

Detachment of fine-grained thin particle layers from filter media

zur Erlangung des akademischen Grades eines
DOKTORS DER INGENIEURWISSENSCHAFTEN (DR.-ING.)

von der KIT-Fakultät für Chemieingenieurwesen und Verfahrenstechnik des
Karlsruher Instituts für Technologie (KIT)

genehmigte
DISSERTATION

von
Patrick Morsch, M.Sc.
aus Bad Dürkheim

Erstgutachter:	Prof. Dr.-Ing. habil. Hermann Nirschl
Zweitgutachter:	Prof. Dr.-Ing. Siegfried Ripperger
Tag der mündlichen Prüfung:	1. Juli 2021

Acknowledgement

This dissertation was written between 2016 and 2021 at the Institute of Mechanical Process Engineering and Mechanics (MVM) at the Karlsruhe Institute of Technology (KIT), under the supervision of Prof. Dr.-Ing. habil Hermann Nirschl, whom I would like to thank in particular for his excellent support and motivation during my doctorate. Thank you for the educational time! I thank him for giving me the chance to do my PhD.

I would like to thank Prof. Dr.-Ing. Siegfried Ripperger for taking over the co-lecture.

I also would like to thank the German Research Foundation (DFG) for financial support within the framework of IGF project no. 18591 N „Ablösung feinstkörniger dünner Partikelschichten von Filtermedien durch Rückspülfiltration“ and IGF project no. 19716 N „In-Situ Reinigungsverfahren von Membranfilterpressen mit sensorgesteuerter und bedarfsorientierter Automatisierung“.

I would also like to thank Dr.-Ing. Harald Anlauf and Dr.-Ing. Marco Gleiß for their professional discussions and engagement during my doctoral studies.

I would like to thank Hans Guigas, Olaf Jörg, Stefan Kollbach, Andreas Lumpp, Thomas Reutter, Berndhard Schweigler, Adam Tobias and all colleagues from the Mechanical Workshop for their support in the design, fabrication and assembly of my experimental unit. In addition, I would like to thank Andreas Baum and Alexandr Lungul for their help with IT and software, as well as Ms. Kerstin Bertsch for her support in the photo lab. I would like to thank Klaus Hirsch and the colleagues from the PMT laboratory for the measurements carried out.

I would also like to thank my colleagues for the very nice time and help. This is especially true for Volker Bächle, Timo Dobler, Bernd Fränkle, Felix Gerbig, Sarah Illies, Lucas Jakob, Manuel Konrath, Stefanos Melekidis, Philipp Menesklou, Richard-Sebastian Möller, Benjamin Radel, Frank Rhein, Thomas Rudsuck, Steffen Schmelzle, Nicolas Schork, Sebastian Schuhmann, Marvin Winkler and Tolga Yildiz.

I also had several students whom I would like to thank. Special thanks go to Adrian Arnold, Maurus Bauer, Jana Lia Christoph, Picabo Sara Dewes, Simon Egner, Yannick Feith, Sven Fietz, Sebastian Fuchs, Christoph Kessler, Jérôme Kühn, Linda Möhlendick, Felix Müller, Kristin Neubauer, Vien Nguyen, Moritz Rettenmayr, Henning Schulze and Vasco Welter.

Special thanks and tributes are also due to the "Circle of Trust". This needs no further elaboration. Glory goes to the Circle!

Zusammenfassung

Die vorliegende Arbeit beinhaltet die wissenschaftliche Ausarbeitung zur Ablösung von Filterkuchenfragmenten von Filtergeweben und ist zeitlich in den Vorgang der Regeneration einzuordnen, welcher nach der eigentlichen Filtration stattfindet. Der Fokus liegt dabei auf dem Kuchenabwurf bei der Rückspülfiltration und der Oberflächenreinigung von Kammerfiltern und beinhaltet eine umfangreiche Variation von Prozessvariablen. Aufbauend darauf erfolgte die Charakterisierung des Kuchenabwurfs anhand des vorliegenden Milieus (Abwurf in Flüssig-/ Gasphase), des Prozesses (Reinigung mit und ohne Hilfsmittel) und der Art des Abwurfs (Vollständiger Kuchenabwurf, guter/schlechter partieller Abwurf, Resuspendieren). Auf Grundlage dieser Beobachtungen wurde ein Bewertungs- und Vorhersagemodell zur Regeneration mittels Kuchenabwurf erarbeitet und in den Kontext nachfolgender Reinigungsprozeduren (Intragewebsreinigung) gesetzt.

Die Experimente zeigen deutlich, dass die Regenerationsvorgänge „Filterkuchenabwurf“ hochgradig vom Milieu der Reinigung abhängen. Im Falle der Rückspülfiltration mit Kuchenabwurf in Flüssig- und Gasphase weisen deutliche Unterschiede in den Abwurfmechanismen auf. So zeigt der Abwurf in Flüssigphase keinen Einfluss des Rückspüldruckes im technisch relevanten Druckbereich von 0,1 - 2 bar auf. Lediglich die Dauer des Regenerationsvorgangs variiert, ist aber im Kontext der Filtrationszeit als vernachlässigbar klein einzuordnen. Sehr gute Regenerationsgüten sind mit Rückspülvolumina unter $2 \text{ l}\cdot\text{m}^{-2}$ zu erreichen. Zur Reduzierung des notwendigen Rückspülvolumens empfiehlt es sich starre Gewebe zu verwenden. Dehnbare Gewebe können das Rückspülvolumen deutlich erhöhen. Hier ist durchaus eine Druckabhängigkeit des Dehnungsverhaltens der Filtergewebe festzustellen. Die Beschreibung des Dehnungsverhaltens ist mittels elementarer Mechanik möglich. Zur Bestimmung von guten Kuchenabwürfen muss zwischen Multifilament- und Monofilamentgewebe unterschieden werden. Die Abwürfe von Multifilamentgewebe sind kohäsionsdominiert und die notwendigen Kuchendicken lassen sich mittels eines Gesamtwiderstandes und dem spezifischen Kuchenwiderstand bestimmen. Beim Abwurf von Monofilamentgewebe muss der Gewebewiderstand zur Berechnung der notwendigen Kuchendicke herangezogen werden. Mit beiden Vorhersagemodellen konnte bei Multifilamentgewebe und Monofilamentgewebe ein guter Abwurf prognostiziert werden. Der Kuchenabwurf selbst lässt sich dabei in Anlehnung an eine Reaktion 1. Ordnung approximieren. Ein genereller Einfluss von Rauigkeit der Gewebeoberfläche und der Regenerationsqualität beim Kuchenabwurf innerhalb einer Gewebeart war nicht zu beobachten.

Im Gegensatz dazu steht der Gasabwurf, dessen Regenerationsperformance maßgeblich durch den Impuls festgelegt wird und zeitlich deutlich schneller erfolgt als der Abwurf in Flüssigphase. Hier empfiehlt es sich, dehnbare und locker aufgespannte Gewebe für den Abwurf zu verwenden. Je höher der Druck und je größer der Beschleunigungsweg, desto mehr Masse des Filterkuchens wird abgeworfen. Auch beim Abwurf in Gasphase nach vorheriger Flüssigfiltration ist beim Kuchenabwurf keine Abhängigkeit von der Rauheit des Filtergewebes zu beobachten.

Im Vergleich zur Rückspülfiltration findet die Regeneration durch Entfernung verbleibender Kuchenfragmente auf der Gewebeoberfläche des Kammerfilters mittels Düsenstrahl zielgerichtet statt. Dieser Schritt ist prozesstechnisch nach Öffnen der Kammerelemente mit nachfolgender, unvollständiger Kuchenloslösung einzuordnen. Dies erfordert das Entfernen der Kuchenfragmente von der Oberfläche und ist im konkreten Fall, verfahrensbedingt, bedarfsgerecht, durch die Entwicklung einer automatisierten Reinigung, möglich. Die Übertragbarkeit des Reinigungskonzept auf andere technische Oberflächen ist daher möglich. Die Untersuchungen haben gezeigt, dass die Reinigungsgüte geringfügig vom Druck, aber in hohem Maße von den Kontaktpartnern Gewebe – Düse – Kontamination abhängt. Ein Trend Richtung „Größere Masche – Schlechtere Regeneration“ lässt sich bei einer Vielzahl an untersuchten Geweben, welche webartbezogen in Gruppen kategorisiert wurden, beobachten. Multifilamentgewebe haben sich, entgegen den Erwartungen, als besonders einfach zu reinigen herausgestellt. Monofilamentgewebe, hergestellt aus Kunststofffasern haben geringfügig bessere Reinigungseigenschaften als Monofilamentgewebe aus Metallfasern, mit Fokus auf die Menge des eingesetzten Regenerationsfluids. Dieser Unterschied nivelliert sich jedoch mit abnehmender Maschenweite. Bei Düsen hat sich besonders die Flachstrahldüse als zweckmäßig zur Reinigung von Oberflächen herausgestellt. Der Reinigungsvorgang selbst lässt sich, analog zur Rückspülung in Flüssigphase, nach Vorbild einer Reaktion 1. Ordnung approximieren. Dadurch ist es möglich, die Reinigungsqualität der Kombination Gewebe – Düse durch zwei Konstanten zu charakterisieren. Bei der Reinigung verschiedenster Kontaminationen hat sich gezeigt, dass auf die jeweilige Charakteristik des Partikelsystems (Neigung zu verbacken, Trocknungsgrad etc.) eingegangen werden muss. Die Verwendung eines intelligenten Filtersystems (Bildanalysetechnik) verbessert die Schmutzerkennung und begünstigt die bedarfsgerechte Reinigung. In Summe ist eine Reduktion des eingesetzten Reinigungsmittels von 30 - 60 %, bezogen auf eine festgelegte „Standardreinigung“ mit ca. 2,1 ml pro cm² Filterfläche, möglich.

Abstract

The present work contains the scientific study of the detachment of filter cake fragments from filter cloths and is to be classified chronologically in the process of regeneration, which takes place after the actual filtration. The focus is on cake removal during backwashing filtration and surface cleaning of chamber filters and includes an extensive variation of process variables. Based on this, the characterization of cake discharge was based on the environment present (liquid/gas phase discharge), the process (cleaning with and without aids), and the type of discharge (complete cake discharge, good/bad partial discharge, resuspending). Based on these observations, an evaluation and prediction model for regeneration by means of cake shedding was developed and placed in the context of subsequent cleaning procedures (intraweave cleaning).

The experiments clearly show that the regeneration process "filter cake discharge" is highly dependent on the cleaning environment. The backwashing filtration with subsequent cake discharges in liquid or gas phase show clear differences in the discharge mechanisms. For example, discharge in liquid phase shows no influence of the backwashing pressure in the technically relevant pressure range of 0.1 - 2 bar. Only the duration of the regeneration process varies, but in the context of the filtration time it is negligibly small, and in contrast to discharge in gas phase it is larger by a factor of 10. Very good regeneration grades can be achieved with backwashing volumes below $2 \text{ l} \cdot \text{m}^{-2}$. To reduce the required backwashing volume, it is recommended to use rigid fabrics. Stretchable fabrics can significantly increase the backwashing volume. Here, a pressure dependence of the expansion behavior of the filter fabric can certainly be observed. The description of the elongation behavior is possible by means of elementary mechanics. To determine good cake discharge, a distinction must be made between multifilament and monofilament fabrics. The regeneration of multifilament fabrics is cohesion dominated and the necessary cake thicknesses can be determined by means of a total resistance and the specific cake resistance. For the regeneration of monofilament fabric, the fabric resistance must be used to calculate the necessary cake thickness. With both prediction models, the regeneration can be predicted for demultifilament and monofilament fabrics. The cake discharge itself can be approximated by a 1st order response. A general influence of the roughness of the fabric surface and the regeneration quality on cake release within one fabric type could not be observed.

This contrasts with gas discharge, the regeneration performance of which is largely determined by the impulse and takes place much faster than discharge in liquid phase. Here, it is recommended to use stretchable and loosely stretched fabrics for the discharge. The higher the

pressure and the greater the acceleration distance, the more mass of filter cake is discharged. Even when discharge in gas phase after previous liquid filtration, no dependence on the roughness of the filter cloth can be observed in the cake discharge.

Compared to backwashing filtration, regeneration takes place in a targeted manner by removing remaining cake fragments on the fabric surface of the chamber filter by means of a nozzle jet (with auxiliary equipment). In terms of process technology, this step is to be classified after opening of the chamber elements with subsequent, incomplete cake detachment. This requires the removal of the cake fragments from the surface and is possible in the specific case, process-dependent, as required, by the development of an automated cleaning system. The transferability of the cleaning concept to other technical surfaces is therefore possible. The investigations have shown that the cleaning quality depends slightly on the pressure, but to a large extent on the contact partners tissue - nozzle - contamination. A trend towards "larger mesh - poorer regeneration" can be observed in many examined fabrics, which were categorized into groups regarding their weave type. Contrary to expectations, multifilament fabrics proved to be particularly suitable for cleaning. Monofilament fabrics made of synthetic fibers have slightly better cleaning properties than monofilament fabrics made of metal fibers, focusing on the amount of regeneration fluid used. However, this difference levels out with decreasing mesh size. In the case of nozzles, the flat jet nozzle has proved to be good for cleaning surfaces. The cleaning process itself can be approximated along the lines of a 1st order reaction, analogous to backwashing in liquid phase. This makes it possible to characterize the cleaning quality of the fabric-nozzle combination by two constants. When cleaning a wide variety of contaminations, it has been shown that the respective characteristics of the particle system (tendency to cake, degree of drying, etc.) must be considered. The use of an intelligent filtering system (image analysis technology) allows an improvement of the dirt detection and favors an improvement of the cleaning according to the needs. In total, a reduction in the cleaning agent used of between 30 and 60 % is possible, based on a defined "standard cleaning" with approx. 2.1 ml per cm² of filter surface.

Content

Symbol directory	X
Latin formula symbols	X
Greek formula symbols	XII
1. Introduction	1
2. Theoretical fundamentals and state of the art.....	7
2.1. Basics of filtration	7
2.2. Separation processes on fibre/fabric - mechanisms of particle separation.....	12
2.3. Deviations from idealised cake filtration	15
2.4. Regeneration of technical surfaces - adhesive forces.....	18
2.4.1. Fluid bridge forces	19
2.4.2. Van der Waals force	21
2.5. Cleaning/regeneration in process engineering - state of the art	25
3. Experimental methods and equipment	31
3.1. Characterisation of the surface contamination	31
3.2. Pressurised filter cell	33
3.3. Laser Scanning Microscope (LSM)	34
3.4. Backwashing filter.....	36
3.5. Chamber filter	39
4. Results and Discussion.....	41
4.1. Backwashing properties of candle filters as a function of the particle system in liquid phase	42
4.2. Backwashing properties of candle filters as a function of the filter fabric in liquid phase	45
4.3. Further development of the prediction model for metal-based monofilament fabrics according to [1,2]	47
4.4. Effects of the bulging behaviour of the filter fabric during the backwashing procedure in liquid phase	50

4.5.	Backwashing properties of candle filters in gas phase.....	52
4.6.	Backwashing properties of candle filters as a function of the filter fabric in gas phase	54
4.7.	Surface cleaning of filter fabrics in chamber filters by automated and demand- controlled nozzle cleaning.....	55
5.	Conclusion and outlook.....	61
5.1.	Conclusion.....	61
I.	Backwashing properties of candle filters as a function of the particle system in liquid phase.....	62
II.	Backwashing properties of candle filters as a function of the filter fabric in liquid phase.....	63
III.	Effects of the bulging behaviour of the filter fabric during the backwashing procedure in liquid phase	64
IV.	Backwashing properties of candle filters in gas phase.....	64
V.	Surface cleaning of filter fabrics in chamber filters by automated and demand- controlled nozzle cleaning.....	65
5.2.	Outlook.....	67
Appendix	69
A.	Darcy equation via Navier-Stokes equation.....	69
B.	Hermans & Bredée – Derivation.....	70
C.	Filter Equation – Derivation.....	71
D.	Backwashing filter – Detailed R & I - flow diagram	72
E.	Statement from the copyright conditions of Elsevier.....	73
F.	Attached publication [1].....	74
G.	Attached publication [2].....	87
H.	Attached publication [3].....	98
I.	Attached publication [4].....	106
J.	Attached publication [5].....	116
K.	Attached publication [6].....	125

L. Extended investigation of [4]	138
References	151
Publications	165
Posters and presentations	167

Symbol directory

Latin formula symbols

A	Flowed through area / m^2
a	Drying constant I / -
\AA	Ångström / $\text{m} \cdot 10^{-10}$
A_{Contact}	Contact area / m^2
A_i	Partial filter area / m^2
A_{Tot}	Total filter area / m^2
b	Drying constant II / -
d_p	(volume equivalent) particle diameter / $\text{m} \cdot 10^{-6}$
F_{Adhesion}	Adhesion force / N
F_{Boarder}	Boundary forces / N
$F_{\text{Capillary}}$	Capillary force / N
F_{Cohesion}	Cohesive force / N
$F_{\text{Detachment}}$	Detachment force / N
F_{Surface}	Surface force / N
F_{VdW}	Van der Wall's force / N
H_{FC}	Filter cake height / $\text{m} \cdot 10^{-3}$
$H_{\text{FC, Mono}}$	Calculated filter cake thickness for cake discharge of monofilament fabric / m^{-1}
$H_{\text{FC, Multi}}$	Calculated filter cake thickness for cake discharge of multifilament fabric / m^{-1}
K	Carman-Kozeny constant / -
K_{HB}	Hermans & Bredée factor / unit depending on separation mechanism
K_{Turb}	Constant of the turbulence term of the Darcy-Forchheimer equation / -
L	Tube length / m
m_{remain}	Remaining cake mass on the fabric during gas discharge / $\text{kg} \cdot 10^{-3}$
m_{removed}	Discharged cake mass from the fabric at gas discharge / $\text{kg} \cdot 10^{-3}$
$m_{\text{removed, dry}}$	Discharged dried cake mass from the fabric at gas discharge / $\text{kg} \cdot 10^{-3}$
$m_{\text{removed, wet}}$	Wet cake mass discharged from the fabric at gas discharge / $\text{kg} \cdot 10^{-3}$
n	Compression exponent / -
p_c	Capillary pressure / Pa

p_D	Dewatering pressure / Pa
p_L	Liquid pressure / Pa
p_s	Solid frame pressure / Pa
q	Hermans & Bredée exponent / -
R	Resistance value / m^{-1}
R	Flow resistance / m^{-1}
$r = r_1 = r_2$	Radius / $m \cdot 10^{-6}$
$R_{F,0}$	Initial resistance / m^{-1}
R_{FC}	Filter cake resistance / m^{-1}
R_{FM}	Fabric resistance / m^{-1}
$R_{FM,0}$	Pure water fabric resistance / m^{-1}
$R_{FM,Surface}$ Deposition	Fabric resistance with interaction of a particle system deposited on the fabric surface / m^{-1}
R_i	Partial resistance of a filter cake segment / m^{-1}
R_{IR}	Interference resistance / m^{-1}
$R_{Periphery}$	System and support fabric resistance / m^{-1}
R_q	Roughness / $m \cdot 10^{-6}$
R_{Tot}	Total flow resistance / m^{-1}
S	Saturation / -
S_∞	Limit saturation / -
t	Time / s
U	Surface energy / $J = N \cdot m$
V_F	Filtrate volume / m^3
\dot{V}_F	Filtrate volume flow / $m^3 \cdot s^{-1}$
$\dot{V}_{F,max}$	Initial filtrate flow / $m^3 \cdot s^{-1}$
$\dot{V}_{F,min}$	Minimum filtrate volume flow / $m^3 \cdot s^{-1}$
$V_{Filter\ cake}$	Volume of filter cake / m^3
V_H	Cavity volume / m^3
V_L	Liquid volume / m^3
x	Particle size (Not further defined) / $m \cdot 10^{-6}$
z	Distance / $m \cdot 10^{-6}$

Greek formula symbols

$\alpha_{\text{approximated}}$	Approximated degree of contamination / -
α_{FC}	Specific cake resistance / m^{-2}
$\alpha_{\text{FC},0}$	(Initial) specific cake resistance / m^{-2}
β	Final contamination degree / -
γ	Surface tension / $\text{N} \cdot \text{m}^{-1}$
γ_{Kinetic}	Cleaning kinetics during nozzle cleaning / $\text{cm}^2 \cdot \text{ml}^{-1}$
Δp	Pressure drop / Pa
Δp_{Tot}	Total pressure drop / Pa
Δp_i	Partial pressure drop of a filter cake segment / Pa
Δp_0	(Initial) pressure loss / Pa
Δt_{Setup}	Duration of the backwash cycle / s
$\Delta \dot{V}$	Difference in volume flow / $\text{m}^3 \cdot \text{s}^{-1}$
ε	Porosity / -
ε_0	(Initial) porosity / -
$\varepsilon_{\text{Filter cake}}$	Porosity of the filter cake / -
η	Dynamic viscosity / $\text{Pa} \cdot \text{s}$
η_f	Dynamic viscosity / $\text{Pa} \cdot \text{s}$
κ	Particle concentration / $\text{m}^3 \cdot \text{m}^{-3}$
ρ	Density / $\text{kg} \cdot \text{m}^{-3}$
ρ_{liquid}	Liquid density / $\text{kg} \cdot \text{m}^{-3}$
σ_Z	Tensile strength / Pa
φ	Sphericity / -

Chapter 1

1. Introduction

Separation of solids from process streams takes place in almost every process plant. Cake-forming filtration in solid-liquid separation has excelled for the treatment of low-concentration suspensions and offers energetic advantages over other separation principles. The fields of application of these filter apparatuses are various and include the filtration of sols in electrochemical and galvano-technical processes (e.g. anode sludge treatment), the recirculation of catalysts in chemical and pharmaceutical processes, the purification of edible oils and fats in food processing technology, as well as the purification of process (water) streams in the petroleum and mining industry (tailings). A significant increase in recent years can also be seen in environmental technology. Here, the reduction of plastic pollution (keyword "microplastic") in rivers and oceans, the separation of microalgae for energy generation and the effective separation of tailings to reduce the anthropogenic impact on the existing fauna and flora are three examples of the application of filtering separators. With these tasks, the user's demands on the filters in terms of separation efficiency, process stability, and service life also increase accordingly. In addition to the actual separation performance (quality of the filtrate, level of hydraulic loading), regular replacement or regeneration of the filter mesh must be embedded in the process sequence to ensure a good process stability and service life. The reason is the increasing flow resistance with the increasing filter cake thickness and the blocking of the filter cloth during service life. Considering the reduction of disposable products, the regeneration of the fabrics is a common way to reduce the costs and decrease the initial resistance between filtration cycles. This regeneration can be realized by the filter cake discharge respectively the removal of the filter cake from the filter cloth surface. This requires models for the prediction of this detachment behavior and the improvement by an adapted choice of filter fabric as an essential gain in knowledge to achieve a complete detachment of the filter cake from the fabric. This relationship is a consequence of tissue-particle interaction and is investigated in this thesis.

During this regeneration, the filter cake should be thrown off as completely as possible so that the mesh can again reach the required filtrate flow at the start of filtration. Figure 1 shows the exemplary course of the filtrate volume flow \dot{V}_F of the cake-forming filtration for several filtration cycles. The initial filtrate flow $\dot{V}_{F,\max}$ and how it decreases during filtration and with the filter cake building up in the direction of $\dot{V}_{F,\min}$ (dashed line) can be seen. Once there, the

filter cake is discharged in the time interval Δt_{Setup} . If this discharge takes place completely, the filtrate flow in the following filtration cycle reaches $\dot{V}_{F,\text{max}}$ again. If cake fragments remain on the surface, this reduces the filter area and the initial volume flow of the following filtration cycle (solid line). These remaining fragments can accumulate during several filtration cycles and lead to an overall reduction in filtration performance by decreasing the initial volume flow. The question to be answered is how this detachment behavior can be influenced by intelligent selection of the filter fabric and the cleaning parameters. A major influence of the interaction between particles and filter fabric can be assumed, which also needs to be clarified. The final goal is to increase the efficiency of filters by increasing the regeneration efficiency by predicting the detachment behavior.

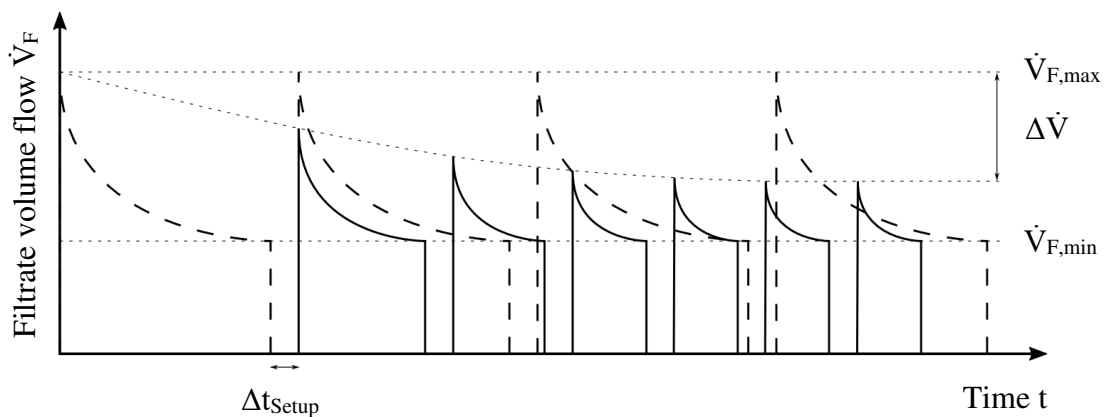


Figure 1: Exemplary course of the filtrate volume flow \dot{V} over time t for filtration cycles with a good regeneration (dashed line, started by $\dot{V}_{F,\text{max}}$ till $\dot{V}_{F,\text{min}}$) and for a poorly regenerated fabric with the reduced initial filtrate volume flow by $\Delta \dot{V}$ for the subsequent filtration cycles. In this case, the number of backwashing cycles, characterized by Δt_{Setup} , increases.

In this work, the regeneration processes after cake-forming filtration, with focus on the removal of the filter cake, are investigated. A distinction is made between cake removal without and with aids. Cake removal without aids is technically represented by the backwashing filters. Here, the built-up filter cake is detached from the filter fabric by means of flow reversal and removed. In the case of cake removal with aids means, the cake is removed by an automated nozzle system coupled with image evaluation. The respective regeneration processes have a test matrix adapted to the process. This can be found in the respective publication.

The dissertation is divided into seven subsections in Chapter 4. Results and Discussion (page 41), following the regeneration mechanisms without and with aids, according to the respective publications, starting after Appendix E (page 73):

1) Backwashing properties as a function of the particle system in a liquid environment.

The starting point is an investigation into regeneration by cake detachment/discharge during backwashing filtration. The general question to be addressed is whether it is possible to predict detachment behavior and what mechanisms take place during cake

detachment. This process is insufficiently investigated, and the question arises at which process conditions an effective cake discharge can be expected. For this reason, the process variables backwashing pressure, cake thickness and particle system (size, shape, mineralogy) were varied. The objective is a methodical description of the discharge process and the elaboration of essential influencing variables.

For this purpose, defined cake thicknesses were approached and backwashed using 7 different particle systems. The aim is to generate a cake discharge as complete as possible. Another part of the investigation was the variation of the backwashing pressure as a freely selectable process parameter. The filter fabric used is a fabric with multifilament fiber structure (multifilament fabric). During this investigation, the dependence of pressure, particle system and cake thickness during regeneration were determined and described with four different discharge types. Finally, a predictive model was developed for the discharge process based on pressurized filter cell tests. The results are summarised in chapter 4.1 (page 42) and described in full in Appendix F (page 74). [1]

2) Backwashing properties as a function of the filter fabric in a liquid environment.

The experience from [1] was used to describe the fabric influence during regeneration using cake discharge. In addition to the influence of the particle system, the selection of the filter fabric is expected to exert a significant influence on cake discharge. This influence was quantified by testing selected fabrics for their regenerability.

By using multifilament and monofilament fabrics, the model of [1] could be extended/confirmed to other multifilament fabrics. Another observation is that regeneration in monofilament tissues follows different discharging mechanisms. The investigation includes plain and twill weave of monofilament fibre structure. A major influencing factor here is the particle size and shape and the associated deposition behavior in the meshes of the monofilament fabrics. An influence of adhesion is therefore given and resulted in a prediction model based on the filter medium resistance and the specific cake resistance. A particle shape dependent factor was introduced, which allows the calculation of the cake thickness for a good cake release. Due to the finite number of the experimental scale, the question arises whether this model can be transferred to other monofilaments of different materials (metal weaves). The results are summarised in chapter 4.2 (page 45) and described in full in Appendix G (page 87). [2]

3) Further development of the prediction model for metal-based monofilament fabrics according to [1, 2]

Based on the methodology described in [2], the investigation was extended to include 9 metal fabrics (plain and twill weave) of monofilament fibre structure. After the prediction model has proven successful for a representative group of tissues (multifilaments and monofilaments), the model is extended to other tissue groups such as metal tissues.

For these fabrics, too, a complete cake discharge was generated and compared with the model from [2]. In the course of this investigation, the particle shape-dependent factor was further refined and shows the transferability of the model to further monofilament fabrics of different weave type and material.

The sum of the investigation now allows the prediction of the necessary cake thickness for a complete cake discharge for polymer and metal fabrics $\leq 25 \mu\text{m}$, weaved into plain and twill weaves. The results are summarised in chapter 4.3 (page 47).

4) Description of the bulging behavior of the tissues during backwashing in liquid phase.

During backwashing in liquid phase, a clear influence on the bulging behavior was found in [1,2]. This bulging behavior during backwashing in the liquid phase contributes to an increase in the necessary backwashing volume and demonstrably worsens the quality of the cake discharge. Based on this observation, a physical description of this process was carried out based on the elongation behavior of selected filter cloths. These measurements can be used to optimize the so-called register spacing of the filter elements in the apparatus and contribute to increasing the filter area per footprint and reducing the backwashing volume. In general, it is recommended that a tightly fitting fabric for backwashing in liquid phase provides significant advantages regarding the reduction of the specific backwashing volume. Nevertheless, a mechanical deformation takes place. A physical quantity could be determined to describe this bulging behavior as a function of the fabric tension, the backwashing pressure and the mesh size. The investigation answers the question of the arrangement of the filter elements in the vessels (register spacing) and is a first step towards the optimization of filter apparatus. The results are summarised in chapter 4.4 (page 50) and described in full in Appendix H (page 98). [3]

5) Backwashing properties in a gaseous environment

Regeneration in a gaseous environment after previous gas filtration is the subject of many publications. Gas discharge after previous liquid filtration, on the other hand, is not. Due to the insufficient investigation of gas discharges after previous liquid filtration, this process is to be investigated in more detail. Based on the experience from [1-3], it can be assumed that the discharge follows other mechanisms. Therefore, a definition of sensitive backwashing variables was made in the case of discharge in the gas phase, after prior liquid filtration. In addition to the backwashing pressure and the cake thickness, this also includes cake drying processes such as drying pressure and drying time. A difference to the drop in [1] could be identified and described. In addition, process variables such as backwashing pressure, liquid saturation and cake thickness were elaborated as particle system-dependent influencing factors. The fabric and its stiffness also play a role here. The investigation allows to conclusively clarify the frequently discussed question regarding the detachment behavior between gas and liquid discharge but poses further questions regarding the fabric dependence in the case of cake discharge in gas phase. The results are summarised in chapter 4.5 (page 52) and described in full in Appendix I (page 106). [4]

6) Backwashing properties as a function of the filter fabric in a gaseous environment

Based on [4], the investigation is also extended to different types of fabrics (plain weave, twill weave and satin weave) of monofilament fiber structure. Since clear differences can already be observed in the discharge in liquid phase, this is also expected for the discharge in gas phase. It is shown that the roughness and stiffness of the fabrics have a significant influence on the throw-off quality. Furthermore, the investigation shows that acceleration of the filter fabric by oversizing the fabric tube diameter, in relation to the candle element, contributes significantly to the improvement of the throw-off behavior and to the reduction of the backwashing pressure. The results are summarised in chapter 4.6 (page 54).

7) Surface cleaning of filter fabrics by nozzles

In the case of particularly strongly adhering contaminants, an undirected regeneration as in the case of cake discharge reaches its limits. Here, cleaning support is necessary and is technically realized using nozzles. These nozzles are to approach contaminated

areas and clean them as required. The aim is to investigate the effect of various nozzles on the filter fabrics to provide empirical values for cleaning tasks.

In this study, selected nozzles are evaluated in the context of cleaning adhering filter cakes. The influence of fabric types is also shown on the basis of monofilament and multifilament fabrics. The performance and quantification of the cleaning is carried out on a specially developed image evaluation software, which allows a demand-based cleaning entirely in the sense of Industry 4.0. The question to extend this application to other technical surfaces is discussed and allows to further develop the regeneration with aids. The results are summarised in chapter 4.7 (page 55) and described in full in Appendix J (page 116) and Appendix K (page 125). [5,6]

Chapter 2

2. Theoretical fundamentals and state of the art

This chapter describes the technical fundamentals for filtration, with emphasis on cake-forming filtration, and the regeneration of technical surfaces, with emphasis on filter fabrics. The respective chapters give a broad overview of the topic. The theory defined for the respective elaboration can be taken from the respective publication.

2.1. Basics of filtration

Mechanical separation techniques feature many physical principles for the separation of particle-loaded suspensions and their implementation in the equipment used to separate the solid, disperse phase from the liquid, continuous phase. These differ in their mode of operation, degree of separation, scalability and other technical differentiation criteria, and it is up to the process engineer to select a suitable apparatus for the process in question. [7–9]

In the separation of low-concentration suspensions from a liquid process stream, cake-forming filtration has established itself as a suitable separation principle and many apparatuses are based on this physical process. The choice of apparatus is based on the value product to be recovered from the process. If the liquid phase is the value product to be recovered, the process is generally referred to as clarification filtration. Processes that aim to recover the solid phase are also referred to as separation filtration. [10,11]

Independent of this distinction, the process of filtration has accompanied anthropogenic development for thousands of years, e.g. for the filtration of food and drinking water [12]. A first mathematical description was given by the French water engineer Henry Darcy in 1856, who observed the linear relationship between the height of a sand fill and the volumetric flow rate in water treatment for the city of Dijon, France [13]. This linear relationship, referred to as the Darcy equation, is described mathematically in Eq. 1 and is considered a hydraulic pondon to Fourier's equation from heat conduction [14] or Fick's law from diffusion [15]. The pressure drop Δp acting in a sand fill is a function of the resistance value R , the dynamic viscosity η , the filter area A and the volume flow \dot{V}_F . There is therefore a direct proportionality $\Delta p \propto \dot{V}_F$. At the same time, the German engineer Julius Ludwig Weisbach formulated the same observation, which is why this equation is also called the Darcy-Weisbach equation [16]. However, this designation has not become generally accepted, so that usually only the Darcy equation is mentioned.

$$\Delta p = R \cdot \eta \cdot \dot{V}_F \cdot A^{-1} \quad \text{Eq. 1}$$

The basis of this equation was developed years earlier by physicist Jean Léonard Marie Poiseuille in 1840/41 [17–19] and engineer Gotthilf Heinrich Ludwig Hagen in 1839 [20] in general for laminar flow of incompressible Newtonian fluid in a pipe stiffener and published as the Hagen-Poiseuille equation [21]. This relationship is illustrated in Eq. 2. Again, there is proportionality between pressure drop and volume flow $\Delta p \propto \dot{V}_F$, the resistance term R of the Darcy equation is replaced by geometrical quantities such as the length of the tube L through which the fluid flows and its transverse area A .

$$\Delta p = 8\pi \cdot L \cdot \eta \cdot \dot{V}_F \cdot A^{-2} \quad \text{Eq. 2}$$

While the Hagen-Poiseuille equation describes the laminar flow of pipes with a significantly greater length than diameter¹, the introduction of the resistance term R according to Darcy allows the transfer to a multitude of laminar flowing bulk materials [23]. Today, these resistances are listed in table books for various bulk materials and allow the filter apparatus to be designed even without empirical determination of the flow resistance [24–26].

The Darcy equation underwent further development by the physicist Josef Kozeny (1927) and engineer Philip C. Carman (1937) for transfer to bulk materials with known particle diameter d_p . This relationship is shown in Eq. 3 and is generally known as the Carman-Kozeny equation. The drag term is described by the height of the bulk or filter cake H_{FC} , the volume equivalent particle diameter d_p , and the porosity of the bulk ε . In addition, the equation contains a constant K , which must be determined empirically. In subsequent publications, this constant is also expressed by the sphericity ϕ in terms of $K = 180 \cdot \phi^{-2}$ [27,28]. Looking at Eq. 3, the pressure drop Δp is inversely proportional to the particle diameter d_p squared $\Delta p \propto d_p^{-2}$. Thus, decreasing the particle size from 100 μm to 10 μm increases the pressure drop by a factor of 100.

$$\Delta p = [H_{FK} \cdot K \cdot (1 - \varepsilon)^2 \cdot \varepsilon^{-3} \cdot d_p^{-2}] \cdot \eta \cdot \dot{V}_F \cdot A^{-1} \quad \text{Eq. 3}$$

Building on the Carman-Kozeny equation, Sabri Ergun, a Turkish-born chemical engineer, published the Ergun equation in 1952, named after him, which transfers the equation to packed columns and adds a turbulence term. This is shown in Eq. 4. This equation allows the calculation of the pressure drop of a gas- and liquid-flowed column and has its origin in filtration but is needed in thermal process engineering. Here, the smooth transition between the sub-disciplines of process engineering becomes clear. The basis of the application-related Ergun equation is the Darcy-Forchheimer equation ($+ \rho \cdot K_{\text{Turb}}^{-1} \cdot (\dot{V}_F \cdot A^{-1})^2$), which extends the Darcy equation

¹ The change in pipe friction coefficient λ is minor in the laminar region ($\lambda=64 \cdot \text{Re}^{-1}$), but must be taken into account in the turbulent region, adapted to the physical system (e.g., formula according to Blasius, Nikuradse, Colebrook, or the common Moody diagram). [22]

by a turbulence term [29] and can be derived via the Navier-Stokes equation (see Appendix A. A. Darcy equation via Navier-Stokes equation, page 69) [30]. This turbulent component was already recognized by Hagen and is considered in his description of flows in pipe services but interpreted as negligible [20]. Since the technical relevance of the turbulence term is also negligible for liquid filtration, reference is made here to the catchy literature [31,32].

$$\begin{aligned} \Delta p = & [H_{FK} \cdot 150 \cdot (1 - \varepsilon)^2 \cdot \varepsilon^{-3} \cdot d_p^{-2}] \cdot \eta \cdot \dot{V}_F \cdot A^{-1} \\ & + [H_{FK} \cdot 1.75 \cdot \rho \cdot (1 - \varepsilon) \cdot \varepsilon^{-3} \cdot d_p^{-1}] \cdot \dot{V}_F^2 \cdot A^{-2} \end{aligned} \quad \text{Eq. 4}$$

With increasing industrialization, the demands placed on filters in terms of separation efficiency, particle retention and filtrate purity increased. This led to the further development of filter meshes through more detailed differentiation of the separation mechanisms in and on the mesh. Macroscopically, this was done for the first time by Hermann and Bredée in 1936 on the basis of the differential equation shown in Eq. 5, for filtrations at constant pressure, and refers to the following 4 separation mechanisms:

- Cake-forming filtration ($q = 0$),
- Standard filtration ($q = 1,5$),
- Intermediate filtration ($q = 1$),
- Clogging filtration ($q = 2$).

This equation allows to determine predominant separation mechanisms such as those of depth filtration ($q=1.5$) and cake-forming filtration ($q=0$), on the basis of measurable quantities such as pressure drop and volume flow rate by means of an exponent q and the factor K_{HB} [10,33]. In addition, a direct transfer into the common equations is possible. This is illustrated by the cake-forming filtration treated here in Appendix B. Hermans & Bredée – Derivation (page 70). Here, by means of coefficient comparison, the derivation into the Darcy equation and its modification into the filtration equation, which will be treated in detail in the following, is possible. Further developments of these equations for non-Newtonian fluids and membrane filtration applications have also been published [34–36]. [37]

$$\frac{d^2 t}{dV_F^2} = K_{HB} \cdot \left(\frac{dt}{dV_F} \right)^q \quad \text{Eq. 5}$$

Due to the technical relevance of the Darcy equation in filtration, a series of further developments followed with reference to the flow resistances. For this purpose, a more detailed description of the resistance R from Eq. 1 was given as the cake resistance R_{FC} and the fabric resistance R_{FM} , which are connected in series. While the fabric resistance remains constant and is therefore, due to interaction with the particle system, also called initial resistance $R_{F,0}$, the cake resistance grows because of the cake thickness. Here, there is a relationship between the cake thickness H_{FC} and the filtrate volume V_F and leads to an overall description of the

resistance R according to Eq. 6. Here, the cake resistance is shown as the product of the specific cake resistance α_{FC} and the filter cake thickness.

$$R = \alpha_{FC} \cdot H_{FC} + R_{FM} \quad \text{Eq. 6}$$

Based on the effective resistances in Eq. 6 and the Darcy equation in Eq. 1, the general filtration equation used today (Eq. 7) results and can be transferred to existing process designs such as constant pressure loss $\Delta p = \text{constant}$ or constant volume flow $\dot{V}_F = \text{constant}$. For this purpose, the filtrate volume flow \dot{V}_F is considered differentially (dV_F/dt) and integrated. The derivation for this is given in Appendix C. Filter Equation – Derivation (page 71) and requires the introduction of the volume constant κ as the ratio of the filter cake volume, expressed as the product of the filter area with the cake thickness $A \cdot H_{FC}$, divided by the filtrate volume V_F . Based on this, the filtration equation for cake-forming filtration can be transferred into the usual form as a $t/V_F - V_F$ - diagram, for determination of the resistances.

$$\Delta p = (\alpha_{FC} \cdot H_{FC} + R_{FM}) \cdot \eta \cdot \frac{dV_F}{dt} \cdot A^{-1} \quad \text{Eq. 7}$$

In the case of fabric resistances, it has been shown that the interaction between the fabric and the first particle layer during filtration leads to an increase in the flow resistance of the fabric compared to the pure water resistance and reduces the fabric resistance heavily [38]. This is a consequence of bridging, mesh blocking of the tissue and reduction of the flowable area due to surface occupancy of individual particles and/or particle clusters and has been taken into account by introducing an interference resistance R_{IR} [39–43]. This considers the increase in flow resistance and increases the resistance of the tissue due to particle interaction. The basis of the interference resistance is an extended description of the resistances according to Eq. 8. While the plant and piping resistance of the periphery $R_{Periphery}$ is usually negligible compared to the fabric and cake resistance, the interference resistance plays a significant role and, with the specified increase in the initial resistance, can lead to a significant reduction relative to the pure water resistance. If not considered, this would lead to an overestimation of the filtrate flow and thus to an underestimation of the necessary filter area. Figure 2 shows a schematic diagram of the flow resistances acting in cake-forming filtration. The periphery resistance is negligible for very fine particle systems, as mentioned above, but may become a factor to be considered if the combination of pipe diameter and support fabric is unfavourable [44,45].

$$R_{Tot} = R_{FC} + R_{FM} + R_{IR} + R_{Periphery} \quad \text{Eq. 8}$$

From a practical point of view, a counteraction takes place through the integral consideration of the filtration, instead of the differential. This means that the design of the filter apparatus is based on the volume flow with existing filter cake. Nevertheless, the introduction of the interference resistance led to a more detailed description of the cake structure, and the

interactions between the particle system, filter cloth, supporting cloth, and plant periphery are a process to be considered during filtration. [38,44,45]

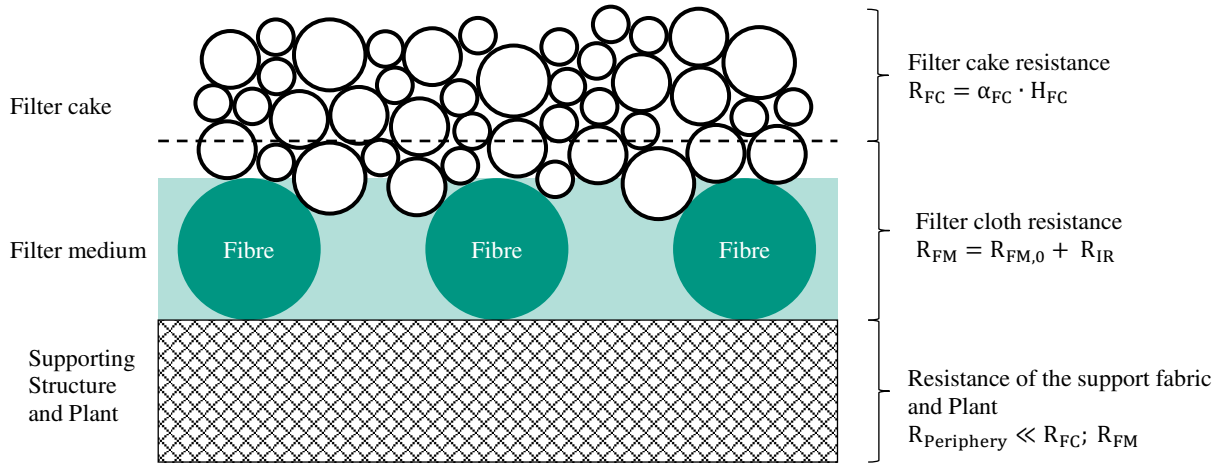


Figure 2: Schematic representation of the flow resistances in cake-forming filtration. The filter cake resistance R_{FC} increases with the filter cake thickness H_{FC} . The filter media resistance R_{FM} depends on the mesh size and weave type ($R_{FM,0}$) and the interaction with the particle system (R_{IR}). The supporting fabric and the line routing of the system form a further resistance $R_{Periphery}$, which is usually significantly lower than cake and fabric resistance. [46]

The equations presented in this chapter from the field of flow through porous structures, filtration and particle-loaded flows are to be understood as an overview. More detailed descriptions can be found in the respective publications. The essential equation for this elaboration is the filter equation (Eq. 7) considering the effective resistance (Eq. 8).

2.2. Separation processes on fibre/fabric - mechanisms of particle separation

As described in the previous chapter, the interaction of particles and tissue leads to an increase of the flow resistance, related to the pure water resistance of the tissue. Macroscopically, the consideration of this effect was done by introducing the interference resistance [40]. These effects lead to the microscopic distinction into 3 possible separation mechanisms [38,41,47]:

- Bleeding,
- Clogging/
Pore Penetration,
- Surface Deposition.

This distinction depends largely on the relationship between particle size and mesh size. According to [38], in an ideally monomodal and spherical particle system, bleeding, i.e. flowing through the filter mesh, is to be expected with mesh sizes smaller than 65 % of the particle diameter to be filtered. In this case, the particles form bridges during filtration, which initiate the actual filtration. If the mesh is unsuitable for the filtration of a given particle system (meshes too large in relation to the particle size distribution), this leads to long turbidity times and recirculation of the filtrate until the bridges are formed.

For particle sizes between 65 and 130 % of the mesh size, clogging or pore penetration is to be expected. Here, the particle size roughly corresponds to the mesh size and this leads to clogging models, close to the sphere-hole model according to [40] with complete or partial clogging of the pore/mesh. This leads to the highest increase in mesh resistance.

The final deposition mechanism is Surface Deposition. In this case, the particles deposit as a clear boundary on the filter mesh. This can be observed with particles that are 1.3 times larger than the mesh of the fabric. The increase in fabric resistance becomes smaller again and is only slightly higher than the pure water resistance, as a result of partially covered pores. While bleeding is especially expected for very small spherical particles, a dominant surface deposition can be assumed with decreasing sphericity and increasing size relative to the mesh size of the fabric [38]. The deposition mechanisms are shown schematically in Figure 3.

Since real particle suspensions are usually not monomodal, spherical particle systems, but bi- to multimodal particle systems with deviation from the ideal sphericity, these mechanisms are superimposed. This lead, for example, to turbidity at the beginning of filtration, even with particle systems whose modal value is larger than the mesh size of the filter fabric.

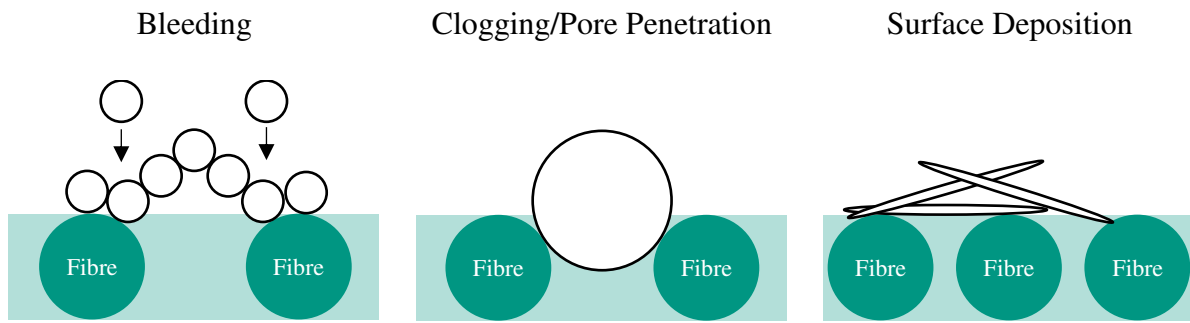


Figure 3: Schematic representation of the deposition mechanisms in a mesh. The distinction is made by the ratio of particle size to mesh size and can be divided into bleeding, clogging/pore penetration and surface deposition. In real systems, these mechanisms are superimposed. [46]

Cake-forming filtration is based on the mechanisms shown in Figure 3 and passes through them during a filtration cycle. The characteristics depend again mainly on the ratio of mesh size to particle size. At the beginning of filtration, smaller particles flow through the pores/meshes with the consequences of turbidity in the filtrate. From a process engineering point of view, recirculation is required here until the particle size in the filtrate falls below the specified limit value. Larger particles, which are deposited in and on the meshes, facilitate the formation of bridges. Once the first particle layer has built up, the larger particles form a porous structure in which the finer particles are deposited. Filtration processes such as precoat filtration are based on this principle [48–50]. The separation mechanisms involved can be summarized as follows [51,52]:

- Diffusion,
- Sedimentation,
- Interception,
- Inertia,
- Sieving effect.

The acting deposition mechanism, analogous to the deposition on the meshes, also depends on the scale of the particles. Very small particles in the sub-micrometer range ($x < 0.1$ to $2 \mu\text{m}$) exhibit diffusion deposition. This is due to collisions of the surrounding fluid molecules as a result of thermal motion. Such collisions also affect larger particles but lead to an abrupt change in direction only for smaller ones. Thus, diffusion is characterized by a sudden random motion of the particle, which can be interpreted as Brownian motion (see Figure 4). If this movement leads to a collision between particle and filter medium/filter fiber or deposited particle, known adhesive forces cause deposition on this surface (see chapter 2.4. Regeneration of technical surfaces - adhesive forces, page 18). [51]

Another separation mechanism is by sedimentation. Especially very large density differences between continuous and disperse phase, as well as very large particles lead to this separation mechanism. The particle leaves the flow line as a result of the weight force in the gravity field and remains on the surface with which it interacts. Sedimentation during filtration can strongly

influence the filtration and leads, among other effects, to an increase in the initial resistance, facilitates bridging and, in the case of vertically mounted filter elements, can stand in the way of a homogeneous filter cake structure. For this reason, flow velocities of 3-5 times the sedimentation velocity of the particle are required for horizontally mounted filter elements in order to support a homogeneous filter cake build-up [53].

Separation by interception or the barrier effect is mainly observed for particles whose flow line is close to the surface to be separated. Here, separation can be expected at distances smaller than the radius of the particle [54]. This deposition mechanism should not be confused with that of inertia and sieving effect. The former is because heavy/inert particles cannot follow this flow exactly when the flow is redirected at curved surfaces. If the particle collides with an obstacle before it has had a chance to adapt to the new flow line, separation occurs. Separation by the sieve effect occurs in/on the meshes of the fabric and the pores of the structure. This is caused by the geometric size difference between the particle and the free flow cross-section and leads to the particle remaining at this location. The separation efficiency related to the particle size of meshes can be done by porometry, microscopy and filtration test. While porometry² as an indirect measurement method depends on many factors such as liquid agent, measurement procedure and evaluation methodology [55,56], microscopy and filtration test provide a direct measurement method to determine the effectively deposited particle size [57–59]. A linear relationship between the presented direct and indirect measurement methods is given, knowing the mesh/pore geometry [60]. The pore size and thus separation efficiency by sieving action of particle structures can be done using the Young-Laplace equation and states that the formed pores of a monomodal particle system with $\frac{2}{3} \cdot$ particle diameter can be estimated [61].

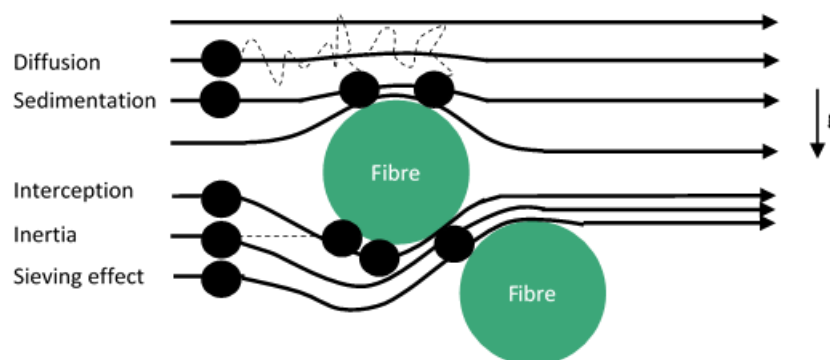


Figure 4: Schematic representation of the deposition on a single fiber. The main influencing factor here is also the particle size. This is incorporated into the predominant deposition mechanism on the single fiber, such as diffusion, sedimentation, interception, inertia and sieving effect. Illustration based on [51,52].

As can be seen from the previous sections, the main influencing variable in filtration is given by the ratio of mesh to particle size distribution. These have a direct effect on the

² See ASTM F316 – 03 and ASTM D6767 – 20

hydrodynamics of the filtration and thus also on the quality of the filtrate, as measurable variables. A wide variety of refinement steps, such as hydrophobing and/or calendaring of the meshes, are possible to improve the separation efficiency [57,58,62–64]. Here again, the importance of the selection of the filter fabric, which must be made by the process engineer, becomes clear.

The experiment to determine suitable fabric-particle combinations is still necessary for this purpose [65]. However, numerical flow simulation, including DEM simulation, provides a suitable means for predicting the separation efficiency [66–68]. The underlying force balance and calculation methodology is being successively extended and has the potential in the long term to replace experimentation for determining the separation processes. [69,70]

2.3. Deviations from idealised cake filtration

As mentioned in chapter 2.2, the deposition processes bleeding, clogging and surface deposition take place superimposed due to the deviation of real particle systems from the monomodal-spherical ideal system. In the mathematical description of filtration, this is considered, for example, by applying constants, e.g. in the Carman-Kozeny equation (Eq. 3). The adjustment for the correct description of the pressure loss is to be understood as a retroactive improvement of the prediction model and should result in a linear course of the $t/V_F - V_F$ application in the cake-forming filtration. In contrast to this, the VDI guideline 2762-2 provides direct physical causes for deviating behaviour during filtration. This results in a deviating course of the $t/V_F - V_F$ application from the ideal straight line and complicates or prevents a correct determination of the specific cake and filter medium resistance α_{FC} and R_{FM} . Figure 5 shows an example of five possible deviations (B-F) from the ideal curve (A) in the $t/V_F - V_F$ (a) or differentially in $dt/dV_F - V_F$ application (b).

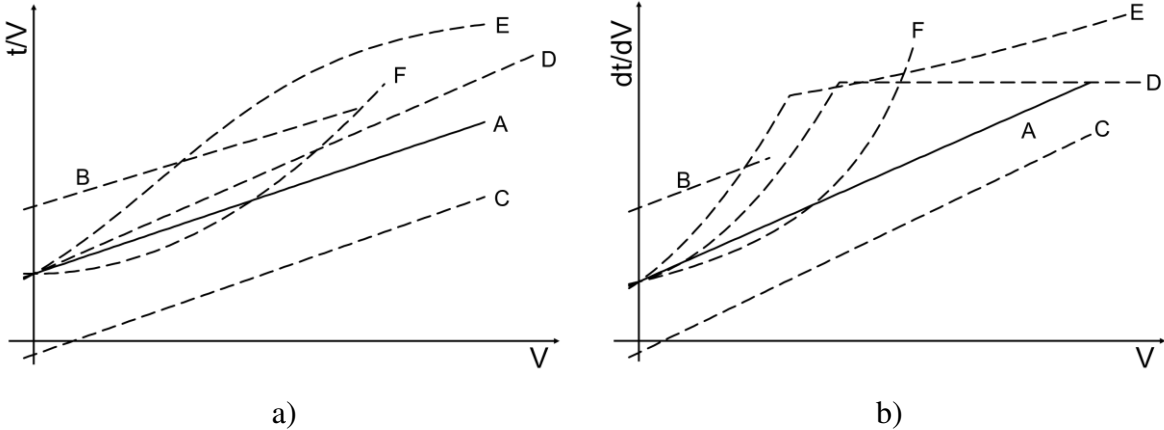


Figure 5: Schematic representation of the deviation from the ideal course of cake-forming filtration according to VDI Guideline 2762-2. Shown is the integral representation via the $t/V_F - V_F$ application (a) and the differential representation $dt/dV_F - V_F$ application (b). [71]

Particularly problematic in the operation of filters is the sedimentation of particles (B) [72–75]. This leads to unwanted classification and an inhomogeneous filter cake. In terms of process technology, the reaction can be an increased inflow velocity over the filter surface [53]. This process becomes clear through an increase in the y-abscissa, i.e. initial resistance, because of the particle cover layer present at the beginning. If particle sedimentation is excluded as the cause by knowing the particle size distribution, this can also be a consequence of the particle occupancy in the meshes (interference resistance).

Particularly strong manifestations of this behaviour are represented by D, E and F. Due to the segregation of the coarse material and the associated sedimentation of the coarse material, the cake structure is inhomogeneous and leads to a decrease in the growth rate (D). This becomes clear through the decrease in the gradient. This can be observed in coarser particle systems with a low proportion of fines, where strong sedimentation is to be expected. As a rule, it is also accompanied by an increase in the y-abscissa. In the case of a broader particle size distribution with a significant proportion of fines, this process is more pronounced (E). Here, sedimentation of the coarse material takes place and the cake is built up by the particles of the fine material fraction on and in the filter cake. A particularly pronounced case is shown in course F, the basis of which can be traced back, among other things, to a bimodal distribution with a clear difference in position of the modal values of the particle system to be filtered. In this specific case, the particles of the fine fraction are separated in the filter cake (depth filtration). This leads to the closing of the pores and to a disproportionate increase of the total resistance. In case of a strong deviation from the ideal course due to a convex measurement course, 2 possibilities can be reacted to during the evaluation:

- I. Evaluation based on depth filtration, which is becoming increasingly dominant,
or
- II. Consideration of the compressibility of the filter cake.

The evaluation by another filtration mechanism (I; See Appendix B. Hermans & Bredée – Derivation, page 70) such as intermediate, standard (depth) or clogging filtration can lead to the desired straight-line equation and allow the evaluation of the sought parameters. Experience shows that this can take place for the entire filtrate volume or sequentially if several mechanisms take place and dominate at different times during the same filtration. It is also conceivable that a compressible particle structure is present (II). In this case, too, the course F can be observed and is a consequence of the decreasing pore size distribution/porosity due to the solid structure pressure on the filter cake. This relationship is illustrated in Figure 6 and can have several causes for the compressible behaviour:

- Rearrangement of particles [76],
- Physio-chemical interactions between fine particles [77–80],
- Deformations of particles [81–84],
- Particle fracture [85].

While the porosity ε and the specific cake resistance α_{FC} are constant for incompressible cakes, the porosity decreases, and the specific cake resistance increases towards the filter fabric for compressible cakes. This is a direct consequence of the increasing solid structure pressure p_s compared to the liquid pressure p_L . The description of this relationship is described phenomenologically in some publications [86,87]. Especially simple power approaches as in Eq. 9 have prevailed here [86,88,89].

$$\frac{1-\varepsilon}{1-\varepsilon_0} = \frac{\alpha_{FC}}{\alpha_{FC,0}} = \left(\frac{\Delta p}{\Delta p_0}\right)^n \quad \text{Eq. 9}$$

By adapting the compression exponent n , the influence on porosity and specific cake resistance can be easily expressed by means of a constant and used to assess the material behaviour [80].

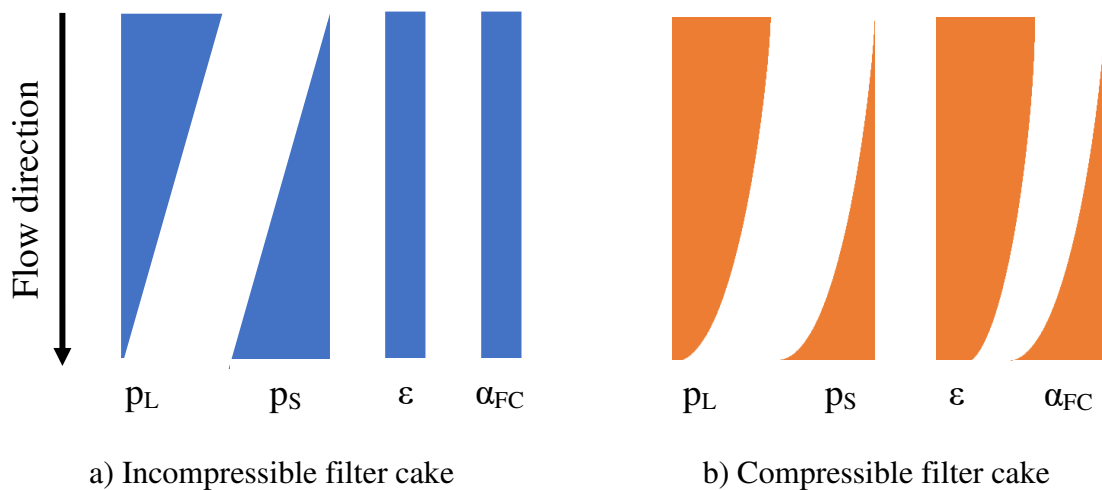


Figure 6: Course of the liquid pressure p_L , solid structure pressure p_s , the porosity ε , as well as the specific cake resistance α_{FC} for an incompressible (a) and a compressible filter cake (b) according to [87].

The last curve shown in Figure 5 is C, which represents a smaller abscissa value. One reason for this behaviour is floating particles because of hydrophilic particles or an unintentional, too many particle penetration at the beginning of filtration. This results in a lower initial resistance and can lead to a negative value in extreme cases. This is to be interpreted as unphysical, as it leads to a negative filter mean resistance. In real terms, therefore, there is an initial flow according to Darcy until a filter cake builds up.

In summary, the particle system affects filtration and knowledge of the material behaviour must be considered in the filtration behaviour.

The deviations from the material behaviour described in the previous sections are due to the separation behaviour of the particles. However, the existing flow also influences the flow

behaviour, as considered in the Darcy-Forchheimer equation. For homogeneously flowing filter cakes with Reynolds numbers < 1 , turbulent flow increasingly takes place. This is to be expected especially in gas filtration and liquid filtration with high flow velocity and must be considered by means of the turbulence term when calculating the pressure loss ($\Delta p \propto \dot{V}_F^2$). In addition to gas filtration, this turbulent particle flow also finds technical application in the fluidised bed and pneumatic conveying of particle flows [90,91]

Another influencing factor is the cracking of the filter cake [76,92]. This clearly shows that the design of filters must be considered. This also includes operations after the filtration process, such as drying and regeneration, which are described in the following subchapter.

2.4. Regeneration of technical surfaces - adhesive forces

The regeneration of technical surfaces has been the focus of scientific research for quite some time and thus follows the trend to safely design and clean production-relevant and product-contacting plant components [93–96]. This resource-saving way of thinking is very much in the focus of "sustainability" campaigns of large industrial representatives of the respective industry and, apart from image cultivation, also offers process-technical advantages for the improvement of existing plants. For this purpose, cleaning concepts from a wide variety of industries are used and transferred to the respective cleaning task. The food and pharmaceutical industries are particularly well represented here, as in both cases cross-contamination has strong effects up to the point of consumption [97–99].

Filter fabrics are a particularly difficult surface to clean, as the periodic sequence of warp and weft threads leads to a surface with many clearance volumes. The question of cleaning is therefore an essential aspect for the stable operation shown in Figure 1. Ensuring this requires knowledge of the forces acting on the contamination to be cleaned and the contaminated technical surface. This was done, for example, by [100] for experiments on the detachment behaviour of filter fabrics. For an effective detachment of the filter cake, the detachment force $F_{\text{Detachment}}$ must exceed that of the adhesion force F_{Adhesion} , so that a removal of the cake occurs. If the internal strength, called cohesion F_{Cohesion} , in the contaminant is greater than that of the detachment force, the removal of the contaminant takes place in a coherent particle fragment. This is preferable in the case of filtration and is shown in an inequality in Eq. 10 [101,102].

$$F_{\text{Cohesion}} > F_{\text{Detachment}} > F_{\text{Adhesion}} \quad \text{Eq. 10}$$

Process engineering itself knows a variety of adhesion mechanisms, some of which are desirable, but also undesirable. Examples of desired adhesion are particle/particle adhesion in the production of agglomerates (built-up and pressed agglomerates) or the powder coating of

surfaces (coating). Transferred to an application in solid-liquid separation, flocculation within liquids to improve sedimentation and filtration properties is an essential process in which adhesive forces play an important role in improving separation properties. Nevertheless, there are also processes in which strongly acting adhesive forces lead to negative product properties. Examples here are the formation of lumps in fine, very cohesive powders, for example in pharmaceutical technology, which can contribute to segregation. Another problem is the adhesion of powders in containers, which, if insufficiently cleaned, is contrary to the FIFO concept (First In - First Out) from food technology and can lead to cross-contamination in batch operation [103]. Here, adhesive forces must be reduced and cleaning intensified.

These examples clearly show that knowledge of the acting adhesive forces contributes significantly to the improvement of the process [104]. This applies not only to the actual process (filtration) but also to subsequent process steps (cleaning/regeneration) and requires knowledge of the acting adhesive forces and the ability to describe their characteristics. A possible categorisation was made by differentiating between 4 groups based on their effective adhesion mechanisms [105,106]:

- Solid state bridges,
 - Sintered bridges
 - Crystallisation
- Liquid bridge forces,
 - Liquid bridges
 - Adsorption layers
- Attractive forces,
 - Van der Waals forces
 - Electrical conductors
 - Electrical insulator
 - Electrostatic forces
- Form-fitting bonds.

Due to the scope of this topic, the adhesive forces of the liquid bridges and the Van der Waals forces relevant to this work will be discussed [107–109].

2.4.1. Fluid bridge forces

Fluid bridges and their forces are the result of fluids, predominantly low viscosity, between two and more particles. These form edge forces F_{Boarder} , which act as the sum of the surface tension in the fluid $F_{\text{Surface}} = \gamma \cdot U \cdot \cos(\alpha)$ and the capillary force inside the fluid bridge $F_{\text{Capillary}} = p_C \cdot A$. If a boundary angle α below 90° occurs, there is a concave bridge surface, assuming an ideal circular meniscus, and a negative pressure and thus an attraction of the interacting particles in the aggregate. The determined bridge contour was first described by the so-called Young-Laplace equation, which is also the basis of porometry [110]. A physically based calculation of the acting adhesive forces within a particle collective is the content of many publications and was first carried out by the diagram of Schuber and Rumpf, who defined the relationship

between liquid saturation in the material and the tensile strength [105,111]. The tensile strength within the particle structure σ_z can be calculated via the formula defined in Eq. 11 and is generally calculated from the porosity in the material ε , the acting adhesive force F_{Adhesion} and the representative particle size x in the particle aggregate.

$$\sigma_z = (1 - \varepsilon) \cdot \varepsilon^{-1} \cdot F_{\text{Adhesion}} \cdot x^{-2} \quad \text{Eq. 11}$$

According to [61], the calculation of the tensile strength within a fluid-filled structure is dependent on the saturation, the proportion of fluid V_L in the void volume of the structure V_H , with a range of values $S = V_L/V_H$ from 0 to 1. The transferable tensile strength can be divided into three ranges of dominant mechanisms of action [106]:

- Capillary area (S ~ 0.8 ... 1.0),
- Transition area (S ~ 0.3 ... 0.8),
- Liquid bridge area (S ~ 0 ... 0.3).

In the capillary region, at a saturation of 1 to 0.8, the aggregate is almost saturated with liquid. Here, the very strong capillary pressure bonds dominate and the transferable tensile strength in the structure can be calculated as the product of the saturation and the capillary pressure p_c . As saturation decreases, for example due to mechanical drying or thermal drying, the material passes through a transition area where the superposition of capillary and liquid bridging forces defines the transferable tensile strength in the material. This is related to the random distribution of pore sizes in real packings [111], and leads to the well-known hysteresis behaviour during wetting and drying and cracking in the structure as a result of the tensile stress gradient due to saturation differences [92]. At saturations below 0.3, liquid bridges dominate, and the transferable tensile strength depends, among other things, proportionally on the surface tension γ (Proportionality: $\sigma_z \propto (1 - \varepsilon) \cdot \varepsilon^{-1} \cdot \gamma \cdot x^{-1}$).

At saturations below 0, liquid bridges are no longer present and the strength in the particle structure is only dependent on interparticle adhesive forces and solid bridges crystallised out of the liquid. The latter form the largest acting adhesive forces. However, such low saturations can only be achieved by thermal drying, since the capillary and bridge fluids can be mechanically drained (open pores), but the adhesive and internal fluids can only be removed thermally (blind and closed pores) [38,112,113]. The mechanical drying of filter cakes is described in VDI 2762 - 3. This standard also contains an empirical model for describing the drying time for idealised, homogeneous cake structures with uniform mechanical drying. This is shown in Eq. 12 and depends on further variables such as drying pressure and particle size/shape [114]. The saturation S can be estimated with the equilibrium saturation S_∞ and the drying constants a and b ($a = 0.3 \pm 3.0$; $b = 2.0 \pm 0.5$). However, the experiment to determine the actual saturation is

still necessary and, in addition to the drying kinetics, also provides conclusions about the process of shrinkage and the phenomenon of cracking. Shrinkage can be divided into 3 areas, analogous to tensile strength, and is most pronounced in the capillary area and virtually non-existent in the bridge area [115].

$$\frac{(S - S_{\infty})}{(1 - S_{\infty})} = \left(1 + a \cdot \frac{\Delta p - p_D}{\alpha_{FC} \cdot \varepsilon \cdot \eta_f \cdot H_{FC}} \cdot t \right)^{-b} \quad \text{Eq. 12}$$

At saturations above 1, the transition to suspension is given, as there is more liquid volume than void volume. By definition, a suspension is then present that cannot transmit any tensile force, provided the surrounding fluid exhibits Newtonian fluid behaviour. The liquid bridge bonds are, besides the solid body bridges, among the strongest acting adhesive forces and are greater by up to 2 powers of ten than the Van der Waals forces described below. [106]

2.4.2. Van der Waals force

In addition to the liquid bridges, the Van der Waals forces also act, although to a minor degree. The forces act without contact because of interactions at the molecular level. For this reason, a physically based calculation is only possible through a model description. This was done for the first time by Hamaker (1937) by describing the interaction between two spheres of different diameters [116]. The basis of his derivation is the interaction between dispersive energies U of atoms and molecules as a function of distance z and particle radius r_1 and r_2 published by London in 1937 [117]. In connection with the differential consideration $F_{vdW} = -d/dz U(z)$, a transfer to different geometries takes place along the lines of [118]. This resulted in the formula in Eq. 13 [116]. In the case of two spheres with identical radius $r = r_1 = r_2$ Eq. 13 simplifies to $F_{vdW} = [H / (12 \cdot z^2)] \cdot r$.

$$\text{Sphere/Sphere: } F_{vdW} = \frac{H}{6 \cdot z^2} \cdot r_1 \cdot r_2 \cdot \left(\frac{1}{r_1 + r_2} \right) \quad \text{Eq. 13}$$

In these equations, H stands for the Hamaker constant, which can be determined experimentally and depends on the materials, and thus the molecular density and polarisability, of the contact partners. Various calculation possibilities of mixed materials and prediction models for this constant have already been published and show the important position of this adhesive force model [119–121]. At the present time, this constant can be taken from table books. An overview of important Hamaker constants in vacuum and in water are shown in Table 1. Here it becomes clear that the Hamaker constant is strongly dependent on the surrounding environment. The difference between liquid and gas phases is particularly strong and can lead to a significant increase in the Hamaker constant [122]. An interesting subdivision is made according to [123]

on the basis of substance groups. Here, the following order of magnitude applies to pure substances:

- $(20 - 45) \cdot 10^{-20}$ J: Metals and carbons,
- $(5 - 20) \cdot 10^{-20}$ J: Oxides und silicates,
- $(5 - 15) \cdot 10^{-20}$ J: Salts,
- $(3 - 8) \cdot 10^{-20}$ J: Polymers,
- $(4 - 7) \cdot 10^{-20}$: Solvents.

The variables r_1 and r_2 are the radii of the interacting spheres and the sphere, respectively, and z is the distance between the contact partners. This is often given in Ångström and must be in the range of 0.4 to 50 nm for the adhesive force model to be valid.

Table 1: Overview of the Hamaker constants in vacuum and water of selected materials [122].

Material	H in vacuum in 10^{-20} J	H in water in 10^{-20} J
Limestone	15	3.8
Quartz	6.5	0.83
Rutile (TiO ₂)	43	26
Alumina (α -Al ₂ O ₃)	14	5.3 – 6.7
Hydrocarbon	5 – 7	0.3 – 0.9
Polyvinyl chloride (PVC)	7.8	0.76
PTFE	3.8	0.33
Si ₃ N ₄	-	4.8 – 5.9
Silicone	-	9.75

This model for describing the interaction of two "ideally smooth spheres" can also be transferred to other geometries [118]. This was done for the contact pairing plate / sphere (Eq. 14) and plate / plate (Eq. 15; With the present contact area A_{Contact}) for ideally smooth surfaces. The former case can also be considered as a sphere/sphere model with a clear difference in size between the two sphere radii $r_1 \ll r_2$. In this case, only one radius must be taken into account when considering the distance of the interacting atoms/molecules. As a result, Eq. 13 changes into Eq. 14 and the latter is larger by a factor of 2. In the case of interaction of two plane plates, the contact area is not affected by curvature. This leads to a constant distance in each spatial plane and the surface energy U is consequently inversely proportional to the distance z^2 . Integrated, this leads to the adhesive force shown in Eq. 15.

Comparing the equations, it is noticeable that the adhesive force between two identical spheres can only be 50% of the adhesive force between a plate and sphere, with the same Hamaker constant.

$$\text{Plate/Sphere: } F_{\text{vdW}} = \frac{H}{6 \cdot z^2} \cdot r \quad \text{Eq. 14}$$

$$\text{Plate/Plate: } F_{\text{vdW}} = \frac{H}{6 \cdot z^3} \cdot A_{\text{Contact}} \quad \text{Eq. 15}$$

Due to the assumption of an ideally smooth sphere, deviations from the real measured adhesive forces, e.g. determined with an atomic force microscope (AFM), can be observed at Eq. 13 to Eq. 15 [124,125]. As a rule, the measured adhesive forces are less pronounced than those calculated based on ideal contact partners [126]. Based on this observation, the sphere/plate model was extended to include a roughness measurement in the form of a semicircle on the surface of the sphere or plate. This hemisphere symbolises a roughness peak of defined height and increases the distance between the contact partners. The adjusted formula is shown in Eq. 16 and Eq. 17.

$$\text{rough Sphere/Plate: } F_{\text{vdW}} = \frac{H}{6} \cdot \left(\frac{r_2}{z^2} + \frac{r_1}{(z+r_2)^2} \right) \quad \text{Eq. 16}$$

$$\text{rough Plate/Sphere: } F_{\text{vdW}} = \frac{H}{6 \cdot z^2} \cdot \left(\frac{r_1 \cdot r_2}{r_1 + r_2} + \frac{r_1}{\left(1 + \frac{r_2}{z}\right)^2} \right) \quad \text{Eq. 17}$$

A detailed examination of these equations shows that they are composed of two summands. This becomes clear at Eq. 16, where the larger sphere with the radius r_1 and the distance of $z + r_2$ interacts with the ideally smooth plate. In addition, another interaction between the hemisphere with radius r_2 , which represents the roughness, and the ideally smooth plate is considered. For roughness elevations $> 0.01 \mu\text{m}$ (roughness elevation in the atomic range), the equation leads to a significant reduction of the interactions compared to the ideally smooth sphere/plate and a global adhesion force minimum at surface roughnesses of approx. 0.01 to $0.1 \mu\text{m}$. This model is valid for roughness elevations $r_2 \leq r_1$. For $r_2 > r_1$, the rough sphere / smooth plate model leads to an overestimation of the adhesive force compared to the ideal model.

The rough plate / smooth plate model (Eq. 17) can be understood as the interaction of a small sphere with a larger sphere and an ideally smooth plate with the larger sphere. This is also how both summands of this equation are composed. This model also provides similar results for roughness elevations $> 0.01 \mu\text{m}$. In contrast to the model from Eq. 16, however, it transitions continuously to Eq. 14 for $r_2 \rightarrow \infty$. An overestimation of the adhesive force as for Eq. 16 does not take place.

A further development of the idea of expressing the roughness survey by an idealised hemisphere took place by Rabinovich et al. (2000). The idea behind this model was to characterise the roughness of the plate by a technically measurable parameter. For this purpose, the definition of the averaged roughness R_q was based on DIN EN ISO 25178. The roughness

R_q enters into a semi-empirical equation that represents the measured adhesive force on an idealised sphere (see Eq. 18). This is a modification of Eq. 17, in which r_1 corresponds to the ideally smooth sphere r , and the roughness survey r_2 is expressed by $1.48 \cdot R_q$. The factor 1.48 is to be understood as an empirical value. With this equation, the adhesive force can be determined based on real surface roughness. It is valid for surfaces with low roughness and high periodicity of the greatest roughness. This contrasts with filter fabrics, which have a low periodicity, alternation of warp raising and lowering, with high roughness elevation. [127]

$$F_{vdW} = \frac{H \cdot r}{6 \cdot z^2} \cdot \left(\frac{1}{1 + \frac{r}{1.48 \cdot R_q}} + \frac{1}{1 + (1.48 \cdot R_q \cdot \frac{1}{z})^2} \right) \quad \text{Eq. 18}$$

Shortcomings of these models can be found in their technical transferability. In real processes, there are usually not single particles but whole particle collectives with multiple contact possibilities. This is not considered by the single particle forces. Considerations of integral measurement methods have been carried out [128–130], The respective transferability to a concrete process engineering application area is necessary [131]. At present, the calculation of adhesive forces by DEM simulations in particle structures is increasingly taking place to simulate process engineering processes such as the mixing of particle collectives and the formation of filter cake structures [132,133]. But also dynamic simulation based on laboratory tests of cake behaviour is also gaining in importance [134]. This also applies to the deposition of particles on filter cloth [66,69] and enables the determination of the adhesive force in a particle collective based on adhesive force measurements on the individual particle. However, measurements of the adhesive forces in the particle collective are also becoming the focus of current research [135].

2.5. Cleaning/regeneration in process engineering - state of the art

The cleaning or regeneration of surfaces takes on an essential role in process engineering. In addition to the obvious process of spoilage in food processing technology due to rotting processes, the chemical, mechanical, pharmaceutical and thermal process technology sectors are also affected by the pressure to improve the cleaning process. The reasons here are the reduction of batch carry-over and the guarantee of stable process conditions. According to [136], successful cleaning is characterised by the following two features:

- I. The surface does not impair subsequent process steps (in terms of time, location) and
- II. the reliability of the product is ensured.

The definition of cleaning on the basis of these two characteristics takes into account process-related (I) and product-specific (II) characteristics to characterise cleaning and aims at a safe/stable process and a durable product [137]. A direct distinction regarding the optically/sensorically detectable, permanent detachment of adhering materials is made according to [138]. In this general distinction, the predicate "clean surface" is given when non-defined substances are successfully detached from a surface. While [136] focuses on consequences for the process and the product, [138] provides a direct description of the surface by imaging methods and is further refined by [139] into "physical" and "chemical" clean. The former distinction considers optically perceptible impurities, while the latter refers to chemically/analytically detectable impurities and is thus of particular importance for the food and pharmaceutical industries, in the form of detection methods (e.g. VDMA leaflet Riboflavin test) [140–142].

While the above-mentioned sources are mainly concerned with the description of the cleaning result, cleaning is classified by Sinner's circle on the basis of the factors chemistry, mechanics, time and temperature. Various further developments of this model have expanded the process variables to include the plant periphery and process controlling (extended Sinner's circle), as well as the cleaning sequence, cleaning programmes and cleaning possibilities of the CIP procedure (3D Sinner's circle) [143]. The interaction of "description of the surface" and "categorisation of the cleaning procedure" should result in a definition of the cleaning quality that is as precise as possible.

Transferred to technical applications, the cleaning of pipelines and heat exchangers from (bio-)fouling [144], the clogging of bubble-cap internals in (rectification) columns [145] and fermentation cloths in food technology [146] can be mentioned as examples. The fouling present there can be divided into three categories [120]:

- Particulate contamination: particles that cannot be further dissolved, of defined and stable shape,
- Cohesive contaminant films: area-like contamination that separates from the surrounding, continuous phase,
- (Chemical) Soluble dirt films/particles: area-like contamination that can be decomposed by chemical/thermal action.

According to [147], the item "(Chemically) soluble contaminant films/particles" is described in more detail. This is expanded by differentiating between "water-soluble contamination", "swelling contamination" and "emulsifiable contamination" (e.g. lipoids). The technical relevance in this paper lies in the particulate impurities, which interact with each other in the form of a filter cake. Depending on the contamination present, hydraulic (continuous/pulsative flow), mechanical (scraper; sonic) or diffusive (dissolution) mechanisms may dominate for cleaning. Consequently, a precise knowledge of the type and extent of adhesion is required to ensure effective cleaning.

While the type is defined by the three categories according to [120], the determination of the characteristic is done by the adhesive forces defined in chapter 2.4. and the corresponding formulae. A distinction is made between adhesion and cohesion as the sum parameter of the effective adhesive forces. While adhesion is to be understood as the acting force between the soiling and the surface, i.e. mostly heterogeneous contact partners, cohesion is the adhesion within the soiling, which is to be understood as a homogeneous contact partner. For effective cleaning, the Eq. 10 defined on page 18 applies, which states that for complete detachment of the soiling, the cohesive force must be greater than the detachment force. In addition, the detachment force must exceed the adhesion force [100]. Removal of the contamination also applies if the detachment force exceeds that of the cohesion. For this reason, the focus of a large number of studies on release behaviour is on adhesion as the determining force [109,148–150]. The forces of adhesion and cohesion are schematically illustrated in Figure 7.

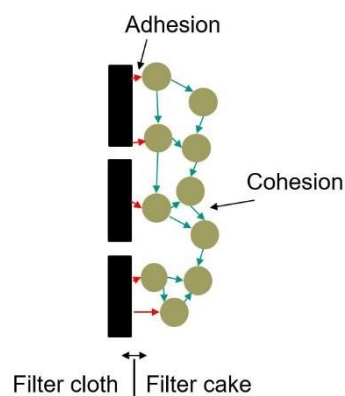


Figure 7: Schematic representation of adhesion and cohesion within a particle structure.

Transferred to applications in process engineering, the focus is particularly on technical surfaces and the impairment of the intended purpose through the adhesion of contaminants to them. Selected examples are discussed in the following:

- A. In the case of heat exchangers, adhesions are caused by biofilms (dairy industry), crystals/encrustations (pharmaceutical industry), mussel infestation (energy industry). A detailed overview of the affected industries is listed in [144]. The technical relevance is made clear by the fact that the VDI Heat Atlas provides tabulated correction values for the heat transfer coefficient in these processes.
- B. In the food industry, adhering microorganisms are of particular importance. In this case, not only is the process impaired, but there is also a direct impact on the taste, shelf life and compatibility of the food produced. For this reason, cleaning/ construction/ evaluation regulations have become established. Of importance are the Cleaning-in-Place (CIP) and Sterilisation-in-Place (SIP) processes to remove contamination between batches. This goes hand in hand with a design requirement such as 'maximising minimised dead space' to prevent contamination within an apparatus. The European Hygienic Engineering & Design Group (EHEDG) method has become established for demonstrating cleaning [151–155]. A very good overview of the topic "cleaning" and "fouling" can be found in [151].
- C. In the context of this thesis, filtration, as a sub-discipline of mechanical process engineering and a separation principle in many of the above-mentioned branches of industry, is of particular importance. Here, too, the trend in recent years has been towards effective cleaning of the filter fabrics [156,157]. As a difference to the other examples of build-up mentioned, the remaining of particles on the filter fabric is desired for the time being, especially if it is the value product, and even necessary for effective separation. Remaining filter cake after cake discharge is undesirable and can be divided into two groups [4,158]:
 - Intra-cloth contamination - particles remaining in the tissue meshes,
 - Surface contamination - filter cake remaining on the fabric surface.

This residual filter cake when discharged on the surface and within the fabric leads to degradation of process performance. As can be seen from the Darcy equation (Eq. 1, page 8), the volume flow and the filter area are linearly proportional to $\dot{V}_F \propto A$. If the surface area is doubled, the volume flow is also twice as large for the same pressure loss Δp . If the surface is now occupied, this reduces the volume flow by the amount of the occupied surface. In the filtration cycle, this area is of increased flow resistance, analogous to the parallel circuit in electrical engineering, and influences the cake formation. Inhomogeneous cake formation can be the result, which in turn affects the cake discharge.

A complete cake discharge is therefore desired. In Figure 8a, occupied filter cake areas for inhomogeneous cake formation and their fluidic consequences are shown schematically. The total pressure drop Δp_{tot} can then be calculated as the reciprocal of the sum of the reciprocals of the partial pressure drops Δp_i , analogous to the parallel connection in electrical engineering. Areas with a smaller cake have a lower pressure drop and are preferentially flowed through. Here the partial volume flow \dot{V}_i of the segment increases. The low pressure drop of these partial segments corresponds to a correspondingly low partial resistance R_i and leads to the analogous relationship of the total resistance R_{tot} to the partial resistances R_i as the total pressure drop Δp_{tot} to the partial pressure drop Δp_i (see Figure 8b). In terms of process technology, this becomes clear through a lower initial volume flow due to the greater resistance when filter cake fragments remain and more frequent regeneration cycles (Figure 1, page 2).

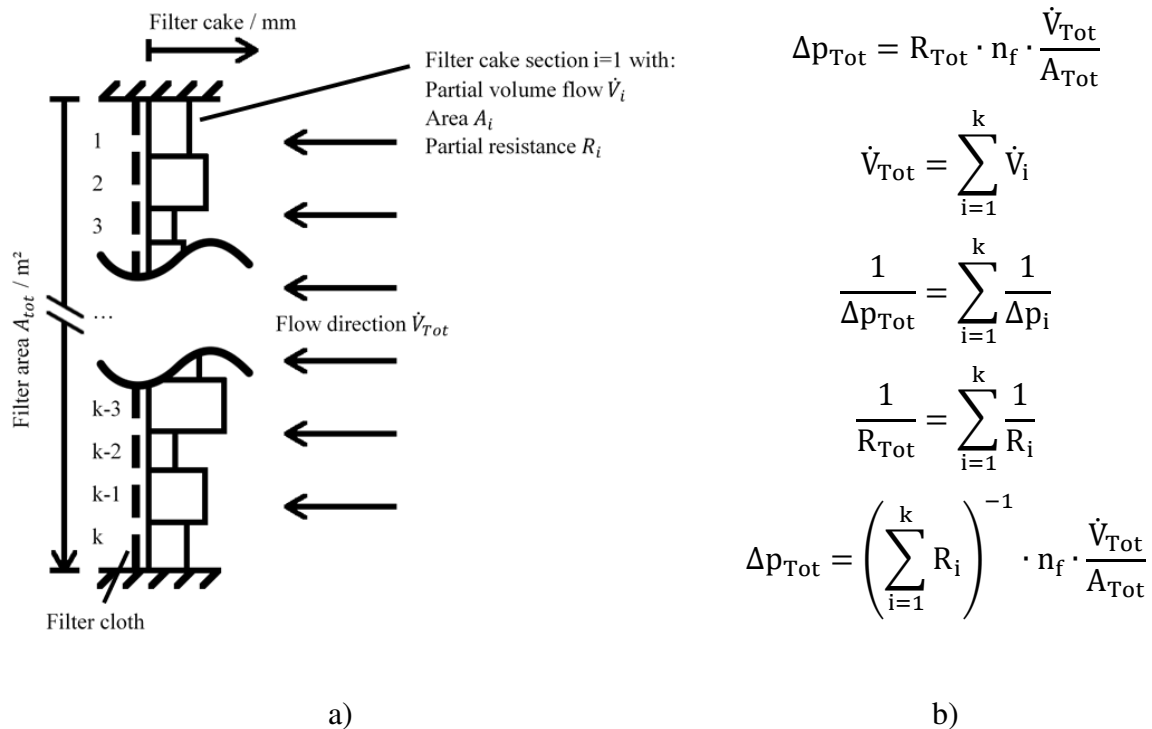


Figure 8: Exemplary occupation of the surface by remaining particle adhesion (a) and its mathematical effect on the filter performance (b)

To avoid inhomogeneous cake build-up and high initial volume flows, but also batch carry-over in sensitive process engineering processes, various cleaning concepts for cake discharge have been developed. A schematic representation of cleaning concepts is shown in [159]. These can be divided into the following groups according to their focus:

- I. Reduction of the adhesive force,
- II. Benefit of the earth's gravity,
- III. Vibration input,
- IV. Mechanical removal,
- V. Nozzle cleaning.

In I. Reduction of the adhesion force, cake release should be achieved by intelligent fabric selection [160]. The aim is to reduce the adhesion force between the particle layer close to the fabric and the fabric itself. [128] provides a measurement method based on the Jenicke shear cell to determine the adhesion force between filter cake and tissue. Based on the considerations in I. Reduction of the adhesive force, the selection of the appropriate filter fabric has a significant influence on cake detachment [100]. In II. Benefit of earth gravity, the effect of the weight force of the cake to e.g. swing the filter element is improved and is often combined with I. [161–165]. The case III. vibration/force application follows the consideration that the filter cake is partially loosened by the vibration/shock and leads to an integral detachment of the entire cake [166,167]. This is illustrated in IV. Mechanical removal by mechanical devices such as scrapers, which is associated with greater death times [168–170]. The use of nozzles to clean the tissue surface is also common practice and is often done by hand [171]. Figure 9 illustrates the cleaning concepts as schematic diagrams.

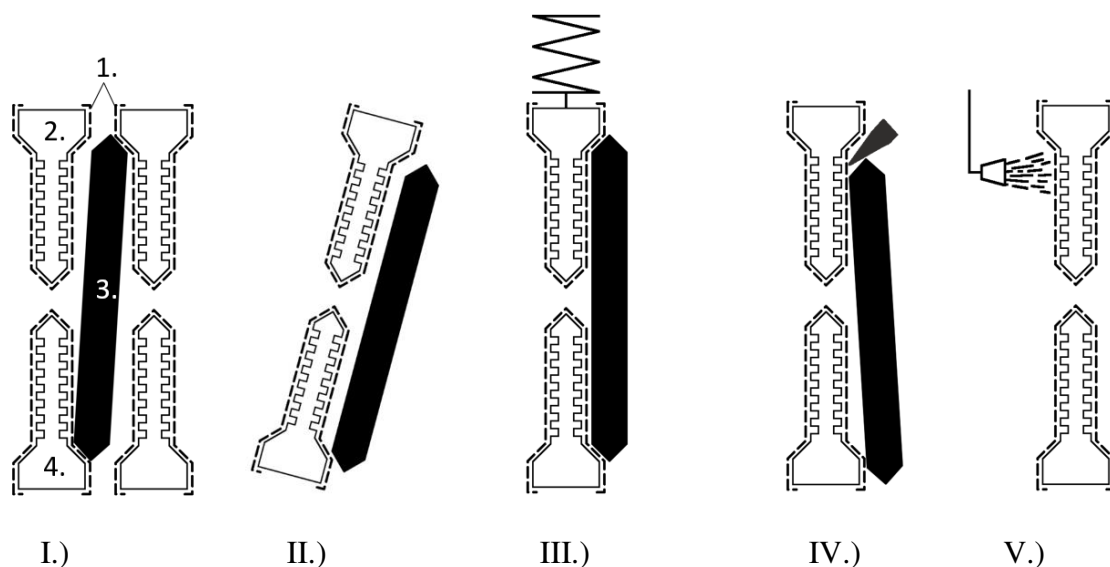


Figure 9: Schematic representation of cleaning concepts for filter cloth (1) on a chamber filter element (2, 4). Shown are detachment mechanisms of the cake (3) by fabric selection (I.), tilting of the filter elements (II.), a vibration device (III.), a mechanical scraper (IV.) and a cleaning nozzle (V.). Illustration inspired by [159].

In summary, it can be said that cleaning depends on the environment, the contamination and the industry. While the food and pharmaceutical industries have very high purity requirements, this is less the case in the metal industry. Transferred to filtration, which is used in a wide range of industries, cake discharge is necessary to reduce flow loss and ensure stable process control. For this reason, this thesis deals with cake discharge with and without aids. Subsequent cleaning steps for removing contamination within the fabric meshes (intra-fabric cleaning) are conceivable and must be compared with the present cleanliness requirement [172,173].

Chapter 3

3. Experimental methods and equipment

The following subchapters describe the parameters and test facilities used to evaluate the cleaning. These are presented in general terms. For a more detailed description, please refer to the respective publication [1–6] starting on page 73. The presented chapters cover the essential point of image evaluation in the characterisation of the surface, followed by important measurement equipment with indirect (pressurised filter cell, laser scanning microscopes) and direct influence (backwashing filter, chamber filter) on the measurement results.

3.1. Characterisation of the surface contamination

The content of this thesis is the cleaning of technical surfaces (filter fabrics) by removing particle accumulations on the fabric after filtration. Previous studies have addressed the removal of soluble/insoluble individual particles and biofilms [120,158,172,173]. While indirect measurement methods such as the heat transfer coefficient can be used for biofilm/fouling, for example heat exchangers in the dairy industry [144], imaging and gravimetric methods provide direct conclusions about physically remaining residual impurities. The underlying formula is always the same and must be adapted to the system under investigation (see Eq. 19).

$$\text{Surface contamination (x)} = \frac{\text{Contaminated area at characteristic } x \geq x_0}{\text{Contaminated area at the starting characteristic } x_0} \quad \text{Eq. 19}$$

The quality of the cleaning depends on the determined surface coverage for the process characteristic x and is related to the surface coverage at the starting point x_0 of the measurement. The residual contamination is thus in a definition range of 0 to 1, where 0 defines a clean surface and 1 the occupancy at the start of the process. Also common is the inverse description from 0 to 1, where 0 equates to the start of cleaning and 1 to complete removal of the observed surface occupation [147,174]. The content is always the same and describes the course of the cleaning. This also applies to deviating descriptions of the residual contamination by imaging methods such as cleaning degree [147], dirt index DI [146], regeneration efficiency [101], or even the surface contamination [1-2], discharged mass fraction [4] or standardized degree of contamination [5, 6].

In combination with a process characteristic x to be evaluated, such as the cleaning time or the cleaning agent used, in combination with the quantification of the surface, thus enables the definition of a cleaning kinetics and the quantitative evaluation of the cleaning. This allows the

comparison of the most diverse cleaning scenarios of fabric-particle combinations in backwashing filtration [1,2,4] and fabric-particle-nozzle combinations in the case of chamber filter cleaning [5,6]. Transferred to the evaluation of filter cake discharge, two process variables are decisive in the evaluation of regeneration:

- Time,
- Specific backwashing volume.

These are synchronised with the surface quality as part of the investigation and then illustrated. This allows the discharge to be transferred into a temporal context and, by means of volumetric measurement, the cleaning agent consumption to be discussed. Figure 10 shows an example of the image evaluation of the surface coverage, starting with the original image (a), the area adjustment (b) and the binary image (c). It is particularly important for imaging procedures to cover the occupied surface as completely as possible during image evaluation. While an erroneously too large determination of the occupied area would lead to a worse evaluation of the cleaning (false positive finding), a too low detection (false negative finding) is to be interpreted as a better cleaning than present. The latter is to be defined as a greater error with a view to correct validation.

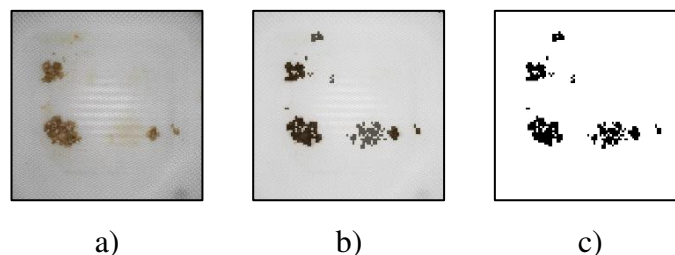


Figure 10: Exemplary representation based on the image evaluation presented in [1,5]. The original image (a), the area adjustment (b) and the binary image (c) are shown. The exact description of the respective procedure is documented in [1,5] (see Appendix E, page 73, and Appendix J, page 116).

While imaging has proven to be the first choice for evaluating cleaning processes in and through liquid phase, indirect and gravimetric measurement methods are the preferred means of evaluation for cake removal in and through the gas phase [4]. For this case, the pressure loss of the medium during gas filtration and/or the weight increase of the filter fabric has proven to be a suitable quantification characteristic. Transferred to the framework condition in this thesis, the discharged cake fragments are evaluated gravimetrically. The reason for this is the faster process compared to the liquid discharge, which makes image evaluation more difficult. For the transfer, Eq. 19 is adapted accordingly and the surface occupancy is defined by the “discharged mass fraction” and remaining mass on the filter cloth. The total mass is to be understood as the sum of both. The exact description is described based on backwash filtration in subchapter 3.4. Backwashing filter and [4].

3.2. Pressurised filter cell

The pressurised filter cell according to VDI guideline 2762-2 is the standard measuring equipment for determining the specific cake resistance α_{FC} and the fabric resistance R_{FM} in the case of cake-forming filtration (see Figure 11) [175]. Furthermore, the measurement enables the determination of the dominant separation mechanisms according to Hermann and Bredée (see chapter 2.1 Basics of filtration and Appendix B, page 70). Based on this measurement principle, many publications have been made with reference to filter cake structure [77,175] and tissue interactions [38,40,44,176,177] during filtration, as well as dehumidification processes during drying of the filter cake [178,179]. The determined quantities can be used directly for the design of filter apparatus. The measurement procedure follows the following schedule:

- I. Selection of the tissue-particle combination,
- II. A) Preparation of the suspension,
B) Installation of the filter fabric,
- III. Adjusting the filtration pressure,
- IV. Feeding the suspension into the filling tube,
- V. Start filtration; measure filtrate volume over time.

After selecting the tissue and particle system to be tested, the suspension is prepared. For a realistic representation of the filtration, it is important to ensure that the suspension concentration in the laboratory test corresponds to that of the pilot plant. There is a direct correlation between cake build-up and turbidity in the filtrate as a function of the suspension concentration [180]. As a rule of thumb, it should be noted that smaller suspension concentrations lead to longer turbidity. The reason for this is the influence of bridge formation described in the chapter 2. The suspension is fed into the filling pipe (1) and the filter flange (2) of the pressure nutsch and filtered through the filter cloth (3) by means of a pressure gradient. There, the particle system is separated from the liquid phase and the filtrate flowing through passes the support fabric and the funnel before it is recorded gravimetrically. The determined filtrate-time curve is transferred to a $t/V_F - V_F$ -diagram according to appendix C (page 71) to determine the specific cake resistance and the fabric resistance.

The flow of the support structure (4) and the funnel (5; representative of the following system parts) must be designed in such a way that they have a significantly lower flow resistance. This also applies to the flow of the filtrate stream. Here, it must be avoided that it flows as a direct jet orthogonally onto the gravimetric measuring device. The generated impulse falsifies the fabric resistance. [40]

The specific cake and fabric resistances used in this study, as well as the definition of the dominant separation mechanisms, were determined with this measuring device.

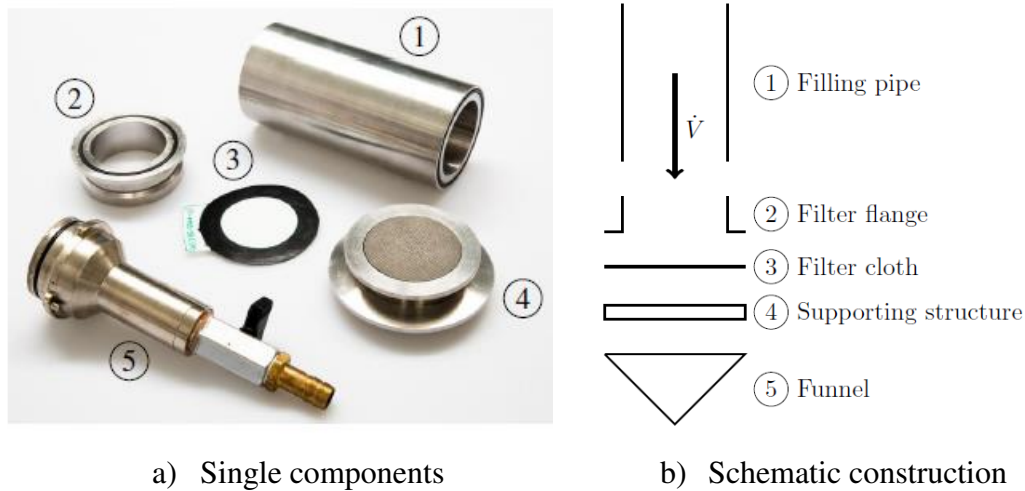


Figure 11: Representation of the individual parts of the pressurised filter cell according to VDI guideline 2762-2 (a) and schematic representation of the construction (b).

3.3. Laser Scanning Microscope (LSM)

While the process-technical characterisation of the filtration is essentially carried out with the pressurised filter cell presented in chapter 3.2., the filter tissues used are categorised by imaging, using a laser scanning microscope (LSM) from Keyence. For this purpose, the tissues are fixed to a microscope slide and then visualised. The categorisation is essentially carried out according to the following criteria:

- I. Characterisation of the weave according to DIN ISO 9354,
- II. Measurement of the fabric resistance to VDI 2762-2,
- III. Definition of surface roughness according to ISO 25178,
- IV. Fabric thickness according to ISO 5084,
- V. Further specifications (specific weight, fibre thickness, mesh size, material).

The characterisation of the weave type according to DIN ISO 9354 is essentially based on 4 points and results in a numerical code, which draws conclusions about the weave type (10: plain weave; 20: twill weave; 30: satin weave), the number of warp lifts and lowerings, the number of threads that experience the same weaving procedure in parallel and the offset of the fibre until the weave pattern is repeated. The standard originates from the textile industry and allows even complicated descriptions of complex weave types. Transferred to a technical context, however, information such as mesh size, material and flow behaviour is missing. For this reason, the information was expanded to include the filter fabric resistance (see chapter 3.2.) and the surface roughness according to ISO 25178, as an important influencing factor in

adhesion, as well as manufacturer information on mesh size (porometry), material and fabric type. Here it has been shown that the description of the fabric type, especially for fabrics with a higher number of warps lifting and lowering, does not always have to correspond to that according to DIN ISO 9354. In addition to this information, there is also the specific weight of the fabric, the thread thickness of warp and weft fibre, as well as the fabric thickness. The table concludes with an LSM image, based on which four of the seven columns of the table are made (excluding the image column). The resulting overview is illustrated in the table header shown in Table 2.

Table 2: Table header for exemplary representation of the tissue data

Fabric type / mesh size in μm / material	Weave according to DIN ISO 9354	Filter cloth resistance according to VDI 2762-2 m^{-1}	Weight per unit area $\text{g} \cdot \text{m}^{-2}$	Surface roughness (ISO 25178) μm	Thread thickness warp/ weft μm	Fabric thickness (ISO 5084) μm	Image

The LSM was also used to characterise the particle systems (shape). For this purpose, the particle system was prepared on microscope slides. However, this measurement was supplemented with further particle characterisation procedures. These were partly carried out by external companies and can be summarised as follows:

- Particle size distribution by means of laser light diffraction by a measuring device from Helos Rodos,
- Material composition by means of chemical analysis, carried out by the company HPF minerals,
- Specific cake resistance according to VDI guideline 2762-2.

Due to the different particle systems used, reference is made at this point, analogous to the filter fabrics, to the respective publication.

3.4. Backwashing filter

One of the two experimental units for characterising the detachment behaviour of filter cakes is the laboratory-scale backwashing filter. This cake discharge is a discharge without aids. The essential parts of this system are shown in Figure 12. The following regeneration steps are possible with the help of this system:

- Filter cake discharge in liquid phase,
- Filter cake discharge in gas phase.

Each test procedure begins with the filtration of the particle suspension. For this purpose, the process chamber is filled with suspension until it flows over an overflow (I). The filtration pressure can be adjusted with the throttle valve installed there. Once the filtration pressure is reached, the filtrate line can be opened and allows the filter cake to build up. The test procedure calls for the filtrate to be recirculated at the beginning of filtration because of turbidity. The quality characteristic "turbidity" is also recorded and allows studies on particle retention and filtration performance. If the turbidity is at a stationary state, the minimum filtrate turbidity is reached with the tissue-particle combination present and the actual filtration begins. This is carried out until a defined amount of filtrate is reached and the suspension is replaced by clear water (II.a). Here, there is a direct correlation between filtrate volume V_F , particle concentration κ , filter area A and the filter cake thickness H_{FC} produced (Eq. 20). This allows the filter cake thickness to be controlled via the filtrate volume and leads to very reproducible filter cake thicknesses. After complete displacement of the suspension by clear water, the cake discharge can now be monitored optically. This is done by reversing the flow (III.a) through the filtrate line. The process is visualised with the lighting up of a LED and allows the subsequent assignment of the image sequences with a respective backwashing volume (see chapter 3.1.). In this way, the quality of the cake discharge can be supplemented with the information "specific backwashing volume".

$$H_{FC} = \kappa \cdot \frac{V_F}{A} \quad \text{Eq. 20}$$

Apart from filtration, the gas-phase discharges differ from the liquid-phase discharges in that there is no displacement by clear water, but the suspension must be drained and dried at the same time (II.b). This process must take place in a superimposed manner to prevent partial detachment from the filter cake and thus poor drying results. Only drying allows effective detachment of the filter cake and can be done by compressed air or steam [112,179]. The evaluation of the drying quality is based on the saturation (Eq. 21), which is achieved by differential weighing and drying of the discharged filter cake. After successful drying, the filter

cake is also discharged through the filtrate line. For this purpose, an impulse is applied to the inside of the fabric by means of compressed air, which accelerates the fabric and the cake and, after abrupt deceleration due to the geometric nature of the filter fabric tube, leads to detachment. Due to the significantly shorter time sequence of this process, no optical but a gravimetric evaluation of the discharge quality is carried out (Eq. 22). For this purpose, the discharged filter cake m_{removed} is collected with a collector under the filter candle and calculated with the remaining filter cake on the cartridge m_{remain} to the discharged mass fraction. This allows the discharge quality to be quantified as a function of various process variables such as backwashing pressure, filter cake thickness and acceleration path.

$$\text{Saturation } S = \frac{m_{\text{removed,wet}} - m_{\text{removed,dry}}}{\rho_{\text{liquid}} \cdot V_{\text{Filter cake}} \cdot \varepsilon_{\text{Filter cake}}} \quad \text{Eq. 21}$$

$$\text{Discharged mass fraction} = \frac{m_{\text{removed}}}{m_{\text{removed}} + m_{\text{remain}}} \quad \text{Eq. 22}$$

A detailed representation according to DIN EN ISO 10628 can be found in Appendix D. Backwashing filter – Detailed R & I - flow diagram (page 72). Also documented is the flow chart for controlling the respective valves for the test procedure. The test matrix for the discharge in liquid and gas phase includes the following variables [1,2,4]:

Liquid discharge

- Backwashing pressure
- Filter cake thickness
- Fabric (weave, mesh size, material)
- Particle system (shape, size)

Gas discharge

- Backwashing pressure
- Filter cake saturation
- Filter cake thickness
- Fabric (weave, mesh size, strength/stiffness)
- Particle system (shape, size)

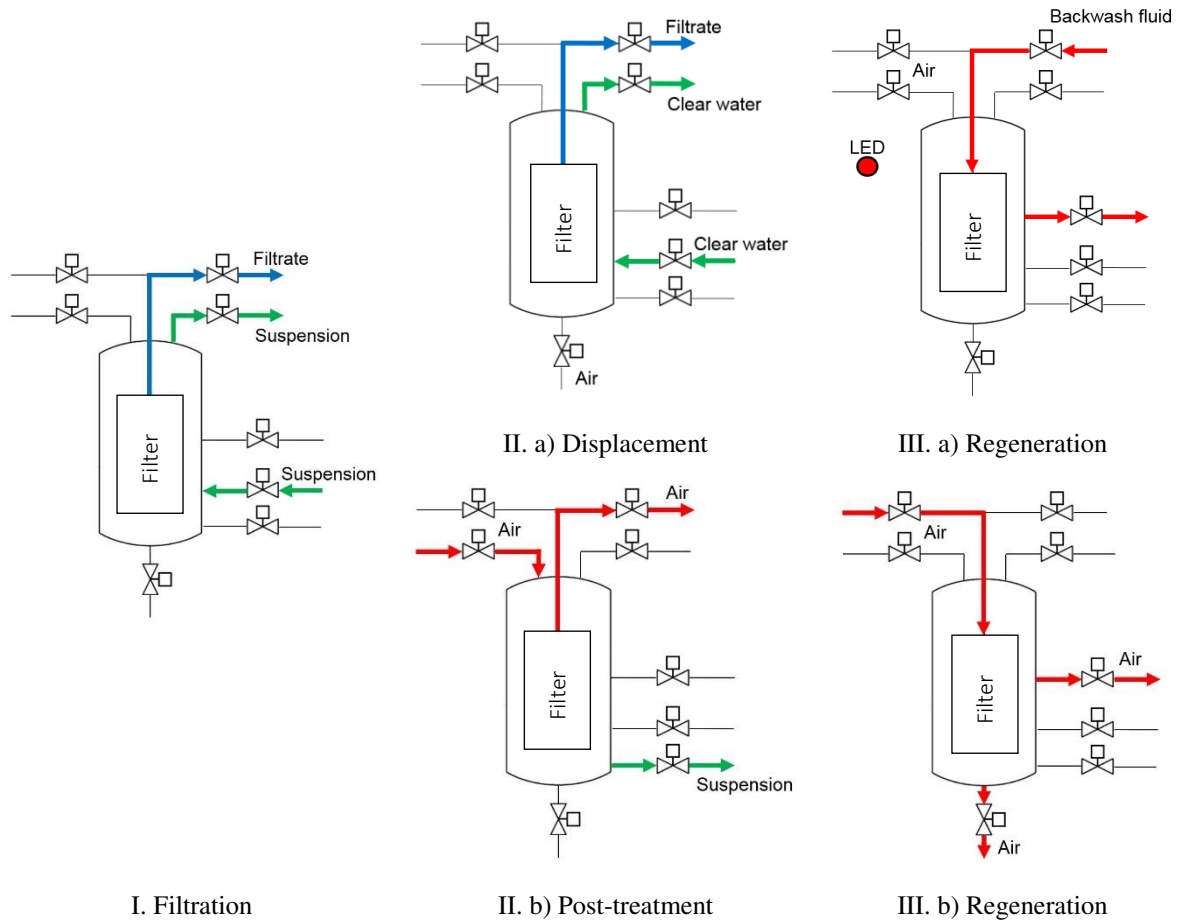


Figure 12: Schematic representation of the essential steps for regeneration by means of cake discharge without aids in a liquid and gaseous environment. After the filter cake (I) has been built up, the suspension is displaced by clear water (II.a) for visual observation of the cake discharge. If this is possible, the cake is discharged by flow reversal (III.a). This process is visually indicated by an LED and thus allows the image sequences to be associated with the backwashing volume. The discharge in gas phase takes place by drying the filter cake after filtration (II.b). After a defined drying time, there is a direct transition to regeneration by means of a compressed air pulse (III.b). The more detailed chart is shown in Appendix D. Backwashing filter – Detailed R & I - flow diagram (page 72).

3.5. Chamber filter

The experimental setup for characterising the detachment behaviour of filter cakes with aids is based on a laboratory chamber filter with an automated cleaning unit. This setup reflects a widespread area of application in which the retention of particle clusters on the surface and the subsequent removal of these on and in the fabric through cleaning steps is a necessary process step [181]. Current cleaning concepts, if implemented at all in the process, are manual and require a lot of time, manpower and cleaning agents. The development of this system is in the context of Industry 4.0 and is intended to support future concepts for cleaning with aids and the documentation of the cleaning result.

The system concept is shown schematically in Figure 13a and includes the coupling of a mechanical actuator and a computer interface. The mechanical actuator is realised by an XYZ stage, which controls a camera and a nozzle system. This unit allows the recording of the area to be cleaned and the cleaning itself by means of a nozzle lance. The measurement data acquisition processes the captured image and determines contaminated areas and how to approach them. Once this is done, the measurement data acquisition sends control commands to the mechanical actuator, which initiates the cleaning. After cleaning has been carried out, the result is recorded and evaluated again. The result is an iterative cleaning process in which the user can view and retrace the cleaning process at any time. For this purpose, it is only necessary to extend the image evaluation shown in Figure 10 (page 32) by the points coordinate generation (Figure 13b) based on the cleaning radius of the nozzle and cleaning sequence (Figure 13c) on the basis of the travelling salesman algorithm.

In the context of this thesis, this concept was implemented and results in contaminated surface - Specific cleaning amount - diagrams at different fabric - nozzle - contamination - combinations with subsequent evaluation by means of an approximated cleaning curve based on the occupied surface shown in Eq. 19. The underlying formula is shown in Eq. 23 and corresponds to a first order reaction [182]. The degree of cleaning is approximated using the residual impurity after the cleaning procedure and the kinetics and allows the cleaning to be interpreted using two constants. The variables used are described by the final contamination degree β and the cleaning kinetic γ_{Kinetic} .

$$\alpha_{\text{approximated}} = (1 - \beta) \cdot e^{-\gamma_{\text{Kinetic}} \cdot \text{Spec. Cleaning Amount}} + \beta \quad \text{Eq. 23}$$

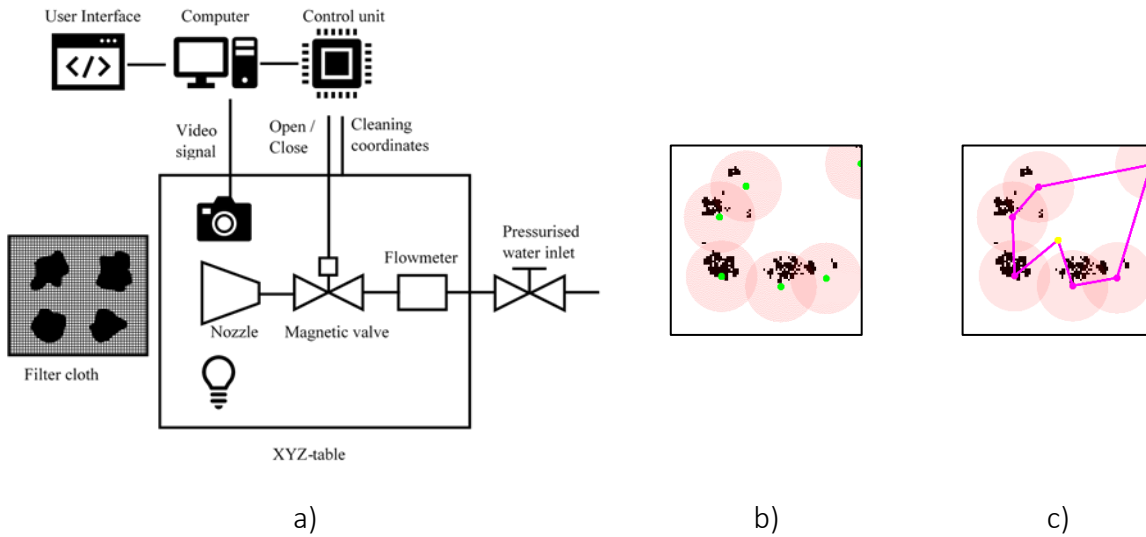


Figure 13: Schematic representation of the regeneration by cake discharge using aids. The implementation was carried out by coupling the image evaluation and a mechanical unit (XYZ table), which is equipped with a camera and a nozzle lance (a). This enables the targeted and demand-oriented cleaning of contaminated areas on surfaces and is used specifically for filter fabrics within the scope of this project. The necessary processing steps of coordinate generation (b) and calculation of the cleaning sequence (c) are also shown in Figure 10 (page 32).

Chapter 4

This chapter directly addresses the results published in [1–6]. For the materials used, reference is made to the respective publication, which is attached from Appendix E. starting with page 73:

Appendix F. Attached publication [1]	page 74
Appendix G. Attached publication [2]	page 87
Appendix H. Attached publication [3]	page 98
Appendix I. Attached publication [4]	page 106
Appendix J. Attached publication [5]	page 116
Appendix K. Attached publication [6]	page 125
Appendix L. Extended investigation of [4]	page 138

The corresponding author contribution is attached to the respective publication.

4. Results and Discussion

The following chapter deals with essential investigations in the field of tissue cleaning and filter regeneration by cake discharge. It is important to distinguish between two possible types/sequences of this cleaning process:

- I. Intra-cloth cleaning
- II. Filter cake discharge

The cleaning of individual adhering particles in the fabric, referred to here as I. Intra-cloth cleaning, is the content of some publications in the field of food process engineering and chemical process engineering [147,174]. Temporally, the reduction of individual particles in and on the filter fabric or technical surfaces is to be classified after the successful II. Cake removal. The focus of this work is therefore on the insufficiently investigated filter cake discharge. The evaluation of the regeneration quality is therefore based on the discharge of the complete cake and not on individual particles.

4.1. Backwashing properties of candle filters as a function of the particle system in liquid phase


Backwashing filter is the designation for discontinuous filters that regenerate the fabric by means of backwashing after filtration, thus increasing the efficiency of the subsequent filtration process. Backwashing is characterised by a flow reversal in the filtrate line and a flow through the filter fabric, starting from the filtrate side. The field of application of these filters is very extensive and includes treatment steps from electroplating (anode sludge filtration) to the filtration of cell cultures. The backwashing filter is technically realised by providing a backwashing tank in which filtrate is provided for subsequent regeneration. This liquid flows through the filter element in reverse to the direction of filtration and regenerates the filter fabric. This can be done by cake removal and/or the removal of individual particles from the fibres of the filter. Accordingly, this filtrate holdup must be dimensioned to be small, which goes hand in hand with a low backwashing volume. At present, the design of these filters focuses on filtration. The decisive factors are the retention of particles (filtrate quality) and a sufficiently high filtrate volume flow (hydraulic load of the filter in $\text{m}^3 \cdot \text{m}^{-2} \cdot \text{h}^{-1}$). The backwashing process, as well as the apparatus parts for regeneration, are designed very conservatively. There is no design based on a scientific study. It should be noted here that poor regeneration has a direct effect on the free filtration area. A direct influence on the filtration performance is therefore given if the regeneration step only takes up a fraction of the process time in relation to the filtration time [183]. The improvement of regeneration is thus an excellent optimisation parameter for improving the filtration process.

For this reason, an initial investigation was carried out into the main influencing variables in backwashing filtration with a view to improving the cleaning result. The focus of this investigation is on the influence of the following process variables on the discharge process and the necessary backwashing volume to achieve this regeneration quality:

- Particle system (shape/size),
- Filter cake thickness and
- Backwashing pressure.

Here, a significant influence of the particle system in connection with the filter cake thickness was observed. The specific cake resistance, which depends on the particle size and shape, results in a defined porosity of the particle structure. The spherical and smaller the particle, the lower the porosity and the specific cake resistance of the particle system increases. In the methodological characterization of the discharge, a trend could be observed that particles with

a large specific cake resistance require a small necessary cake thickness for a good regeneration. The cause was found to be the greater flow resistance of the cake compared to the flow around and detachment of the filter cake from the tissue. This fact led to the identification of 4 different types of discharge with a decrease in filter cake thickness:

- Complete discharge,
 - Incomplete, good discharge into fragments,
 - Incomplete, bad discharge into fragments,
 - Resuspended discharge.
- 

Filter cake thickness
 $H_{FC} \downarrow$

In the case of complete discharge, the filter cake is discharged over the entire area. Here, the effective cohesion is significantly greater than the adhesion of the particle layer to the filter fabric (see Eq. 10). After the detachment, the filter cake sediments in its entirety. The surface purity is very good. A similarly good regeneration is achieved by the incomplete, good cake discharge. In this case, the cake is also discharged over a large area, with the difference that the filter cake is partially broken up. The cohesion is therefore partially subject to the acting detachment force. This results in sedimentation of filter cake fragments of different sizes. The surface cleanliness afterwards is still very good to good and there is only a negligible influence on the backwashing time. On the other hand, there is the incomplete, bad cake discharge, a break-up of the filter cake into many small fragments with partial filter cake fragments remaining on the surface of the fabric. This type of discharge affects subsequent filtration cycles and must be avoided. Due to the decreasing filter cake thickness, the adhesion exceeds that of the cohesion and the detachment force, which is the explanation of the remaining fragments on the surface regarding the acting forces. The necessary backwashing volume increases strongly. In the case of the fourth type of discharge, resuspension, there is no filter cake in the true sense of the word and the small number of built-up particle layers pass directly back into the suspension. This discharge does not follow the mechanisms of cake discharge and the regeneration quality is accordingly poor. In the framework of [1], the discharge types are shown based on selected image sequences (page 74).

To calculate the necessary cake thickness for a very good regeneration quality, a total resistance of the cake of 2 to $5 \cdot 10^{10} \text{ m}^{-1}$ divided by the specific cake resistance of the respective particle system has proven to be useful. The determined cake thickness was proven to lead to a good regenerability of the tissue with further particle systems used. In addition, the backwashing volume required for this was lowest with a complete cake discharge. When varying the backwashing pressure in the technically relevant range up to 2 bar, no pressure dependency of the backwashing volume up to the cake discharge could be determined, but a dependency of

the backwashing time could be established. However, this time is negligible in relation to the filtration time.

A detailed description of the backwashing process was also provided. The results are published in [1] (see Figure 14). The publication is attached in Appendix F (page 74).

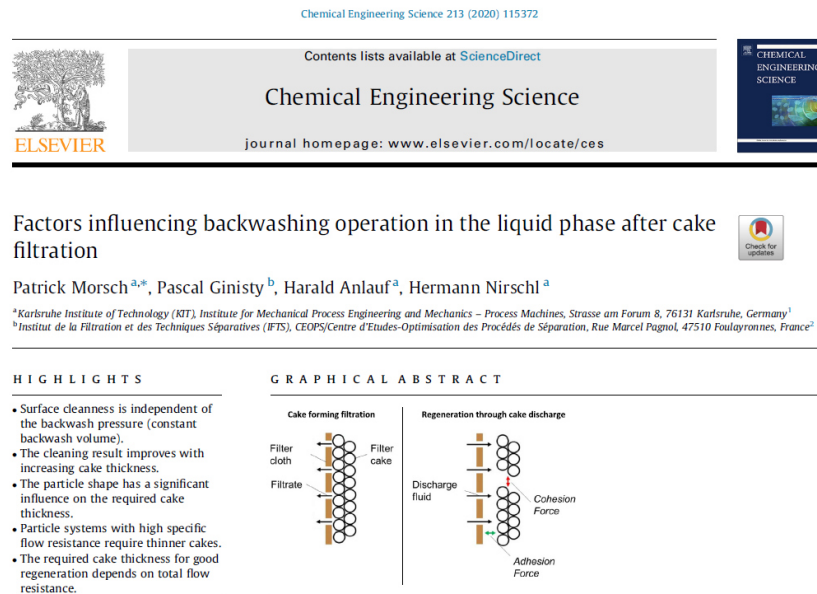


Figure 14: Cover sheet of the publication [1]. Regeneration was investigated by building up and discharging particle systems of different shapes and mineralogy on the surface of the filter as a filter cake. The backwashing pressure and filter cake thickness were varied. The different types of discharge were characterised and placed in the context of good regeneration quality. The publication is attached in Appendix F (page 74) of this paper.

4.2. Backwashing properties of candle filters as a function of the filter fabric in liquid phase

While the focus of [1] is on the variation of process variables (pressure, filter cake thickness, backwashing volume) for different particle suspensions with the same filter fabric, an essential influencing factor of regeneration is given by the filter fabric itself [100]. For this reason, the investigation of a wide variety of fabrics is essential for the development of a prediction model. For this purpose, the test procedure is to be carried out analogously to [1], but with different filter fabrics on the laboratory candle filter. Filter fabrics interwoven with monofilament yarn (six fabrics) and with multifilament yarn (three fabrics) were examined. For the monofilament fabrics, a further distinction was made between plain and twill weave with mesh sizes $< 22 \mu\text{m}$. All fabrics are made of synthetic fibres.

An important observation is that the regeneration process "cake discharge in liquid phase" shows clear differences between multifilament and monofilament fabrics. In multifilament fabrics, the discharge is cohesion-dominated, i.e. a certain cake thickness must be exceeded for complete cake discharge to occur. The cake thickness considers the porosity of the particle structure and results from the contact points between the particles. Both variables depend significantly on the particle size and shape and can be indirectly expressed by the specific cake resistance. Nearly spherical particles form very compact cakes and, compared to similarly sized needle-shaped particles, have a correspondingly high specific cake resistance [77]. In [2] it was observed that good regeneration can be observed when a critical filter cake thickness is exceeded. This can be estimated by means of an empirically determined total flow resistance $R_{\text{FC}} \geq 5 \cdot 10^{10} \text{ m}^{-1}$ divided by the specific cake resistance α_{FC} of the respective particle system (see Eq. 24) for all investigated multifilament fabrics. This means that particle systems with high specific resistance α_{FC} , equating to low porosity (and nearly spherical particles) and thus higher cohesion in the filter cake, need a smaller cake thickness for complete discharge than particle systems with lower specific resistance.

$$H_{\text{FC,Multi}} = \frac{R_{\text{FC}}}{\alpha_{\text{FC}}} \quad \text{Eq. 24}$$

However, the regeneration step of monofilaments follows different mechanisms. In six fabrics it was found that the ratio of mesh size and particle size has a strong effect on the cake thickness required for complete discharge. The discharge behaviour is exactly opposite to that of multifilament fabrics. Here, particle systems with a lower specific cake resistance have a smaller cake thickness required for complete cake discharge. The explanation from [2] includes the different deposition behaviour of "bleeding", "clogging" and "surface deposition" (see

chapter 2.2., page 12) and their effect on particle deposition in the meshes. This approach states that larger particles create a more defined particle layer between the first particle layer of the filter cake and the mesh. The tissue resistance of particles with "surface deposition" is consequently smaller than in the case of interaction by "clogging" and, in part, "bleeding" and is, presumably, to be equated with straighter contact points at the tissue surface [38]. Consequently, the particle systems with a small specific cake resistance also require a small cake thickness to achieve a good regeneration quality.

Consequently, the model presented in Eq. 24 cannot be applied to monofilament fabrics and led to the elaboration of a new predictive model for monofilament fabrics (see Eq. 25). By calculating the specific cake resistance α_{FC} with the filter fabric resistance $R_{FM, \text{Surface Deposition}}$, determined by pressurized filter cell tests with a particle system with unique "Surface Deposition", and a, particle shape dependent factor, the calculation of a minimum cake thickness is also possible here. The factor determined is $3 \cdot 10^{-2}$ for orthorhombic particles, $15 \cdot 10^{-2}$ for flaky and $46 \cdot 10^{-2}$ for needle-shaped particle systems. A trend towards larger factors with increasing deviation from the ideal sphericity was observed. A more precise definition of this factor must be made by expanding the test matrix.

$$H_{FK, \text{Mono}} = \frac{R_{FM, \text{Surface Deposition}}}{\alpha_{FC} \cdot \text{Factor}} \quad \text{Eq. 25}$$

The results are published in detail in [2], which is attached in Appendix H (page 98) (cover sheet see Figure 15).

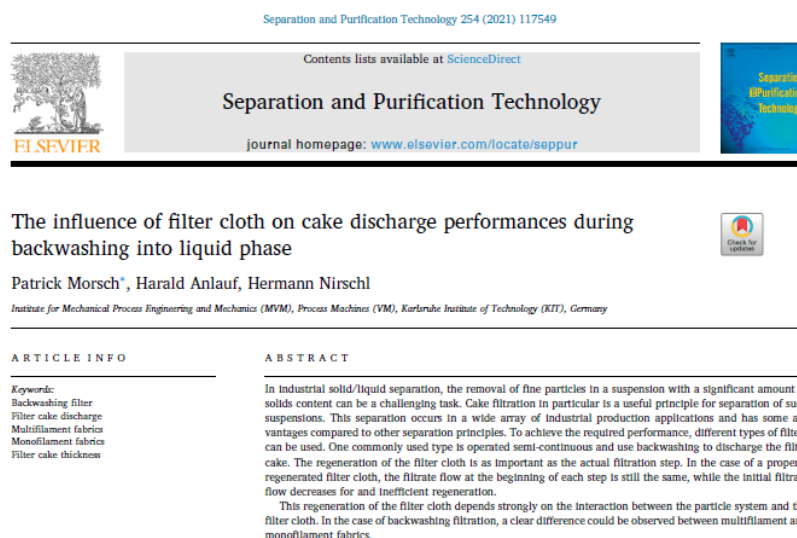
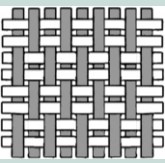
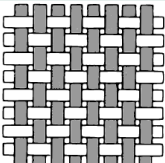


Figure 15: Cover sheet of the publication [2]. Regeneration was investigated by building up and discharging 3 particle systems of different shapes and mineralogy on the surface of 9 filter fabrics as a filter cake. The fibre type, mesh type and mesh size were varied. The different types of fabrics were characterised and compared with each other. Based on this, two prediction models were developed for different mesh types (multi-/monofilament). The publication is attached in Appendix H (page 98) of this paper.

4.3. Further development of the prediction model for metal-based monofilament fabrics according to [1,2]

In addition to polymer-based multifilament and monofilament fabrics, metal fabrics are also used in filter apparatus. Among other things, they are used for particularly abrasive products. The conflict between plastic and metal mesh is therefore "price vs. service life". Metal mesh manufacturers advertise the mechanical stability of their products, which the buyer has to take into account with a higher price compared to synthetic fabrics. In the case of chemical stability, metal fabrics, especially in the acidic environment, are often at a disadvantage compared to fabrics made of the resistant polyethylene or polypropylene. The suitability and profitability are therefore linked to the process and the added value and must be specifically adapted. Because of the technical relevance, it is necessary that these metal fabrics are also examined for their backwashability. For mesh sizes below 25 μm , this type of fabric is represented by plain and twill weaves with two warp elevations on 2 warp sinkings (see Table 3). Because of the similar floating to a plain weave, these fine twill weaves are also called twill plain weaves. The experimental range includes 4 of these fabrics with 9, 11, 15 and 21 μm , as well as 5 plain dutch weaves with 6, 10, 14, 20 and 25 μm . The majority of the meshes are made of 1.4404 stainless steel, which is particularly corrosion-resistant due to its high chromium and nickel content in combination with molybdenum. However, 1.4301 and 1.4306 are also used, which have a good tendency to corrosion due to chromium and nickel components similar to 1.4404 [184]. Due to the material, all fabrics have very thin fibres compared to synthetic fabrics (compare Table 3 in Appendix H, page 98). The production-technical possibility of spinning such thin fibres is directly related to the greater strength of metal compared to polymers. As a result, very thin fabrics with lower surface roughness and many meshes per unit area can be woven. Calendering of these fabrics is not necessary. On the other hand, the specific weight is significantly higher for the same mesh size. Due to the high mesh density, these fabrics are very porous, which leads to clear water resistances $R_{\text{FM},0}$ in the range 10^7 to 10^8 m^{-1} . However, interaction with particles results in an initial resistance of a similar order of magnitude (tending to be somewhat lower) to that of synthetic fabrics in the range 10^9 to 10^{10} m^{-1} . The test matrix does not contain any multifilament metal fabrics, as this type of fabric is not included in the portfolio of metal fabric manufacturers and is therefore of no technical relevance.

Table 3: Examined metal tissues following [1, 2]. The categorisation used in [2] is continued here.

Fabric type / mesh size in μm / material		Weave according to DIN ISO 9354	Mesh per filter area mm^{-2}	Filter cloth resistance according to VDI 2762-2 m^{-1*}	Weight per unit area $\text{g} \cdot \text{m}^{-2}$	Surface roughness (ISO 25178) μm	Thread thickness warp / weft μm	Fabric thickness (ISO 5084) μm	Schematic weaving patterns, based on [185]	
Twill	9	1.4404	20-02 02-01-02	834	$2.1 \cdot 10^{10} \pm 5.4 \cdot 10^9$	343	4	19 / 30	66	
	11	1.4404		455	$2.0 \cdot 10^{10} \pm 6.7 \cdot 10^9$	425	6	20 / 31	82	
	15	1.4404		206	$1.7 \cdot 10^{10} \pm 4.4 \cdot 10^9$	757	7	21 / 64	144	
	21	1.4306		171	$2.0 \cdot 10^{10} \pm 1.3 \cdot 10^{10}$	692	6	44 / 47	142	
Plain	6	1.4404 / 1.4301	10-01 01-01-00	1452	$1.3 \cdot 10^{10} \pm 1.0 \cdot 10^{10}$	188	4	13 / 36	65	
	10	1.4404		869	$1.4 \cdot 10^{10} \pm 1.0 \cdot 10^{10}$	287	5	19 / 45	94	
	14	1.4404		407	$1.6 \cdot 10^{10} \pm 1.1 \cdot 10^{10}$	444	8	26 / 60	132	
	20	1.4404		309	$1.7 \cdot 10^{10} \pm 1.4 \cdot 10^{10}$	437	9	27 / 61	145	
	25	1.4404		260	$1.6 \cdot 10^{10} \pm 1.5 \cdot 10^{10}$	450	9	29 / 60	150	

* Based on mean filter cloth resistance measured with Particle system from [1, 2]

With regard to the regenerability of metal fabrics, it can be said that effective and complete discharge can already be expected with very thin filter cakes ($< 1 \text{ mm}$) for the majority of the fabrics examined. Since discharge in the liquid phase involves "flowing through" the mesh with subsequent detachment of the filter cake, an improvement in cake discharge compared to polymer fabrics was expected due to the large porosity of metal mesh. Although the observation that "filter cakes made of coarser particles are better discharged due to surface deposition" [2] is true, a significantly better discharge compared to polymer fabrics with a lower specific backwashing volume is not the case. Accordingly, the factor introduced from Eq. 25 for metal mesh is of a similar order of magnitude. The differences are due to the fabric resistance and the cake thickness and are documented in Table 4 with the comparison from [2]. While according

to [2] this factor could be summarised for polymer fabrics made of plain weave and twill weave, the metal-based fabrics show clear differences. For this reason, the factor was determined independently of each other.

When comparing the metal-based plain weaves with the polymer fabrics, an increase in the factor from 0.03 to 0.08 can be observed for orthorhombic particles. However, this should not be interpreted as a decrease in the necessary cake thickness, as the fabric resistance in Eq. 25 also has an effect. The cake thicknesses determined for the complete discharge of the metal meshes tend to be greater, while the fabric resistance is lower at the same time. Accordingly, the factor is mathematically larger for the prediction of the cake thickness for metal fabrics. The trend towards a larger factor with increasing deviation from the ideal sphericity is given, even if the differences between the particle systems are smaller for the metal plain weaves. For example, the factor for flaky is 0.10 and needle-shaped 0.17 and thus significantly lower than for the synthetics. A differentiation in the prediction is therefore necessary.

In the case of metal-based twill fabrics, this difference between the particle shapes is again more pronounced, which is ultimately due to slight variations in the fabric resistance across all 3 particle systems. Here, the metal-based twill fabrics show more similarities with the group of plastic fabrics from [2] due to the decreasing mesh density. With regard to the required cake thickness, this is similar for the orthorhombic particle system to that of the metal-based braided fabrics, the filter cakes of flaky and needle-shaped particles are significantly smaller in the range < 0.9 mm. This results in a factor of 0.41 for flaky particles and 0.31 for needle-shaped particles. The observed trend with regard to particle shape is not given here.

In conclusion, it can be said that between mesh sizes, material and separation mechanisms, the factor is suitable as a sum parameter for 3 groups of monofilament fabric types of different material.

Table 4: Summary of the factor for calculating the minimum required cake thicknesses of monofilament filter fabrics as a function of the particle shape based on Eq. 25, following the procedure from [2] (See Appendix H, page 98).

Particle system	Factor for complete discharge		
	Polymer-based weave [2], Appendix H, page 98	Metal-based plain weave	Metal-based twill weave
Orthorombic	0.032 ± 0.019	0.081 ± 0.036	0.168 ± 0.067
Flaky	0.153 ± 0.091	0.103 ± 0.057	0.405 ± 0.059
Needle-shaped	0.459 ± 0.142	0.167 ± 0.063	0.305 ± 0.097

4.4. Effects of the bulging behaviour of the filter fabric during the backwashing procedure in liquid phase

During the investigation of [1,2] it was observed that the bulging behaviour of the filter fabric, i.e. the deformation of the filter fabric as a result of the flow through it, can essentially contribute to the increase of the specific backwashing volume. For this reason, a more detailed investigation of this behaviour was carried out. This investigation is based on two test apparatuses for characterising the force-elongation behaviour of filter fabrics and the bulge behaviour during the flow:

- A. Tensile testing machine,
- B. Leaf filter.

With the Tensile testing machine (A), selected fabrics have been cut and tensile loaded based on ASTM Standard 6614-07. The measuring device allows the dedicated recording of the change in length (elongation) with the associated force. The result of this investigation shows the highly anisotropic behaviour of filter fabrics under load and allowed the differentiation into 3 ranges:

- I. High elongation with low force,
- II. Exponential force increases with comparatively low elongation increase,
- III. Further increase in force at low elongation.

At the beginning of the force application, the meshes align themselves within the fabric and can be deformed. A large change in elongation with a relatively small force effect is the result (I). After the meshes have aligned, the force increases exponentially with relatively little change in length. Here friction takes place between the fibres at the looping points (II). While in I there was still a change in length due to mesh displacement, II is characterised by increasing direct force action on the fibres. The force-elongation behaviour then continues in the direction of the strength of the material used, considering the notch effect (the maximum breaking force of woven fabrics is always less than that of the pure material). This can be done by further increase of force at lower elongation (III) or an asymptotic approach to a maximum value and depends on the elongation and the pattern of the fabric. The slope from this force-elongation curve is used to calculate the geometrical moment of inertia, which is the basis of the prediction concept. Since the slope varies, this behaviour had to be considered in the calculation.

The actual bulge during backwashing is then determined using the leaf filter (B). For this purpose, the filter fabric is mounted on the frame of the leaf filter, which allows a defined pretension. The mounting can be done in warp as well as in weft direction of the fabric. During the bulging process with variable pressure and pretensioning, the bulge is recorded by image technology. This bulge, in conjunction with the strength values from A, allow the determination of a geometrical moment of inertia for fabric, which can be used for future predictions of bulge. Four selected filter fabrics were investigated for the study. Based on this investigation, it is possible to adjust the arrangement of filter elements in the backwashing filter regarding regeneration.

The results are published in detail in [3], which is attached in Appendix G (page 87). (See Figure 16 for cover sheet).



Figure 16: Cover sheet of the publication [3]. Backwashing was further investigated regarding the deformation of the filter fabric. For this purpose, 4 filter fabrics were mounted in a leaf filter, which allows different preloads of the fabric. The aim is to physically describe the deformation based on elementary mechanics. For this purpose, the fabric type, mesh size, warp/weft orientation, pretension and backwashing pressure were varied. Based on this, a geometrical moment of inertia was determined for the fabrics, which enables the calculation of the bulge. The publication is attached in Appendix G (page 87) of this paper.

4.5. Backwashing properties of candle filters in gas phase

The use of backwashing filters has proven itself in a variety of industries due to their adaptability regarding the post-processing of the filter cake. In addition to the already presented discharge of the filter cake in liquid phase, backwashing filters also offer the option of discharging the filter cake in gas phase [4]. While discharge in liquid phase involves subsequent thickening of the filter cake at the bottom of the vessel and subsequent discharge, a further step, drying of the filter cake, is necessary when discharging the cake in gas phase. For this purpose, the filter cake must be flown through by means of a gas/steam flow, which displaces the remaining liquid from the capillaries of the cake. What remains is a dried filter cake of defined residual moisture, which is thrown off and discharged directly from the filter apparatus.

The study published in [4] includes the variation of the following four process variables when using 2 filter cloths (plain and satin weave) and 4 particle systems:

- I. Backwashing pressure,
- II. Filter cake thickness,
- III. Filter cloth diameter,
- IV. Filter cloth type.

While no pressure dependency was found for discharge in the liquid phase [1], there is a clear pressure dependency for discharge in the gas phase. With increasing pressure, the proportion of discharged filter cake also increases. This is the first indication of different discharge mechanisms between liquid and gas phase discharges. These different mechanisms then become visible when comparing the images of the two types of discharge. While the discharge in liquid phase can be described as a flow through the filter cloth with sliding of the filter cake, the discharge in gas phase must be described as a throw-off of the filter cake with an impulse (comparison Fig. 5 in Appendix H (page 98) and Fig. 8 in Appendix F (page 74)). This fact is also shown when comparing the time of discharge of both regenerations, where the discharge in gas phase is significantly faster than the discharge in liquid phase (approx. 10 % of the duration of the discharge in liquid phase under identical process conditions).

The amount of filter cake discharged also depends strongly on the filter cake thickness, the degree of drying and the mesh type and installation. Analogous to the backwashing pressure, an increase in the cake thickness can also be expected to lead to an increase in the discharge quality.

In the comparison of the filter fabrics used in [4], thin, filigree fabrics are recommended for discharge in the gas phase. Plain fabrics have prevailed over the much stiffer twill and satin fabrics. In addition, the possibility of a relative movement of cake and fabric favours the discharge. Loosely stretched fabrics throw off effectively at a significantly lower backwashing pressure and thus offer a possibility to reduce the backwashing pressure. Loosely stretched

fabrics throw off effectively at a significantly lower backwashing pressure and thus offer a possibility to reduce this process variable. In the case of stiffer twill and satin fabrics, this is even necessary to initiate cake discharge.

Within the framework of an elaboration, the differences between the two types of discharge were worked out and parameters important for gas discharge were elaborated. The results were also compared with regeneration steps from gas filtration and are published in detail in [4], which is attached in Appendix H (page 98) (see cover sheet Figure 17).

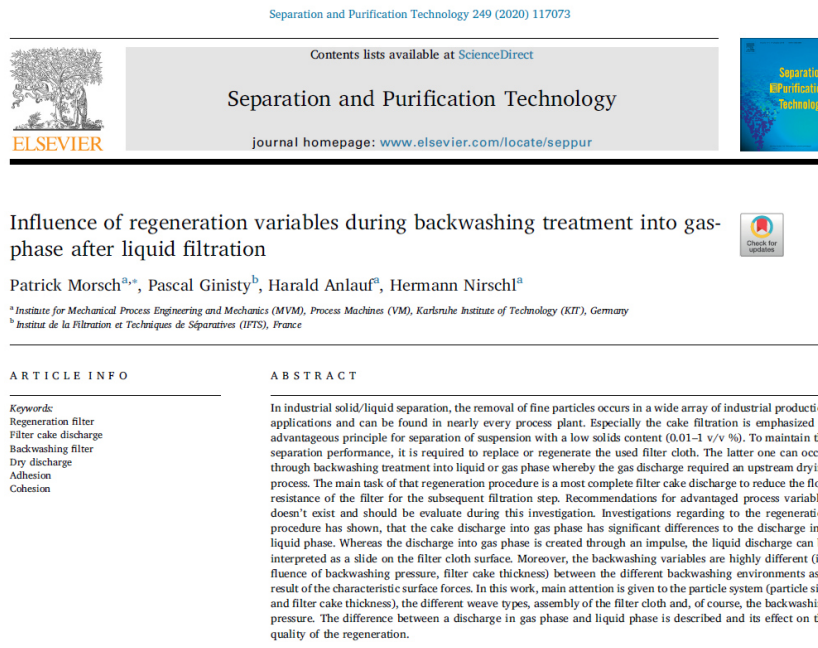


Figure 17: Cover sheet of the publication [4]. Regeneration was investigated by building up particle systems of different shapes and mineralogy on the surface of the filter as a filter cake, drying them and discharging them. The backwashing pressure, filter cake thickness and degree of drying were varied. The publication is attached in Appendix H (page 98) of this paper.

4.6. Backwashing properties of candle filters as a function of the filter fabric in gas phase

In addition to the basic investigation of the discharge behaviour in gas phase after prior liquid filtration, a variation of the filter fabrics for the gas discharge was also carried out, based on the fabric influence in liquid backwashing [2]. The detailed description is attached in Appendix L (page 138) and includes, analogous to [4], the variation of the process variables backwashing pressure (I.), filter cake thickness (II.), filter cloth diameter (III.) and filter cloth type (IV.).

The variation of the backwashing pressure (I.) of different fabrics have confirmed that in the case of gas phase backwashing there is a clear pressure dependence. This contrasts with liquid backwashing and confirms the different detachment mechanisms. It has been shown that lighter, more filigree fabrics have a better cake release (comparison Table 7 and Figure 21, page 141ff). This fact becomes clear when comparing the specific weight and thickness of the fabrics. Here, the plain weaves show a clearly better detachment behaviour due to larger discharged mass fractions compared to the heavy and thick twill and satin fabrics. The latter fabrics achieve insufficient cake detachment in the examined pressure range.

When the cake thickness is varied (II.; Figure 22, page 145), the plain dutch weaves also show complete discharge even with the thinnest filter cakes. The twill and satin fabrics require a significantly greater cake thickness for a discharge quality of similar quality. The installation situation of the fabric on the filter candle has proven to be a strong influencing factor. Fabric surfaces with a significantly larger diameter than that of the filter candle throw off better (III.). In this way, even very inert/heavy and rigid mesh types can achieve adequate cake discharge (IV.). In the context of a patent investigation, the need for tissue movement in some filter candles designed for gas discharge and the process of drying were considered [186–189].

In the context of extending the experiments with reference to gas discharge, the difference between backwashing in liquid and gas phase after previous liquid filtration has been clearly demonstrated. It is recommended that the respective filter elements also be adapted to the regeneration process. The results are documented in detail in Appendix L (page 138).

4.7. Surface cleaning of filter fabrics in chamber filters by automated and demand-controlled nozzle cleaning

While the filter cake is removed in the backwashing filtration by means of flow reversal (chapters 4.1 to 4.6), a large number of filter fabrics and other technical surfaces are cleaned of contamination by nozzles, scrapers and other hydraulic and/or mechanical cleaning units. The excerpt from the patents mentioned in Figure 9 (page 29) gives an insight into the necessity of adequate cleaning concepts for the regeneration of filter fabrics. Cleaning by means of nozzles is, in the case of chamber filters, a widespread application with potential for optimisation. In this process, remaining particle contaminations on surfaces are removed by means of a liquid jet. Currently, this is done manually and with conservative cleaning concepts, which is associated with high time and cleaning agent consumption. For this reason, an evaluation of this cleaning process and the elaboration of influencing factors such as fabric and nozzle type were carried out. The content is the implementation of automated cleaning based on image evaluation, which provides new possibilities regarding cleaning quality and cleaning documentation of technical surfaces. The investigations themselves are divided into 3 steps:

- I. Conceptual design and construction of the test facility,
- II. software development for the detection, approach and cleaning of contaminated areas,
- III. parameter study using a test matrix consisting of filter fabrics, nozzle types and particle contaminations.

The realisation of point I is done by coupling a regular CNC machine with a self-built cleaning lance head with camera and exposure ring. The camera forms the connecting element and delivers the status of the surface to be cleaned to a software, which evaluates the degree of cleanliness and assigns coordinate points to contaminations (II). The structure and the image evaluation including the generation of coordinates are described in detail in [5]. These coordinates are sent to the CNC and allow the targeted investigation of selected process variables (III). The investigation includes the variation of the process variables cleaning pressure, nozzle type and distance, contamination type and fabric type. When varying the backwashing pressure, only a slight pressure dependence can be observed regarding the number of cleaning cycles. Surface coverage and detergent consumption are almost identical in the pressure range investigated and show first parallels between backwashing by flow reversal and nozzle cleaning. The effective adhesive force of the wet contamination is reduced by the liquid and allows it to slide on the liquid film. However, the assumption of a general pressure dependence even with dried, strongly adhering contamination and cleaning in the fabric meshes

(intra-cloth cleaning) should not be assumed. As expected, the variation of the nozzle type showed clear differences, with full-cone nozzles and flat-jet nozzles being preferred. The nozzle distance is directly related to the geometry of the nozzle jet and requires an adaptation of the demand-based cleaning to the effective cleaning area of the nozzle for further reduction of the cleaning agent expenditure. In addition to this adaptation, the type and degree of dryness of the contaminant must also be considered in the design of demand-oriented and automated cleaning. In the case of dried contamination, the cleaning agent consumption can be reduced by rest periods after rewetting. In the variation of fabrics, fine-mesh fabrics with a monofilament fiber structure and multifilament fabrics for surface cleaning have been particularly successful. Here, too, parallel to backwashing filtration is possible. The investigation is described in [5, 6] (see Appendix J, page 116 and Appendix K, page 125) and following this section for the investigation of further filter fabrics, to extend [6]. The cover sheets of the published papers are illustrated in Figure 18 and Figure 19.



Figure 18: Cover sheet of the publication [5]. For the investigation, the surface of a filter fabric was covered with a defined contamination matrix and cleaned by nozzles. The cleaning was automated based on an image evaluation, which is presented in this paper. The focus is on the variation of image evaluation parameters, cleaning distance and pressure, and nozzle type. The comparison and quantification of the cleaning is done by means of specific cleaning amount and the surface characterisation of the tissue after cleaning. The publication is attached in Appendix J (page 116) of this paper.



Influence of the filter cloth and nozzles type on the in-situ cleaning procedure of filter presses



Patrick Morsch^{a,*}, Jérôme Kühn^a, Roman Werner^{b,*}, Harald Anlauf^a, Dominik U. Geier^b, Thomas Becker^b, Hermann Nirschl^a

^aKarlsruhe Institute of Technology (KIT), Institute for Mechanical Process Engineering and Mechanics (MfM), Process Machines, Strasse am Forum 8, 76131 Karlsruhe, Germany
^bTechnical University of Munich, TUM School of Life Sciences Weihenstephan, Institute of Brewing and Beverage Technology, BioPat and Digitalization, Weihenstephaner Steig 20, 85354 Freising, Germany

HIGHLIGHTS

- The surface contamination is lower with smaller meshes within the same weave type.
- Calendering of the fabric surface does not lead to less surface contamination.
- Multifilament fabrics have the lowest surface contamination with the smallest amount of cleaning agent.
- Mathematical description of the cleaning process by a regressive model possible.
- Full jet nozzle to be preferred for surface cleaning.
- Optimization of the dirt detection by variation with colour filters and light sources possible.

GRAPHICAL ABSTRACT

Exemplary representation of the contaminated surface and the resulting binary image with coordinate generation based on the effective radius of the cleaning nozzle and the shortest way of cleaning procedure (left to right).



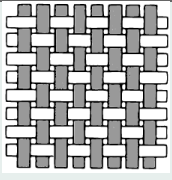
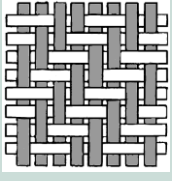
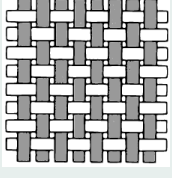
Figure 19: Cover sheet of the publication [6]. For the investigation, the surfaces of filter fabrics were covered with a defined contamination matrix and cleaned by nozzles. The cleaning was automated based on image evaluation. The focus was on the variation of filter fabrics and nozzle type. Comparison and quantification of cleaning is done by specific cleaning amount and surface characterisation of the fabrics after cleaning. The publication is attached in Appendix K (page 125) of this paper.

Based on [5,6], the test matrix was expanded with a special focus on the choice of fabric. Due to the technical relevance, selected metal meshes with mesh sizes from 10 to 182 μm were chosen. Important fabric information, based on the fabric characterisation mentioned in chapter 3.3, is contained in Table 5. The 11 metal meshes used can be divided into 3 groups, which follow the consecutive numbering from [6].

Regarding the mesh data, group 4 contains plain weaves from 45 to 153 μm (mesh number 12 - 15). A comparable group of fabrics in [6], with regard to mesh size, are the twill fabrics contained in group 1 with mesh sizes from 20 to 215 μm . Due to the material, metal fabrics can be woven with very thin threads relative to the mesh size. The reason for this is the increased strength of steel compared to synthetics. This becomes clear by looking at the fibre thickness in Table 5 compared to the meshes in [6] and results in a lower mesh thickness and surface roughness compared to synthetic meshes of the same mesh size. The specific weight is also greater with coarser mesh sizes. However, this difference to synthetic fabrics levels out with decreasing mesh size. The reason for this is the significantly higher porosity of metal mesh compared to synthetics of small mesh sizes in the lower two-digit micrometre range. The combination of thinner fibres and higher porosity thus compensates for the higher density of the material. Calendering of the fabrics to achieve the smallest mesh sizes is not necessary. Also included in the test matrix are twill fabrics with the usual weave of 2 warp lifts and 2 sinks for metal fabrics. The mesh size of this fabric group 5 (fabric numbers 16 - 18) is also based on

fabric group 1 in [6] and establishes the reference to the same weave type. Here, the fact of more filigree fibres in metal fabrics compared to polymer fabrics, and the associated physical differences, also becomes clear. The last group of weaves, 6, from Table 5, comprises four more plain weaves of finer mesh size. As a continuation of group 4 only conditionally possible as a result of the finer weave structure, this fabric group 6 allows the validation of the observed trend with regard to surface cleanliness from [6]. In addition, due to the smallest mesh size, a comparison with the multifilament fabrics contained in [6] is possible.

Table 5: Examined metal fabrics following [5,6]. The numbering of the tissues/tissue groups presented in [6] is continued here.

No.	Group/ Fabric type / Fibre type / mesh size μm		Weave according to DIN ISO 9354	Weight per unit area $\text{g}\cdot\text{dm}^{-2}$	Surface roughness (ISO 25178) μm	Thread thickness warp/ weft μm	Fabric thickness (ISO 5084) μm	Schematic weaving patterns based on [185]	
12	4	Plain	10-01 01-01-00	153	25.9	115	240/348	750	
13				122	15.3	72	144/281	503	
14				73	10.4	47	93/134	341	
15				45	8.2	37	72/131	230	
16	5	Twill	20-02 02-01-01	182	28.3	154	133/246	742	
17				82	16.4	36	80/150	394	
18				47	11.8	23	58/93	256	
19	6	Plain	10-01 01-01-00	74	11.1	49	84/188	364	
20				40	6.7	32	44/106	228	
21				19	4.4	17	28/44	138	
22				10	2.9	12	21/33	94	

The evaluation of the surface cleanability according to [6], with significant cleaning agent consumption of 1.5 and 2.5 ml per cm^2 , is shown in Figure 20. The trend of decreasing mesh size and improving surface cleanliness observed in [6] for group 1 can also be confirmed for the metal meshes. Here, all 3 groups show an improvement in surface cleanliness with decreasing mesh size. Only the degree varies and tends to be better in the case of synthetic fabrics. For example, the synthetic mesh No. 2 / No. 3 ($164 \mu\text{m}$ / $120 \mu\text{m}$; see Appendix K on page 125) has a surface purity of approx. 0.3 / 0.25 at $1.5 \text{ ml}\cdot\text{cm}^{-2}$ and 0.2 at $2.5 \text{ ml}\cdot\text{cm}^{-2}$, while metal meshes of similar mesh size (No. 12, 13 and 16) achieve surface purities of > 0.4 for $1.5 \text{ ml}\cdot\text{cm}^{-2}$. Only when $2.5 \text{ ml}\cdot\text{cm}^{-2}$ is reached does the surface purity of meshes No. 13 and 16 approach that of the synthetic meshes, at approximately 0.3. With focus on monofilament fabrics of smaller mesh size around $40 \mu\text{m}$ (No. 4, 8, 11 for synthetic fabrics and No. 15, 18

and 20 for metal fabrics) this trend changes. Here, metal fabrics with a surface coverage of approximately 0.15 / 0.05 at 1.5 / 2.5 ml·cm⁻² have a lower surface coverage than plastic fabrics with a surface coverage of approximately 0.25 / 0.15 at 1.5 / 2.5 ml·cm⁻² with the same cleaning agent consumption. This also becomes clear when comparing the 20 µm fabrics No. 5 and No. 21, so that metal fabrics with the finest mesh sizes (No. 21/22) merge into the surface quality of the multifilament fabrics (No. 9/10). This behaviour can also be explained by the weaving characteristics of metal fabrics and is a consequence of the fine, highly porous structures of the metal fabrics with small mesh sizes. According to the manufacturer, the metal fabrics have a high mesh density due to the small fibre diameters. Therefore, there is little surface area for particles to adhere to. As a result, impurities can be detached more easily. This explanation is also consistent with the good surface cleanability of multifilament fabrics. Although these have thicker threads in the fibre composite, they consist of very fine fibrils. These define the micro level of the surface and create a low number of contact points between the contamination and the fabric and thus a very good cleanability of the surface. However, this measurement method does not provide information about the cleaning within the fibrils (intra-cloth contamination).

In summary, metal fabrics of larger meshes are more difficult to clean from surface contamination than polymer fabrics. However, this trend reverses with smaller mesh sizes. Metal meshes with the finest meshes of 10 - 20 µm have excellent properties regarding cleanability as a result of the high porosity.

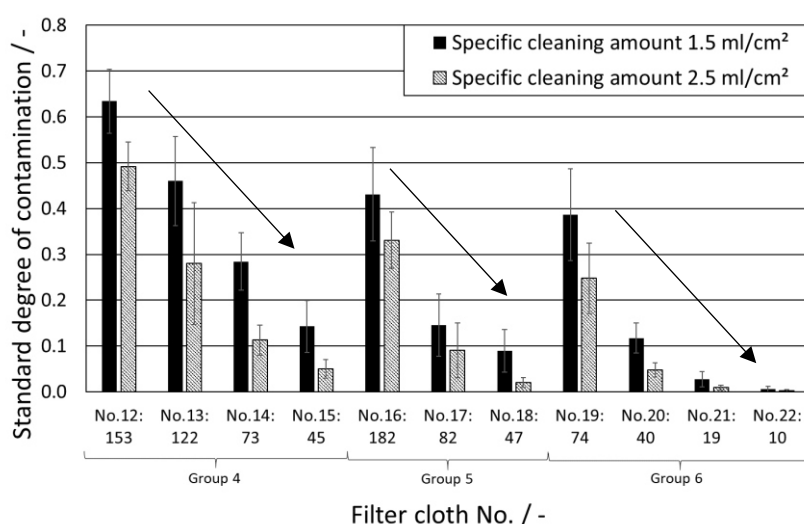


Figure 20: Surface coverage of filter fabrics No. 12 to 22 according to the evaluation methodology published in [5,6]. This shows the surface coverage at 1.5- and 2.5-ml cleaning agent consumption per cm² filter surface. The cleaning curves can be approximated using Eq. 23 (page 39) and Table 6 described below with a coefficient of determination R² of at least > 0.9 (coarse mesh fabrics No. 12, 13 and 16) or > 0.95, respectively.

The surface cleanability is assessed using the partial section at 1.5 and 2.5 ml·cm⁻² shown in Figure 20, which is, however, suitable for assessing the cleanability of a wide range of tissues

[6]. The original course corresponds to a 1st order reaction and can be approximated using the equation presented in Eq. 23. The basis for this is a kinetics term, which specifies the cleaning speed in clean area per ml of cleaning fluid, and a final surface coverage after 10 cleaning cycles. Analogous to the fabrics from group 1 (see Appendix K, page 125), fabrics with a coarser mesh size (large value for the final surface coverage) are also "slower" to clean. This is shown by the smaller kinetics term. A mutual dependence of the two variables cannot be denied. If a fabric can be cleaned quickly, a straighter surface coverage can usually be expected. In a comparison of fabric groups 4, 5 and 6, this trend is present in all fabrics. If the mesh size decreases, the kinetic term increases significantly, and the surface coverage approaches 0. The conclusion from [6] that a very good surface cleanability is given with kinetic values of > 3 can be confirmed and corrected downwards using meshes no. 21 and 22. With metal fabrics, a surface movement of $\leq 5\%$ can already be expected with kinetic values of ≥ 0.94 .

Table 6: Overview of the variables "kinetics γ_{Kinetic} " and "final contamination degree β " for the equation presented in Eq. 23 and [6] to approximate the cleaning process in nozzle-assisted surface cleaning.

Group	Filter cloth	Kinetic / $\text{cm}^2 \cdot \text{ml}^{-1}$	Final contamination degree / -
4	No.12: 153 μm	0.43	0.33
	No.13: 122 μm	0.64	0.14
	No.14: 73 μm	0.94	0.05
	No.15: 45 μm	1.40	0.03
5	No.16: 182 μm	0.68	0.19
	No.17: 82 μm	1.57	0.05
	No.18: 47 μm	1.81	0.02
6	No.19: 74 μm	0.90	0.16
	No.20: 40 μm	1.44	0.04
	No.21: 20 μm	2.97	$3 \cdot 10^{-3}$
	No.22: 10 μm	3.37	$3 \cdot 10^{-3}$

Chapter 5

5. Conclusion and outlook

The focus of the research is the identification of essential regeneration parameters in the cleaning of technical surfaces, especially filter fabrics, from adhering filter cake. For this purpose, a distinction is made between "filter cake removal with and without aids".

For discharge without aids, a backwashing filter system was designed and constructed on a laboratory scale in order to be able to investigate the discharge process. The quantification of the discharge quality was carried out using imaging and gravimetric methods. An important point is to distinguish between "filter cake discharge in liquid phase" and "filter cake discharge in gas phase". Both processes follow different mechanisms, which is elaborated and discussed in [4]. In the following subchapter 5.1. Conclusion, the highlights of these publications are presented in summary form.

A cleaning system was developed for cleaning the surface with aids, which enables the automated cleaning of the surface by coupling image evaluation and a mechanically adjustable nozzle lance. The quantification of the nozzle cleaning is carried out by means of a BaseCase and is related to the specific cleaning agent expenditure normalised to the filter surface. In this way, the cleaning characteristics of different fabrics and nozzles could be described and approximated by means of a two-parameter model. The process of automated cleaning, i.e. the coupling of image evaluation and mechanical cleaning unit, as well as the parameter study are elaborated and documented in [5,6].

After successful cake discharge, it is conceivable that the fabric undergoes further cleaning according to the mechanisms presented in [147,174]. In this way, in addition to the built-up filter cake, which represents the main pressure loss during cake-forming filtration, remaining particles on and in the fabric are also removed. The necessity of this process must be evaluated for the respective process.

The results of the research from [1–6] are summarised in the subchapter.

5.1. Conclusion

The results elaborated within the framework of the research project and their impact on the application of cleaning technical surfaces with and without aids are summarised accordingly in the subchapters of chapter 4 and the impact of the results is subsequently assessed.

I. Backwashing properties of candle filters as a function of the particle system in liquid phase

Using the laboratory candle filter shown in chapter 3 (Figure 12, page 38), the filter cake discharge was assessed without any aids. For this purpose, the backwashing properties of the filter cake thickness and the backwashing pressure of seven particle systems with different particle shapes, particle sizes and mineralogy were investigated on a multifilament fabric with a mesh size of 20 μm . As an aid, the discharge was evaluated by means of image analysis. An essential evaluation criterion is the assessment of the type of discharge. For this purpose, four different possibilities of filter cake discharge were worked out:

- | | |
|--------------------------------------|--------------------------------------|
| I. Complete discharge, | III. Incomplete, bad cake discharge, |
| II. Incomplete, good cake discharge, | IV. Resuspended discharge. |

Complete (cake) discharge (I) describes the removal of the filter cake from the filter fabric as a cohesive whole and is characterised by very good surface cleanliness. In this case, the cohesion in the cake is sufficiently pronounced so that no break-up of the filter cake can be observed because of the downward weight force of a partial section of the filter cake. Incomplete, good cake discharge (II) also provides good to very good surface purity. In this case, the filter cake breaks up, but the fragments are large enough to overcome the adhesion and the filter cake slides off the fabric surface. Because of this rupture, a higher specific backwashing volume is required. Insufficient surface cleanliness is provided by Incomplete, bad cake discharge (III) and resuspension of the filter cake (IV). In both cases, the cohesion is not sufficiently pronounced due to an insufficient filter cake thickness, which leads to many cracks in the cake during backwashing. These are then preferentially flowed through, resulting in insufficient cake discharge. Both types of discharge are characterised by a low degree of regeneration / high surface coverage with a high specific backwashing volume. This is particularly critical to consider, as filtration concepts such as intermittent cake filtration [87] aim for short filtration periods with subsequent backwashing but rely on a high degree of regeneration. Taking the regeneration quality into account, this process can therefore only be carried out for particle systems with very cohesive particle layers.

When varying the backwashing pressure in the technically relevant range of 0.1 to 2 bar, it can be observed that the pressure only influences the regeneration time, but not the backwashing volume. Higher pressures therefore lead to a shorter backwash, which is, however, negligible in the context of the filtration time [183]. The quality of the filter cake discharge increases with the filter cake thickness and tends to be better suited for particle systems with higher specific filter cake resistance. The total resistance of the filter cake has been found to be the sum

parameter. This includes variables such as porosity, which is indirectly related to the particle shape and the contact points in the cake structure. It was found that from a total resistance of the filter cake of $5 \cdot 10^{10} \text{ m}^{-1}$ a complete discharge, with a specific backwashing volume of $< 2 \text{ l} \cdot \text{m}^{-2}$, can be observed. The transfer between the particle systems is possible by dividing this total resistance by the respective specific filter cake resistances and directly provides the cake thickness to be aimed at. Here it is clear that the regeneration of this multifilament fabric is cohesion dominated. The transfer to other tissues was carried out in a follow-up study.

II. Backwashing properties of candle filters as a function of the filter fabric in liquid phase
When the investigation was extended to include different types of fabric [2], it was found that other multifilament fabrics $\leq 20 \text{ }\mu\text{m}$ also exhibit the same backwashing behaviour as in [1]. The total resistance of the filter cake of $\geq 5 \cdot 10^{10} \text{ m}^{-1}$ has proven to be a good transfer parameter here. An orthorhombic particle system with the largest specific cake resistance had the smallest necessary cake thickness, while an acicular particle system had the largest necessary cake thickness with the smallest specific cake resistance. For transfer to other multifilament fabrics, this transfer criterion can be applied to fabrics with mesh sizes below $20 \text{ }\mu\text{m}$.

When this model is extended to monofilament fabrics, an exactly opposite behaviour to the multifilament fabrics can be observed. Here, the orthorhombic particle system has the largest cake thickness and the needle-shaped particle system the smallest. Accordingly, there must be a different occupation behaviour of the tissue surface. Using the different deposition mechanisms in and on the tissue according to chapter 2.2, it became clear that tissue with an increased risk of bleeding and pore clogging requires a thicker cake thickness for good discharge. This is due to the higher interaction forces between the particles. Particles which, due to their shape and size, lay clearly on the meshes require a smaller cake thickness. Here, the discharge is adhesion-dominated and associated with the particles remaining in the mesh. Evaluation of many filter tissue – particle – contaminations allowed the development of a prediction model based on filter media resistance (Eq. 25). Determined according to VDI guideline 2762-2 with a particle system with clean surface deposition, divided by the specific cake resistance of the particle system to be discarded and a particle shape-dependent factor. This made it possible to create a prediction model for the group of monofilament fabrics as well [2]. Extending this model to metal fabrics confirmed this predictive model and refined the form factor (see chapter 4.3, page 47).

III. Effects of the bulging behaviour of the filter fabric during the backwashing procedure in liquid phase

During backwashing in liquid phase, it can be clearly seen that a deformation of the filter fabric takes place before the filter cake is thrown off. This is even more pronounced the more filigree the filter fabric used is. First calculations of the necessary liquid volume have shown that a substantial part of the necessary backwashing volume goes into the bulging of the filter fabric (50-60%; see IGF project 18591 N). Consequently, not only the backwashing tank becomes larger, but also the time needed to fill it during filtration (increase in filtrate holdup). For this reason, a study was conducted to calculate the bulge based on elementary mechanics and how it can be reduced. As a result, a geometrical moment of inertia of filter fabrics was determined, which allows the description of the bulge behaviour. Based on this, the spacing of the filter elements can also be adapted to the bulging behaviour of the filter fabric. In the technically relevant range for backwashing filtration (low pressure with moderate pretensioning of the filter fabric), a surface moment of inertia of $10^4 - 10^5 \text{ mm}^4$ can be expected. The bulging of the fabric is equated to that of a bending beam clamped on both sides. The highly anisotropic force-elongation behaviour of filter fabrics must be considered. It applies that the more stable fibre direction (warp or weft direction) is to be placed on the shorter filter geometry (superposition principle). This can further reduce the bulging behaviour. Also helpful is a certain pretensioning of the fabric. However, care must be taken here to ensure that the pretensioning and the acting force do not lead to plastic deformation of the fabric during straining. [3]

While bulging of the tissue occurs as a side effect to be "endured" during backwashing in the liquid phase, this is essential for success during backwashing by a gas pulse. Both regeneration variations have different characteristics and are therefore the subject of further investigation [4].

IV. Backwashing properties of candle filters in gas phase

In addition to backwashing in liquid phase, which often takes the role of a thickener and/or liquid clarifier in the process, this application also takes place as filter cake discharge in gas phase. The selection of the appropriate regeneration step is usually directly linked to the role of the value product. While in the former case the focus is on the liquid phase, in the case of discharges into the gas phase the particle system is often regarded as the value-added product. For this reason, in addition to a high degree of separation efficiency of the fabric, the cake must be discharged as completely as possible. Remaining particles on the tissue are to be interpreted

as bound capital and minimised if possible. For this reason, cake discharge in the gas phase was investigated separately from discharge in the liquid phase and compared with each other.

In contrast to discharge in liquid phase, discharge in gas phase is highly dependent on the backwashing pressure. Like the discharge of the filter cake after gas filtration, there are only two types of discharge:

- Complete discharge,
- Incomplete cake discharge.

Complete discharge describes the complete removal of the filter cake from the surface and is the counterpart to complete discharge in the liquid phase. In the case of incomplete discharge, which is also referred to as "patchy cleaning" in gas filtration [101,102], residual contamination remains on the surface and reduces the efficiency of the regeneration. A further distinction as in liquid backwashing is not possible due to the acting forces.

A clear difference between gas and liquid discharge is the pressure dependency during discharge in gas phase, which is like a pressure pulse. This can be seen in the horizontal movement of the filter cake during regeneration (see Appendix H, page 98). This force vector is not visible during discharge in liquid phase. Accordingly, fabrics that allow more movement in front of the filter cake are much easier to clean. Light, stretchable filter fabrics whose fabric diameter is ideally significantly larger than the diameter of the filter element (larger acceleration path) are therefore recommended for gas discharge. The inertia of the filter cake also plays a role. Thicker cakes have a higher inertia. Once the mass of the cake is accelerated, this leads to a larger amount of cake being thrown off [100]. Accordingly, this also applies to a larger specific cake mass. Care must be taken to ensure that the saturation falls below a maximum value (25 %), otherwise no discharge can take place due to the large liquid bridge forces [190]. It can also be observed that very thick filter tissues of low elasticity (for fine meshes significantly satin tissues) are poorly or not at all suitable for discharges into the gas phase. Here, oversizing the diameter of the filter bag compared to that of the filter element is necessary for successful regeneration of rigid filter tissues.

V. Surface cleaning of filter fabrics in chamber filters by automated and demand-controlled nozzle cleaning

The chamber filter shown in chapter 3.5 (Figure 13) was used to assess the filter cake discharge with aids. The difference to the previous investigations is that the cleaning is now directed at a defined area of the surface to be cleaned. This is realised by a nozzle system which is coupled with an image evaluation in order to specifically remove remaining impurities on the tissue

surface. This cleaning is used to remove remaining cake fragments from the chamber elements after the actual discharge of the filter cake. A transfer to other systems for surface cleaning of remaining adhesions is therefore possible without any problems and allows an expansion of the system to applications in the field of chemical, food and pharmaceutical process engineering. When varying the process variable cleaning pressure in the technically relevant range of 5 to 8 bar, only a slight pressure dependency of the cleaning result was found. This must be viewed critically, as strongly adhering contaminants, as well as contaminants in the fabric (intra-cloth contamination), must be removed with higher cleaning effort / cleaning pressure [181,191]. This requires higher intensities of the cleaning jet on the surface and the possibility of rewetting in case of adhering contaminations [97]. Here, the duration of action has been found to be a strong variable in cleaning adherent contaminants. This can also be realised by varying the nozzle distance. A large influence was found with a variation of this process variable. This is also due to the automated generation of coordinates for the approach of the contamination. A smaller distance is characterised by a smaller covered area / effective area by the nozzle and accordingly leads to an increase in the points to be approached and thus the specific cleaning agent requirement. A difference can also be observed between the nozzle types. For the study, similar nozzles were selected regarding the flow rate, with different jet profiles, full-cone, flat-jet and full-jet nozzles. Because of this study, full-jet and flat-jet nozzles are particularly recommended. With a suitable choice of nozzle and coordinate generation, it was possible to save cleaning agent in the range of 30 to 60 % compared to a conventional base case. [5]

An essential investigation is the variation of filter fabrics for cleaning. For this purpose, polymer-based monofilament fabrics (group 1 and group 2) of different weave and decreasing mesh size were compared and evaluated with the same variation of multifilament fabrics (group 3). There was a clear trend towards decreasing surface coverage with decreasing mesh size [6]. The results were extended and confirmed with metal meshes (group 4 to 6). One explanation is the smoother surface of meshes of finer mesh size. Calendering did not lead to improved surface cleanliness. The multifilament fabrics performed best in terms of surface cleanliness and specific cleaning agent requirements. Here, the conclusion to backwashing filtration is possible, as these fabrics are cohesion-dominated, and adhesion plays a minor role in cleaning. The mathematical description of the cleaning process using a first-order regressive model allows the comparison of the investigated fabric-nozzle combination based on a cleaning kinetic and final contamination degree (Eq. 23, page 39). Here, an extension of this matrix to include further contaminants is conceivable. In this way, a future selection of the nozzle for

cleaning purposes can be determined based on the cleaning task instead of the fluid mechanical parameters of the nozzle.

5.2. Outlook

The models developed for backwashing filtration in [1,2] provide initial possibilities for predicting the backwashing regeneration and its quality on the basis of sum parameters and empirically determined factors. In [1,4], following [100,146,159], measurements for the characterisation of the acting forces of adhesion and cohesion are already included. The long-term goal is to replace the sum parameters of the flow resistances by the acting forces based on a force balance. First tendencies are shown in [1,4], but the connection of adhesion and cohesion is difficult, because particle influence in the shear planes, especially in the adhesion measurement, can strongly change the result. High standard deviations are the consequences. Here, a refinement of the measurement method with the fabrics used is recommended as the next step. However, the focus may be on a simple and practicable measurement method, analogous to the determination of flow resistance, for predicting regeneration quality.

In the course of this, the test matrix can be expanded to include filter cloth, also of coarser mesh size. This raises the question of how the filter cake is discharged with filter fabrics of coarser mesh size and at what point the cake is discharged automatically by the weight of the filter cake as a result of the decreasing adhesion force with coarser particle systems. A reduction of the mesh size is also conceivable, if this is possible in the future from a weaving technology point of view. Tests already carried out with fine and low-porosity fabrics, which lead to fabric resistances $R_{FM} \geq 10^{11} \text{ m}^{-1}$, have proved difficult to regenerate. Backwashing for membranes is also an issue and has already been investigated for hollow fibre membranes [192,193]. Investigation of the backwashing behaviour of membranes is recommended, in view of the growing areas of application. The experimental setup presented in chapter 3. is suitable for this purpose and can be used to conduct experiments and collect data.

Further developed backwashing concepts for reducing the backwashing volume or reducing the system periphery of the backwash concept are also a possibility for optimising this process. In the case of cleaning, pulsation flow has proven to be an adjusting key for reducing the backwashing volume [147]. Applications in cake discharge need to be further investigated. Shock wave technology has also been shown to be suitable for cleaning surfaces [194]. The transfer to cake discharge is also conceivable. Finally, a holistic consideration of the regeneration process, i.e. the coupling of cake removal with intra-cloth cleaning, should take place in future. By combining the results contained in this paper [1,2,4] in conjunction with the

cleaning of individual particles [147,174], an optimal cleaning of the filter fabric should take place. Validation must then be carried out by describing particles remaining in the fabric.

The automated cleaning of filter fabrics with aids can also be further optimised, following the example of CNC machines from manufacturing technology. Equipped, for example, with a tool turret that intelligently adapts the cleaning unit to the contamination. The connection with an AI that recognises this independently paves the way for a completely autonomous Industry 4.0.

Appendix

A. Darcy equation via Navier-Stokes equation

The Darcy equation applies to laminar, slow flow, which is why turbulence is also negligible and only must be considered for high volume flows and/or compressible fluids. The Darcy equation is then extended by a turbulence term, analogous to the Forchheimer or Ergun equation. For aggregate structures through which fluid flows, the pressure loss is mainly generated by viscous friction $\eta \cdot \Delta v_x$. The flow through a porous structure can, in addition to the framework conditions of laminar and slow flow, also be considered as taking place in one direction and with a constant volumetric flow over the cake length. This reduces the Navier-Stokes equation to the following terms [195,196]:

$$\rho \cdot \frac{dv_x}{dt} = -\frac{\partial p}{\partial x} + \eta \cdot \Delta v_x + f_x \quad (\text{I})$$

Since the Darcy equation deals with the steady-state flow of a porous bed, the time derivative $\frac{d}{dt}$ is zero. This simplifies the Navier-Stokes equation to the simplified Stokes equation. The gravitational acceleration f_x (external forces) can also be defined as negligible in a first approximation. This changes (I) into the following form:

$$\frac{\partial p}{\partial x} = \eta \cdot \Delta v_x \quad (\text{II})$$

By expressing the Laplace operator by means of a second-order permeability tensor under the assumption of constant viscous friction [30] and the porosity of the present bulk ϕ , (II) can be rewritten as $\Delta v_x = -\frac{\phi \cdot v_x}{k_{xy}}$:

$$\frac{\partial p}{\partial x} = -\frac{\eta \cdot \phi \cdot v_x}{k_{xy}} \quad (\text{III})$$

Neglecting the flow orthogonal to the direction of flow, this term can be transformed into the well-known Darcy equation for a defined pressure difference along the length of the porous bed H and the flow velocity as volume flow \dot{V} through the unit area. The permeability is to be understood as the reciprocal of the flow resistance.

$$\Delta p = \frac{\eta \cdot \dot{V}}{k \cdot A} = \frac{R \cdot \eta \cdot \dot{V}}{A} \quad (\text{IV})$$

B. Hermans & Bredée – Derivation

Differential equation of cake filtration ($q=0$) at constant pressure ($\Delta p = \text{const.}$) according to Hermans and Bredée:

$$\frac{d^2 t}{dV_F^2} = K \cdot \left(\frac{dt}{dV_F}\right)^q \quad \rightarrow \quad \frac{d^2 t}{dV_F^2} = K \quad \text{(I)}$$

Solving the differential equation yields:

$$\frac{d}{dV_F} \cdot \frac{dt}{dV_F} = K \quad \rightarrow \quad d\left(\frac{dt}{dV_F}\right) = K \cdot dV_F \quad \text{(II)}$$

$$\frac{dt}{dV_F} = K_1 \cdot V_F + K_2 \quad \rightarrow \quad dt = (K_1 \cdot V_F + K_2) \cdot dV_F \quad \text{(III)}$$

$$t = 0.5 \cdot K_1 \cdot V_F^2 + K_2 \cdot V_F + K_3 \quad \text{(IV)}$$

With the boundary condition $V_F(t=0) = 0$ applies:

$$K_3 = 0 \quad \text{(V)}$$

$$\frac{t}{V_F} = 0.5 \cdot K_1 \cdot V_F + K_2 \quad \text{(VI)}$$

From a coefficient comparison it follows for the filtration equation:

$$\frac{t}{V_F} = \frac{0.5 \cdot \alpha_{FC} \cdot \eta \cdot \kappa}{A^2 \cdot \Delta p} \cdot V_F + \frac{R_{FM} \cdot \eta}{A \cdot \Delta p} \quad \text{(VII)}$$

$$\text{follows: } K_1 = \frac{\alpha_{FC} \cdot \eta \cdot \kappa}{A^2 \cdot \Delta p} \quad \text{und: } K_2 = \frac{R_{FM} \cdot \eta}{A \cdot \Delta p} \quad \text{(VIII)}$$

Should the filtration take place at constant volume flow, the differential equation changes as

$$\text{follows: } \frac{d(\Delta p)}{dV_F} = K \cdot (\Delta p)^q \quad \text{(IX)}$$

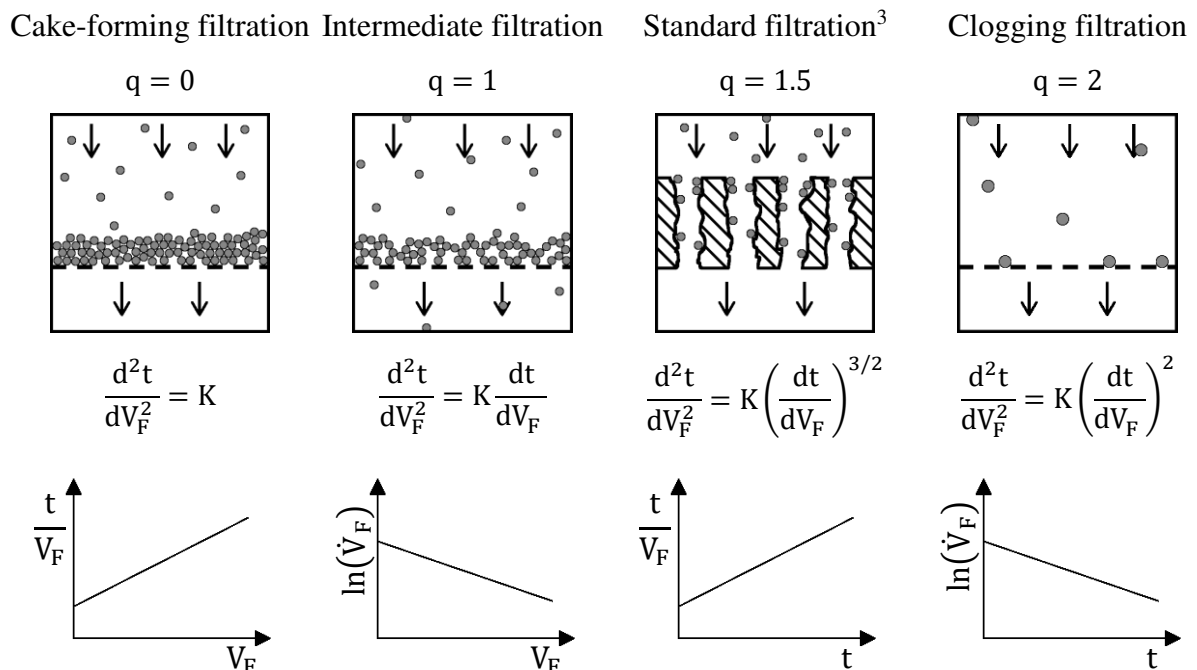


Figure based on the separation mechanisms of [37].

³ Also known as depth filtration

C. Filter Equation – Derivation

The effective flow resistances R can be differentiated into the time-dependent or filtrate volume-dependent filter cake resistance R_{FC} and the filter medium resistance R_{FM} . The former can also be expressed by the specific cake resistance and the cake thickness. Due to the interactions between the particle system and the fabric, the filter medium resistance at the beginning of filtration is also referred to as the initial resistance $R_{F,0}$, which is highly dependent on the particle system and how it is deposited on/in the meshes of the fabric.

$$R = R_{FC}(t) + R_{FM} = \alpha_{FC} \cdot H_{FC}(t) + R_{FM} = \alpha_{FC} \cdot H_{FC}(t) + R_{F,0} \quad (I)$$

To distinguish the filtration guide in constant pressure $\Delta p = \text{constant}$ and constant volume flow $\dot{V}_F = \text{constant}$ is the introduction of the volume ratio of the filter cake and the filtrate volume, which is denoted as κ .

$$\kappa = \frac{V_{FC}(t)}{V_F(t)} = \frac{H_{FC}(t) \cdot A}{V_F(t)} = \text{const.} \quad (II)$$

This enables the transfer into a straight-line equation with which the process constants "specific cake resistance α_{FC} " and "filter medium resistance R_{FM} "/"initial resistance $R_{F,0}$ ", can be determined.

$$\Delta p = \frac{\left(R_{FM} + \frac{\alpha_{FC} \cdot \kappa \cdot V_F}{A}\right) \cdot \eta}{A} \cdot \frac{dV_F}{dt} \quad (III)$$

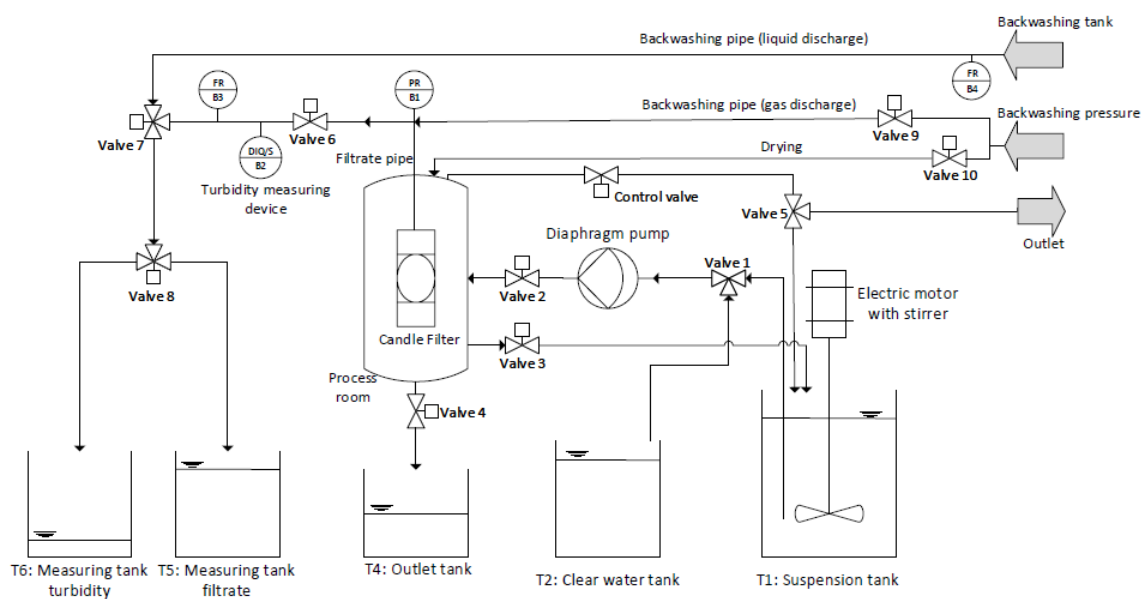
$$\begin{aligned} \frac{t}{V_F} &= a_0 + a_1 \cdot V_F \\ \Delta p = \text{constant:} \quad \frac{t}{V_F} &= \frac{R_{FM} \cdot \eta}{A \cdot \Delta p} + \frac{0.5 \cdot \alpha_{FC} \cdot \eta \cdot \kappa}{A^2 \cdot \Delta p} \cdot V_F \end{aligned} \quad (IV)$$

$$\begin{aligned} \Delta p &= a_0 + a_1 \cdot t \\ \dot{V}_F = \text{constant:} \quad \Delta p &= \frac{R_{FM} \cdot \eta \cdot \dot{V}_F}{A} + \alpha_{FC} \cdot \eta \cdot \kappa \cdot \left(\frac{\dot{V}_F}{A}\right)^2 \cdot t \end{aligned} \quad (V)$$

The third operating principle is the simultaneous change of flow rate and pressure $\dot{V}_F = f(\Delta p)$, which can only be solved numerically.

D. Backwashing filter – Detailed R & I - flow diagram

The simplified experimental set-up of the backwashing filter from Figure 12 (page 38) is shown in detail in this appendix, following the rules for the presentation of R & I flow diagrams. The experimental set-up includes a suspension tank (T1) for receiving the particle solution. This is pumped into the process chamber by a diaphragm pump via valve 1 and valve 2. Here, filtration takes place via the candle filter. The process chamber is flooded, and the filtration pressure is set via the control valve, a continuously adjustable valve. For this purpose, the suspension flows back into the suspension tank via valve 5. After the pressure has been set, valve 6 opens and filtration begins. The turbidity is first collected separately in tank T6 for subsequent analysis. Once this turbidity blow is over, valve 8 can be used to switch over to filtrate measurement. Here a defined volume is filtered according to chapter 3.4. This is followed by regeneration. For this purpose, valve 1 is used to switch to the clear water tank T2 and displace the suspension in the process chamber. This allows visual observation of the regeneration. To prevent dilution of the suspension, valve 5 is also switched over. In this way, the clear water flows directly out of the system at the head of the process chamber. If the filter candle is visible, the backwash pipe can be changed by switching valve 7. Now backwashing fluid flows through the mesh against the direction of the filtrate and removes the cake. For this purpose, the pump is switched off. The discharged cake can be removed from the system by means of valve 4. For backwashing by gas, valve 10 is opened first and the cake is dried through the usual filtrate line. At the same time, the process chamber is freed from suspension by valve 3. After a set drying time, the gas pulse is initiated by opening valve 10 and closing valve 6. The cake discharge is initiated and can be evaluated gravimetrically.



E. Statement from the copyright conditions of Elsevier

The publications presented below [1-6] are in accordance with the copyright guidelines of the publisher Elsevier. Here is an excerpt from Elsevier's copyright conditions (accessed online on 16 January 2021 at www.elsevier.com/about/policies/copyright#Author-rights):

Personal use

Authors can use their articles, in full or in part, for a wide range of scholarly, non-commercial purposes as outlined below:

- Use by an author in the author's classroom teaching (including distribution of copies, paper or electronic)
- Distribution of copies (including through e-mail) to known research colleagues for their personal use (but not for Commercial Use)
- **Inclusion in a thesis or dissertation (provided that this is not to be published commercially)**
- Use in a subsequent compilation of the author's works
- Extending the Article to book-length form
- Preparation of other derivative works (but not for Commercial Use)
- Otherwise using or re-using portions or excerpts in other works

These rights apply for all Elsevier authors who publish their article as either a subscription article or an open access article. In all cases we require that all Elsevier authors always include a full acknowledgement and, if appropriate, a link to the final published version hosted on Science Direct.

F. Attached publication [1]

Verification of the contribution from the co-authors

Title: Factors influencing backwashing operation in the liquid phase after cake filtration

Journal: Chemical Engineering Science

Authors: P. Morsch, P. Ginisty, H. Anlauf, H. Nirschl

Position in the dissertation:

The content of this paper has been included in Chapter 4.1 and 5.1

Contribution of Patrick Morsch

- Conceptual design and construction of the backwash system, as well as planning of the test procedure.
- Execution of backwash tests and data evaluation.
- Summary of the data and evaluation of the results.
- Writing the chapters and performing the source research.

Contribution of Pascal Ginisty

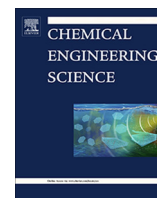
- Provision of a force gauge (penetrometry). Support of the work by strength measurements within the framework of a cooperation between IFTS and KIT.

Contribution of Harald Anlauf

- Support of the work by references in literature, test setup, test procedure. Proofreading of the paper (technical).

Contribution of Hermann Nirschl

- Support of the work by references in literature, test setup, test procedure. Proofreading of the paper (technical).



Factors influencing backwashing operation in the liquid phase after cake filtration



Patrick Morsch^{a,*}, Pascal Ginisty^b, Harald Anlauf^a, Hermann Nirschl^a

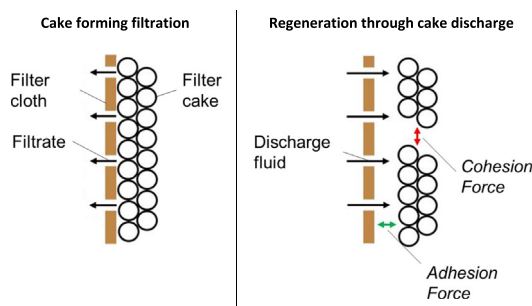
^a Karlsruhe Institute of Technology (KIT), Institute for Mechanical Process Engineering and Mechanics – Process Machines, Strasse am Forum 8, 76131 Karlsruhe, Germany¹

^b Institut de la Filtration et des Techniques Séparatives (IFTS), CEOPS/Centre d'Etudes-Optimisation des Procédés de Séparation, Rue Marcel Pagnol, 47510 Foulayronnes, France²

HIGHLIGHTS

- Surface cleanness is independent of the backwash pressure (constant backwash volume).
- The cleaning result improves with increasing cake thickness.
- The particle shape has a significant influence on the required cake thickness.
- Particle systems with high specific flow resistance require thinner cakes.
- The required cake thickness for good regeneration depends on total flow resistance.

GRAPHICAL ABSTRACT



ARTICLE INFO

Article history:

Received 20 May 2019

Received in revised form 20 November 2019

Accepted 22 November 2019

Available online 27 November 2019

Keywords:

Regeneration filter
Backwashing filter
Filter cake discharge
Liquid discharge
Filter cake thickness
Cohesion
Adhesion

ABSTRACT

The separation of solids from process streams takes place in almost every process plant. In particular, cake-forming filtration in the liquid environment is advancing as a widespread method of separating low-concentration suspensions from their solids content and offers energy advantages over other separation principles. In addition to the actual separation performance, the filter fabrics must be regularly replaced or regenerated. The reason for this is the growing resistance because of the increasing filter cake thicknesses. Considering the reduction of disposable products, the regeneration of the fabrics is an interesting possibility to reduce costs and to guarantee a stable process control. This can be achieved by means of filter cake discharge. In the course of this regeneration, the filter cake should be discharged as completely as possible so that the fabric reaches the required initial filtrate flow of the previous filtration cycle again.

Investigations concerning cake discharge have shown that the regeneration step can be divided into different discharge mechanisms (complete, partial, resuspended) which result in different cleaning qualities. In the context of this study, backwashing processes with different backwashing parameters (pressure, cake thickness) as well as different particle shapes and their influence on the regeneration quality of filter fabrics are presented and discussed.

The focus of this work is the investigation of the backwashing process “cake discharge” as a subsequent and necessary step in cake-forming filtration. Within the scope of this study, a test setup was designed which allows the variation of different process variables and tissue-particle combinations. The experimental setup is kept simple and allows easy reproduction of experiments. The aim is the integrated consideration of the influencing variables on the regeneration quality. The variables cake thickness, particle shape and backwash pressure were investigated within the scope of this study.

* Corresponding author.

E-mail addresses: patrick.morsch@kit.edu (P. Morsch), pascal.ginisty@ifts-sls.com (P. Ginisty), harald.anlauf@kit.edu (H. Anlauf), hermann.nirschl@kit.edu (H. Nirschl).

¹ Web: www.mvm.kit.edu.

² Web: www.ifts-sls.com.

A significant influence of backwash quality on the examined multifilament filter fabric for particle systems $\leq 20 \mu\text{m}$ can be attributed to the particle shape and filter cake thickness. Here, a good regeneration quality can be achieved after exceeding a defined filter cake resistance. This depends significantly on the specific filter cake resistance and thus determines the required cake thickness. Particle systems which, due to their shape and size, have a lower specific cake resistance therefore require a higher cake thickness for a good cleaning result. As a rule of thumb, the absolute filter cake resistance can be estimated with $\geq 4 \cdot 10^{10} \text{ m}^{-1}$. A possible influence of the backwash pressure was investigated and can be denied in the range of 0.1–2 bar. The necessary backwash volume in l/m^2 was constant over this pressure range. Only the regeneration time decreased, which, relative to the filtration time, is considered insignificant.

© 2019 Elsevier Ltd. All rights reserved.

Nomenclature

$\Delta p_{\text{Backwash}}$	pressure difference [bar]	$\dot{V}_{\text{regen.}}$	minimum filtrate flow before regeneration [m^3/s]
ΔV_A	difference between initial filtrate flows [m^3/s]	$x_{50, 1}$	length-related modal value of particle distribution [m]
A	filter surface [m^2]	$x_{50, 3}$	mass/volume-related modal value of particle distribution [m]
D	diameter of penetration die [m]	α_H	specific flow resistance [$1/\text{m}^2$]
H_{FC}	filter cake thickness [m]	ε	porosity [–]
L	length of penetration depth [m]	η	dynamic viscosity [Pa s]
S_V	specific surface [m^2/m^3]	κ	concentration value [–]
$t_{\text{regen.}}$	filtration time at regeneration start [s]	μ	flow factor [–]
\dot{V}_A	initial filtrate flow [m^3/s]	$\tau_{\text{Penetration}}$	penetration resistance of filter cake [mN/mm^2]
V_f	volume [m^3]		
ΔV_f	filtrate flow [m^3/s]		

1. Introduction

In industrial solid/liquid separation, the removal of fine particles ($\leq 10 \mu\text{m}$) from a suspension with a low solids content (0.01–1 v/v %) is a challenging and demanding task. The reasons are the compressibility of filter cakes consisting of fine particles, the high flow resistance, and bleeding through the meshes/pores. This separation task can be found in a wide range of production and treatment. Examples are the filtration of lacquer, hydraulic fluid, wastewater, and many areas in the automobile industry. Apart from the different geometries of filter elements and types of filter cloth, the required purity is the main challenge of solid/liquid separation. Many types of filters are available, which are based on different separation mechanisms. A particular focus should be placed on cake filtration with the associated flow resistance inside the built-up filter cake. Flow resistance can be described by the already known Carman-Kozeny equation. Filters based on cake separation mechanism have to be regenerated regularly, because the filter cake decreases the volumetric flow and/or increases the filtration pressure depending on the operation mode of the filtration process (Rushton et al., 2008).

To reduce the impact of this physical behavior, the filter cake should be removed regularly. This can be achieved by removal with and without discharge support. Examples of discharge-supported cake removal systems are vacuum, scraping, and nozzle systems. The basic principle of these systems is “removal through local and defined forces” from the upper surface of the filter cake. This requires additional mechanical and electronic equipment within a regular filter system. Systems without discharge support also require a detachment force. However, this force is provided by a fluid stream and not by a mechanical discharge aid. An example of such filter systems is the regular backwashing filtration system. This type of filter starts regeneration with an inverted flow through the filtrate outlet. During this process, the filter cloth is permeated by the backwashing fluid and the filter cake is detached. Then, the filter cake discharges and a subsequent filtration cycle

can start. Such kind of backwashing filters can be used in gas and liquid filtration, with subsequent regeneration occurring in gas and liquid phases. The focus of this study is the regular backwashing operation for filtration and regeneration in the liquid phase. In this context, the influence of filter cake thickness, particle shape, and backwashing pressure will be discussed.

2. Mechanisms of filter regeneration

In case of cake filtration with a constant filtration pressure, filtrate flow \dot{V} decreases with increasing filter cake thickness. This is a result of the separated particles on the surface of the filter cloth. Particle separation depends on particle concentration inside the suspension and causes the filtrate flow to decrease as a function of time t . Hence, periodical regeneration at defined times $t_{\text{regen.}}$ during cake filtration is required for a stable process. During cake filtration, the selected filter will be used (semi-)discontinuously and the “filtration” process is just as important as the subsequent “regeneration” of the filter cloth. In case of an improperly regenerated filter, the intervals between the filtration processes will become shorter. This is reflected by the decrease of the initial filtrate flow \dot{V}_A over the filtration periods ($\Delta \dot{V}_A$) to a minimum filtrate flow ($\dot{V}_{\text{regen.}}$) requiring regeneration. This behavior is presented by the filtrate flow – time plot in Fig. 1. For a properly regenerated filter (a), filtrate flow at the beginning of each step is equal. In case of an improperly regenerated filter (b), however, the initial filtrate flow decreases. (Rushton and Griffiths, 1972)

Obviously, there is a considerable potential for improvement in many industrial cases. A properly regenerated filter cloth highly depends on the interaction between the particle system and the filter cloth (weave type, thread thickness, material) (Müller et al., 1987). In order to guarantee removal of the filter cake, the applied removal force has to be higher than the adhesive forces. To remove the filter cake in large fragments, the removal force also has to be

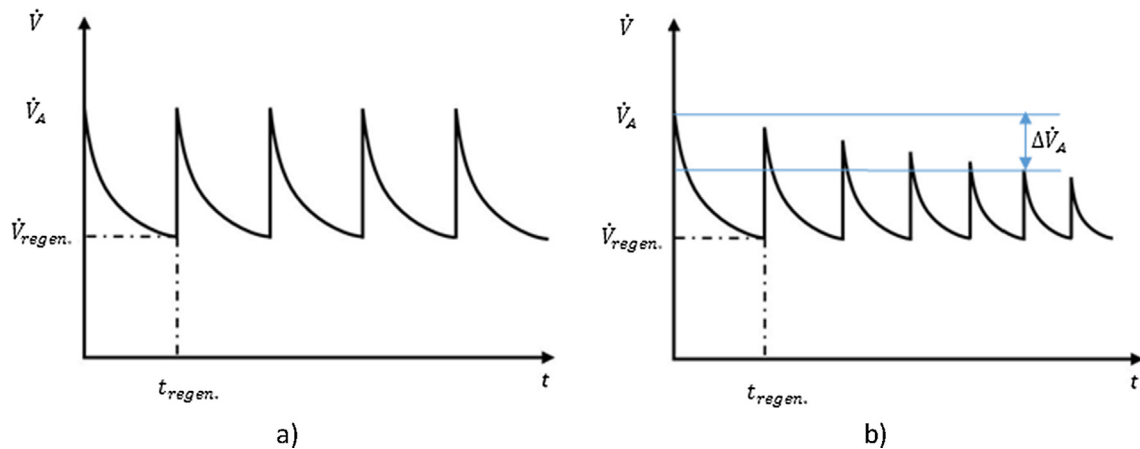


Fig. 1. Filtrate flow-time diagrams and schematic representation of process management with a properly regenerated filter cloth (a) and an improperly regenerated filter cloth (b).

lower than the cohesive force. Both conditions are summarized by the following inequations:

- Detachment force > Adhesion on filter cloth (F_A)
- Detachment force < Cohesion in filter cake (F_C)

These two forces depend on process conditions, such as the porosity of the filter cake (Morris et al., 1987; Charleton and Heywood, 1983). Fig. 2a) schematically shows the discharge of a filter cake with these two forces. The resulting cloth surface when the conditions are not met is shown in Fig. 2b). In this case, some filter cake fragments remain on the filter cloth surface and decrease the filtrate flow at the beginning of the subsequent filtration cycle, as is shown in Fig. 1b).

The regeneration of a filter cloth is determined by the process conditions during filtration and should require a short time compared to the whole filtration process (Ripperger, 2008). Regeneration of such a filter cloth by backwashing treatment is based on the experience of the industrial user and/or requires constant tests to determine the backwashing pressure and volumetric flow required for a well-cleaned filter cloth. This may sometimes lead to an increased backwash volume or to a poorly cleaned filter cloth. A higher backwash volume increases the filtrate residence time and requires a corresponding plant design, whereas a poorly cleaned filter cloth directly decreases the process performance. Current literature only refers to improving the filter by decreasing surface roughness and provides no information about the required regeneration process conditions (Rushton et al., 2008; Müller et al., 1987). In addition, cake removal mainly covers “dry cake removal” into a gas phase without any method to define the backwash

process conditions (Rushton et al., 2008; Charleton and Heywood, 1983). Research in the past few years focused on the cleaning behavior of a filter centrifuge (Stahl et al., 2013; Stahl et al., 2008) or regeneration of the filter cloth by removal of single adhering particles with different kinds of flow mechanisms (Weidemann et al., 2014; Leipert and Nirschl, 2012; Burdick et al., 2005). For water treatment and sand filters for depth filtration, the focus was placed on liquid discharge after liquid filtration (Fitzpatrick, 1998; Amirtharajah, 1985). However, a catalog of measures for the regeneration of filter cloths with cake discharge in backwash treatment is still lacking. Necessary regeneration parameters such as backwash pressure and backwash volume depending on different filter cloth-particle combinations have not been investigated. Potential methods will be examined within the context of this study.

3. Method

The backwash treatment is evaluated in an experimental setup reduced to the essential area and shown in Fig. 3. The test can be divided into two sequences. Sequence 1 is the filtration process shown in Fig. 3a). During this step, the filter cake is built until a defined thickness is reached. Then, the suspension is replaced by clean water. In sequence 2, the filter cake is discharged. The backwash fluid flows through the filtrate pipe back to the filter element. The filter cake is detached from the filter cloth and discharged. The required amount of backwash volume is measured by a flow meter. For a systematic process evaluation, the start of image evaluation is synchronized with the backwash volume via an LED, as shown in Fig. 3b).

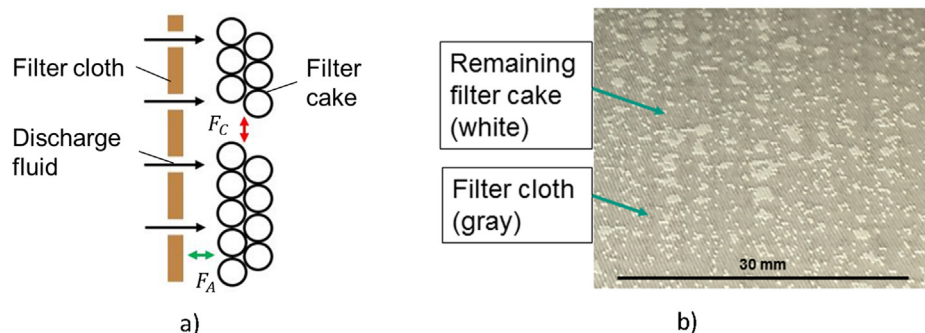


Fig. 2. Forces acting inside a filter cake during the backwash procedure (left side). For regeneration, adhesion (F_A) has to be smaller than the discharge force. When these conditions are not fulfilled, particles remain on the filter surface (right side).

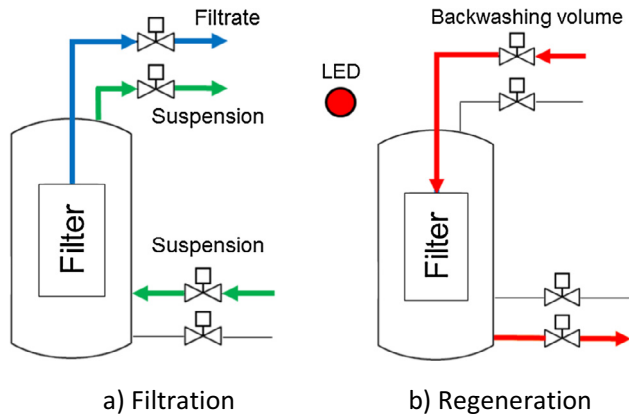


Fig. 3. Schematic flow chart of the experimental plant during filtration (a) and during regeneration with a counter-current flow (b).

With this method, the influence of three main parameters is investigated:

- Filter cake thickness
- Particle size/shape
- Backwashing pressure

To quantify the success of a backwashing treatment in the liquid phase, the amount of particles remaining on the filter cloth surface and the required backwashing volume are determined. For this, three different particle systems with different shapes (orthorhombic, flaky, and needle-shaped) are filtered to produce different cake thicknesses and then discharged (see chapter “Material”). Of particular interest is the discharge behavior of the particle system at varying filter cake thicknesses and, of course, the influence of the particle shape. As a hypothesis, it can be expected that higher filter cakes have an increased cohesion force F_C and are discharged in bigger fragments (the specific cohesion in mN/mm^2 ($\cong \text{kPa}$) is supposed to be constant). The required filter cake thickness can be adjusted with the help of the concentration of the suspension and a constant filtrate volume based on Eq. (1). The filter cake thickness depends on the concentration value κ , the filter surface A , the filter cake thickness H_{FC} , and the filtrate volume V_f , as shown in Eq. (1). The laboratory filter has an available filter area of $\approx 103.6 \text{ cm}^2$, with a filter diameter of 30 mm and a length of 100 mm. With increasing concentration, the filter cake thickness increases and can be adjusted reproducibly at a low measurement expense. Preliminary experiments have shown that the particle concentration does not affect the cake formed during filtration.

$$H_{FC} = \kappa \cdot V_f / A \quad (1)$$

In addition, the influence of backwashing pressure is investigated. For this, the backwashing pressure is varied between 0.1 bar and 2.0 bar. With regard to cohesion, different backwashing pressures vary the stress on the filter cake, which is expected to negatively influence the required backwashing volume. Therefore, the tests are carried out at a constant filter cake thickness that can be adjusted with the concentration of the suspension (Eq. (1)).

Apart from the analysis of the required backwashing volume, the discharge of the filter cake was investigated with image evaluation. This evaluation proceeds as follows:

- I. The relevant images are recorded at defined times during a discharge procedure.
- II. The image is converted into a binary format, with high contrast between the filter cake and the remaining part of the image.

- III. The remaining filter cake areas are compared and defined as contaminated areas at time t , with the whole filter cake at the beginning being defined as contaminated area in the beginning, which results from “surface contamination” (see Eq. (2)).

The observation of the discharge is based on a representative surface of the cylindrical candle filter. For this purpose the camera (model: Canon Eos D7) is aimed frontally at the candle and videos with a resolution of 1920×1080 at 25 frames per second are taken. After the cake has been built, the cake is discharged directly into the liquid environment and the discharged filter cake fragments are observed over time. Image evaluation allows to compare defined levels of cleanliness and the corresponding backwashing volumes for different process variables. This is needed for filter cake discharge until no filter cake fragments are detached anymore.

$$\text{Surface contamination } (t) = \frac{\text{Contaminated area at time } t}{\text{Contaminated area at the beginning}} \quad (2)$$

4. Materials

The filter element is a laboratory-scale candle filter shown in Fig. 4. The diameter of this candle is 30 mm, the length of the supporting tissue is 110 mm. For the experiment, the filter cloth is coated with liquid rubber on both ends and placed over the supporting filter tissue. After that, the filter cloth is fixed at the top and bottom using clips. Now, the filter candle is ready for experiments and can be installed in the test section. The used filter cloth is a twill weave with multifilament yarns for weft threads and monofilament yarns for warp threads. The mesh size amounts to $20 \mu\text{m}$ and the material is polypropylene. This filter cloth was chosen after previous tests using a leaf filter. These tests revealed that the elasticity of the filter cloth has a big impact on the backwashing volume. For this reason, a robust filter cloth without any buckling during reverse flow was chosen.

The particle systems investigated with respect to backwashing filtration mainly differ in the shape factor, as shown in Fig. 5. This leads to different porosities and specific flow resistances of the built-up filter cakes. In case of orthorhombic quartz particles P1, the filter cake is very compact and the specific flow resistance $\alpha_H = 1.59 \cdot 10^{14} \text{ 1}/\text{m}^2$ is the highest of the three particle systems. The particle system consists mainly of SiO_2 (98%) with traces of Al_2O_3 (1.5%) and components $<0.1\%$ (CaO, MgO, Fe_2O_3 , Na_2O , K_2O). The flow resistances of flaky (P2) and needle-shaped (P3) mixed particles of quartz ($\sim 50\%$), calcium oxide (45–47%), and lower shares of minority components $<1\%$ (Aluminium oxide, magnesium oxide, iron oxide, sodium oxide, potassium oxide) are $\alpha_H = 2.66 \cdot 10^{13} \text{ 1}/\text{m}^2$ and $\alpha_H = 1.25 \cdot 10^{13} \text{ 1}/\text{m}^2$ and are considerably smaller compared to quartz. This is due to the more porous structures of the built-up filter cakes and the resulting higher permeabilities, which is reflected by the Carman-Kozeny equation shown in Eq. (3). This equation shows that the pressure difference of a filter cake Δp depends on the specific surface area $S_V (=6/\bar{x}_{sa}$ for a spherical particle), the porosity ε , a flow factor μ (≈ 2.0 – 2.5), and some other values known from the Darcy equation (dynamic viscosity η_f , filter cake thickness H_{FC} , and filtrate flow \dot{V}_f). Eq. (3) shows that the pressure drop increases with decreasing particle size (increase of S_V) and/or with decreasing porosity of the filter cake ($\Delta p \propto (1-\varepsilon)^2/\varepsilon^3$). Transferred to the particle systems used, the orthorhombic quartz particles have the highest flow resistance, because the particles are quite small and the filter cake is very compact (less porous). Compared to the flaky particles, the particle

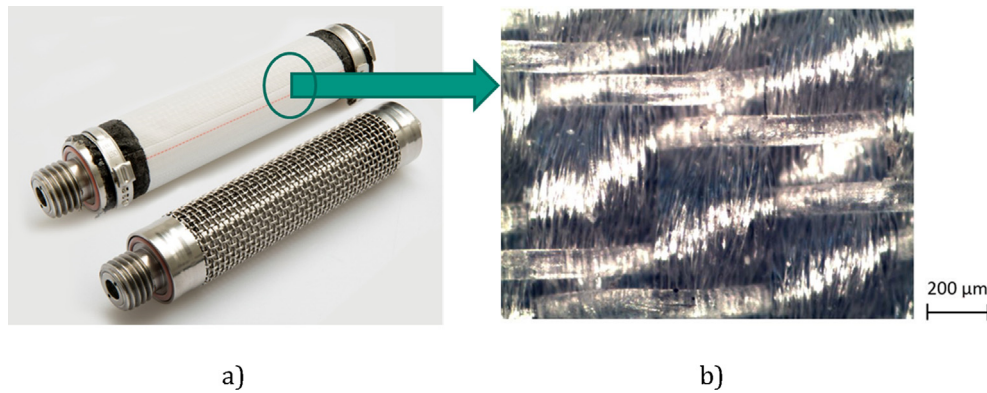


Fig. 4. Illustration of the laboratory-scale candle filter with and without filter cloth covering the supporting tissue (a) and enlarged image of the used filter cloth (b).

P1 SF300	P2 Tremim 283-100	P3 Tremim 939-304
$x_{50,3} = 10 \mu\text{m}^*$	$x_{50,3} = 12 \mu\text{m}^*$	$x_{50,1} = 21 \mu\text{m}^*$
$\alpha_H = 1.59 \cdot 10^{14} \text{ 1/m}^2$	$\alpha_H = 2.66 \cdot 10^{13} \text{ 1/m}^2$	$\alpha_H = 1.25 \cdot 10^{13} \text{ 1/m}^2$
98 % SiO ₂	51 % SiO ₂	49 % SiO ₂
(1.5 % Al ₂ O ₃ , 0.1 % CaO +	45 % CaO	47 % CaO
MgO, 0.05 % Fe ₂ O ₃ , 0.1 %	(1 % Al ₂ O ₃ , 1 % MgO, 0.3 %	(0.6 % Na ₂ O + K ₂ O, 0.5 %
Na ₂ O + K ₂ O)	Fe ₂ O ₃ , 0.1 % Na ₂ O, K ₂ O)	Fe ₂ O ₃ , 0.4 % Al ₂ O ₃ , 0.4 %
		MgO)
a)	b)	c)

*: Based on measurements of Quarzwerke GmbH

Fig. 5. Particle systems investigated for cake discharge in the liquid phase. The shapes of these particle systems vary from orthorhombic (a), to flaky (b), to needle-shaped (c) and result in different porosities and specific flow resistances α_H . The pictures and average particle sizes are provided by Quarzwerke GmbH. The specific flow resistances are measured with a pressure filter cell according to VDI 2762-2.

sizes are the same. Consequently, the shape results in a higher porosity and an accordingly smaller flow resistance. The needle-shaped particles have the lowest flow resistance, because the particle size and porosity are higher.

$$\Delta p = 2 \cdot \mu \cdot \frac{S_V^2 \cdot (1 - \varepsilon)^2}{\varepsilon^3} \cdot \eta_f \cdot H_{FC} \cdot \dot{V}_f = \alpha_H \cdot \eta_f \cdot H_{FC} \cdot \dot{V}_f \quad (3)$$

As a result of higher porosity, the number of contact points is smaller. Hence, it can be expected that the cohesion force F_C decreases. This is reflected by tensile strength measurements. Looking at the force condition given in the chapter "Mechanisms of filter regeneration" the porosity of the filter cake must be higher for a complete discharge. Smaller particles lead to smaller capillaries in the filter cake, as is evident from the calculated capillary pressure. The diameter of the pore d_H is estimated to be $2/3 \cdot \bar{x}_{sa}$ (capillarity of aggregated material). When the diameters of the aggregated material are smaller, the amount of liquid flowing through the filter cake is also smaller and prevents fragments of the filter cake from being discharged. In summary, a filter cake with a higher flow resistance should therefore be advantageous for discharge in the liquid phase (hypothesis).

To further characterize the particle systems used (s. Fig. 5), the particle size distribution was determined by a laser diffraction sys-

tem made by Helos Rodos. The distribution curves (sum/density distribution) are shown in Fig. 6(a) and (b). For the orthorhombic SF300 (P1), a very steep sum distribution can be observed. The mass or volume-related median value $x_{50,3}$ is 10.73 μm . This corresponds to the manufacturer's specifications. With regard to the distribution curve (Fig. 6(b), SF300 (P1) is bimodally distributed. There is a local maximum at a value of $\approx 1.5 \mu\text{m}$. Presumably, this maximum is responsible for a further increase of the specific cake resistance. Compared to SF300 (P1), the platelet-shaped Tremim 283-100 (P2) particles show a less pronounced increase in the sum distribution. This is particularly obvious for the density distribution. In the case of Tremim 283-100, the $x_{50,3}$ value is measured to be 10.19 μm , which differs from the manufacturer's specification by 2 μm . This difference may be due to the form factor and the measuring system, although Quarzwerke GmbH do not provide any information on the measuring system used. In addition, a bimodal distribution with a local maximum of 1.5 μm is measured. Although the $x_{50,3}$ value is similar to that of SF300 (P1), a significantly reduced specific cake resistance can be observed. Considering the distribution curves, this reduction is attributed to the form factor and the resulting change in porosity. The largest difference between the manufacturer's specifications and the measured values is obtained for the needle-shaped Tremim 939-304 (P3). Here, an $x_{50,3}$ value of 6.68 μm with a monomodal particle size distribution is measured. The difference is caused by the fact that the Helos Rodos laser diffractor calculates the mass or volume equivalent of a sphere. This leads to the comparatively small value, while the manufacturer specifies an average length $x_{50,1}$ of 21 μm . This size results in the erroneous assumption of a higher resistance for the needle shape and the porosity associated with it.

In the experiments filter cake thicknesses varied between 0.3 mm and 3.3 mm. For a reproducible filter cake thickness, filtration was carried out at a constant filtrate volume of 2 litres. The variation of the cake thickness was adjusted by suspension concentration (see Eq. (1)). As the concentration increases, the built-up cake increases at a constant filtrate volume. This enabled a very well reproducible cake thickness within a measurement series. The necessary concentrations of the cake thicknesses are summarized in Table 1. It becomes clear that the particle system with the lowest specific resistance (Tremim 939-304) also has a lower mass at the same cake thickness. This is equivalent to a lower volume fraction and thus a higher porosity compared to SF300 and Tremim 283-100.

5. Interpretation

Our study covers the filter cakes produced by filtration and their discharge. Three possibilities of cake discharge are identified:

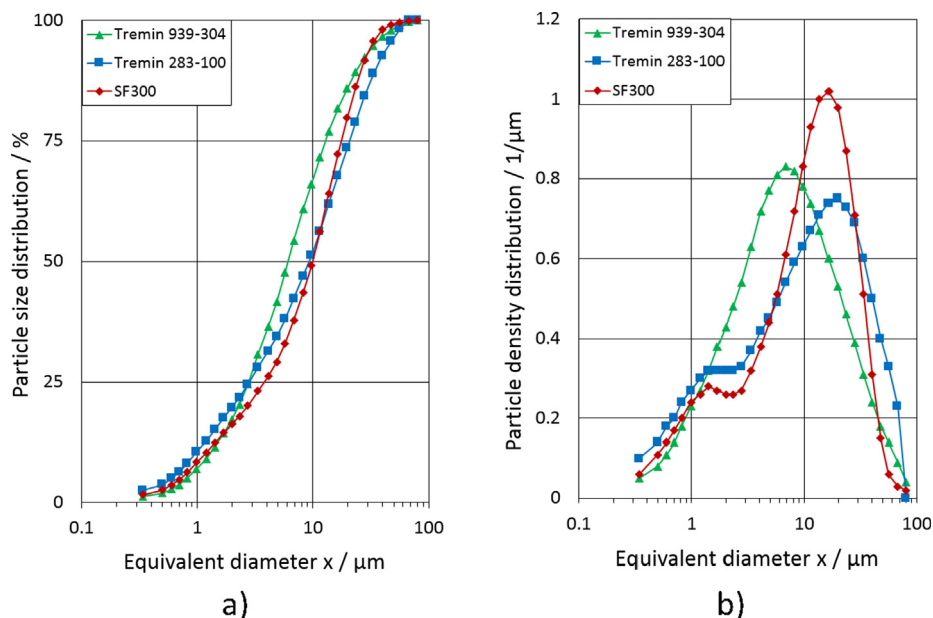


Fig. 6. Sum distribution (a) and density distribution (b) of the particle systems represented in Fig. 5, based on a mass or volume distribution.

Table 1

Representation of the desired cake thickness and the necessary suspension concentration at a constant filtrate volume of 2 litres.

Filter cake thicknesses [mm]	Suspension concentration [g/l]		
	SF300	Tremin 283-100	Tremin 939-304
0.3	1.4	1.4	0.5
0.5	2.9	2.8	0.9
0.9	5.0	4.9	1.6
1.3	7.1	6.9	2.3
1.7	10.0	9.7	3.2
2.1	–	11.9	3.9
2.5	–	14.3	4.7
2.9	–	16.8	5.4
3.3	–	19.3	6.4

- Complete discharge
- Incomplete cake discharge
- Redispersed particle/cake

In case of a complete discharge, the adhesion force is overcome and the cake is discharged in one piece. In this case, cohesion is assumed to be high enough to resist the detachment force. Hence, this type of cake discharge can be expected for very compact filter cakes. During an incomplete cake discharge, adhesion is overcome as well, but cohesion is smaller than the detachment force because of less number of contact points inside the cake. Consequently, the cake is discharged in smaller pieces/fragments. This behavior is critical especially for long filter elements for two main reasons. Firstly, the filter cake remains on the cloth surface. This blocked filter area is then not available for subsequent filtration cycles and leads to a decrease of the free filtration surface. Secondly, the settling velocity of fragments after discharge decreases significantly. This may result in a considerable increase of setup time in the process. An extreme case of incomplete cake discharge is a redispersed particle/cake. In this case, the built-up filter cake merely consists of a few particle layers. The cohesion in these few particle layers is not sufficient to counteract the break-up. The cake is discharged in small particle agglomerates, which are perceived as resuspensions and a cake discharge does not take place. The regeneration result is the worst of the three cake discharge types. In Fig. 7, the

discharge types “complete discharge” (a) and a “good incomplete discharge” in smaller fragments (b) are shown. The discharge type “bad incomplete discharge” with very small fragments and a high surface contamination (c) and “redispersed particle/cake” (d) are also shown. In the latter case, the resuspension becomes clear through the increase in turbidity.

To determine the influence of filter cake thickness on the discharge mechanism, different filter cake thicknesses were generated by constant pressure filtration at one bar. Then, the built-up filter cake was discharged at a backwashing pressure of 0.5 bar. The start of backwashing is indicated by a LED, which also allows to synchronize the image sections with the backwashing volume. No further movement of the cake in image evaluation is defined as the end of backwashing. From the frame rate of image evaluation and the time of backwashing flow, the backwashing volume required for discharging a cake can be determined. This was carried out for the three particle systems at filter cake thicknesses ranging from 0.3 mm to 3.3 mm. The required backwashing volume is plotted versus the specific backwashing volumes and different filter cake thicknesses in Fig. 8.

In the case of orthorhombic particles, complete discharge can be reached for very thin filter cakes. At a thickness of around 0.5 mm, the filter cake is lifted and deposited in very large pieces. This is equivalent to a total flow resistance of the filter cake of $7.95 \cdot 10^{10}$ 1/m. In this context, it should be noted that the size of dropped fragments increases when the thickness of the filter cake increases from 0.3 to 0.5 mm. A change from partial to complete cake discharge can be observed from $4.77 \cdot 10^{10}$ to $7.95 \cdot 10^{10}$ 1/m total flow resistance of the filter cake. The required backwashing volume decreases from 2 l per m^2 filter surface to 1 l/m^2 . This is confirmed by image evaluation. A thicker and more complete filter cake deposits which is broken up by the backwashing volume much faster. When looking at the prediction intervals (95%), the range of the changed discharge mode between 0.3 mm and 0.5 mm is not very significant. Hence, a maximal backwashing volume of 2 l/m^2 can be expected. Bigger cakes need less backwashing volume (1 l/m^2).

Compared to the flaky and needle-shaped particle systems, the orthorhombic filter cake is very stable. Cohesion of the former particle systems inside the cake decreases. This is reflected by the decreased specific flow resistance and negatively affects cake

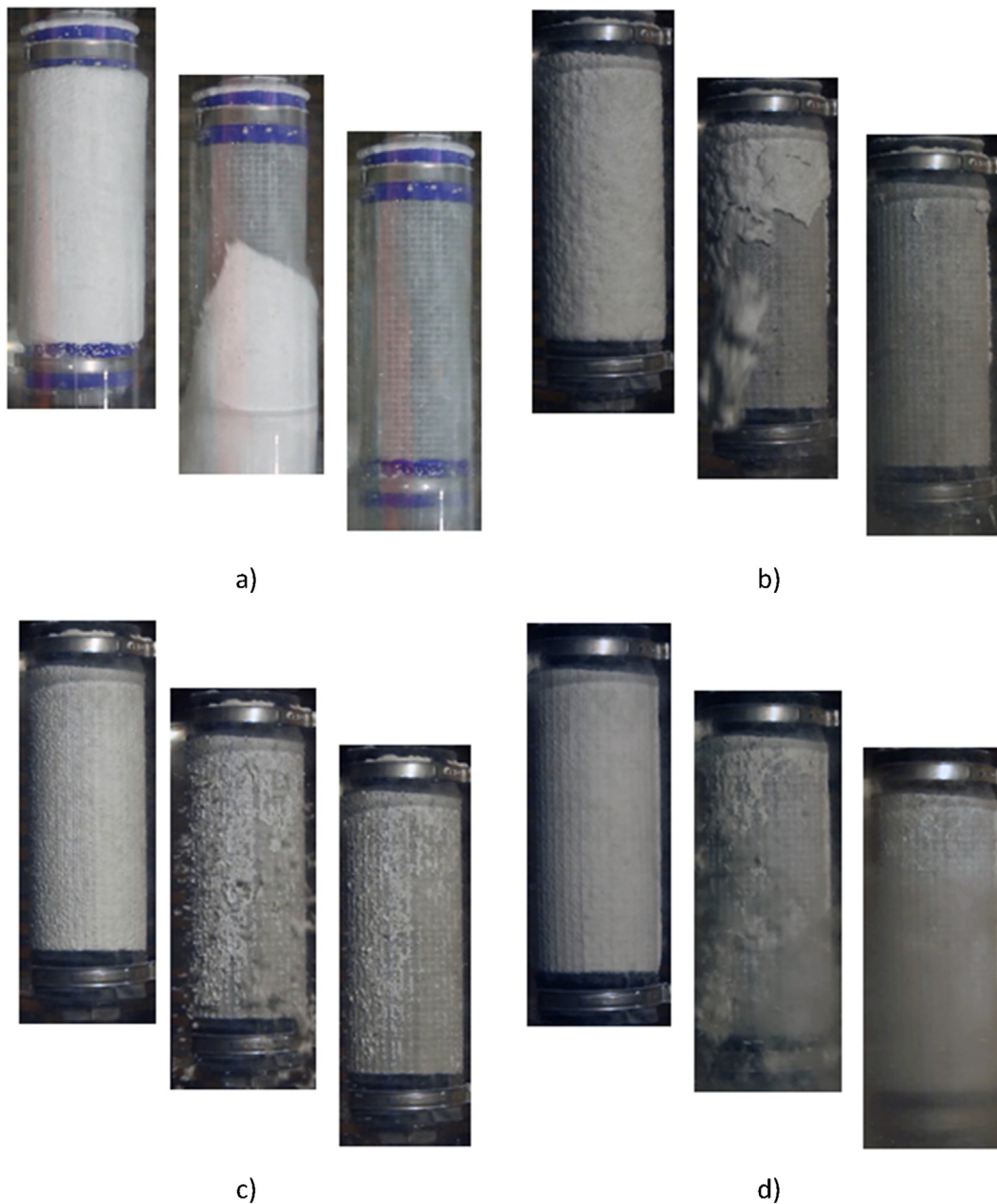


Fig. 7. Exemplary illustration of regeneration of the lab-scale candle filter after cake filtration during a complete discharge (a), an incomplete, good discharge into fragments (b), an incomplete, bad discharge into fragments (c) and the resuspended discharge (d).

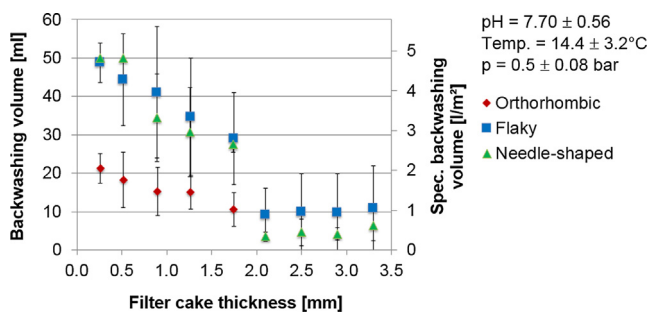


Fig. 8. Backwashing volume and specific backwashing volume for the laboratory-scale candle filter as a function of the filter cake thickness with a 95% confidence interval based on a sample size of $n = 5$. Especially for flaky particles, reproducibility is scattered widely.

discharge. The result of a decreased cohesion is that the cake is discharged in one piece at higher filter cake thicknesses only. Reduced cohesion also results in an increase of the backwashing volume required for smaller cake thicknesses. The cake breaks up and the backwashing volume flows through the section from where the filter cake has already been discharged. This is also visible in Fig. 8. Very low cakes of flaky particles are removed partly or even redispersed. For cake thicknesses of about 1.7 mm, “total discharge” takes place with approximately 1 litres of backwashing volume per m^2 filter surface. This is indicated by a drop in the required backwashing volume in Fig. 8. It is confirmed by image evaluation, where discharge of one large piece is much faster compared to smaller pieces. A filter cake of flaky particles with a thickness of ≥ 1.7 mm is discharged completely. This corresponds to a total flow resistance of the filter cake of $\geq 4.52 \cdot 10^{10}$ 1/m.

Compared to the orthorhombic and flaky particle systems, needle-shaped particles form the filter cake with the highest porosity. For this reason, very thin filter cakes need a backwashing volume higher than 50 ml ($\approx 5 \text{ l/m}^2$). For filter cakes $\leq 0.5 \text{ mm}$, a high contamination remains on the filter surface after discharge (see Fig. 8). Then, the backwashing volume decreases with increasing cake thickness and the discharge tends to be more “complete.” When exceeding a critical level similar to that of the flaky particle at $\geq 1.7 \text{ mm}$, the cake is discharged completely. This corresponds to a total flow resistance of $2.13 \cdot 10^{10} \text{ 1/m}$.

When looking at Fig. 8, the main problem is that the abort criterion is defined by the detachment of all fragments. For this reason, fragments remaining (partial discharge) at the top of the candle filter increase the required time of backwashing treatment and result in higher scattering of the backwashing volume. For better comparability, it is required to look at the defined backwashing time and compare surface contamination and backwashing volume.

For this purpose, the “surface contamination” value is defined (Eq. (2)) based on image evaluation of the discharge sequence. The image evaluation reveals the detachment behavior of the particle system and allows comparing the backwashing volumes required for the same surface contamination. This is the main advantage compared to Fig. 8. At the beginning, surface contamination amounts to 1 and approaches 0 for a complete discharge. Of course, 0 cannot be reached due to the fragments remaining and image noise during evaluation. Hence, a smaller surface contamination means a more complete regeneration step.

The detachment behaviors of the needle-shaped particle systems are exemplarily plotted in Fig. 9 for three filter cake thicknesses and a constant backwashing pressure of 0.5 bar. In case of a filter cake thickness of 0.3 mm, surface contamination is reduced to $79 \pm 11\%$ after 2 s with a required backwashing volume of $7.6 \pm 0.2 \text{ ml}$ ($\approx 0.7 \text{ l/m}^2$) and to $75 \pm 10\%$ after four seconds ($15.9 \pm 0.1 \text{ ml}$ or $\approx 1.5 \text{ l/m}^2$) to a remaining surface contamination of $66 \pm 18\%$ and $48.5 \pm 0.8 \text{ ml}$ ($\approx 4.7 \text{ l/m}^2$) backwashing volume at the end of the backwash process ($\approx 12 \text{ s}$). In this case, the subsequent filtration cycle is much shorter and the regeneration periods are reduced strongly. However, complex particle systems, such as needle-shaped particles, may cause many problems when using special filtration techniques, e.g. intermittent cake filtration (Alles et al., 2001). Short filtration periods with the corresponding low filter cake thicknesses reduce the filtration area and impede the whole filtration process. This can be avoided by longer filtration periods with filter cake thicknesses of 0.9 and 1.7 mm. The reduction in the first two seconds is not as strong as for orthorhombic particle systems, but after the fourth second, surface contaminations of 21.6 ± 7.5 and $18.8 \pm 7.4\%$, respectively, can be reached with a backwashing volume of $15.9 \pm 0.1 \text{ ml}$ ($\approx 1.5 \text{ l/m}^2$).

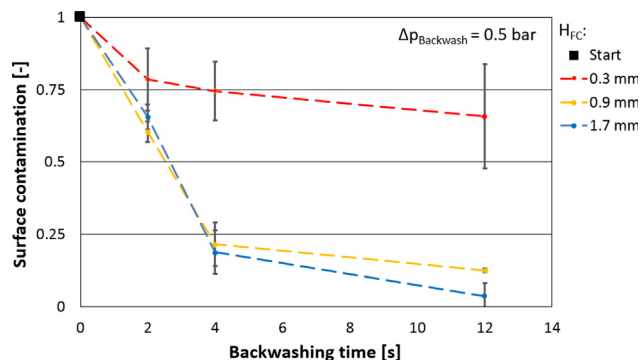


Fig. 9. Graphic representation of surface contamination versus backwashing time for the needle-shaped particle system Tremin 939-304 (P3).

After 12 s of regeneration ($\approx 4.7 \text{ l/m}^2$), surface contamination decreases to $12.5 \pm 4\%$ (0.9 mm) and $3.6 \pm 0.7\%$ (1.7 mm), respectively. This also shows that an increased cake thickness decreases surface contamination at a constant backwashing volume or reduces the required backwashing volume for the same surface contamination.

This trend can also be confirmed for the orthorhombic particle system, the main decrease of surface contamination (from 1 to ≈ 0.25) takes place in the first 2 seconds. This corresponds to a total backwashing volume required of $9.8 \pm 0.2 \text{ ml}$ or $\approx 1 \text{ l/m}^2$ s. Subsequent discharge until the fourth second reduces surface contamination to 18% for 0.3 mm and 9.6% for 0.5 mm only. The required backwashing volume is doubled for this small reduction of surface contamination ($18.5 \pm 0.3 \text{ ml}$ or $\approx 2 \text{ l/m}^2$). At the fourth second, most of the 0.9 mm filter cake has been discharged, while image noise and fragments remain at the top of the filter candle. Further discharge does not take place and after 8 s, the filter cake remaining at the candle top is also removed and surface contamination decreases to 3% with a required backwashing volume of $35 \pm 0.5 \text{ ml}$ ($\approx 3.5 \text{ l/m}^2$). The same surface contamination (3.6%) can only be reached for the 0.5 mm filter cake after 12 s of discharge with $50.8 \pm 0.4 \text{ ml}$ ($\approx 5 \text{ l/m}^2$). In case of a filter cake thickness of 0.3 mm, the surface contamination remaining at the end of regeneration amounts to $15 \pm 6\%$ and reduces the filter surface area available for subsequent filtration steps. For orthorhombic particle systems, surface contamination tends to be reduced with increasing backwashing time and filter cake thickness.

This behavior can also be seen with the flaky particle system. With the filter cake thickness increasing from 0.3 over 0.5 to 0.9 mm, surface contamination is reduced from $61.6 \pm 15.4\%$ to $48.9 \pm 19.5\%$, to $6 \pm 7.2\%$. But evaluation of this particle system during backwashing is very difficult, because a part of the particle layer is resuspended. Hence, it is only possible to evaluate the systems after second 2 and at the end of regeneration to obtain the trend.

In summary, Fig. 9 confirms the results from Fig. 8 and shows that the backwashing volume required for the same surface contamination depends on the filter cake thickness and the shape of the particle system. More porous filter cakes tend to have a higher surface contamination because of a smaller specific flow resistance and require bigger filter cakes for a good cleanliness of the filter area.

It can be noted that all complete cake discharges respectively a good regeneration procedure take place at a total flow resistance of $\geq (2-5) \cdot 10^{10} \text{ 1/m}$ (see Table 2, P1 - P3). In the case of the SF300 (P1), the complete cake discharge with 0.9 mm is suitable, but good cleaning already takes place with cake thicknesses of 0.5 mm ($7.95 \cdot 10^{10} \text{ 1/m}$). Based on this knowledge, the discharge behavior of this filter cloth can be predicted with an easy pressure filter cell (VDI 2762-2). For this, particle systems of a similar size but different chemical composition are chosen (see Table 2, P4 - P7). The idea behind this test procedure is a transfer of the necessary cake thickness by calculation according to Eq. (4). This allows the backwash quality for other particle systems to be estimated with just a few experiments. The total resistance of $2-5 \cdot 10^{10} \text{ 1/m}$ is divided by the specific cake resistance. The result is the required cake thickness.

$$H_{FC} = \frac{(2-5) \cdot 10^{10} \text{ m}^{-1}}{\alpha_H} \quad (4)$$

Based on this, the necessary cake thicknesses for P4 - P7 were calculated according to the model systems P1 - P3. Filter cakes with defined thicknesses are built and discharged until a complete discharge can be observed. The cake thickness required for a complete cake discharge is summarized in Table 2 for all particle

Table 2

Summary of particle systems used for discharge experiments and their shapes, the filter cake thicknesses required for complete discharge, the specific flow resistances based on VDI Guideline 2762-2, flow resistances, and the specific backwashing volumes for discharging each particle system.

No.	Particle system	Shape	$x_{50,3}$ [μm]	Complete discharge at [mm]	Spec. flow resistance [#] [$1/\text{m}^2$]	Flow resistance [$1/\text{m}$]	Spec. backwashing volume [$1/\text{m}^2$]
P1	SF300	orthorhombic	10	0.9	$1.59 \cdot 10^{14}$	$1.43 \cdot 10^{11}$	1.45
P2	Tremin 939-304	needle-shaped	21*	2.1	$1.25 \cdot 10^{13}$	$2.63 \cdot 10^{10}$	0.48
P3	Tremin 283-100	flaky	12	1.7	$2.66 \cdot 10^{13}$	$4.53 \cdot 10^{10}$	0.96
P4	ATH M15B	orthorhombic & flaky	10	0.7	$3.10 \cdot 10^{13}$	$2.14 \cdot 10^{10}$	1.35
P5	Eskal500	spherical	4.3	0.6	$6.05 \cdot 10^{13}$	$3.45 \cdot 10^{10}$	0.77
P6	Tremica 1305-006 AST	flaky	9.3	2.2	$1.56 \cdot 10^{13}$	$3.41 \cdot 10^{10}$	1.93
P7	Sepasil EK500	spherical	13	1.1	$3.24 \cdot 10^{12}$	$3.63 \cdot 10^9$	0.39

* $x_{50,1}$.

Based on VDI 2762-2.

systems (P1 - P7). For the particle system P4 with the designation ATH M15B (P4), mineralogically an aluminium trihydrate (65% Al_2O_3 , 34.5% H_2O) with traces of <0.1% von CaO, SiO_2 , Fe_2O_3 , the complete cake discharge took place at a cake thickness of 0.7 mm. The particle shape is a mixture of orthorhombic and flaky particles, similar to P1. The analogy to P1 is further illustrated by the necessary backwash volume of 1.35 l/m^2 . Only the spherical Eskal500 (P5), consisting of 99.1% CaCO_3 has an even lower necessary cake thickness of 0.6 mm. With an $x_{50,3}$ value of $4.3 \mu\text{m}$, this particle system is the finest particle system investigated and requires 0.77 l/m^2 for backwashing. A comparison of P4 to P5 confirms the trend that the necessary cake thickness decreases with increasing specific cake resistance. The flaky Tremica 1305-006 AST (P6), consisting of 46% SiO_2 , 32% Al_2O_3 , 10% K_2O , 5% Fe_2O_3 , 0.7% MgO , with a $x_{50,3}$ value of $9.3 \mu\text{m}$ and a low specific cake resistance of $1.56 \cdot 10^{13} \text{ m}^{-2}$, similar to the needle-shaped Tremica 939-304 (P2) with $1.25 \cdot 10^{13} \text{ m}^{-2}$, has the highest required cake thickness of 2.2 mm with the highest required backwash volume of 1.93 l/m^2 . The particle system Sepasil EK500 (P7) has the lowest backwash volume of 0.39 l/m^2 . This spherical particle with a $x_{50,3}$ - value of $13 \mu\text{m}$ consists of 99.4% Al_2O_3 , with traces of 0.3% Na_2O , 0.2% SiO_2 and 0.05% Fe_2O_3 and requires a cake thickness of 1.1 mm for complete ejection. Only this particle system exhibits a deviation because of the smaller specific cake resistance of 10^{12} m^{-2} . In this case, a higher cake thickness is necessary, which would nevertheless lead to a better regeneration in the real process (false positive result).

To summarize, with a backwash volume of $\geq 0.5 \text{ l/m}^2$ and $\leq 2 \text{ l/m}^2$ (Ripperger, 2008) all particle systems with a specific cake resistance $> 10^{13} \text{ m}^{-2}$ can be completely cleaned. The only condition for a complete cake discharge is that the cake height provides a total resistance of at least $4 \cdot 10^{10} \text{ m}^{-1}$.

Cohesion and detachment behavior of the particles during cake removal may vary depending on the number of contact points, shape, physico-chemical properties, material, and other factors. In case of a lower cake and thus lower total resistance, it can be expected that the contamination on the filter surface is much higher and some further cleaning operation has to be implemented (increased backwashing volume, pulsed backwashing). In case of a higher cake, the particles remaining on the filter surface decrease and the subsequent cleaning procedure for intra-cloth cleaning can be reduced to a minimum, when using a well-known cleaning mechanism (Stahl et al., 2013; Weidemann et al., 2014).

The cake thicknesses listed in Table 2 for a complete discharge are based on the cracks produced in the filter cake during backwashing. If hardly any cracks are produced because of high internal strength, the discharge is considered to be complete. Particle systems, in particular the three main systems investigated here, differ

considerably. While SF300 (P1) requires a very small cake thickness for a complete discharge, thicknesses are higher for Tremica 283-100 and Tremica 939-304. The latter, in turn, differ only slightly in the required cake thicknesses. These differences are caused by the different properties in terms of contact points and particle-particle interactions, as described in the previous chapter. They are a direct consequence of different cohesions in the filter cake. The correlation here is exactly the opposite of that of cake thickness: particle systems with high cohesion require smaller cake thicknesses for a complete discharge. Accordingly, SF300 (P1) is assumed to have a significantly higher cohesion than Tremica 283-100 (P2) and Tremica 939-304 (P3).

Various types of shear cells are used in bulk material mechanics to determine the internal strength of a bulk material. Their measuring principle is that the bulk material is subjected to shear loading. Different compaction conditions can be achieved. In the concrete case of backwashing filtration, the compressible filter cake can be assumed to have an elastic behavior after removal of the filtration pressure (Alles et al., 2001). For this reason, shearing can take place without pre-compaction.

In this paper, the internal strength is determined using a penetration test instead of a ring shear device. This does not reflect the internal cohesion, but rather the resistance to the penetration of a test body. Nevertheless, the condition should apply that more compact filter cakes have a lower penetration depth with the same force or a higher force with the same penetration depth. For this purpose, a die of a defined size (diameter D) is pressed into the filter cake. Then, the penetration resistance $\tau_{\text{Penetration resistance}}$ can be calculated by $F/(\pi \cdot D \cdot L)$ with F being the force required and L the penetration depth. The measurement setup is shown schematically in Fig. 10(a). The only condition is that the cake thickness H_{FC} has a sufficient height ($L < H_{\text{FC}}$). This can be achieved by using filter cakes with thicknesses $> 10 \text{ mm}$ and a maximum penetration force of 60 N. If the cake thicknesses are too small, the particles would not be compacted but deformed. This cannot be interpreted as penetration resistance, but as deformation resistance.

The three main particle systems SF300, Tremica 283-100, Tremica 939-304 and the particle system with the largest cake thickness Tremica 1305-006 AST were measured to test the above hypothesis. The four particle systems and the measured penetration resistance are shown in Fig. 10(b). SF300 has the highest penetration resistance with $412.8 \pm 89.5 \text{ mN/mm}^2$. This was expected due to the orthorhombic shape, as denser packings and, hence, lower porosities can be produced. Tremica 283-100 has the second largest penetration resistance measured of $128.4 \pm 34.6 \text{ mN/mm}^2$, while Tremica 939-304 with $38.89 \pm 3.9 \text{ mN/mm}^2$ and Tremica 1305-006 AST with $17.8 \pm 7.2 \text{ mN/mm}^2$ have the smallest values. This is consistent with the minimum cake thicknesses observed for a

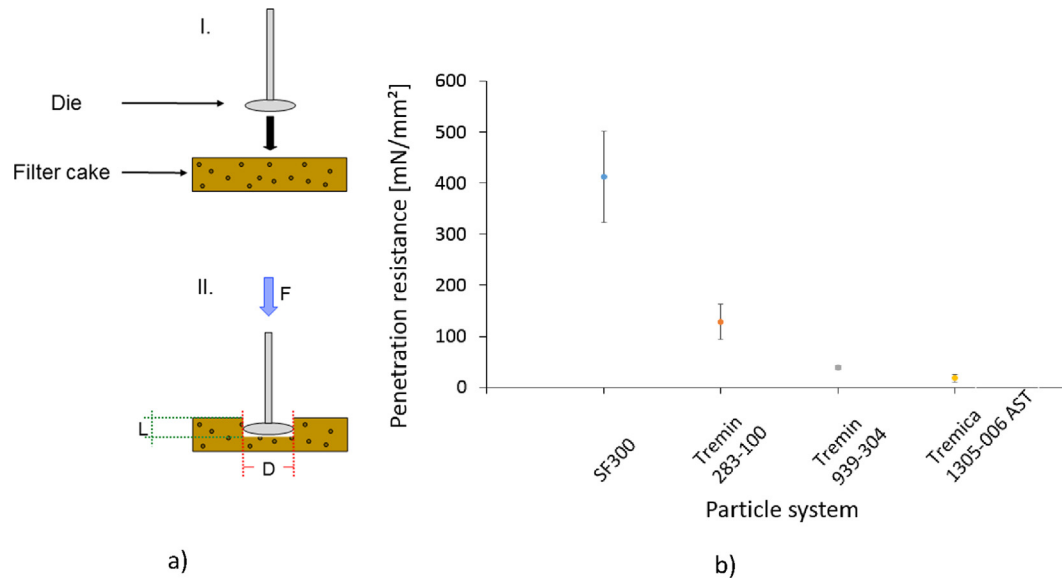


Fig. 10. Schematic representation of the penetration test (a) and the measured penetration resistance in $\tau_{\text{Penetration resistance}}$ mN/mm² (b) for four different particle systems.

complete discharge. Due to the high measuring effort, the measurement procedure of $\tau_{\text{Penetration resistance}}$ is not within the scope of this paper.

Normally, the filter cake thickness is a result of the filtration process and not a function of a free process variable like filtration pressure. Based on the previously shown results, surface cleanliness can be increased by a higher filter cake thickness (reduced surface contamination with remaining particles). However, backwashing is influenced directly by backwashing pressure. In case of the cleaning process of single particles on a filter cloth, higher backwashing pressure leads to an increased level of cleanliness. The hypothesis for cake discharge is as follows:

Higher backwashing pressure leads to an increased stress on the filter cake and results in an increased backwashing volume.

To verify this hypothesis, the same filter cake thickness of 0.9 mm is used for all particle systems shown in Fig. 5. After cake formation, regeneration is performed with a backwashing pressure of 0.1, 0.3, 1.0, and 2.0 bar, respectively. This is equivalent to a constant backwash volume flow of 1.5 ± 0.1 ml/s, 3.1 ± 0.1 ml/s, 6.0 ± 0.1 ml/s and 8.6 ± 0.3 ml/s during regeneration procedure. First attention is given to the backwashing volume until the last fragment is detached from the filter surface, similar to Fig. 8. The required and specific backwashing volumes for the three used particle systems are shown in Fig. 11. For the orthorhombic particles, the required backwashing volume is approximately constant for all backwashing pressures. Of course, the required volume varies as a result of the statistic detachment behavior that is also found in investigations at variable filter cake thicknesses, but the average value stays approximately constant at ≈ 1.5 l/m². With regard to the size of discharged fragments, higher pressure is found to cause detachment of bigger pieces, whereas a decreased pressure also causes the size of the fragments to decrease. The remaining surface contaminations are the same. The expected increase of backwashing volume for partial discharge could not be observed, which is why the previously formulated hypothesis cannot be confirmed. One explanation is that a smaller backwashing pressure leads to a decreased flow through the filter cloth. It can be assumed that smaller backwashing volumes flow through the filter cloth very inhomogeneously. The filter cake is detached partly due to tensile strength resulting from the gravity force pulling on the filter cake. The inhomogeneous flow through the filter cloth results in partial discharge at smaller backwashing pressure. However, the frag-

ments still are big compared to those of the other two particle systems. Hence, regeneration at variable pressure has no influence in case of orthorhombic particles. Additionally, this observation is true for flaky and needle-shaped particle systems. The only parameters that change are the discharge type and the required backwashing volume. Filter cakes consisting of flaky particle systems with a height of 0.9 mm are detached in larger fragments (partly). This is reflected by an increased backwashing volume of ≈ 3 l/m² as a result of an uneven flow through the filter cloth. So, the constant backwashing volume for different backwashing pressures can be confirmed for the flaky particle system. Only the backwashing type (partly or complete) varies with the particle shape. And the same behavior can be observed for needle-shaped particles. Because of the more porous filter cake, the detached fragments are smaller and result in an increased backwashing volume, which is higher than that of the flaky system (≈ 4 l/m²).

Just like the backwashing volume in Fig. 11, the remaining surface contamination is approximately equal, which is shown in Fig. 12 for the needle-shaped particle. For these particles and a backwashing pressure of 0.1 bar (dash-dotted line), the main discharge is reached after 10 s (surface contamination of $32 \pm 7.25\%$). For a further small decrease of surface contamination, discharge has to last 30 s (surface contamination of $24 \pm 6\%$). The backwashing volume required for main discharge after 10 s amounts to 1.6 ± 0.3 l/m². For further surface cleaning, the absolute backwashing volume tends to 4.8 ± 0.2 l/m². A reduction of 8%

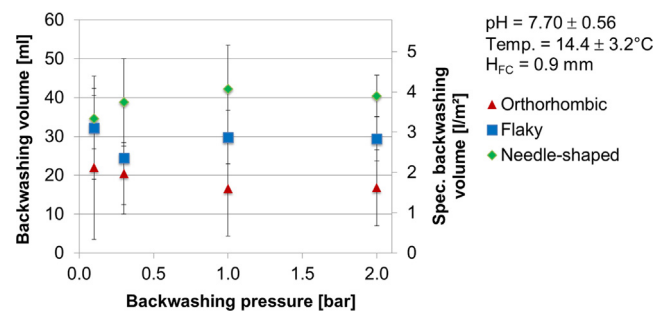


Fig. 11. Backwashing and specific backwashing volumes for the laboratory-scale candle filter as a function of the backwashing pressure with a 95% confidence interval based on a sample size of $n = 5$.

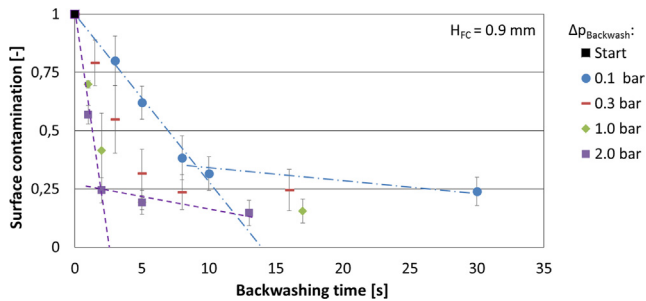


Fig. 12. Influence of the backwashing pressure on surface contamination for the needle-shaped particle system.

surface contamination (reference to the average of the measuring result) increases the backwashing volume by a factor of 3. At 2.0 bar (dashed line), the main discharge occurs within 2 s (surface contamination of $24 \pm 5\%$) and the same level of cleanliness is reached after less than 5 s (dashed line; surface contamination of $19 \pm 3\%$). The required backwashing volume for 2 s amounts to $1.7 \pm 0.1 \text{ l/m}^2$ and for 5 s to $4.1 \pm 0.2 \text{ l/m}^2$. This also demonstrates that backwashing pressure only increases the backwashing time and has no influence on surface contamination. The whole backwashing procedure at 2.0 bar ends after 13 s, with the surface contamination being $\approx 15 \pm 5.4\%$. Small differences of surface contamination between 0.1 and 2 bar result from noise during image evaluation. In summary, the reduction speed of surface contamination increases from 6.8%/s to 9.5%/s for 0.3 bar, to 29%/s for 1.0 bar, to 38%/s for 2.0 bar.

In case of the flaky particle system and a backwashing pressure of 0.1 bar, a surface contamination of $\approx 5\%$ is reached after 15 s ($2.7 \pm 0.3 \text{ l/m}^2$), whereas the same level of cleanliness at 2.0 bar is reached after ≈ 4 s ($3.0 \pm 0.7 \text{ l/m}^2$). The reduction speed of surface contamination to $\approx 5\%$ increases linearly over all backwashing pressures. The reduction speeds for the backwashing pressures are as follows:

- 0.1 bar = 6.4%/s,
- 0.3 bar = 10.8%/s,
- 1.0 bar = 20.25%/s,
- 2.0 bar = 24%/s

As already shown for the needle-shaped particles, the reduction of surface contamination of flaky particles also increases with an increased backwashing pressure. The speed is a little smaller, but the tendency is obvious. And this tendency can also be observed for the orthorhombic particle system. At a backwashing pressure of 0.1 bar, the minimum surface contamination is $13 \pm 4\%$ after 4 s. This main discharge occurs with a required backwashing volume of $0.7 \pm 0.1 \text{ l/m}^2$. Any further backwashing fluid has a minor impact on surface contamination. For backwashing at 2.0 bar, the minimum surface contamination is $9 \pm 5\%$ and can be reached with a backwashing time of 1 s and a backwashing volume of $\approx 1.1 \text{ l/m}^2$. The influence of backwashing pressure on backwashing time is also obvious for the orthorhombic particle system. In summary, the filter cake consisting of orthorhombic particles is mainly discharged in bigger fragments. The reduction speeds of surface contamination are much higher and given in the following list:

- 0.1 bar = 21.75%/s,
- 0.3 bar = 28.3%/s
- 1.0 bar = 61%/s,
- 2.0 bar = 91%/s

The backwashing pressure has no influence on the remaining surface contamination and the required backwashing volume. For this reason, a smaller backwashing pressure can be chosen.

6. Conclusion

The experiments show that the thickness of the filter cake and shape of the particle system have an influence on the backwashing volume and surface contamination after backwashing. When reaching a defined filter cake thickness, discharge will be more successful. This filter cake thickness depends on the overall flow resistance of the filter cake, which includes the porosity and contact points. For very porous filter cakes and, hence, smaller specific flow resistances, the height has to exceed that of filter cakes consisting of very compact particle systems. Knowledge of the used filter cloth allows determining the cake thickness required for a complete discharge with an easy pressure filter cell according to VDI 2762-2. A complete discharge is also advantageous for subsequent sedimentation. Very small fragments need a lot of time for sedimentation. Taking into account the size of the industrial filter candles (≤ 2.5 m), low settling velocities of the fragments have a high impact on the process efficiency. For effective and stable processing, it is not always possible to filtrate until the required filter cake thickness for a complete discharge is reached. However, from time to time, it is recommended to do so, because the filter surface will be cleaner and the subsequent filtration performance will increase.

The backwashing pressure has no influence on the required backwashing volume. Only the speed of discharge increases, but compared to the filtration time, the regeneration time can be neglected (Ripperger, 2008). The surface contamination remaining at a higher backwashing pressure is equal to that remaining in case of a lower backwashing pressure. For this reason, smaller facilities can be used (backwashing vessel etc.) depending on which way the pressure is provided (pump, piston, and pressurized air). The investigations for different backwashing pressures also show that the way of discharge and the particle shape directly affect the required backwashing volume.

To sum up, the shape of the particle system and the filtration time or filter cake thickness have the biggest impact.

7. Outlook

Based on this research, it is recommended to enlarge the period of filtration for an increase of filter cake thicknesses. Too short filtration intervals decrease the efficiency of the regeneration step because of filter cake fragments remaining on the filter cloth surface. This corresponds to a smaller filter area. In case of special filtration processes, such as intermittent filtration, the advantage of fast periods between filtration and regeneration can be neglected for very adhesive particle systems. Looking at the remaining particle layers and filtration processes, such as precoat filtration, the effect of bad surface regeneration on turbidity at the beginning of the subsequent filtration step still remains to be determined. For this, different discharge modes of the same particle system should be compared with respect to particle concentration in the filtrate flow.

Another issue is the right selection of the filter cloth. There are various kinds of filter cloths with different physical and chemical properties on the market. To determine their suitability for backwashing filtration, these cloths should be subjected to the procedure described in the “method” section. Preliminary studies with a leaf filter have shown that the weave type has a big influence on the filter cake thickness required for complete discharge.

Declaration of Competing Interest

The authors declare that they have no known competing financial interests or personal relationships that could have appeared to influence the work reported in this paper.

Acknowledgement

The IGF Project 18591 N is supported via German Federation of Industrial Research Associations (AiF) within the programme for promoting the Industrial Collective Research (IGF) of the German Ministry of Economic Affairs and Energy (BMWi), based on a resolution of the German Parliament. The authors would also like to thank all colleagues and students for the support in writing this paper.

References

- Alles, C.M., Anlauf, H., Stahl, W., 2001. Process Strategies for Cake Filtration with Fine Particles. Nürnberg, June 26–28.
- Amirtharajah, A., 1985. *Water Res.* 19, 5.
- Burdick, G.M., Berman, N.S., Beaudoin, S.P., 2005. *Thin Solid Films* 488, 1–2.
- Charleton, A.J., Heywood, N.I., 1983. *Filtration & Separation*, 20 Nr. 5.
- Fitzpatrick, C.S., 1998. *Filtr. Sep.* 35, 1.
- Leipert, C., Nirschl, H., 2012. *F & S International Edition*, 11.
- Morris, K., Allen, R., Clift, R., 1987. *Filtration & Separation*, 24 Nr. 1.
- Müller, H.R., Kern, R., Stahl, W., 1987. *Filtration & Separation*, 24 Nr. 1.
- Ripperger, S., 2008. *Filtrieren und Separieren*, 22 Nr. 2.
- Rushton, A., Ward, A.S., Holdich, R.G., 2008. *Solid-Liquid Filtration and Separation Technology*. Wiley-VCH, Hoboken [eng].
- Rushton, A., Griffiths, P.V.R., 1972. *Filtr. Sep.*, 9.
- Stahl, S., Spelter, L.-E., Nirschl, H., 2008. *Chem. Eng. Technol.* 31, 11.
- Stahl, S., Leipert, C., Nirschl, H., 2013. *Sep. Purif. Technol.* 110.
- Weidemann, C., Vogt, S., Nirschl, H., 2014. *J. Food Eng.* 132.

G. Attached publication [2]

Verification of the contribution from the co-authors

Title: The influence of filter cloth on cake discharge performances during backwashing into liquid phase

Journal: Separation and Purification Technology

Authors: P. Morsch, H. Anlauf, H. Nirschl

Position in the dissertation:

The content of this paper has been included in Chapter 4.2 and 5.1

Contribution of Patrick Morsch

- Conceptual design and construction of the backwash system, as well as planning of the test procedure.
- Execution of backwash tests and data evaluation.
- Summary of the data and evaluation of the results.
- Writing the chapters and performing the source research.

Contribution of Harald Anlauf

- Support of the work by references in literature, test setup, test procedure. Proofreading of the paper (technical).

Contribution of Hermann Nirschl

- Support of the work by references in literature, test setup, test procedure. Proofreading of the paper (technical).



The influence of filter cloth on cake discharge performances during backwashing into liquid phase



Patrick Morsch*, Harald Anlauf, Hermann Nirschl

Institute for Mechanical Process Engineering and Mechanics (MVM), Process Machines (VM), Karlsruhe Institute of Technology (KIT), Germany

ARTICLE INFO

Keywords:

Backwashing filter
Filter cake discharge
Multifilament fabrics
Monofilament fabrics
Filter cake thickness

ABSTRACT

In industrial solid/liquid separation, the removal of fine particles in a suspension with a significant amount of solids content can be a challenging task. Cake filtration in particular is a useful principle for separation of such suspensions. This separation occurs in a wide array of industrial production applications and has some advantages compared to other separation principles. To achieve the required performance, different types of filters can be used. One commonly used type is operated semi-continuous and use backwashing to discharge the filter cake. The regeneration of the filter cloth is as important as the actual filtration step. In the case of a properly regenerated filter cloth, the filtrate flow at the beginning of each step is still the same, while the initial filtrate flow decreases for and inefficient regeneration.

This regeneration of the filter cloth depends strongly on the interaction between the particle system and the filter cloth. In the case of backwashing filtration, a clear difference could be observed between multifilament and monofilament fabrics.

For multifilament filter cloths, it is possible to calculate the minimum required cake thickness for a complete discharge by means of the total resistance, i.e. the product of the specific cake resistance multiplied by the cake thickness. For 3 investigated fabrics with mesh size $\leq 20 \mu\text{m}$, a complete cake discharge could be achieved by all 3 model particle systems. It is noticeable that the minimum required cake thickness decreases with increasing specific resistance. As soon as the cake thickness with the respective specific cake resistance of the particle system exceeds the value $5 \cdot 10^{10} \text{ m}^{-1}$, a complete discharge can be observed. The cake thicknesses found within the same particle system were very similar between the 3 fabrics investigated. Based on this observation, the release of cakes from multifilament fabrics appears to be dominated by cohesion of particles in the cake. The adhesion from the first particle layer to the fabric does not seem to be a significant influencing factor.

The situation is different for monofilament fabrics. This behaviour is different from the multifilament fabrics in the cake thickness. Here, smaller cake minimum required cake thicknesses were observed for small specific cake resistances. This is due to the particle deposition mechanism within the fabric. A lower specific cake resistance is associated with a larger particle size and/or a different particle shape (greater deviation from the ideal sphericity). Larger particles relative to the mesh size of the filter fabric preferably form a clean interface between the particle layer and the filter fabric (surface deposition). This leads to a lower interference and better cake discharge. This behaviour could be estimated by dividing the filter media resistance (determined by a particle system whose particle size is significantly larger than the mesh size of the fabric), by the specific cake resistance multiplied by a particle shape-dependent factor (Eq. (2)). The shape-dependent factors were determined to be 0.03 for orthorhombic, 0.15 for flaky and 0.46 for needle-shaped particles and thus increases with increasing deviation from the ideal sphericity. By including the filter medium resistance, the influence of the fabric and the adhesion of particles to the fabric is to be expected. Validity of this model was proven with 6 filter clothes with $\leq 22 \mu\text{m}$ mesh (3 twill and 3 plain weave).

Similar behaviour between multifilament fabric and monofilament fabric could only be observed with the required minimum backwashing volume for a complete discharge. The required necessary backwash volume is always $\leq 2 \text{ l/m}^2$. In summary, this study shows the regeneration performance of different filter cloth types (multifilament and monofilament) can be predicted by different models.

* Corresponding author.

E-mail address: patrick.morsch@kit.edu (P. Morsch).

<https://doi.org/10.1016/j.seppur.2020.117549>

Received 29 November 2019; Received in revised form 4 August 2020; Accepted 5 August 2020

Available online 12 August 2020

1383-5866/ © 2020 Elsevier B.V. All rights reserved.

Nomenclature

Symbol	Description [Unit]
H_{FC}	Filter cake thickness [mm]
$x_{50, 3}$	Mass related modal value [μm]
$x_{50, 1}$	Length-related modal value [μm]
α_H	Specific filter cake resistance [m^{-2}]

1. Introduction

For the removal or separation of particle-loaded process streams, mechanical process engineering has a wide variety of equipment based on different physical removal principles. The mechanisms of density separation and separation by filtration, i.e. geometric dimensions, are particularly important concepts. While separation by means of density separation includes treatment basins in sewage treatment plants up to centrifuges in the pharmaceutical industry, the group of filtering separators is no less broad and includes precoat filters in the food industry up to the separation of cellulose fibres [1].

Both separation mechanisms have their own specific advantages. While rotating separators such as the decanter can continuously discharge highly loaded process streams dry, filtration is suitable for low loaded process streams. Due to its large field of application, cake-forming filtration is of particular industrial interest here [2].

The separation performance is essentially influenced by the choice of the suitable filter cloth. If the mesh size and weave are unsuitable for the process stream to be filtered, this is evident by a very high and long-lasting turbidity or a high residual load of particles in the filtrate stream (bleeding) or the filter cloth (clogging) [3–6]. In addition to effects on the actual filtration process, the selection of the filter cloth also affects the necessary regeneration (filter cake discharge). Which fabrics are suitable for a good discharge, however, was not investigated due to a generally valid systematic and scientific case analysis and is essentially based on the experiences of the respective operators of such filter devices. Scientific work in the field of liquid filtration refers exclusively to cake discharges in gas phase with the application focus chamber filter and similar [2,7–10].

The effect of an unsuitable filter cloth for the particular separation task in combination with an equally unsuitable regeneration is dramatic (see Fig. 1). For good regeneration, the initial volume flow of each filtration cycle should be in the same order of magnitude as the previous cycle ($\dot{V}_{F,max}$). This reduces the number of necessary standstill times (Δt_{Setup}) during regeneration. In the event of poor regeneration, the initial resistance decreases. This is a result of remaining particles in and on the filter cloth and has the consequence that the regeneration cycles, by faster reaching $\dot{V}_{F,min}$, increase and the total filtrate volume decreases compared to the good regeneration.

The backwashing behaviour of fabrics of candle filters with a combination of multifilament warp and monofilament weft threads, as well as fabrics consisting exclusively of monofilament threads, will be

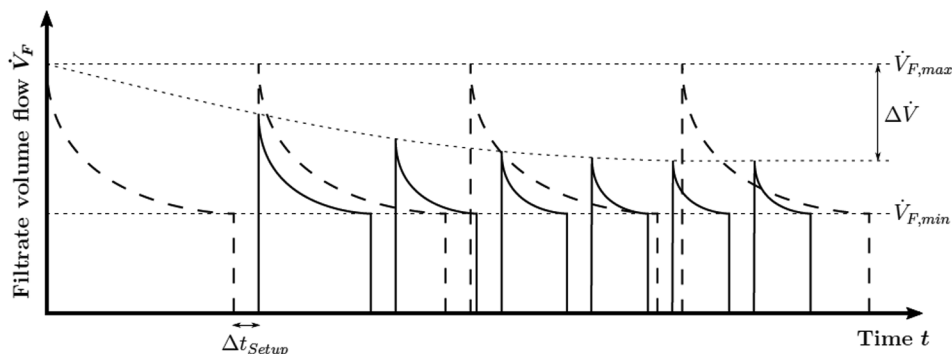


Fig. 1. Effect of inadequate regeneration on the filtrate volume flow \dot{V}_F at the beginning of each filtration cycle. or good regeneration, the initial volume flow of each filtration reaches the initial volume flow of the previous filtration cycle $\dot{V}_{F,max}$. With increasing retention of particles on and in the fabrics, this initial resistance is reduced by $\Delta \dot{V}$. As a result, the regeneration cycles (Δt_{Setup}) increase min when $\dot{V}_{F,min}$ is reached.

investigated within the scope of this paper. The aim is to develop a transfer criterion to ensure good regeneration. This paper refers to an earlier paper which focuses on the effect of backwash pressure and the minimum required cake thickness in case of a variation of the particle system [11].

2. Theory

Cake-forming filtration combines the surface filtration with those of the depth filtration. First, the process stream to be filtered flows through the selected filter fabric, whereby the disperse particle phase to be separated is removed. A phenomenon can be observed that is referred to in expert circles as “bleeding”, i.e. the penetration of particles at the beginning of filtration. This particle penetration decreases with the growth of the first particle layers. During this time, the filtrate flow is returned until a lower limit value of the particle load in the filtrate is reached. While the properties and the duration of this turbidity depend on the sieving effect of the fabric, the filter cake takes over the main separation performance with increasing filtration duration. The initial surface filtration (screen filtration) is thus replaced by the filter cake, which also separates finer particles in its inner structure (depth filter).

The separation process of the filter cake (size of the capillary as a function of the filtering particles, etc.) is the subject of numerous scientific studies. Only orientation aids are given for the selection of suitable filter fabrics. For example [1], recommended for chamber filters that the flow resistance of the filter cloth should be in the range of 2–15% of the filter cake. For higher flow resistances of the cake, the tendency is towards 15%, while coarser particles should tend towards filter cloth resistances of 2%. The mutual influence of the particles deposited in the meshes of the filter cloth is not considered. Only [2] considers that the key influence on flow resistance, especially with compressible particles, is determined by the first particle layer in connection with the mesh (mesh type, mesh size, etc.). This phenomenon is made clear by the fact that the total resistance is greater than the sum of the partial resistances, consisting of filter medium resistance and filter cake resistance. This increase is considered as interference resistance and can be determined by experiments according to VDI 2762-2 [12]. In addition to these elaborations, recommendations are also given on the properties of the individual fabric types and woven fibres [3,4], which are, however, to be understood at most as a tendency, but not as a fixed rule.

This applies in particular to regeneration during cake-forming filtration. This is achieved by cake removal, for example by cake discharge in backwash filtration. There are no scientific papers which provide recommendations for a good regeneration. For this reason, this is carried out within the scope of this elaboration with a view to the choice of mesh.

Filter fabrics are to be understood as the heart of candle and leaf filters. Due to the different experience of the manufacturers of such apparatuses, a correspondingly high number of different weaves is available on the open market. In addition to the usual differences in

weave, twill or satin, these differ in the sequence of the wrap around of the threads, the number of fibres per weaving thread (so-called yarn) and the offset of the yarns until the weaving pattern is repeated. DIN ISO 9354 (Fig. 2) provides a good possibility for characterization.

Within the scope of this standard, the 4 differentiation criteria mentioned are summarized as a number sequence, which makes it possible to record the woven pattern at a glance. The numerical code begins with the weaving pattern as the upper group. A distinction is made here between plain (10), twill (20) and satin (30) and requires the creator of the number code to assign the fabric to one of these large groups. These three groups can also be described by the numbers 11, 21 and 31, which directly target the second part of the numerical code, namely the number of warp lifts or decreases. If, for example, the weaving pattern starts with a warp lift, the first code ends with 0, and if the warp is lowered with 1. Starting from this, the number of fibres that the warp thread passes through above and below the fabric is indicated. For example, a fabric that starts with a warp lift and 3 threads above and one understretch is set to 03 01. The following numerical code includes the number of threads which run parallel to each other through the same process in the weaving pattern. This is followed by the offset, which describes when the weaving pattern repeats itself periodically, i.e. after how many threads the weaving pattern starts again with a warp lift or drop. As an example, a twill fabric, starting with a warp lift, can be named, which overruns 3 threads and underruns 1 with one thread. This would be 20-03 01-01 - 03, whereby the offset as a result of the warp lifting and lowering would be 03. The technical term for this fabric would be the so-called oblique degree body and could also be characterized as 21-01 03-01 - 03, starting with a warp reduction. Based on this distinction all fabrics of this paper are characterized.

The differentiation of fabrics according to DIN ISO 9354 offers many advantages to characterize fabrics according to their structure and weave and to group them together. However, references to the fibres used (monofilament / multifilament) and their specific advantages (permeability, strength) do not provide this distinction and are difficult to detect due to the wide range of fabrics. However, experience has shown that trends can be deducted [13] and they are summarized in Table 1 where 6 important properties are compared:

- Particle retention
- Permeability (flow capability)
- Cake dryness
- Maximum cake discharge
- Filter medium life
- Resistance to blinding

In the case of the yarns, the staple yarn is particularly good at particle retention, but there are striking disadvantages in low permeability, cake dryness, cake discharge and resistance to blocking. For this reason, these fibers are of no technical importance in backwash filtration. With regard to monofilaments and multifilaments, monofilaments always have the advantage over multifilaments, apart from retention. For this reason, the focus of this development is on these two fibre types.

The weaving patterns are differentiated according to [13] in the three groups plain, twill and satin fabrics. In addition, the so-called plain reverse dutch weave (PRD) is presented, a fabric with a strongly

unequal diameter ratio between warp and weft threads. This makes very fine meshes and smooth fabrics possible. This is clearly shown by the best retention, drying behaviour and service life. In the case of production, release behaviour and resistance to clogging, the satin fabric is advantageous. The twill fabric always moves in the midfield in all six differentiation criteria [13].

This raises the question of why users should use fabrics other than PRD or satin fabrics at all. One answer with regard to [13] is certainly that for the specific application a fabric is sought which covers all sub-areas well. However, it must also be taken into account that Table 1 can only be regarded as trends. The multitude of offered fabrics with different permeability, roughness, mesh ratios make it difficult to make a general statement. Here a systematic variation of fibre diameter etc. would be necessary, which in turn directly influences permeability and roughness. For this reason the table is only used as a comparison tool for the validation of observations. Attention is paid to fabrics which are used in industry.

These include multi-/monofilaments of the twill weave and mono-/monofilaments of the braid and twill weave. These are presented in the chapter Materials.

Research results relating to the effect of particles on the filter medium resistance have shown that the interaction between particle collective and filter fabrics has a significant effect on the flow resistance [3-6,14]. Tichy et al. introduces the interference resistance to describe this behaviour in addition to the filter cake and filter medium resistance. This resistance takes into account the interaction between the particle collective and the filter fabric on the initial resistance in the form of an increase in resistance and is directly attributable to the deposition behaviour of the particles on and in the mesh of the filter material [15].

This behaviour has already been studied by increasing the initial resistance between filtration with a suspension R_T in relation to the flow resistance with pure water R_0 . For this purpose, Purchas et al. (2002) divided the separation in the meshes into three areas, which refer to the filtration mechanisms and processes of surface and clog filtration as well as the particle breakthrough [3,16].

- Surface Deposition
- Clogging
- Bleeding

The distinction is made on the basis of the ratio between particle size D in the suspension to the mesh size of the fabric d_p used and the filament diameter d_f . This ratio provides information on the interaction of particles and filter cloth.

Bleeding: If the particles are smaller than 65% of the mesh diameter, turbidity occurs through the fabric. The particles penetrate the fabric completely. However, some of the particles adhere adhesively to the fabric fibres, resulting in a narrowing of the mesh diameter. With increasing particle penetration, the pores close and the filter medium resistance increases significantly compared to the pure water resistance. For particle sizes smaller than 40% of the mesh size, the formation of liquid bridges is much more difficult, which is contrary to the suitability of the fabric for the separation task at hand.

Clogging: By further increasing the particle size between 65 and 130 % of the mesh size, this behaviour is further enhanced. Now no collective of significantly smaller particles, which have built up to bridges

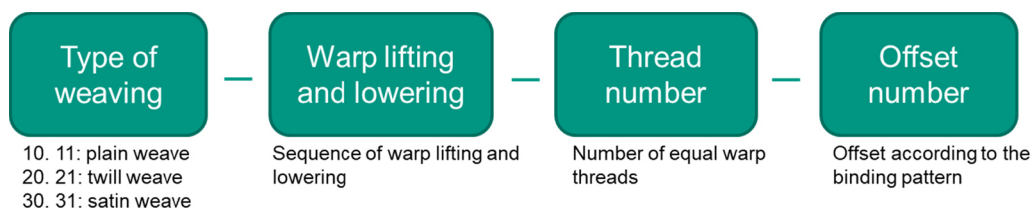


Fig. 2. Presentation of the differentiation criteria for the characterization of a fabric according to DIN ISO 9354.

Table 1
Cake filtration performance of yarns and fabrics styles (Ranking, starting from top to bottom) according to [13].

	Particle retention	Permeability (flow capability)	Cake dryness	Maximum cake discharge	Filter medium life	Resistance to blinding
Fibre Form	Spun staple	Mono	Mono	Mono	Spun staple	Mono
	Multi	Multi	Multi	Multi	Multi	Multi
Weave Pattern	Mono	Spun staple	Spun staple	Spun staple	Mono	Spun staple
	PRD	Satin	PRD	Satin	PRD	Satin
	Plain	Twill	Satin	PRD	Twill	Twill
	Twill	Plain	Twill	Twill	Plain	PRD
	Satin	PRD	Plain	Plain	Satin	Plain

over the meshes, block the mesh, but individual particles actively adhere to the meshes and significantly clog them. This behavior, also known as pore penetration, increases the filter medium resistance to a maximum until a decrease occurs again. This behaviour can be understood as a consequence of the significantly larger particles and the decreasing probability that these particles are deposited exactly on the respective meshes or that they occupy them perfectly. With regard to regeneration, clogging behaviour can be considered dramatic, as the particles first have to be removed from the fabric in order to reduce the initial resistance.

Surface Deposition: By further increasing the particle size (> 130% of the fabric mesh), the particles are increasingly deposited on the fabric surface. A clear boundary is created between the filter cake and the mesh. This leads to a smaller increase in fabric resistance. It is to be expected that this value for a significantly larger particle size, relative to the mesh size, will be close to that of the pure water resistance. However, the study by Purchas et al. (2002) ends with a particle 180% larger than the mesh size and a resistance that is larger by a factor of 1.8 in relation to the pure water resistance. In the case of surface deposition, the larger particles cover the meshes of the fabric and thus cause a decrease in the free area, which is equivalent to an increase in resistance. This is known as the spherical-hole model [15]. For this case of surface deposition, a very good regeneration can be expected due to the clear separation limit between particle collective and fabric.

At this point it must be mentioned that the value of the filter cloth resistance under real conditions (with particle interaction) can much higher than presented in [15]. This effect must be measured with the given filter cloth - particle system - combination in each case, taking [11] into account. Furthermore, the presented clear differentiation in bleeding, clogging and surface deposition as separation behavior of a real particle system does not take place. Rather, these effects overlap as a consequence of the particle size distribution in a real system.

The effect of the regeneration quality is based on the differentiation of the three penetration mechanisms of the particles into the fabric and is of particular importance for the Interpretation chapter.

3. Method

The regeneration behaviour is investigated on a laboratory candle filter, based on [11]. This is mounted in a process chamber where three essential process steps are carried out:

- I. Filtration
- II. Displacement
- III. Regeneration

In the case of filtration, the process chamber is first flooded with suspension and a pressure is set by means of an overflow valve. Then the filtrate line opens, and the filtration begins. The filtration is carried until the filtrate is clear and a predetermined amount of filtrate has been collected. The amount of filtrate corresponds to the cake thickness and allows a good reproducibility of the test procedure. When this filtrate volume is reached, the suspension is displaced in the process chamber by clear water. The purpose of this step is to be able to record the discharge in the subsequent step by means of image technology. After complete displacement of the suspension, regeneration is initiated by flashing of an LED. Then the backwash volume flows against the filtrate flow and removes the cake fragments. The process is recorded by image technology and is known in industry as cake discharge. This step is carried out using various fabrics and particle systems, which are presented in the following chapter “Materials”. The sequence of the experiments is shown in Fig. 3.

The technical image evaluation is carried out based on selected image sections at certain points in time. The remaining cake fragments are placed in relation to the initial state and connected to the backwashing volume required until then. Thus, the decrease of the filter cake occupied area during the cake release can be displayed time-resolved and compared with the necessary backwash volume. The underlying equation is shown in Eq. (1). The surface not regenerated (still has cake on it) at time t corresponds to the cake occupied area at time t divided by the cake covering area at the beginning of regeneration. This value ranges from 1 to 0. The cake thickness is obtained by measuring

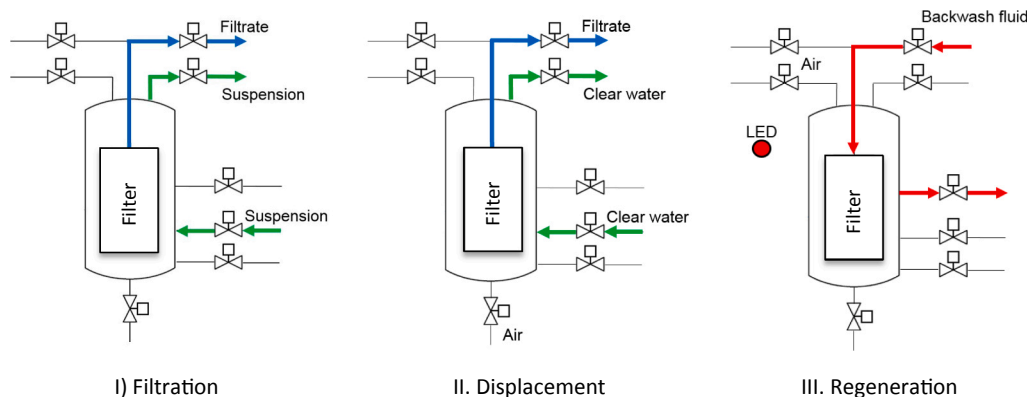


Fig. 3. Schematic flow chart of the experimental plant during filtration (I.), displacement suspension with clear water (II.) and regeneration through discharging into liquid phase (III.)

the cake thickness at the beginning of the regeneration. [11]

$$\text{Surface Contamination (t)} = \frac{\text{Area still occupied by cake at time t}}{\text{Cake area at the beginning}} \quad (1)$$

Using this evaluation method, the different release behaviour of fabrics can be compared. The materials used are described in the following section.

4. Material

Within the scope of the investigations, selected fabrics are placed on the laboratory filter candle mounted ($\varnothing = 30$ mm, length available for filtration 110 mm). These fabrics are sewn together to form a 30 mm diameter filter bag and the assembly areas, and the seam are sealed with liquid rubber. At the upper and lower end of the filter candle there are ~ 20 mm mounting surfaces for fixing the fabrics with clamps, which are not intended for filtration. The total length of the filter candle is therefore ~ 150 mm.

The first series of tests is carried out with twill woven filter fabrics. A special feature is the connection of multifilament warp threads, while the weft threads are monofilament. The contents of the test are 10 and 20 μm polypropylene and 11.5 μm PVDF fabric. Due to the type of weave (regarding the number of offsets), these fabrics show a clear difference in weight per unit area. While the fabric with the smallest offset number has the lowest weight (20 μm , 1.7 g/dm^2), the weight per unit area increases with increasing offset number (10 μm , 2.8 g/dm^2 ; 11.5 μm , 5.5 g/dm^2). The same behavior applies to the mean arithmetic surface roughness S_a , which is the smallest with 43 μm for fabrics with a smaller offset number but larger mesh size, and ~ 80 μm for fabrics with the same mesh size and larger offset number. The same trend can also be observed for the thread diameter and the fabric thickness, which are directly connected to each other. In total, the 3 fabrics have clear differences in roughness, mesh size and material and are therefore suitable for this study. A technical overview of the three fabrics is shown in Table 2.

For the second test series, monofilament/monofilament filter fabrics are examined which show clear differences to the previous filter fabrics. Contents are 3 woven fabrics of the plain and twill type with similar mesh sizes. The plain fabrics comprise 12, 14 and 22 μm , while the twill fabrics comprise 11, 14 and 20 μm . With regard to the materials, the majority are PET fabrics (12 & 22 μm braid and 11 and 20 μm twill), while the 14 μm plain consists of PA6.6 and the 14 μm twill consists of PP. With regard to the basis weight, the twill fabric tends to be heavier than the dutch weave, as it tends to require thicker threads for weaving with the same mesh width. This also becomes clear when measuring the threads and fabric thickness. With regard to roughness, there is no rule. The fabric type with the lowest roughness (12 μm plain) also has the highest roughness (14 μm plain), while the roughness value of the twill fabric varies from 30 to 40 μm . The overview of the fabrics is

summarized in Table 3, where the direct difference to the multifilament/monofilament fabrics from Table 2, which tend to be heavier and rougher, becomes clear.

The cleanability of the fabrics is assessed using the particle systems shown in Table 4. Filter cakes of defined thickness are built up for this purpose. The focus is on when the cake is completely discharged as a so-called complete discharge (patchy cleaning). The particle systems are selected on the basis of their clearly different shapes. This results in differently densely packed filter cakes and thus flow resistances. The investigation is carried out using the orthorhombic particle system (P1) with an $x_{50.3}$ value of 10 μm , which has the highest specific resistance α_H of $1.59 \cdot 10^{14}$ $1/\text{m}^2$. In addition, the flaky-shaped particles (P2) with an $x_{50.3}$ of 12 μm and $\alpha_H = 2.66 \cdot 10^{13}$ $1/\text{m}^2$ and the needle-shaped particle system (P3) with an average length $x_{50.1}$ of 21 μm and, as expected, the lowest flow resistance of $\alpha_H = 1.25 \cdot 10^{13}$ $1/\text{m}^2$. Due to the different shape, it can be assumed that both the deposition of the particles on the filter surface and the internal strength of the cake exhibit significant differences. These have a direct effect on the dropping behaviour. In the following chapter, the ejection behaviour of these 3 particle systems on the fabrics is presented.


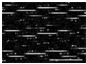

5. Interpretation

It is already known from previous investigations that the regeneration step “filter cake discharge” is essentially influenced by the filter cake thickness [Sources]. In general, a thicker filter cake provides a better regeneration quality. The so-called complete discharge, the complete detachment of the filter cake in one piece with subsequent sliding away from the filter surface, has proven to be a sign of quality. It was found that the total flow resistance, the product of the specific cake resistance α_H multiplied by the cake thickness H_{FC} , can be transferred between different particle systems. This was done with the particle systems shown in Table 4 by a series of tests in which the cake thickness was increased sequentially for each filtration process until a complete slipping occurred during the discharge process. This cake thickness was then used for multiple determination. A pressure dependence of the backwashing process could not be determined in this work because higher pressure only accelerated the backwash process, but the amount of backwash volume remains the same in the investigated range of 0.1–2.0 bar [11].

It was found that with the 20 μm twill fabric (multifile/monofilament) from Table 5 and a total resistance of $7 \cdot 10^{10}$ m^{-1} the complete discharge is independent of the particle system. Thus, the minimum required cake thickness for a good discharge could be predicted by dividing above total resistance value by the specific cake resistance of the respective particle system.

The question that arises here is can this principle of determining the minimum required cake thickness by the total resistance be applied to other fabrics. For this reason, two further multifilament/monofilament

Table 2
Characteristics of the multifilament filter cloths for the first test series.

Fabric type / mesh size [μm] / material	Weave according to DIN ISO 9354	Filter cloth resistance according to VDI 2762-2 [m^{-1}]	Weight per unit area [g/dm^2]	Surface roughness (ISO 25178) [μm]	Thread thickness warp/ weft [μm]	Fabric thickness (ISO 5084) [μm]	Image (The scale equals to 2 mm)
Multifilament Filter Cloth							
Twill 20	PP 20-02 02-01-03 Equal burr twill	$1.77 \cdot 10^{10} \pm 7.88 \cdot 10^9$	1.7	43	428 /106	390	
10	PP 20-02 03-01-04 Broad-billed twill	$9.82 \cdot 10^9 \pm 2.92 \cdot 10^9$	2.8	79	654 /146	560	
11.5	PVDF 20-02 05-01-06 Steep burr twill	$1.17 \cdot 10^{10} \pm 7.32 \cdot 10^9$	5.5	82	738 /111	550	

*Based on mean filter cloth resistance measured with Particle system P1, P2 and P3 (see Table 4).

Table 3
Representation of the monofilament filter cloths for the test series.

Fabric type / mesh size [μm] / material	Weave according to DIN ISO 9354	Filter cloth resistance according to VDI 2762-2 [m ⁻¹]*	Weight per unit area [g·dm ⁻²]	Surface roughness (ISO 25178) [μm]	Thread thickness warp/weft [μm]	Fabric thickness (ISO 5084) [μm]	Image (The scale equals to 1 mm)		
Monofilament Filter Cloth									
Twill	11	PET	20-03 01-01-03	7.63·10 ¹⁰ ± 1.63·10 ¹⁰	2	29	132 / 429	245	
	14	PP	20-02 01-01-02	1.52·10 ¹⁰ ± 1.40·10 ⁹	1.25	40	168 / 161	200	
	20	PET	20-03 01-01-03	1.56·10 ¹⁰ ± 3.33·10 ⁹	2	30	128 / 160	260	
Plain	12	PET	10-01 01-01-00	2.03·10 ¹⁰ ± 1.89·10 ⁹	0.5	9	100 / 45	80	
	14	PA6.6		9.41·10 ⁹ ± 1.37·10 ⁹	1	86	100 / 75	160	
	22	PET		9.38·10 ⁹ ± 2.12·10 ⁹	1.75	31	126 / 176	185	

* Based on mean filter cloth resistance measured with Particle system P1, P2 and P3 (see Table 4).

Table 4
Particle systems investigated for cake discharge in the liquid phase. The shapes of these particle systems vary from orthorhombic (a), to flaky (b), to needle-shaped (c) and result in different porosities and specific flow resistances α_H. The pictures and average particle sizes are provided by Quarzwerke GmbH. The specific flow resistances are measured with a pressure filter cell according to VDI 2762-2.

P1	P2	P3
SF300	Tremin 283-100	Tremin 939-304
x _{50,3} = 10 μm* α _H = 1.59·10 ¹⁴ 1/m ² 98% SiO ₂ (1.5% Al ₂ O ₃ , 0.1% CaO + MgO, 0.05% Fe ₂ O ₃ , 0.1% Na ₂ O + K ₂ O)	x _{50,3} = 12 μm* α _H = 2.66·10 ¹³ 1/m ² 51% SiO ₂ 45% CaO (1% Al ₂ O ₃ , 1% MgO, 0.3% Fe ₂ O ₃ , 0.1% Na ₂ O, K ₂ O)	x _{50,1} = 21 μm* α _H = 1.25·10 ¹³ 1/m ² 49% SiO ₂ 47% CaO (0.6% Na ₂ O + K ₂ O, 0.5% Fe ₂ O ₃ , 0.4% Al ₂ O ₃ , 0.4% MgO)
a)	b)	c)

* Based on measurements of Quarzwerke GmbH.

filter fabrics were have been investigated. One is a fabric with a smaller mesh size (10 μm) and one is a fabric made of another material (11.5 μm: PVDF). The investigation of the bindings has also shown that these fabrics differ, for example, in the number of offsets. The minimum required cake thicknesses observed from experiments for the three particle systems are summarized in Table 5. It can be seen that the two

meshes of similar mesh size (10 and 11.5 μm) behave similarly with regard to the required cake thickness. In the case of the three investigated particle systems, the cake thicknesses are almost the same between the investigated 3 multifilament filter cloths. The minimal differences can be neglected. When summarizing the total resistances, the multifilament/monofilament fabrics generate a complete discharge

Table 5
Summary of the necessary filter cake thicknesses for the three twill fabrics examined with multifilament/monofilament yarn combination. From the product of the filter cake thickness and the specific cake resistances from Table 4, an average flow resistance can be calculated for each fabric across all three particle systems.

Fabric type / mesh size [μm] / material	Weave according to DIN ISO 9354	Filter cake thickness for complete discharge [mm]	Average total resistance [m ⁻¹]	
Twill	20	PP	20-02 03-01-04	P1: 0.9 P2: 1.7 P3: 2.0 7·10 ¹⁰
	10	PP	Broad-billed twill 20-02 02-01-03	P1: 0.5 P2: 1.2 P3: 2.1 5·10 ¹⁰
	11.5	PVDF	Equal burr twill 20-02 05-01-06 Steep burr twill	P1: 0.5 P2: 1.2 P3: 2.3 5·10 ¹⁰

from a total resistance $> 5 \cdot 10^{10} \text{ m}^{-1}$. Here it becomes clear that the principle of using total resistance and calculating the required filter cake thickness with the specific flow resistance is **not only** suitable for transfer to other particle systems for the same fabric, like in [11], and also to other filter cloths. If a total resistance is exceeded, a good discharge will take place. Then, the typical backwashing volume for the regeneration of backwashing filters according to [17] of maximum 2 l/m^2 are not exceeded. In the case of all 3 fabrics from Table 5, only backwash volumes of $< 1 \text{ l/m}^2$ were necessary.

The next step of the investigation is the transfer of this principle to fabric with a monofilament/monofilament weaving structure. The evaluation of the minimum required cake thickness was carried out analogous to the multifilament/monofilament fabrics from the previous section.

Fig. 4 shows the course of the surface contamination over the time for the plain (a) and twill fabric (b) as an example for particle system P2 with a cake thickness of 1.2 mm . The crossing of the 2 l/m^2 with reference to [17] is marked by a dotted line. At the end of the backwashing procedure after $12 \text{ s } 5 \text{ l/m}^2$ flowed through the fabric. As the weave progresses, it becomes clear that the speed of the surface quality increases with decreasing mesh width of $22 \mu\text{m}$, $14 \mu\text{m}$ and $12 \mu\text{m}$ respectively. An explanatory approach provides the ratio between mesh size and mean particle diameter. While with the $22 \mu\text{m}$ fabric the $12 \mu\text{m}$ particles can penetrate the fabric, this penetration, assuming, is reduced with the consumer mesh size. With the $12 \mu\text{m}$ fabric, this ratio is 1 and it can be assumed that there is a clearer boundary between the fabric and the particles than with fabrics of larger mesh. Of course, smaller particles of the distribution will also flow into and through the fabric. Nevertheless, this explains why the cake is discharged cleanly with the $12 \mu\text{m}$ fabric, while in the $22 \mu\text{m}$ fabric it still has a surface coverage of $\sim 50\%$ after 1 s . Even after 2 l/m^2 ($\sim 5.5 \text{ s}$) this fabric still has a coating of $\sim 10\%$.

Compared to the course of the twill fabric, it becomes clear that, apart from the $11 \mu\text{m}$ fabric, the discharge behaviour becomes significantly worse and less reproducible. With the $14 \mu\text{m}$ and $20 \mu\text{m}$ fabrics, surface coverings of $40\text{--}60\%$ can be observed after 5 l/m^2 . However, with the $20 \mu\text{m}$ fabric from 2 l/m^2 there is no noticeable decrease in surface coverage. The tendency “Larger mesh = bad discharge” is not given. In a direct comparison of both $14 \mu\text{m}$ fabrics (plain and twill), it becomes clear that the $14 \mu\text{m}$ plain weave has a significantly better discharge behavior than the $14 \mu\text{m}$ twill weave. The

Table 6

Summary of the required cake thicknesses for a complete discharge of the monofilament/monofilament.

Particle system→ Filter cloth↓	Filter cloth resistance measured with particle system P3 [m^{-1}]	Filter cake thickness for complete discharge [mm]		
		P1	P2	P3
Plain	$12 \mu\text{m}$	$7.61 \cdot 10^9 \pm 1.03 \cdot 10^9$	$< 0.5^*$	< 0.5
	$14 \mu\text{m}$	$5.66 \cdot 10^9 \pm 1.75 \cdot 10^9$	1.4	< 0.5
	$22 \mu\text{m}$	$7.49 \cdot 10^9 \pm 1.91 \cdot 10^9$	2.1^*	< 0.5
Twill	$11 \mu\text{m}$	$1.52 \cdot 10^{10} \pm 2.93 \cdot 10^9$	1.4	1.6^*
	$14 \mu\text{m}$	$6.63 \cdot 10^9 \pm 4.51 \cdot 10^8$	1.2^*	2.4
	$20 \mu\text{m}$	$8.65 \cdot 10^9 \pm 1.98 \cdot 10^9$	2.5	2.2

ranking according to [13] can thus be confirmed. In addition, it becomes clear that the rougher fabric ($86 \mu\text{m}$ for the plain and $40 \mu\text{m}$ for the twill fabric) produces a filter cake discharge. One reason is that, due to the lower number of offsets, there is a higher mesh density in the plain weave due to the type of weave, which detaches the cake more homogeneously and thus leads to a complete discharge in the case of already thinner cakes.

The course in Fig. 4 clearly shows the different discharge behaviour of the fabrics. Accordingly, it is to be expected that the fabrics will be completely discharged at different cake thicknesses. For this reason, these fabrics were gradually filtered with thicker cakes to evaluate the regeneration behaviour, analogous to the multifilament/monofilament fabrics and [11]. When the minimum required cake thicknesses for a complete discharge were reached, the multiple determination was carried out. The determined cake thicknesses are documented in Table 6.

In the case of the plain weave and the P3 particle system, cake release takes place at very low cake thicknesses $< 0.5 \text{ mm}$. The difficulty with such low cake thicknesses is that no meaningful image evaluation is possible with further reduction. For this reason, the inequality $< 0.5 \text{ mm}$ cake has been defined as the minimum required cake thickness. If, however, it is to be expected that from a certain thickness of the cake, no complete discharge will be thrown off. What is noticeable, however, is that the particle system with an average length of $21 \mu\text{m}$, with a ratio between the size of the particle system and the mesh size of ≥ 1 , has very good discharges with all three plain weaves and the

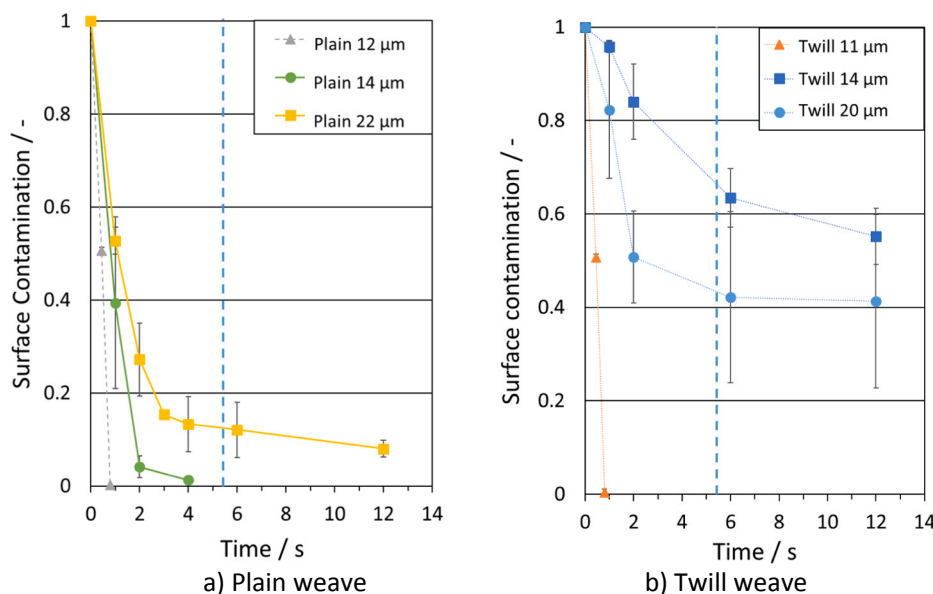


Fig. 4. Exemplary illustration of the discharge behaviour of plain weaves (a) and twill weaves (b) with monofilament warp and weft threads, using the P2 particle system with a filter cake thickness H_{FC} of $1.2 \pm 0.2 \text{ mm}$. The vertical dotted line symbolizes the 2 l/m^2 limit of the backwashing volume.

lowest cake thicknesses. In the case of the P2 particle system, this trend can also be seen in relation to the ratio. While a complete discharge is already produced at 1.4 mm for the 12 μm weave, the required cake thickness increases to 2.4 mm for the 14 μm weave and reaches a required cake thickness of 4.3 mm for the 22 μm weave. It can also be observed here that a further decrease in the ratio between particle size divided by mesh size < 1 leads to a higher minimum required cake thickness. And a similar behavior, although with smaller cake thicknesses, can be observed with particle system P1. However, in the case of fabrics with 12 and 22 μm , no complete discharge of the whole coherent filter cake could be observed [11]. Tangential cracks occurred in the filter cake during regeneration and leads to a discharge in larger fragments. Reasons for this could be that the fabric did not rest completely on the candle surface or that the cake thickness is simply too small for enough cohesion in the filter cake. Nevertheless, the filter cake is discharged extensively in larger fragments and of very good quality with a so-called “good partial discharge” [11]. All in all, a clear trend can be observed in the monofilament/monofilament fabrics regarding the particle/mesh size ratio. In addition, the discharge behaviour is clearly different from that of multifilament/monofilament twill fabrics, which required the thickest minimum required cake thicknesses with the needle-shaped P3 particle system.

If the discharge behaviour of the monofilament/monofilament twill fabric is added, the tendency for the 20 μm fabric can be confirmed. Here the required cake thickness is 2.5 mm for P1 (smallest ratio between particle/mesh sizes), over 2.2 mm for P2 to < 0.5 mm (largest ratio between particle/mesh sizes). However, the transfer to the 11 and 14 μm fabric is not possible. While the 11 μm has no tendency (the required cake thickness is between 1.4 and 1.7 mm), the 14 μm behaves like the multifilament/monofilament fabrics and vice versa regarding the particle/mesh size. Here, the largest cake thickness is required for the P3 particle system. A possible explanation is the lower mesh density (mesh/cm²) because of the higher number of offsets. This becomes clear in the permeability of the fabrics. However, this explanatory approach is only possible to a limited extent, since the 20 μm fabric also has a greater number of offsets, but nevertheless exhibits greater permeability because of the mesh size.

In summary, however, it can be said that monofilament/monofilament fabrics differ significantly from multifilament/monofilament fabrics. A possible transfer criterion based on the model of the total resistance is therefore not possible, since the particle system with the lowest specific flow resistance also has the smallest cake thickness for many fabrics. A prediction concept for the required cake thickness is presented in the following section.

The prediction concept for monofilament/monofilament fabrics is based on a consideration of [14], relating to the selection of filter fabrics. For this purpose, it is determined that the flow resistance of the filter medium should be between 2 and 15 % of the resistance of the filter cake (product of specific cake resistance and cake thickness). Applied to the problem of cake predictions, Eq. (2) can be derived from this consideration. Here there is the ratio between filter medium and specific cake resistance and a correction factor. These three variables should allow the minimum required cake thickness for a good filter cake release.

$$H_{FC} = \frac{\text{Filter Cloth Resistance}}{\text{Specific Filter Cake Resistance} \cdot \text{Factor}} \quad (2)$$

This prediction concept could be successfully performed for all six filter cloth. The basis of the measured filter cake resistance is based on that of particle system P3 (see Table 3). This particle system is to be classified in the area “Surface Deposition” with reference to the ratio of mesh size to particle size according to [3,16]. The deposition behaviour has proven to be particularly suitable for the prediction concept. For mean filter resistances based on the mean value from the particle systems P1, P2 and P3 used, as well as based on the mean filter resistance with P1 and P2, factors with too large a deviation have generated.

Table 7

Summary of the factor for calculating the minimum required cake thicknesses for monofilament / monofilament filter fabrics as a function of particle shape based on Eq. (2) with the filter cloth resistance measured with particle system P3 (see Table 3).

Particle system	Factor for complete Discharge	H _{FC} with surface contamination < 10%
Orthorhombic (P1)	0.032 ± 0.019	0.043 ± 0.017
Flaky (P2)	0.153 ± 0.091	0.281 ± 0.151
Needle-shaped (P3)	0.459 ± 0.142	0.502 ± 0.169

Further experiments with a needle-shaped particle system and an orthorhombic particle system have confirmed the tendency of the filter mean resistance. A needle-shaped particle system with a larger needle length (x50.1 = 33 μm) but a similar ratio of needle length to needle thickness was used. The fabric resistances against P3 vary only in the range of the standard deviation. In the sample with the further orthorhombic particle system (x50.3 = 40 μm , but with a clear fine fraction), the fabric resistance is similar to that of P1. The assumption here was that the larger particles enable surface deposition. However, the shape in combination with the fines content allowed bleeding and clogging. A particle system with a needle-shaped structure is therefore suitable for the evaluation system presented here. This form produces a separation by “surface deposition” and thus a very good prediction of the minimum required cake thicknesses.

On the basis of the data summarized in Table 7 for the factors dependent on the particle systems, the minimum required cake thicknesses for a complete discharge can be reliably predicted. It is also noticeable that the factor increases with increasing deviation from the ideal sphericity of 1. For example, a factor of 0.459 applies to the needle-shaped P3, while the orthorhombic P1 of 0.032 is much smaller. What is also noticeable with monofilament fabrics is that very clean surfaces were already possible with cake thicknesses below that of the complete discharge. For this reason, the factor was determined for surface cleanliness $< 10\%$ with the necessary backwash volumes of 2 l/m². This factor is greater than that for a complete discharge. Nevertheless, the discharge can be characterized as “very good”. For a more detailed investigation, the proportion of the factor for the respective fabric types (weave fabric and body fabric) for the respective fabric types was considered. The weave fabrics with a variation of 0.032 ± 0.019 for P1, 0.153 ± 0.091 for P2 and 0.459 ± 0.142 for P3 show a significantly lower variation than the twill fabrics with 0.043 ± 0.017 for P1, 0.281 ± 0.151 for P2 and 0.502 ± 0.169 for P3. Here, too, the needle-shaped fabric shows a clearly reproducible calculation.

The reason for the deviations of the twill fabrics is the 11 μm weave, which has a significantly worse prediction. This fabric stands out with a higher filter medium resistance as well as a high offset number in the weave type. Both factors are connected because the offset determines the mesh density on the fabric and thus the free area. Here it must be checked whether fabrics with a high offset can generally be described worse by this model. This will be investigated by further elaboration with regard to satin fabrics, which have the highest offset numbers.

With regard to the fluctuation of the factor for complete discharge, an influence of the measurement error as well as a fluctuation due to larger steps in the filtrate volumes for determining the complete discharge during evaluation cannot be excluded. In summary, however, the use of a factor is quite practicable, since a critical situation only occurs for larger values. In this case, an incorrect smaller cake thickness would be determined. But by the column $< 10\%$ in the first 2 s it becomes clear that for mean value + standard deviation for a complete discharge still \leq factor for surface purity 10% applies. This means that the discharge can certainly be rated as good to very good. In addition, no false negative results can be obtained.

By combining both discharge criteria (complete discharge and $<$

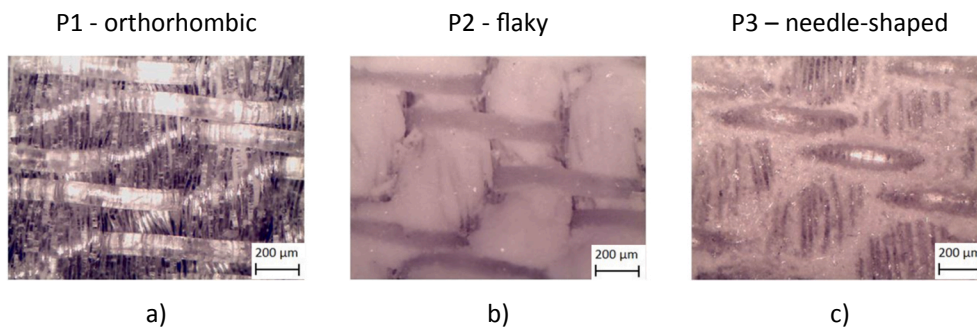


Fig. 5. Microscope images of the remaining particle layers on the 20 µm multifilament filter cloths for the particle system P1 (a), P2 (b) und P3 (c).

10% surface occupation in the first 2 s), it can be ensured that a good discharge is guaranteed, considering the factor for a complete discharge. By using the smaller factor, which is in the denominator in the calculation, the calculated cake thickness becomes thicker for a good regeneration. This is unfortunate in terms of filtration performance but leads to good surface cleaning. With increasing value of the factor, the calculated cake thickness would be thinner. This would lead to a bad discharge. The proof with the surface cleanliness $< 10\%$, however, clearly shows that the factor for a complete discharge is always below this value. Although the cake thickness becomes thinner, the regeneration quality is still “good” to “very good”.

6. Conclusion

The investigations have shown that, in addition to the influence of the particle system, a clear fabric influence prevails in the regeneration quality due to cake release. In the case of multifilament/monofilament fabrics, the release is largely determined by cohesion. For this reason, significantly greater cake thicknesses are required, which is possible not only between the particle systems within a fabric but also under the fabrics due to a minimum total resistance, product of specific cake resistance and cake thickness. This is $5 \cdot 10^{10} \text{ m}^{-1}$ for the investigated fabrics. It can be assumed that if this total resistance is exceeded, irrespective of the shape of the particle system, a complete cake discharge takes place. The regeneration quality can then be rated “good” to “very good”. This means that the cake is thrown in one piece or large fragments and no fragments remain on the fabric. However, it should be noted that the cake discharge does not show any information about the contamination within the fabric. The filter cake has the greatest resistance, especially in the filtration area of very fine particles, and must therefore be removed. Nevertheless, with reference to [11,18–21], a distinction must be made between the filter cake discharge and the subsequent intraweaving cleaning, the removal of remaining particle layers and individual particles in the fabric (clogging). This becomes clear when the Fig. 5 is considered. The following cleaning strategy is based on the current research results: After the cake has been discharged from the fabric at low backwashing pressure [11], an optional further cleaning of the remaining particle residues ideally takes place by a pulsating flow at higher pressure [18–20]. In addition, it becomes visible that the different particles exhibit significantly different detachment behavior. While the orthorhombic particles of P1 leave behind a very clean fabric, the flaky P2 detach in the meshes but remain on the multifilament fibers. The needle-shaped P3 behaves exactly opposite to P2.

The model for multifilament fabrics cannot be transferred to the monofilaments fabrics. For the estimation of the cleanability, the introduction of a ratio between particle size and mesh size has been shown to be useful. If this ratio is ≥ 1 , the boundary between particle layers and filter fabric is clearly pronounced and the cake is easier to remove. Here the assumption suggests that pronounced interference resistances after [15] lead to poorer cleaning results. This is confirmed

by the fact that larger forces are to be expected between particles instead of between particles and fabric [22,23]. By using and adapting a design formula according to [14], it is also possible to calculate the minimum required cake thickness by Eq.2 for 6 of the 6 fabrics investigated. The model can therefore also be applied to twill fabrics, provided that the number of offsets is low, which is associated with a high mesh density (meshes per unit area). Due to the lower number of meshes per unit area, the filter mean resistance increases significantly, and the model exhibits greater deviations with the determined factors (11 µm twill weave). With certain cake thicknesses, the cake was always discharged with a backwash volume of $< 2 \text{ l/m}^2$ [17]. Here it has been shown that the factor is probably related to the shape of the particle system. This correlation will be the subject of further investigation.

CRediT authorship contribution statement

Patrick Morsch: Conceptualization, Methodology, Software, Formal analysis, Investigation, Validation, Resources, Writing - original draft, Project administration. **Harald Anlauf:** Supervision, Writing - review & editing, Funding acquisition. **Hermann Nirschl:** Supervision, Writing - review & editing, Funding acquisition.

Declaration of Competing Interest

The authors declare that they have no known competing financial interests or personal relationships that could have appeared to influence the work reported in this paper.

Acknowledgement

The authors would like to thank the German Federation of Industrial Research Associations (AiF) for the financial support (IGF number 18591N). The authors would also like to thank all colleagues and students for the support in writing this paper. Special thanks go to my student Volker Bächle and Tom Gabor Shange for the support during their time at the institute.

References

- [1] K. Sutherland, *Filters and filtration handbook*, Elsevier, Oxford, 2008 [eng].
- [2] N.P. Cheremisinoff, *Liquid filtration*, Butterworth-Heinemann, Boston, 1998 [eng].
- [3] A. Rushton, *THE CHEMICAL ENGINEER*, 1970.
- [4] G.G. Chase, J. Arconti, J. Kanel, *Sep. Sci. Technol.* 29 (1994) 16.
- [5] E. Kehat, A. Lin, A. Kaplan, *Ind. Eng. Chem. Proc. Des. Dev.* 6 (1967) 1.
- [6] J. Marecek, *Ind. Eng. Chem. Process Des. Dev.* 20 (1981) 4.
- [7] A. Rushton, A.S. Ward, R.G. Holdich, *Solid-Liquid Filtration and Separation Technology*, Wiley-VCH, Hoboken, 2008 [eng].
- [8] K. Morris, R.W.K. Allen, R. Clift, *Filtr. Sep.* 24 Nr. 1 (1987).
- [9] H.R. Muller, R. Kern, W. Stahl, *Filtr. Sep.* 24 Nr. 1 (1987).
- [10] P. Morsch, J. Kühn, R. Werner, H. Anlauf, D.U. Geier, T. Becker, H. Nirschl, *Chem. Eng. Sci.* (2020).
- [11] P. Morsch, P. Ginisty, H. Anlauf, H. Nirschl, *Chem. Eng. Sci.* 213 (2020).
- [12] VDI-Guideline: Mechanical solid-liquid separation by cake filtration -

- Determination of filter cake resistance: 2762-2, 2010.
- [13] D.B. Purchas, *Solid-Liquid Separation Technology: Chapter 3*, Uplands Press, Croydon, 1981.
- [14] A. Rushton, P.V.R. Griffiths, *Filtr. Sep.* (1972) 9.
- [15] J.W. Tichy, *Fortschritt-Berichte VDI Reihe 3, Verfahrenstechnik, Vol. 877: Zum Einfluss des Filtermittels und der auftretenden Interferenzen zwischen Filterkuchen und Filtermittel bei der Kuchenfiltration*, VDI-Verl., Düsseldorf, 2007 [ger].
- [16] D.B. Purchas, K. Sutherland, *eng, Handbook of filter media*, Elsevier Advanced Technology, Oxford, 2002.
- [17] S. Ripperger, *Filtrieren und Separieren* 22 Nr. 2 (2008).
- [18] C. Weidemann, S. Vogt, H. Nirschl, *J. Food Eng.* 132 (2014).
- [19] S. Stahl, C. Leipert, H. Nirschl, *Sep. Purif. Technol.* 110 (2013).
- [20] C. Leipert, H. Nirschl, *F & S International Edition* 11 (2012).
- [21] P. Morsch, P. Ginisty, H. Anlauf, H. Nirschl, *Sep. Purif. Technol.* 249 (2020).
- [22] M. Ferer, D.H. Smith, *J. Appl. Phys.* 81 (1997) 4.
- [23] A. Dittler, M.V. Ferer, P. Mathur, P. Djuranovic, G. Kasper, D.H. Smith, *Powder Technol.* 124 (2002) 1–2.

H. Attached publication [3]

Verification of the contribution from the co-authors

Title: Description of the filter cloth deformation during backwashing filtration

Journal: Separation and Purification Technology

Authors: P. Morsch, M. Bauer, C. Kessler, H. Anlauf, and H. Nirschl

Position in the dissertation:

The content of this paper has been included in Chapter 4.4 and 5.1

Contribution of Patrick Morsch

Conceptualization, Methodology, Software, Formal analysis, Investigation, Validation, Resources, Writing - Original Draft, Project administration

Contribution of Maurus Bauer

Investigation, Writing - Review & Editing

Contribution of Christoph Kessler

Investigation, Writing - Review & Editing

Contribution of Harald Anlauf

Supervision, Writing- Reviewing and Editing, Funding acquisition

Contribution of Hermann Nirschl

Supervision, Writing- Reviewing and Editing, Funding acquisition



Description of the filter cloth deformation during backwashing filtration

Patrick Morsch^{*,1}, Maurus Bauer, Christoph Kessler, Harald Anlauf, Hermann Nirschl

Institute of Mechanical Process Engineering and Mechanics (MVM), Process Machines (VM), Karlsruhe Institute of Technology (KIT), Germany



ARTICLE INFO

Keywords:

Liquid filter cake discharge
Force-stretch behaviour of filter cloth
Backwashing filtration
Filter cloth deformation
Geometrical moment of inertia
Bulging-out behaviour
Register distance

ABSTRACT

The separation of fine particles with filter cloth is a commonly used technique to remove particles from process streams under low-cost and low-maintenance conditions. Such kind of filter apparatus can be found, i.e., in front of distillation columns with the adjusted size. Here, it is possible to have a filter apparatus with filter elements ≤ 2.5 m in length and ≤ 100 elements in one vessel. For a constant and stable process conditions, a periodical regeneration of the filter cloth is absolute required. One option for realizing this procedure is discharging the built-up filter cake in liquid phase (backwashing filtration). Due to the reverse flow, a deformation of the filter cloth occurs. This deformation depends on the assembly situation, mechanical pre-loading of the weave, the environment of the system, the weave type and, of course, the backwashing pressure. The interaction of this variables results in an adjusting of the space between the filter elements and correspond with the required backwashing volume in l/m^2 .

Influence of a contact between two filter elements is not known but can have a negative impact in case of remaining filter cake on surface. Too much space reduces the economy of the apparatus because less filter surface needs the same apparatus footprint. Thus, by knowing how the filter cloth expand, the space can be adjusted on the particular separation task. This can lead to an improvement of the filter surface per apparatus footprint and can be advantageously compared to competing separations procedures. The deformation of the filter cloth during the backwashing treatment is described and discussed in the context of this investigation on the basis of elementary mechanics.

1. Introduction

The separation of particles by means of filter fabrics is a common method for removing particles from process streams in a cost-effective and low-maintenance manner. Such filter apparatuses can be found, for example, upstream of distillation columns and are correspondingly large (filter elements ≤ 2.5 m in length; up to 100 filter elements per apparatus). For constant and stable process control, it is essential to regenerate the filter after complete filtration [1]. One way of achieving this, is to carry out filtration with regular flow reversal (backwashing filtration) [2].

While the theory of filtration has been comprehensively analysed and documented, filter backwashing represents an inadequately investigated application. Knowledge of the theoretical principles of backwashing and the correct choice of cleaning parameters are important for the economical operation of a backwashing filter system.

Regeneration by backwashing results in bulging of the filter cloth due to flow reversal. This behavior has been studied for gas pulse-based cake discharge and depends on the backwashing pressure and the

acceleration of the fabric acting on the cake [3,4]. This deformation depends, among other things, on the installation configuration, the pretension, operation conditions and the pressure acting on the weave.

Fig. 1 shows filter elements installed on one register. It becomes clear that the correct choice of the element distance is largely determined by the deformation of the fabric occurring during regeneration/backwashing. This process is shown schematically in Fig. 1(b) [5]. If the distance between the filter elements is too small, they obstruct each other during backwashing. Efficient cleaning is not to be expected here. If, on the other hand, the register distance and element distance is too large, good cleaning will take place, but the ratio of filter area to apparatus footprint is too small. Knowledge of the bulging behaviour is therefore necessary to optimize the regeneration and filter design economy.

One possibility to describe the deformation behaviour of filter fabrics is provided by the bending beam theory known from technical mechanics [6,7].

The present study assesses whether this theory is suitable for describing the deformation of fabric during backwash filtration. The aim

* Corresponding author.

E-mail address: patrick.morsch@kit.edu (P. Morsch).

¹ Research Fellow.

Nomenclature	
<i>Symbols</i>	
E	Young modulus [N/mm ²]
H	Height variable [mm]
I(x)	Geometrical moment of inertia [mm ⁴]
l _{tot}	Total length of the filter [mm]
q ₀	Line load [N/mm]
w(x)	Bulge [mm ⁴]
x	Length coordinate [mm]

the efficiency of the entire process suffers.

To prevent the filter regeneration from becoming the bottleneck of the filtration process, the present paper deals with the optimization of the spacing among filter elements and registers according to Fig. 1. The aim is to enable an increase of the filtration area by smaller element and register spacings and to achieve an improvement of the regeneration by backwashing.

3. Material and method

As already explained in Fig. 1, it is essential for optimal operation of a filter system to know the bulging of the filter used during regenera-

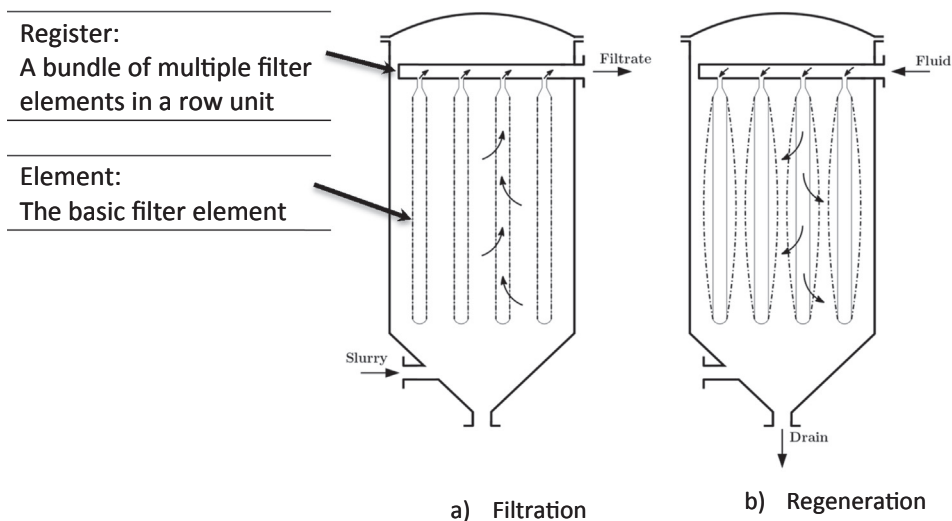


Fig. 1. Backwashing filter during filtration (a) and regeneration (b). The bulging of the filter cloth during backwashing is shown schematically [5].

is to enable an increase in the filter area per footprint based on an accurate description of the expansion behaviour of the filter cloths.

2. Mechanisms of filter cloth deformation

The mechanical behaviour of the filter cloth during regeneration by backwashing is already the subject of many publications in gas filtration and especially in bag filters [3,4,8,9]. In the case of liquid filtration, this process has only been studied for dry cake discharge with a gas backflow [10,11].

The process of liquid filtration in the liquid phase with subsequent cake discharge with a liquid backflow, although extensively practiced in the industry is only currently being investigated [2]. A theoretical description of the mechanical behaviour of filter cloths is completely unknown and is only described by assumed strains and their effects [11]. The filter cloth stretching has a significant influence on the regeneration with regard to the necessary backwashing volume.

Adequate understanding not only in gas backflow for dry cake discharge but also in liquid backflow mode wet cake discharge filtration is an essential step to design backwashing filters. Poor cleaning increases the pressure loss or reduces the available filter area, because of which

this is underlined, for example, by the fact that the bulging of the filter fabric increases the necessary backwash volume by 50–60%.

At present the choice of the register and element spacing is an in-house experience but is not based on knowledge of the mechanical behaviour of the filter cloth. In the context of this work the bulging behaviour of various filter fabrics caused by backwashing is therefore examined in more detail. The procedure of the investigation comprises three points:

- Selection of representative filter fabrics
- Determination of the mechanical properties of the fabrics (force-stretch behaviour)
- Flow through the fabric in a filter system and measure the bulge

After the selection of suitable filter fabrics, the force-stretch behaviour is evaluated. For this purpose, the fabrics are examined in a tensile testing machine. The aim here is to determine the bulging behaviour of the filter cloths used to understand the deformation occurring during backwashing on this basis. Filtration and backwashing then take place in a leaf filter system. Here, the filter fabric is flowed through and the bulge is evaluated by imaging. The selection of the filter fabrics,

Table 1
Overview of the filter fabrics used.

Fabric type/mesh size [μm] /Material	Weave type [DIN ISO 9354]	Weight per area [g/dm ²]	Surface roughness (ISO 25178)	Thread thickness warp/weft [μm]	Fabric thickness (ISO 5084) [μm]	
twill	11 PET	20-03 01-01-03	2	29	132/429	245
	14 PP	20-02 01-01-02	1.25	40	168/161	200
	20 PET	20-03 01-01-03	2	30	128/160	260
plain reverse dutch	12 PET	10-01 01-01-00	0.5	9	100/45	80

as well as the structure of the corresponding tests and their execution are explained in the following chapters.

3.1. Filter fabrics

The basis for the examination are the fabrics listed in Table 1. The filter cloths vary in weave type and pattern in order to achieve a general validity of the measurements performed.

The three twill fabrics examined have mesh sizes of 11 μm, 14 μm and 20 μm. While the 14 μm twill fabric is made of polypropylene (PP), the other two are made of polyethylene terephthalate (PET). The used plain reverse dutch filter cloth also consists of PET and has a mesh size of 12 μm (see Table 1).

Looking at the weave pattern, the 11 μm and the 20 μm fabrics are similar. Here, three warp lifts are followed by a warp lowering. In the case of the 14 μm fabric, the weaving pattern is given by two warp thread transfers to a warp thread underpass. The plain reverse dutch weave shows the usual variation between warp lifting and warp lowering. All fabric types are monofilament in warp and weft direction and have a single-thread weaving pattern.

The number of offsets in the twill fabrics corresponds to the number of warp lifts, which means that there is no twill of the same degree, but an inclined or wide twill. Due to the type of weave, the weight per area of the twill fabrics is considerably greater than those of the plain reverse dutch fabric. Due to the thicker threads, the filter cloths with twill weave are rougher than the plain reverse dutch fabric, which is also noticeable in the overall thickness.

The filter cloths examined within the scope of this work thus show a clear variation in the following points:

- Weave type
- Mesh size
- Material
- Thread/weave thickness

With regards to twill and plain reverse dutch fabrics, this is therefore a representative selection for filter fabrics < 20 μm. Fabrics with satin weave are not included in this paper.

3.2. Experimental set-up – Tensile testing machine

The stress-strain behaviour of the fabrics is determined using a

tensile testing machine. The test setup and execution are based on ASTM Standard 6614–07.

In order to install the fabric in the tensile testing machine, it is clamped in the device shown in Fig. 2(a). The filter frame used here has a width of 50 mm. The fabric is then stretched. The force applied by the pulling device and the corresponding change in length are detected. The measured change in length is related to the initial length of 150 mm (see Fig. 2(a)), resulting in the fabric elongation. The tension acting in the filter cloth is calculated from the recorded force using the fabric width (50 mm) and fabric thickness (see Table 1).

Thus it is possible to record the tension curve of the 11 μm twill fabric in warp direction as shown in Fig. 2(b). The test moves completely in the elastic area of the fabric. Here it becomes clear that the stress can be divided into several areas (see Fig. 2b):

- I. High elongation with low force
- II. Exponential force increase with comparatively low elongation increase
- III. Further increase in force at low elongation

Especially at the beginning of the tensile tests, significant changes in elongation at low force can be observed. If this range is linearized (coefficient of determination > 95%), a slope of ~85 N/mm² is recorded for strains of up to 0.4%. The gradient corresponds to the modulus of elasticity, modelled on Hook's range. With further elongation, the necessary force increases strongly. Here, for example, a modulus of elasticity of 1247.6 N/mm² can be determined for strains of 0.4 to 0.6% for the second range. An increase of the Young's modulus by a factor of fifteen can be explained by different physical processes in the fabric during elongation. While in the beginning (area I) the elongation is mainly caused by a displacement of the fabric meshes in the weaving pattern, in area II the elongation is mainly caused by direct tensile loading of the fibres. For this reason, a strong increase in the modulus of elasticity in the direction of the material characteristic value of PET (according to ISO 527–2 approx. 3600 N/mm²) can be observed. With a further increase in force, the increase in elongation is less pronounced. Thus, a further increase of the Young's modulus to ~1800 N/mm² for elongations up to 1.07% can be observed.

After knowing of the stress-strain curve, the filter cloth is bulged on a leaf filter system. In this test, the fabric is deliberately used as a flat leaf filter to investigate the influence of warp and weft direction. Effects of a cylindrical shape of the filter cloth, as they occur with the widely

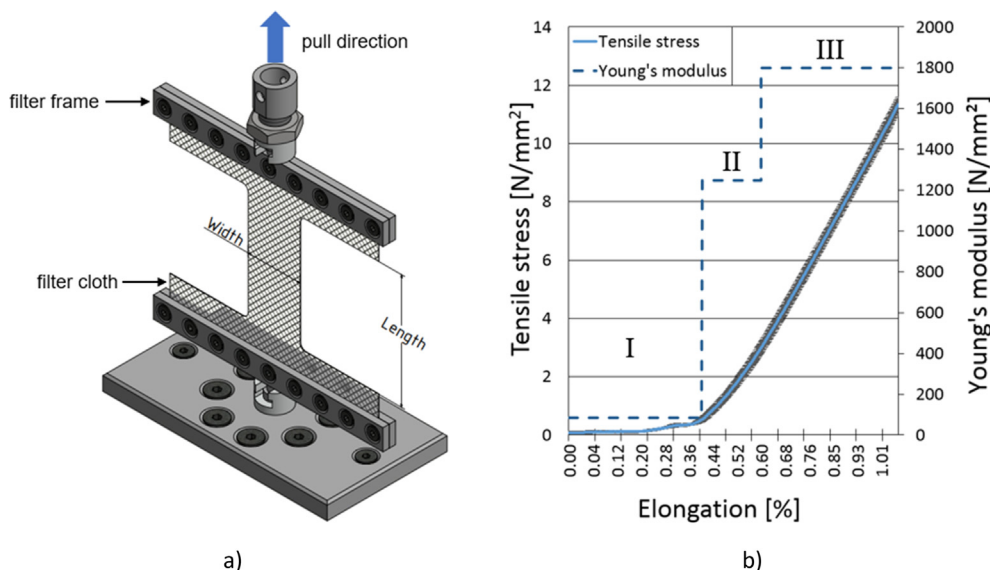


Fig. 2. Illustration of the test setup for determining the tensile strength of filter fabric (a) and exemplary illustration of the stress-strain diagram with linearization and modulus of elasticity for the 11 μm filter cloth in warp direction (b).

used candle filters, are not examined in detail in this paper. The structure and performance of the backwash tests are described in the following chapter.

3.3. Experimental set-up – Leaf filter

The bulge tests are carried out using a leaf filter with a filter area of $150 \times 100 \text{ mm}^2$. Due to the rectangular filter profile, influences of the weaving direction on the fabric deformation can be illustrated. Fig. 3 shows the structure of the filter element. This consists of the actual leaf filter, which is loosely embedded in a stenter frame. If a fabric is mounted on the filter element, the fine thread can be used to move the leaf filter against the fabric. This creates a defined pre-tension of the fabric.

The bulging of the filter cloth occurs at defined pre-tensions of 1 Nm and 10 Nm for different backwash pressures (0.3/1.5/3.0 bar). The individual backwashing processes are recorded visually using a camera. The resulting bulging of the fabric is then determined by image evaluation.

Now that the stress-strain behaviour and the bulge are known, the geometrical moment of inertia $I(x)$ of the filter cloth can be determined according to Eq. (1). The variable is a moment of resistance to bending, which originally comes from the bending beam theory of technical mechanics/statics. In the case of a bending beam clamped on both sides, the differential equation provides the form integrated in Eq. (1) [6,7]. It holds that the greater $I(x)$, the more stable the body is against bending. When transferred to filter fabric, this is equivalent to bulging. This is because the fabric on the leaf filter is also a body clamped on both sides which is deformed with an even load. If the bulge $w(x)$ is now resolved against the bulge, the equation shown in Eq. (2) results.

With the knowledge of $I(x)$ it is then possible to calculate the bulge $w(x)$ of a real backwash process (Eq. (2)). This allows the distance between the filter elements to be adjusted and the filter area utilization to be improved. Since the maximum bulging occurs in the middle of the filter cloth, only the length variable x must be replaced by $\frac{1}{2} \cdot l_{tot}$. The l_{tot} represents the total length of the fabric. The Young modulus must be adapted to the elongation, since fabrics exhibit anisotropic, nonlinear elongation behaviour (see Fig. 2(b)). The description of the individual variables and their origin are summarized under “Sources” in the description of the equation.

$$I(x) = \frac{\frac{1}{24} \cdot q_0 \cdot x^4 - \frac{1}{12} \cdot q_0 \cdot l_{tot} \cdot x^3 + \frac{1}{12} \cdot q_0 \cdot l_{tot}^3 \cdot x}{E \cdot w(x)} \tag{1}$$

$$w(x) = \frac{\frac{1}{24} \cdot q_0 \cdot x^4 - \frac{1}{12} \cdot q_0 \cdot l_{tot} \cdot x^3 + \frac{1}{12} \cdot q_0 \cdot l_{tot}^3 \cdot x}{E \cdot I(x)} \tag{2}$$

Symbol	Unit	Description	Source
q_0	[N/mm]	Line load	Measured and calculated
$l_{tot}; x$	[mm]	Length coordinate	Geometric dimension
$w(x)$	[mm]	Bulge	Optical measurement
E	[N/mm ²]	Young modulus	Stress-strain curve measurement
$I(x)$	[mm ⁴]	Geometrical moment of inertia	Calculated

4. Interpretation

The study carried out in the context of this work can be divided into the following key points:

- I. Determination of fabric-dependent strength values
- II. Determination of the filter bulge at the leaf filter
- III. Calculation of the second moments of area of the fabrics

The following section describes the results of the tensile tests and

the measured bulge during backwashing.

4.1. Tensile test and bulging

As shown in Fig. 2(b), the areas for determining the Youngs moduli can generally be described by three envelopes. These are summarized in Table 2 for the four investigated filter cloths. The Youngs moduli in warp and weft direction of the fabrics are shown for different elongations, as well as the bulge during backwashing as a function of preload (expressed by torque) and backwash pressure (0.3–3.0 bar).

In the case of the 11 μm fabric, there is a strong increase in elongation in the warp direction with minimal effort (see area I in Fig. 2(b)). In this area, the meshes shift against each other. Then, in area II, the modulus of elasticity increases sharply to approx. 1250 N/mm^2 . The modulus of elasticity reaches its maximum value in area III with a value of approx. 1800 N/mm^2 at an elongation of 1.07%. Here the fabric begins to deform plastically. In the case of the tensile tests in the weft direction. Here a significantly greater elongation (up to 1.5%) takes place at a lower stress (290 N/mm^2). The 12 μm weave also exhibits similar behavior, albeit to a lesser extent. Here a stress of $\sim 1500 \text{ N/m}^2$ is measured at a maximum elongation of 1.14% in warp direction, while the modulus of elasticity at similar elongation in weft direction (1.17%) is only $\sim 910 \text{ N/mm}^2$. In the case of the 14 μm twill fabric, the elongation range can be described with only two envelopes. Here a clear difference between warp (1% elongation with 1043 N/mm^2) and weft (3.8% elongation with 76 N/mm^2) is found. The 20 μm fabric behaves analogously to the 11 and 14 μm fabric. In total, however, a clearly anisotropic behaviour of the fabrics can be observed.

With regards to deformation, the expected trend that increasing prestressing will reduce bulging is confirmed. The bulge furthermore increases with rising backwashing pressure.

However, special features can also be observed. In the case of the 11 μm fabric in warp direction, the bulge is similar at backwash pressures of 3.0 bar in the case of a preload of 1 Nm and 10 Nm. Here it can be expected that the fabric will be moved from the elastic to the plastic area by the high load. A permanent change in length with the associated change in elongation is to be expected. The situation is similar at 11 μm in the weft direction. Here even a larger bulge is measured at higher preload. Similar behaviour can also be observed at 12 μm in the weft direction and at 14 μm in the warp direction. Here the added value for practice is, that a too high pre-tension of the fabric is

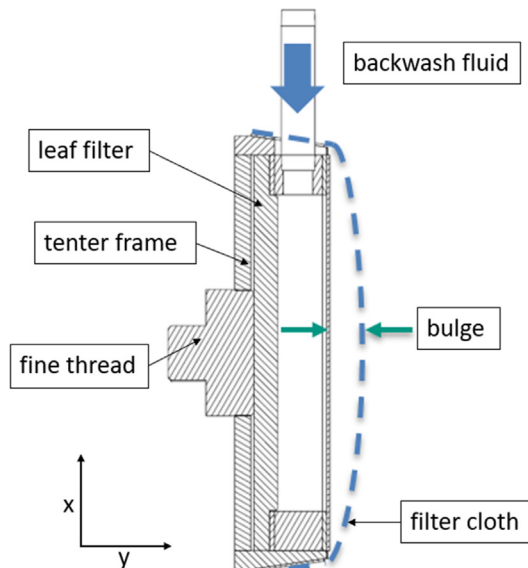


Fig. 3. Sectional view of the leaf filter in the stenter frame with exemplary depicted bulging of the fabric (dashed line) during backwashing procedure.

Table 2
Young moduli and bulges for the four investigated filter fabrics.

Fabric		Young Modulus for defined elongation ranges ϵ [N/mm ²]			Preload torque	Bulge		
Fabric type	thread direction	Area I	Area II	Area III	[Nm]	[mm]		
					Backwash pressure →	0.3 bar	1.5 bar	3.0 bar
11 μm 20-03 01-01-02	warp	0% $\leq \epsilon < 0.40\%$ 84.98	0.40% $\leq \epsilon < 0.60\%$ 1247.60	0.60% $\leq \epsilon < 1.07\%$ 1798.55	1 10	11.3 9.4	16.4 15.5	18.1 17.7
	weft	0% $\leq \epsilon < 0.41\%$ 77.77	0.41% $\leq \epsilon < 0.69\%$ 109.60	0.60% $\leq \epsilon < 1.52\%$ 290.64	1 10	9.5 8.7	10.9 10.5	11.9 12.1
12 μm 10-01 01-01-00	warp	0% $\leq \epsilon < 0.50\%$ 225.98	0.50% $\leq \epsilon < 0.80\%$ 881.93	0.80% $\leq \epsilon < 1.14\%$ 1487.15	1 10	13.9 8.0	16.1 11.8	17.6 14.0
	weft	0% $\leq \epsilon < 0.39\%$ 236.63	0.39% $\leq \epsilon < 0.65\%$ 702.64	0.65% $\leq \epsilon < 1.17\%$ 912.62	1 10	13.8 15.6	14.9 16.7	15.6 17.5
14 μm 20-02 01-01-02	warp	0% $\leq \epsilon < 0.15\%$ 457.08	0.15% $\leq \epsilon < 1.03\%$ 1043.39	-	1 10	17.5 16.8	18.5 18.6	19.1 19.1
	weft	0% $\leq \epsilon < 0.33\%$ 88.39	0.33% $\leq \epsilon < 0.66\%$ 30.02	0.66% $\leq \epsilon < 3.79\%$ 76.76	1 10	14.9 10.7	16.1 11.8	16.6 12.3
20 μm 20-03 01-01-03	warp	0% $\leq \epsilon < 0.35\%$ 130.07	0.35% $\leq \epsilon < 0.50\%$ 1378.11	0.50% $\leq \epsilon < 0.76\%$ 2025.31	1 10	16.3 3.0	17.9 5.0	18.6 6.0
	weft	0% $\leq \epsilon < 0.33\%$ 105.90	0.33% $\leq \epsilon < 0.73\%$ 468.38	0.73% $\leq \epsilon < 0.91\%$ 565.19	1 10	10.0 2.7	10.9 4.7	11.5 5.8

counterproductive for backwash filtration.

Another remarkable observation is, that the weft direction has a smaller bulge than the warp direction. This becomes clear with the 20 μm twill fabric. Although the modulus of elasticity in the warp direction is higher and therefore requires more force per stretch, the bulge for warp direction on the long edge (150 mm) of the filter fabric is greater. This is based on the superposition principle. Under the assumption that the more stable fibre direction determines the bulging, in the case of the warp direction on the 150 mm side of the leaf filter the fabric fibres have a greater possibility of elongation than would be the case with the 100 mm side (load in the weft direction). This behaviour can also be observed for all other fabrics. The added value for practice here is that the fabric fibre with the higher strength should be mounted on the shorter side of right-angled filter elements in order to achieve the lowest possible bulging. In summary, the following findings can be taken from Table 2:

- Anisotropic behaviour of the filter fabrics
- Reduced bulging with stiffer fabric
- Greater bulging when fiber with lower strength is on long filter edge
- Deviations from standard behaviour with larger preloads/backwash pressures

4.2. Geometrical moment of inertia

After the first step in the geometrical determination of strain behavior and bulging, the geometrical moment of inertia (cf. Eq. (1)) are calculated for the different preloads and backwashing pressures. For this purpose, the backwashing pressure in N/mm² is converted into a

line load in N/mm with the geometry of the filter cloth and the moment of inertia is calculated with the aid of the cloth length l_{tot} and the point of maximum cloth bulge $x = \frac{1}{2}l_{\text{tot}}$, the modulus of elasticity $E(\epsilon)$ and the measured bulge $w(x)$ at the point $x = \frac{1}{2}l_{\text{tot}}$.

These are summarized in Table 3 as mean geometrical moment of inertia over the entire range of backwash pressures (0.3, 1.5, and 3.0 bar). This is possible with regards to Eq. (1), since in the case of a higher backwash pressure the bulge also increases. Only the modulus of elasticity increases as a result of the larger bulging and would have to be iteratively adapted to the strain, for example for a simulation.

The connection of the elongation ϵ as a function of the modulus of elasticity is ($\epsilon = f(E)$), because it applies equally to the modulus of elasticity, which increases with increasing elongation ($E = f(\epsilon)$). Taking Table 3 into account, it is noticeable that the second moment of area for all fabrics ranges from $10^5 - 10^6 \text{ mm}^4$ for fabrics $< 20 \mu\text{m}$, backwash pressures from 0.3–3.0 bar and prestressing torques of 1 and 10 Nm. It should be noted that fabrics with lower bulging have a higher modulus of elasticity and the fluctuation of the geometrical moment of inertia, analogous to the bulge, is lower. According to [2], the required backwash volume for cake discharge by liquid backwashing is not pressure-dependent. Only the cake discharge process is accelerated with higher backwashing pressure. From this point of view, smaller backwashing pressures can be selected so that the bulge and thus the geometrical moment of inertia required for the design is smaller (0.3 bar: 4.5·10⁴ to 105). Based on this knowledge, the real bulge can be estimated with a geometrical moment of inertia of 10^5-10^6 mm^4 . For a conservative design, a smaller geometrical moment of inertia must be used so that the bulge is assumed to be larger. The design of the element distances is then based on Fig. 1 as the sum of the double bulge, the double filter

Table 3
Average Geometrical moment of inertia over all backwash pressures 0.3-3.0 bar) and preload torques (1-10 Nm).

Fabric type/mash size [μm]/Material			Weave type [DIN ISO 9354]	Geometrical moment of inertia [mm^4]
Twill	11	PET	20-03 01-01-03	warp: $3.04 \cdot 10^5 \pm 2.80 \cdot 10^5$ weft: $3.52 \cdot 10^6 \pm 2.45 \cdot 10^6$
	14	PP	20-02 01-01-02	warp: $3.13 \cdot 10^6 \pm 2.12 \cdot 10^6$ weft: $4.37 \cdot 10^6 \pm 2.85 \cdot 10^6$
	20	PET	20-03 01-01-03	warp: $2.85 \cdot 10^5 \pm 8.18 \cdot 10^4$ weft: $2.87 \cdot 10^5 \pm 2.34 \cdot 10^5$
Plain reverse dutch	12	PET	10-01 01-01-00	warp: $2.85 \cdot 10^5 \pm 8.18 \cdot 10^4$ weft: $2.87 \cdot 10^5 \pm 2.34 \cdot 10^5$

cake thickness and a safety factor and is shown in Eq. (3).

$$H_{Element} = 2 \cdot H_{Bulge} + 2 \cdot H_{filter\ cake\ thickness} + H_{Safety} \quad (3)$$

The Geometrical moment of inertia resolved for the respective pressure and calculated with the bulge from Table 2 is broken down in Table 4. The example of the 11 μm twill fabric illustrates why the standard deviations in Table 3 are sometimes of similar magnitude to the mean value. Here, for a backwash pressure of 0.3 bar, the calculated geometrical moment of inertia for 11.3 mm bulge (warp direction) has the value 5.64·10⁴ mm⁴ and increases with increasing backwash pressure to 1.34·10⁵ mm⁴ (1.5 bar) and 2.44·10⁵ mm⁴ (3.0 bar). In the weft direction, the increase is less pronounced, but the geometrical moment of inertia of 10⁶ mm⁴ is one order of magnitude greater. The reason for this has already been discussed and is that in the case of “weft direction on long filter element edge” the more stable warp threads lie on the shorter fabric edge. The validity of the superposition principle becomes clear here based on the larger geometrical moment of inertia or the smaller bulge.

Also, the 12 μm weave follows this tendency, whereby for each combination of backwash pressure and preload an increase of one variable is accompanied by an increase of the geometrical moment of inertia. Only at a preload of 10 Nm from 1.5 bar to 3.0 bar the geometrical moment of inertia stagnates due to a plastic deformation of the filigree plain reverse dutch weave due to the slight increase of the bulge and at the same time a strong increase of the geometrical moment of inertia (see Table 2).

This tendency is also confirmed for the 14 μm and 20 μm twill fabric without outliers. Both fabrics even have the highest geometrical moment of inertia in the 10⁷ mm⁴ range in the weft direction. Only the 14 μm fabric shows an abnormality in the warp direction when compared with 1 Nm and 10 Nm pre-tension. The geometrical moment of inertia shows similar values here. This is due to the constant gradient of the modulus of elasticity of 1043.39 N/mm² even at slight elongations of > 0.15%.

In summary, because of their anisotropic force-stretch behaviour, the fabrics do not exhibit any linear stretching during backwashing. However, the description geometrical moment of inertia for different strains is possible and provides values in the range 10⁴–10⁷ mm⁴. The

values for lower backwash pressures (0.3 bar; tendency towards 104 mm⁴) are to be classified as technically relevant. The more stable fibre direction should also be clamped on the shorter edge of the filter geometry.

5. Conclusion

The results of this study show that the Young moduli of filter fabrics exhibit highly anisotropic behaviour. Nevertheless, they can be used to predict strain in backwash filters.

This shows that particularly stiff fabrics have low bulges. This leads to a lower backwashing volume until the fabric is regenerated and smaller possible element distances between the elements.

Furthermore, the more stable weaving direction (warp or weft) for rectangular fabrics must be stretched onto the shorter edge of the filter element. This allows the fabric to expand less, as the more stable thread direction is the deformation determining side. The element distances are reduced.

A certain pre-tension of the fabric also leads to a further reduction in bulging. Alternatives are support grids on the filtrate side. In this case, however, the support grid reduces the free filter area, which is accompanied by a reduction in the filter capacity. Negative effects on the regeneration can only be assumed here (e.g. “interlocking” of the filter cake on the supporting fabric).

Since the strain was known in the previous determination of the second moments of area and the modulus of elasticity could be adapted to it, real designs in the vessel must react to this design by iterative adaptation of the modulus of elasticity. A conservative design in the form of an additional “safety distance” is recommended here. A similar procedure is known in the technical field, e.g. for the design of pressure vessels.

The second moments of area are similar in their tendency (10⁴–10⁵ mm⁴, partly 10⁶–10⁷ mm⁴ for small bulges) for all investigated fabrics (mesh size < 20 μm). Here, the smaller value should be used for a more conservative design. This means that the calculated bulge is assumed to be greater according to Eqs. (1) and (2). It is therefore possible to estimate the bulge.

Table 4
Geometrical moment of inertia based on the bulge from Table 2 over all backwashing pressures (0.3–3.0 bar) and prestressing torques (1–10 Nm) for the four investigated fabrics.

Fabric type/mash size[μm]	Weave type [DIN ISO 9354]	Pressure [bar]	Geometrical moment of inertia 1 Nm pretension [mm ⁴]	Geometrical moment of inertia 10 Nm pretension [mm ⁴]
Twill	11	20-03 01-01-03	warp – 1 Nm: 5.64·10 ⁴	warp – 10 Nm: 9.98·10 ⁵
			weft – 1 Nm: 1.08·10 ⁶	weft – 10 Nm: 3.46·10 ⁶
		1.5	warp – 1 Nm: 1.34·10 ⁵	warp – 10 Nm: 1.42·10 ⁵
			weft – 1 Nm: 3.33·10 ⁶	weft – 10 Nm: 2.49·10 ⁶
		3.0	warp – 1 Nm: 2.44·10 ⁵	warp – 10 Nm: 2.49·10 ⁵
			weft – 1 Nm: 6.07·10 ⁶	weft – 10 Nm: 5.98·10 ⁶
	14	20-02 01-01-02	warp – 1 Nm: 4.36·10 ⁴	warp – 10 Nm: 4.53·10 ⁴
			weft – 1 Nm: 6.95·10 ⁵	weft – 10 Nm: 2.47·10 ⁵
		1.5	warp – 1 Nm: 2.05·10 ⁵	warp – 10 Nm: 2.05·10 ⁵
			weft – 1 Nm: 3.20·10 ⁶	weft – 10 Nm: 1.12·10 ⁷
		3.0	warp – 1 Nm: 3.99·10 ⁵	warp – 10 Nm: 3.99·10 ⁵
			weft – 1 Nm: 6.22·10 ⁶	weft – 10 Nm: 2.15·10 ⁷
20	20-03 01-01-03	warp – 1 Nm: 2.40·10 ⁴	warp – 10 Nm: 2.01·10 ⁶	
		weft – 1 Nm: 1.69·10 ⁵	weft – 10 Nm: 2.82·10 ⁶	
	1.5	warp – 1 Nm: 1.10·10 ⁵	warp – 10 Nm: 6.12·10 ⁶	
		weft – 1 Nm: 7.75·10 ⁵	weft – 10 Nm: 8.06·10 ⁶	
	3.0	warp – 1 Nm: 2.11·10 ⁵	warp – 10 Nm: 1.03·10 ⁷	
		weft – 1 Nm: 1.48·10 ⁶	weft – 10 Nm: 1.29·10 ⁷	
Plain reverse dutch	12	10-01 01-01-00	warp – 1 Nm: 3.83·10 ⁴	warp – 10 Nm: 4.37·10 ⁵
			weft – 1 Nm: 6.31·10 ⁴	weft – 10 Nm: 5.59·10 ⁴
	1.5	warp – 1 Nm: 1.66·10 ⁵	warp – 10 Nm: 3.83·10 ⁵	
		weft – 1 Nm: 2.92·10 ⁵	weft – 10 Nm: 2.60·10 ⁵	
	3.0	warp – 1 Nm: 3.02·10 ⁵	warp – 10 Nm: 3.81·10 ⁵	
		weft – 1 Nm: 5.56·10 ⁵	weft – 10 Nm: 4.97·10 ⁵	

CRediT authorship contribution statement

Patrick Morsch: Conceptualization, Methodology, Software, Formal analysis, Investigation, Validation, Resources, Writing - original draft, Project administration. **Maurus Bauer:** Investigation, Writing - review & editing. **Christoph Kessler:** Investigation, Writing - review & editing. **Harald Anlauf:** Supervision, Writing - review & editing, Funding acquisition. **Hermann Nirschl:** Supervision, Writing - review & editing, Funding acquisition.

Declaration of Competing Interest

The authors declare that they have no known competing financial interests or personal relationships that could have appeared to influence the work reported in this paper.

Acknowledgement

The authors would like to thank the German Federation of Industrial Research Associations (AiF) for the financial support (IGF number

18591N). The authors would also like to thank all colleagues and students for the support in writing this paper. Special thanks go to my student Mr. Simon Egner for the support during their time at the institute.

References

- [1] A.J. Charleton, N.I. Heywood, *Filtr. Sep.* 20 (5) (1983).
- [2] P. Morsch, P. Ginisty, H. Anlauf, H. Nirschl, *Chem. Eng. Sci.* (2019).
- [3] J. Sievert, F. Löffler, *Chem. Eng. Process. Process Intensif.* 26 (1989) 2.
- [4] J. Sievert, F. Löffler, *Filtr. Sep.* 24 (1987) 2.
- [5] Gaudrin, *Filters Gaudrin: worldpatents* (1973).
- [6] D. Gross, W. Hauger, J. Schröder, W. A. Wall, and J. Bonet, *Engineering Mechanics 2: Mechanics of Materials* (Springer Berlin Heidelberg, Berlin, Heidelberg, 2018) [eng].
- [7] D. Gross, W. Hauger, J. Schröder, W. A. Wall, and N. Rajapakse, *Springer textbook: Engineering Mechanics 1: Statics* (Springer, Berlin, Heidelberg, 2013) [eng].
- [8] M. Ferer, D.H. Smith, *J. Appl. Phys.* 81 (1997) 4.
- [9] A. Dittler, M.V. Ferer, P. Mathur, P. Djuranovic, G. Kasper, D.H. Smith, *Powder Technol.* 124 (2002) 1–2.
- [10] H.R. Muller, R. Kern, W. Stahl, *Filtr. Sep.* 24 (1) (1987).
- [11] R. Kern, *Die Optimierung des Kuchenabwurfs beim Scheibenfilter: Eine Voraussetzung für dessen Weiterentwicklung* [ger].

I. Attached publication [4]

Verification of the contribution from the co-authors

Title: Influence of regeneration variables during backwashing treatment into gas-phase after liquid filtration

Journal: Separation and Purification Technology

Authors: P. Morsch, P. Ginisty, H. Anlauf, and H. Nirschl

Position in the dissertation:

The content of this paper has been included in Chapter 4.5 and 5.1

Contribution of Patrick Morsch

- Conceptual design and construction of the backwash system, as well as planning of the test procedure.
- Execution of backwash tests and data evaluation.
- Summary of the data and evaluation of the results.
- Writing the chapters and performing the source research.

Contribution of Pascal Ginisty

- Provision of a force gauge (penetrometry). Support of the work by strength measurements within the framework of a cooperation between IFTS and KIT.

Contribution of Harald Anlauf

- Support of the work by references in literature, test setup, test procedure. Proofreading of the paper (technical).

Contribution of Hermann Nirschl

- Support of the work by references in literature, test setup, test procedure. Proofreading of the paper (technical).



Influence of regeneration variables during backwashing treatment into gas-phase after liquid filtration

Patrick Morsch^{a,*}, Pascal Ginisty^b, Harald Anlauf^a, Hermann Nirschl^a

^a Institute for Mechanical Process Engineering and Mechanics (MVM), Process Machines (VM), Karlsruhe Institute of Technology (KIT), Germany

^b Institut de la Filtration et Techniques de Séparatives (IFTS), France

ARTICLE INFO

Keywords:

Regeneration filter
Filter cake discharge
Backwashing filter
Dry discharge
Adhesion
Cohesion

ABSTRACT

In industrial solid/liquid separation, the removal of fine particles occurs in a wide array of industrial production applications and can be found in nearly every process plant. Especially the cake filtration is emphasized as advantageous principle for separation of suspension with a low solids content (0.01–1 v/v %). To maintain the separation performance, it is required to replace or regenerate the used filter cloth. The latter one can occur through backwashing treatment into liquid or gas phase whereby the gas discharge required an upstream drying process. The main task of that regeneration procedure is a most complete filter cake discharge to reduce the flow resistance of the filter for the subsequent filtration step. Recommendations for advantaged process variables doesn't exist and should be evaluate during this investigation. Investigations regarding to the regeneration procedure has shown, that the cake discharge into gas phase has significant differences to the discharge into liquid phase. Whereas the discharge into gas phase is created through an impulse, the liquid discharge can be interpreted as a slide on the filter cloth surface. Moreover, the backwashing variables are highly different (influence of backwashing pressure, filter cake thickness) between the different backwashing environments as a result of the characteristic surface forces. In this work, main attention is given to the particle system (particle size and filter cake thickness), the different weave types, assembly of the filter cloth and, of course, the backwashing pressure. The difference between a discharge in gas phase and liquid phase is described and its effect on the quality of the regeneration.

1. Introduction

Separation and recovery/recycling of particles separated from liquid streams are commonly used techniques to reduce waste streams, save operating material, and increase the economic efficiency of the process. They are applied for the removal of impurities from salt water streams for electrochemical processes, recovery of catalytic particles in pharmaceutical processes, removal of activated carbon in corrosive solutions, and cleaning of process streams in the natural gas and petrochemicals industries. Separation is particularly profitable in case of low concentrated suspensions. Depending on the valuable product to be separated, two types of filtration processes are distinguished.

In case of clarification filtration, the valuable product is the liquid phase and any particles contained must be removed, as they contaminate the liquid. Here, regeneration starts directly with the subsequent filtration step. The detached filter cake deposits on the bottom of the filter vessel and get removed. Secondly, separation filtration may be aimed at removing the particles as the valuable product. In this case,

subsequent process steps, such as washing out of liquids and drying, are needed. It may be necessary to dry the built-up filter cake mechanically before discharge in the gas phase.

In both cases the periodic discharge of the filter cake and particle cluster from the surface is required. The latter is already part of research projects [1,2], whereas the cake discharge into the gas phase is only known from the previous filtration in gas phase [3]. The cake discharge in gas phase from previous liquid filtration is only known from vacuum filtration with continuous filters and is therefore the content of this paper for discontinuous filters. Regeneration occur with an reverse gas impulse from inside the filter cloth to detach and remove the built-up filter cake. This option is mainly used in discontinuous filters, such as candle and leaf filter systems and thus covers a widespread regeneration process.

2. Theory

Such filtration processes with implemented regeneration are

* Corresponding author.

E-mail address: patrick.morsch@kit.edu (P. Morsch).

<https://doi.org/10.1016/j.seppur.2020.117073>

Received 11 November 2019; Received in revised form 14 April 2020; Accepted 8 May 2020

Available online 13 May 2020

1383-5866/ © 2020 Elsevier B.V. All rights reserved.

Nomenclature			
$\Delta p_{\text{Backwash}}$	Backwashing pressure, bar	p_E	Dehumidification pressure, bar
F_{Detach}	Detachment force, N	S	Saturation, -
F_A	Adhesion force, N	s	Acceleration distance, m
F_C	Cohesion force, N	S_∞	Limit saturation, -
H_{FC}	Filter cake thickness, m	t	time, s
m_{remain}	Mass fraction remaining on filter surface, g	t_E	Dehumidification time, s
$m_{\text{remain, dry}}$	Mass fraction remaining on filter surface after drying, g	v_{max}	Maximum velocity of the filter cloth, m/s
$m_{\text{remain, wet}}$	Mass fraction remaining on filter surface with liquid, g	W	Surface weight, g/m ²
m_{removed}	Discharged mass fraction, g	$x_{i, 3}$	Descriptive Mass/volume-related modal value of particle distribution (i = 10, 50, 90%), m
$m_{\text{removed, dry}}$	Discharged mass fraction after drying, g	α_H	Specific flow resistance, 1/m ²
$m_{\text{removed, wet}}$	Discharged mass fraction with liquid, g	η	Dynamic viscosity, Pa s
		ρ_{Liquid}	Density of the liquid phase, kg/m ³

performed with different types of equipment and can be divided into continuous and discontinuous filters. Examples of continuous filters are drum, disk, and belt filters. Their differences result from time-related and locally resolved stationary filtration conditions. The filtrate flow is constant, because the filter cake is built up, dried, and discharged at different locations. Each of this location is stationary and allows for a continuous filtration flow. Contrary to continuous filters, discontinuous filters are highly transient. This is shown by the fact that the filtrate flow decreases with time as a result of the building up of filter cake. Higher filter cakes with a constant filtrate pressure result in a decrease of the filtrate flow and require periodical removal by discharge. Given the fact that these subsequent process steps (drying, discharging) cannot take place in parallel, the process sequence is split into the three parts of filtration, drying, and discharging. Each part is transient in time and takes place at the same local position. For this reason, good discharge is required to increase the time difference between filtration and regeneration for a good process performance. Examples of such commonly used discontinuous filters are candle filters, which are the focus of this work.

The dominating adhesive forces are defined between the first particle layer and the filter cloth (adhesion) and inside the filter cake proper (cohesion) [4–6]. Adhesion and cohesion may differ considerably depending on the surrounding environment. In case of a liquid phase, the dominating forces are the Van der Waals (VdW) forces. In contrast to the liquid phase, the dominating force in gas phase is the liquid bridge force. These forces may be higher than the effective VdW forces [7]. For this reason, the effective force between filter cake and filter cloth must be reduced by desaturation of the filter cake. Experiments with other filter elements (chamber filters) revealed that cake moisture should have a maximum level of 25% for a good regeneration [8].

With reference to previous investigations, main attention is given to

dry discharge after gas filtration [3,8,9]. It is found that the intensity of discharge (backwashing pressure), filter cake thickness, and geometry of the particles (size and shape) have a strong effect on the discharge behavior. In case of a stable filter cloth, the amount of discharged mass increases with increasing cohesive particles (higher filter cake thickness and smaller particle shape) and higher backwashing pressure in case of backwashing into the gas phase after gas filtration [3]. This increase is much more pronounced in case of an unstable, movable filter cloth and can be formulated mathematically by a normal force balance as derived in Eq. (3) in the chapter 5 [9].

Investigations, based on gas discharge after gas filtration, differs considerably from the discharge behavior in the gas phase after liquid filtration. The filter cake is subjected to a high liquid load, called saturation, whereas gas filtration is affected by air humidity which is infinitely smaller. The latter is associated with a much smaller liquid bridge forces and the saturation level is assumed to decrease the surface load in weight per filter area compared to the former filtration method. To sum up, comparing between these discharge processes is quite difficult, because the boundary conditions of gas and liquid filtration are different.

Investigations of liquid filtration with subsequent drying and discharge are reported for disk filters [3]. This publication also includes a theoretical approach to determining the influence of filter cloth movement based on the discharged mass fraction. These can be used to compare the following results and discuss them for different shapes of the filter element. The effective force in case of discharge (liquid and dry) largely depends on the filter cloth in terms of contact surface (weave type and thread thickness) and less on the material [5,10,11].

For complete discharge, the removal force applied must be larger than the adhesive forces. This universally valid statement was already published by [12] and is independent of the specific adhesive force in the enclosed continuous phase. The effect is summarized by the

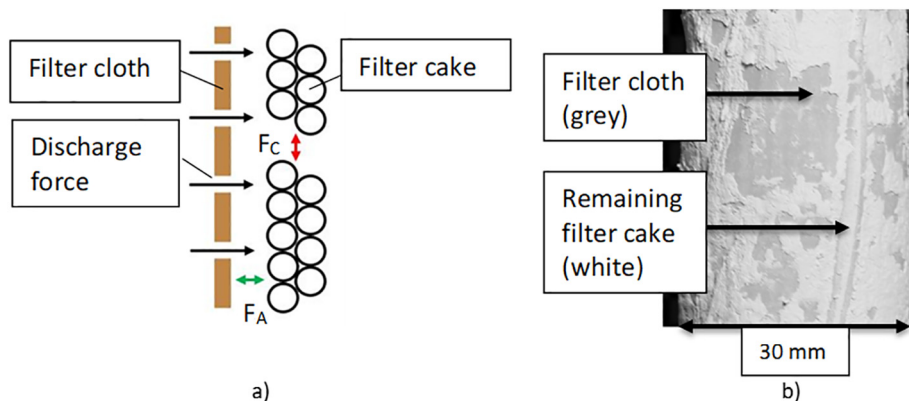


Fig. 1. Force condition inside a filter cake during the backwash procedure (a). Adhesion (F_A) has to be smaller than the discharge force. If these conditions are not fulfilled, particles remain on the filter surface (b).

inequation “Detachment force $F_{\text{Detach}} > \text{Adhesion on filter cloth } F_A$ ”. The detachment force is provided by a pressurized air pulse. This process is supported by the acceleration of the filter cloth with a sudden stop by the mechanical inertia force. Generally, it can be assumed that a more stable filter cloth needs a higher backwashing pressure/backwashing impulse [3]. The same can be expected for filter cloths with a larger contact surface and/or smaller particles [12]. Both values increase the adhesion force.

Apart from adhesion, cohesion is also important with regard to the size of the discharged fragments. For this, cohesion must be much higher than adhesion and discharge is to occur in bigger fragments [3]. And cohesion also affected by the drying procedure. In case of a high desaturation velocity, the saturation gradient is very high between the upper and lower level of the filter cake. This may lead to some cracks inside the filter cake with a lower flow resistance than the remaining cake [13,14]. Hence, the air stream preferably flows through these cracks and results in poor drying. The effects can already be noticed during subsequent discharge, because discharge will not take place at all or be poor, because cracks also reduce the discharged fragments and allow smaller pieces to remain on the filter surface. Bigger fragments are desired, because they are able to carry away more filter cake fragments from the filter surface. The desired force condition for cohesion is reflected by the inequation “Detachment force $F_{\text{Detach}} < \text{Cohesion inside the filter cake } F_C$ ”.

The effective forces are shown schematically in Fig. 1a. The particles remaining on filter cloth surfaces after discharge in the dry phase are shown in Fig. 2b.

3. Method

Within the scope of the investigation, the backwashing properties of various fabrics and particle systems are assessed using a laboratory cartridge filter. The backwashing treatment is evaluated using the experimental setup shown in Fig. 2, which is reduced to the essential area. The test procedure can be split into three main phases in case of dry discharge. Phase 1 covers the filtration process shown in Fig. 2a. During this step, the filter cake is built up until a defined thickness is reached. In this case, suspension flow enters the process chamber at the bottom and leaves at the top. The filtration pressure can be adjusted. The filtrate flows from inside of the laboratory-scaled candle filter through the filtrate pipe and leaves the vessel at the top. After cake buildup, the second phase starts when the suspension is replaced by air pressure in the vessel (Fig. 2b). As a result of the steady air pressure, the filter cake always is subjected to a pressure. When the suspension is replaced by air, the bottom pipe closes and the filter cake is dried mechanically with the help of the filtrate pipe. The drying pressure p_E and drying time t_E can be varied. After drying the filter cake, discharge starts immediately (Fig. 2c). For this purpose, an air pressure flowing opposite to the

filtrate is used. The air pressure acts on the filter cake and filter cloth and a sudden stop with the resulting moment of inertia detaches the cake. In order to release the pressure in the process chamber, the valves open at the bottom of the vessel. The detached filter cake falls onto a metal grid and can be removed. The weight of the filter cake and its saturation can be determined with gravimetric methods after discharge ($m_{\text{removed, wet}}$) and subsequent drying at 100 °C ($m_{\text{removed, dry}}$). This procedure can also be applied to the filter cake remaining on the filter candle ($m_{\text{remain, wet}}$ and $m_{\text{remain, dry}}$). For this, it is necessary to remove the filter cake mechanically. Apart from the saturation of the filter cake (Eq. (1)), the mass fraction of the discharged filter cake (Eq. (2)) can be determined. The interpretation given below will be based on these values.

$$\text{Saturation } S = (m_{\text{removed, wet}} - m_{\text{removed, dry}}) / (\rho_{\text{Liquid}} \cdot V_{\text{Filtercake}} \cdot \epsilon_{\text{Filtercake}}) \tag{1}$$

$$\text{Discharged mass fraction} = m_{\text{removed}} / (m_{\text{removed}} + m_{\text{remain}}) \tag{2}$$

To obtain reproducible test conditions in terms of filter cake thickness, the filtrate volume is kept constant by varying the concentration of the suspension in defined steps. The used particle systems and filter cloths are documented in the following chapter 4.

4. Material

The investigations are carried out using a lab-scale filter element. This laboratory candle filter has a diameter of ~30 mm and the length of the filtration area is 110 mm (total length without thread: 140 mm). The structure of the lab-scale candle filter is shown in Fig. 3a. The filter cloth can be fastened on the supporting tissue with mounting rings. For sample preparation, accurate sealing with a rubber underlay in the mounting area is required. After assembly of the filter cloth, the filter candle can be installed in the test station and is ready for the experiments. For dry discharge, two different filter cloths are studied:

- Plain-Reverse Dutch weave (PRD; Filter cloth #1)
- Satin weave (STN; Filter cloth #2)

In case of PRD, the mesh size determined by a bubble point test is 12 μm. The material is polyethylene terephthalate (PET) and the weave is very filigree/unstable. In contrast to this filter cloth, the satin weave is very stable and has a mesh size of 18 μm. The material is polypropylene (PP). In case of discharges in the liquid phase, the stability and diameter of the filter cloth have a direct effect on the backwashing volume. In case of dry discharge, this behavior can be expected when looking at the test reported in [5,6,15]. For this purpose, however, it is necessary to select a fabric diameter larger than the diameter of the candle filter for accelerating the filter cake. For both materials, two

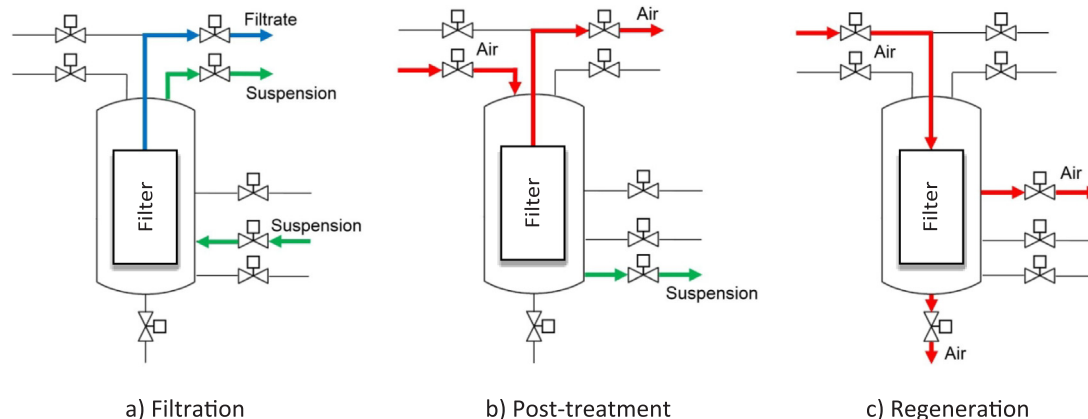


Fig. 2. Schematic flowchart of the experimental facility during filtration (a), replacement of the suspension and drying (b), and discharging into the gas phase (c).

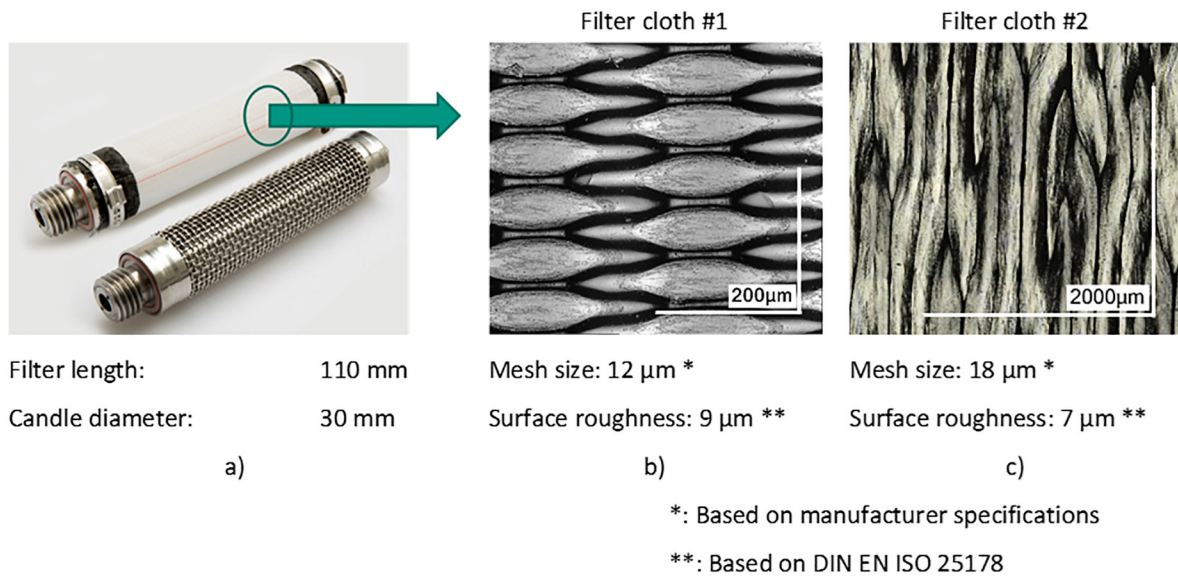


Fig. 3. Illustration of the lab-scale candle filter with and without filter cloth (a) and enlarged images of the used filter cloths of 12 μm plain reverse Dutch weave (PRD) (b) and 18 μm satin weave (STN) (c).

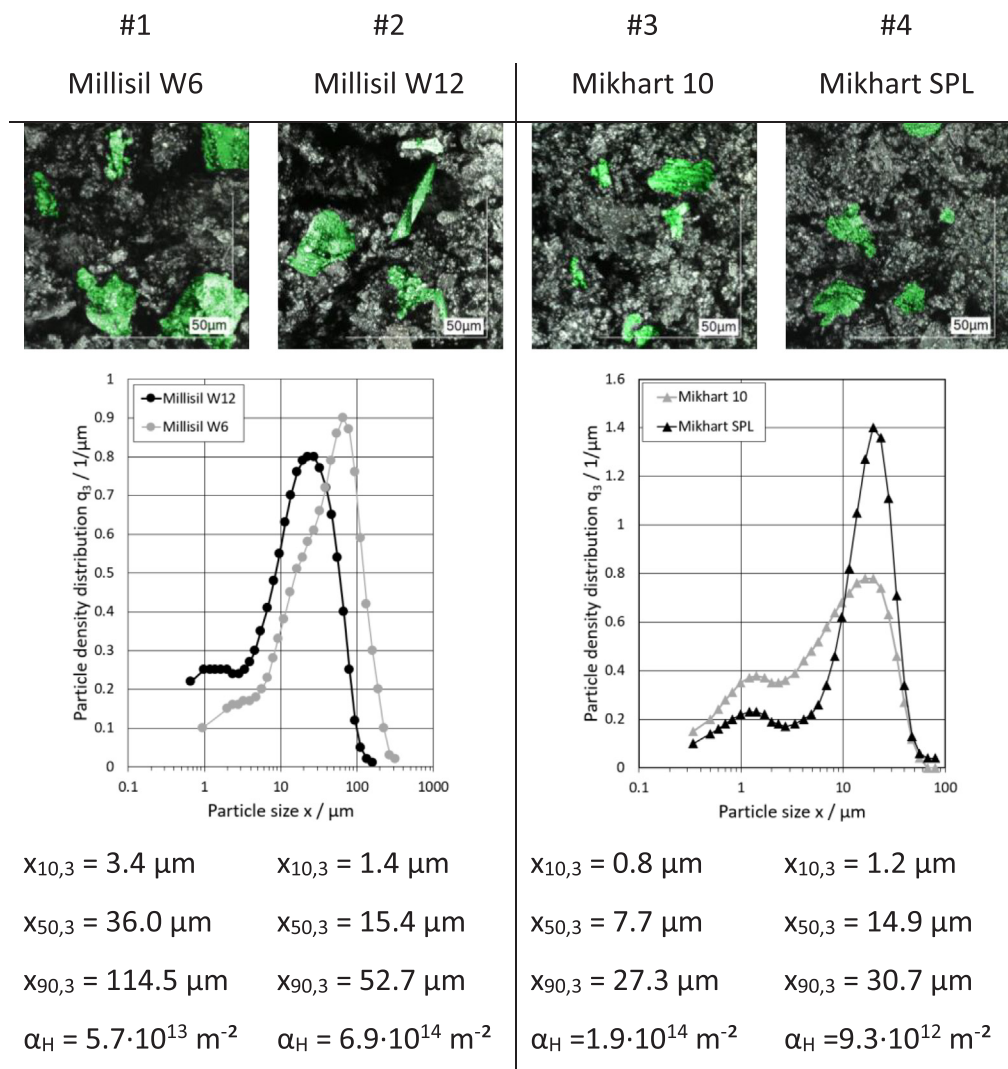


Fig. 4. Particle systems Investigated for cake discharge in the gas phase. The shape of the particles is orthonhombic. The particle sizes results in high specific flow resistances α_H (VDI 2762-2).

different filter cloths (inflexible/flexible) and 3 different filter cloth diameters (30, 35, 40 mm) with a potential motion range of 0, 2.5, and 5 mm are studied. The investigated filter cloths are summarised in Fig. 3 b and 3c. In addition to the mesh size as the manufacturer's specification, the surface roughness according to DIN EN ISO 25178 is also listed. This is approximately similar for both fabrics with 9 μm (Filter cloth #1) and 7 μm (Filter cloth #2).

The investigated particle systems for backwashing filtration mainly differ in particle size, as is shown in Fig. 4. First, attention should be given to the porosity and the resulting capillary pressure for drying. In case of a very high capillary pressure, a high drying pressure is required for lower saturation levels. As already known, the saturation has to decrease before discharge, because a high saturation leads to high cohesive and adhesive forces and results in a poor or more complicated regeneration due to inhomogeneous force distribution [15].

Four particle systems are used, of which two each have the same mineralogical composition but different mass-based median values $x_{50,3}$. This results in different contact points between the first particle layer and the filter cloth (adhesion), and different particle-particle interactions and associated cohesions. The different mineralogical composition of the two particle systems also makes it possible to transfer the results to another particle system [4].

5. Interpretation

Investigations covered the process of filtration with the formation of defined filter cakes, drying by air pressure, and regeneration of the filter by discharge into gas phase. Research revealed two possibilities of cake discharge [19]:

- Complete discharge and
- Incomplete cake discharge

For complete discharge, also called patchy cleaning, the adhesion force over the whole filter is overcome and the whole filter cake is detached and discharged. Of course, cohesion has to be high enough to prevent breakthrough of the air flow [3]. This kind of discharge obviously is preferred, especially when considering subsequent unit operation. After discharge, the aggregate material at the bottom of the vessel is removed and some further process steps may follow. In case of filter cake fragments remaining on the filter cloth, the retention of the valuable product (the particles) increases and the performance of the subsequent filtration process decreases as a result of the decreased filter area. In Fig. 5, the complete discharge is exemplarily shown. Compared

to discharge in the liquid phase, the backwashing time for dry discharge is much shorter [16,19].

When considering the higher adhesive forces in gas phase compared to liquid phase [7], the mechanisms of dry and liquid discharge are supposed to be different. It can be expected that the discharge force has to be higher for a good discharge. The main question is which process variable leads to an increased detachment in dry discharge. To answer this question, four process variables are analyzed:

- I. Backwashing pressure: an increase in this variable increases the stress on the filter cake. According to [3], discharge in gas phase after gas filtration are improved and this can also be expected after liquid filtration.
- II. Filter cloth diameter: An increase in the filter cloth diameter relative to the filter element (e.g. candle filter) increases the acceleration distance and the detachment force [9].
- III. Filter cake thickness: in case of filter presses, heavier filter cakes can be discharged more easily [6]. This behavior can also be expected for candle filters, because the force of inertia increases with the filter cake thickness.
- IV. Filter cloth type: rougher and less elastic fabrics are expected to result in a reduced discharge of filter cake fragments.

5.1. Backwashing pressure (I) and filter cloth diameter (II)

The basic conditions of the experiments were that with filter cloth 1 and different diameters of the filter cloth (30, 35, 40 mm), a cake of $H_{FC} = 1.5$ mm was built up, dried and discharged at air pressures of 1–1.5, 2–2.5 and 3–3.5 bar. The discharged filter cake was collected and described gravimetrically. The filter cake remaining on the filter cloth was subjected to the same process after mechanical removal from the surface of the filter cloth. With the measured masses and Eqs. (1) and (2), a discharged mass fraction – backwashing pressure plot is obtained, see Fig. 5a.

When using a 30 mm filter cloth on a 30 mm filter candle, only ~20% of the filter cake of W6 will be discharged. The amount discharged remains constant from 1 to 3 bar backwashing pressure. This observation leads to the conclusion that the backwashing pressure has no impact on the amount of discharged filter cake like discharging in liquid phase [19]. This result does not agree with the high impact of backwashing pressure observed in [3] for gas filtration/regeneration. Further studies for disk filters in case of liquid filtration and gas discharge revealed that the filter cake may be rewet from the bottom of the candle. This effect leads to a disturbed distribution of adhesion force. As

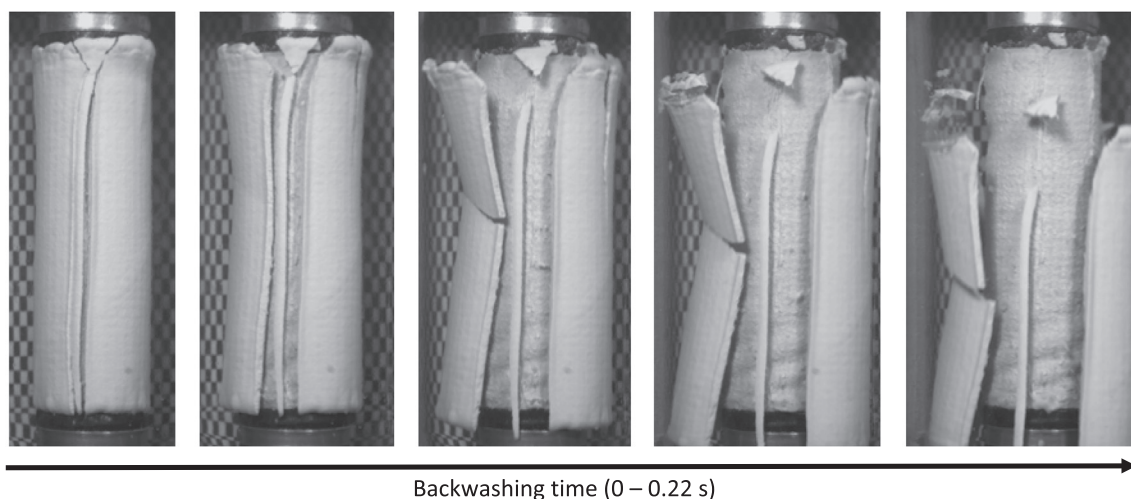


Fig. 5. Regeneration of the lab-scale candle filter (Millisil W6; $H_{FC} = 1.5$ mm; $\Delta p_{\text{Backwash}} = 1$ bar). Discharge in the liquid phase under the same conditions takes six times longer.

obvious from Fig. 7a, this also happens in case of a dry discharge of a 30 mm filter cake. The lower part of the candle locally experiences a saturation = 1 and adhesion decreases. Then, the same amount of filter cake is detached from the rest, which may be interpreted wrongly as a constant mass discharged at increased pressure. Hence, discharge is not a result of an impulse, but a normal fall by gravity.

The impact of the backwashing pressure is reflected by the discharge for a 35 mm filter cloth and particle system W6. With an acceleration of 2.5 mm, ~28% of the filter cake are discharged at 1–1.5 bar. The discharged fragments come from the whole candle area and not only from the lower part (see Fig. 7b). Moreover, the discharged mass fraction increases with the backwashing pressure to ~37% at 2–2.5 bar to ~55% at 3–3.5 bar (11.2 w%/bar). When the filter cloth diameter is increased to Ø 40 mm (5 mm acceleration; 18 w%/bar), the same mass is discharged at 1–1.5 bar like with Ø 35 mm filter cloth and 3–3.5 bar.

When the acceleration distance *s* is doubled, pressure can be reduced by factor of 3. Analogous results are found in [9] for gas filtration and gas discharge (Eq. (3)).

$$v_{\max} = (9 \cdot s^2 \cdot 0.5 \cdot W^{-1})^{1/3} \cdot (d(\Delta p)/dt)^{1/3} \quad (3)$$

According to [9] the maximum speed v_{\max} of the filter cloth depends on the acceleration distance *s*, surface weight *W*, and the increasing differential pressure versus time $d(\Delta p)/dt$. Based on the proportionality $v_{\max} \propto s^{2/3} \cdot (d(\Delta p)/dt)^{1/3}$, the impact of *s* exceeds that of the pressure rising ($d(\Delta p)/dt$). In this context, it means that the same amount of discharged mass fraction can be reached at a much smaller backwashing pressure by increasing the acceleration distance *s*.

When the backwashing pressure is further increased to 2–2.5 bar, the discharged mass fraction amounts to ~72% and a complete discharge is reached at 3–3.5 bar (shown in Fig. 7c). Using this combination of particle system and filter cloth, adhesion can only be overcome by an acceleration distance of 5 mm and a pressure of 3–3.5 bar. Under this condition, the detachment force is higher than adhesion over the whole filter cloth.

In Fig. 6 b, the influence of the filter cloth diameter is obvious for the W6 particle system. This corresponds to an overall increase of discharged mass fraction/ (bar backwashing pressure · filter cloth diameter) by 1.8% and reveals the high impact of the effective acceleration of the filter cloth (1–1.5 bar: 3.7%/mm; 2–2.5 bar: 5.3%/mm; 3–3.5 bar: 8%/mm).

Apart from the particle system W6 with a $x_{50, 3}$ -value of 36 µm, investigation also covers W12, with a $x_{50, 3}$ -value of 15.4 µm (see Fig. 4). Finer particles can be expected to have a higher adhesion to the filter cloth due to the increased number of contact points [17,18]. When looking at W12 (1–1.5 bar; 35 mm), it can be noted that the backwashing efficiency is below the efficiency for W6 at same conditions. With an increase of the backwashing pressure, the discharged mass fraction for W12 is higher.

The increase in the mass fraction discharged at a higher backwashing pressure, however, cannot be explained by the effective adhesive forces. According to Eq. (3), the momentum on the filter cake decreases and results in the discharged mass fraction being smaller at smaller v_{\max} . This can be implemented by a decrease of the surface area *W* and it is the reason for the increase of the discharged mass fraction of W12. A decreasing particle size results in a decrease of the bulk density and, hence, in a smaller number of particles for the same filter cake thickness. This goes hand-in-hand with a smaller surface weight (~3.8 kg/m² for W6 and 2.1 g/m² for W12) and results in a higher v_{\max} and a higher momentum by discharge. To sum up, adhesion is expected to be higher for W12, as is the force for discharging these particles. The same observation can be made for W12 with the filter cloth 1 and a diameter of 40 mm (0.25 bar: 38%; 0.5 bar: 63%; 1.0 bar: 93%). When using W12, a discharged mass fraction of ~63% can be reached when the filter cloth is 40 mm in diameter and 0.5 bar (35 mm requires 3–3.5 bar).

In conclusion, it should be noted that by choosing an adequate acceleration distance *s* and a high velocity of the filter cloth/cake, the discharged mass fraction can be increased.

5.2. Filter cake thickness (III)

Based on the finding that the initial force must be high enough for a complete discharge, it can be assumed that a good discharge can also be reached by a variation of filter cake thickness. To study the impact of filter cake thickness in case of dry discharge, defined filter cake thicknesses of 0.5, 1.5, and 2.5 mm are chosen, dried and discharged. The plot of the discharged mass fraction versus filter cake thickness is shown in Fig. 8.

It is evident that an increase of the filter cake thickness results in an increase of the discharged mass fraction. While only a few fragments are detached at a thickness of 0.5 mm, the weight fraction discharged

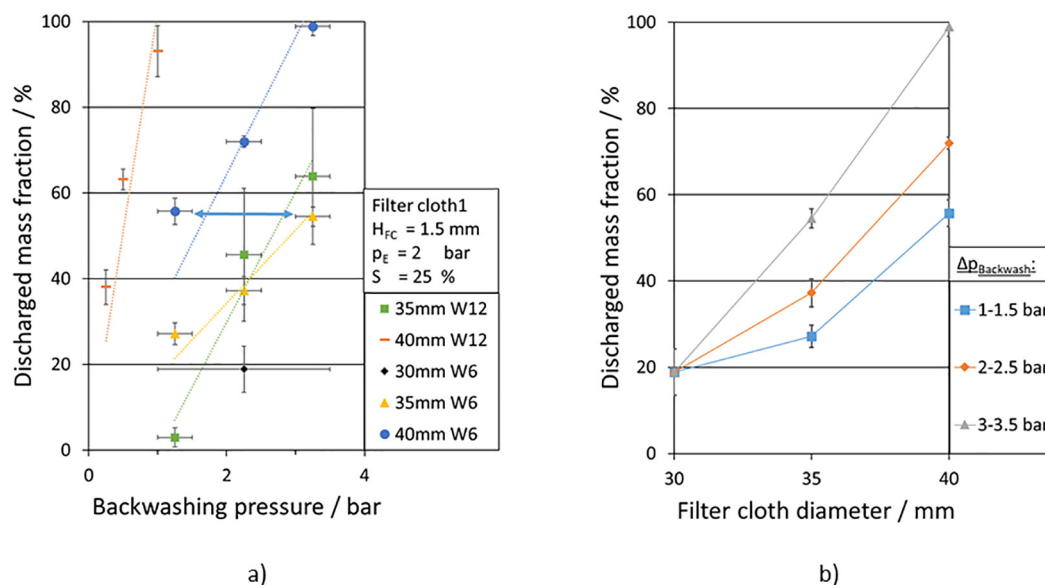


Fig. 6. Discharged mass fraction of the lab-scale candle filter as a function of the backwashing pressure (a) and the diameter of the filter cloth 1 (b) at a constant filter cake thickness $H_{FC} = 1.5$ mm.

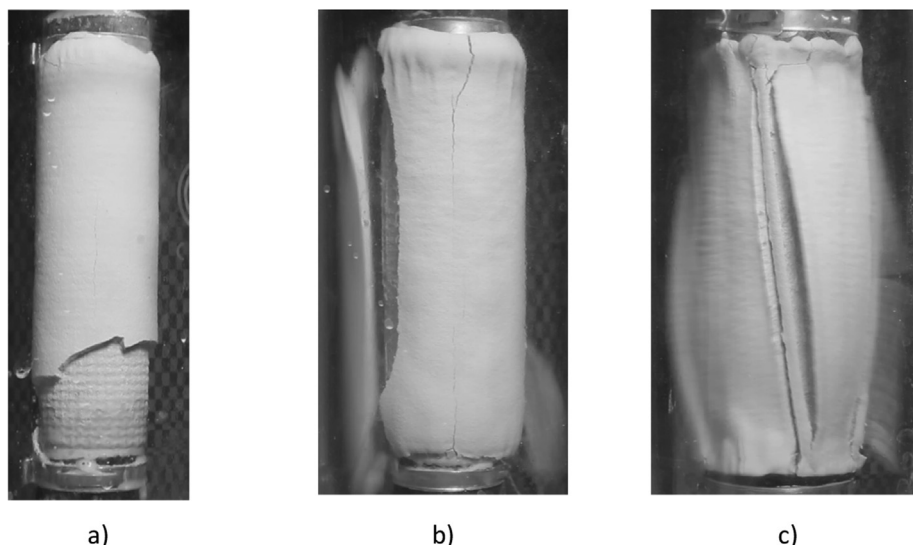


Fig. 7. Filter cake remaining when removing a cake of 1.5 mm thickness by backwashing with air. The filter cloth diameter for a discharge at 30 mm (a), 35 mm (b) and 40 mm (c).

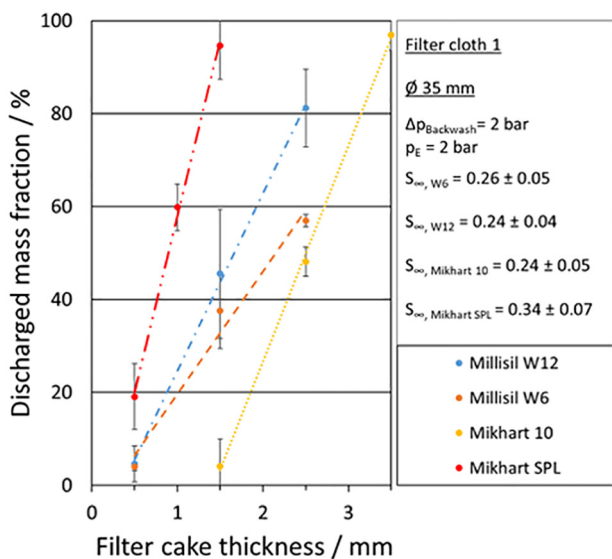


Fig. 8. Discharged mass fraction for the lab-scale candle filter as a function of the filter cake thickness.

increases rapidly with increasing thickness. It is remarkable that a linear behaviour can be observed for all 4 particle systems.

A look to Fig. 8 rises the question, why the mass fractions discharged are higher for smaller particle systems. It is well known that smaller particle systems have a higher number of contact points and therefore adhesion between the surface and filter cloth. But a worse regeneration cannot be observed. An assessment is also made here on the basis of the specific mass on the surface.

At a filter cake thickness of 1.5 mm, W12 has a surface weight of 2.35 kg/m², whereas that of W6 is ~3.05 kg/m². As in case of the variation of the filter cloth diameter, this results in a lower v_{max} and, hence, in a smaller momentum for discharging the built-up filter cake. The result is a higher force of inertia and an increased inertia of the discharged cake. With regard to the Mikhart particle systems, this behaviour is exactly opposite. Here, the coarser Mikhart SPL with a basis weight of 2.40 kg/m² is, as expected, thrown off much better than Mikhart 10 with 1.57 kg/m². With regard to the cake resistance (α_H = 9.3 · 10¹² m⁻²), a more porous structure can be assumed for this particle system with the resulting very good release. The discharge

process is therefore a process in which, on the one hand, the greater adhesion of finer particles to the lower inertia can be counteracted by the smaller surface loading. The liquid load inside the filter cake can increase the liquid bridge forces (adhesion; ∝ x) and also the basis weight of the filter cake (∝ x³). Therefore, it is not possible to make a general statement on the extent of the adhesive forces, including saturation, and the interaction of the fabric (meshes) with the particle size distribution.

When looking at Eq. (3), proportionality of v_{max} to the surface weight W is given by v_{max} ∝ W^{-1/3} and this results in a reduction of v_{max} at higher surface weight W. It must be assumed that the discharge behavior is no mono-variable interaction and depends on more variables than just specific weight. According to the original force condition, the detachment force F_{Detach} counteracts the force of inertia (mass m multiplied by the acceleration a = dv/dt) and adhesion force F_A. This force condition F_{Detach} - F_A = m·a clearly shows that detachment is not only influenced by the speed of discharge, but also by the mass.

With a look to the proportionalities, the presumption is that the increase in weight is more important than the increase on adhesive forces. The accuracy of this derivation can be verified by observing the limit values of chamber filters. In case of these filters used in e.g. beer filtration, the filter cake is detached only as a result of the gravity force and v_{max} is zero.

5.3. Filter cloth type (IV)

In addition to the previously investigated parameters, the filter cloth itself is varied as well. Here, special attention is paid to the stiffness of the tissue. In contrast to the filigree filter cloth 1 (Thickness: 80 μm), filter cloth 2 is of higher strength (Thickness: 714 μm). The two fabrics are shown in Fig. 3. It can therefore be assumed that, as a result of the higher thickness and, hence, lower flexibility, acceleration of filter cloth 2 is smaller than that of filter cloth 1. This is supposed to result in a smaller filter cake discharge. Deviations from this behavior may be caused by different adhesive forces and stiffnesses of the filter cloth exclusively.

For the first validation of the hypothesis “stiffer tissue leads to reduced filter cake discharge,” regenerations are carried out with variable filter cake thicknesses H_{FC} and backwashing pressures Δp_{Backwash} using a tissue diameter of 35 and 40 mm, and the particle system W6. The results can be compared with the values obtained for the 12 μm tissue in Fig. 6. In addition, adhesion measurements are carried out according to [17–19].

A look at the discharge rate in Fig. 9 suggests that a discharge for 35 mm isn't possible (H_{FC} : 6 mm and $\Delta p_{Backwash}$: 4 bar: < 5%).

When the tissue diameter is increased from 35 to 40 mm, the first fragments are loosened at cake heights of 1.5 mm and a backwashing pressure of 2 bar. With increasing cake thickness to 2.5 mm, the quantity of filter cake thrown off increases to 50%. Compared to filter cloth 1, the particle layer remaining on the fabric is much thicker. With a further increase of the cake height to 3.5 mm, a large part of the filter cake is discharged (~69%). Remaining fragments can be found mainly in low-movement zones, such as the upper and lower sides of the filter fabric. In addition, the particle layer remaining on the filter fabric should not be neglected. When the backwashing pressure is increased from 2 to 4 bar, no significant increase in the discharge rate can be observed. While the discharge rate is nearly zero at a cake thickness of 1.5 mm, it amounts to 40% only at 2.5 mm, and to 79% at 3.5 mm. Considering the standard deviation, no significant differences between 2 and 4 bar backwashing pressure must be assumed. The small pressure dependence can be explained by the rigidity of filter cloth 2. Large increases in force cause small changes of elongation only. Hence, higher pressures do not have the desired effect of increased cake discharge. Direct comparison with filter cloth 1 shows that the more elastic and less rough fabric results in discharge rates of ~38% even at a filter cloth diameter of 35 mm and a cake thickness of 1.5 mm.

To study particle masses remaining on the surfaces of different tissues, adhesion measurements were carried out according to [17,18]. For this purpose, a filter cake was built up on a filter fabric with the help of a pressure filter cell and the fabric was then pulled off the surface. The effective force was evaluated using Eqs. (4) and (5).

$$\text{Break-up stress (N}\cdot\text{m}^{-2}\text{)} = (\text{Maximum force}) \cdot (\text{Area of contact with filter cloth})^{-1} \quad (4)$$

$$\text{Break-up energy (J}\cdot\text{m}^{-2}\text{)} = (\Sigma\text{Force}\cdot\Delta x) \cdot (\text{Area of filter cloth})^{-1} \quad (5)$$

from $x = 0$ to $x = x$ Detachment

The break-up stress consists of the maximum force measured in a test relative to the filter area. In addition, a break-up energy is defined taking into account the force as a function of the tensile length. Thus, the different stages of force measurement (static friction, idling and sliding friction according to [18]) are considered according to their proportions. Measurements were made using both filter fabrics shown in Fig. 3 and are summarized in Table 1.

It was found that the break-up stresses in $\text{N}\cdot\text{m}^{-2}$ of filter cloths 1 and 2 differ with respect to the mean value. However, no significant difference can be assumed. This can be explained by the surfaces of the tissues and the acting shear planes in the experiments. Due to the periodic surface of the filter fabric and the shear plane, the first particle layer is not completely moved over the fabric but also over the particle layer. The measured adhesion thus refers to a mixture of particle and filter area. Since the particle-particle interaction is much more pronounced, any differences between the tissues are levelled out. This is clearly shown by the high standard deviation of ~ 30% for both fabrics. Taking the break-up energy in $\text{J}\cdot\text{m}^{-2}$ into account, no difference in position between the two filter cloths used can be detected. Both measured values are in the same range.

Conclusions drawn from these measurements with respect to the discharge rates of the fabrics suggest that discharge is affected only slightly by the adhesion of the fabric types but influenced largely by the stiffness that determines resistance to the discharge impulse and the movement of the fabric (momentum).

6. Conclusion

The experiments show that the filter cloth diameter, backwashing pressure, weave type, and filter cake thickness have a big influence on the discharged mass fraction. It is highly recommended to use a filter

cloth with a diameter enabling proper motion. Only with such acceleration can a discharge be accomplished successfully. In particular, flexible fabrics are suited for a good regeneration. In addition, larger fabric diameters relative to the candle diameter are to be preferred for cake discharge in the gas phase.

Apart from the movement of the filter cloth, backwashing pressure also has a high impact on the discharge process. Higher backwashing pressure leads to a higher impulse which produces a better discharge. Here a clear difference to regeneration in liquid phase can be observed [19]. The combination of the filter cloth diameter and backwashing pressure can lead to a good discharge.

Taking Eq. (3) into account, an increased mass load of the surface, possibly due to a higher cake thickness, will also result in an increase in the mass discharged. This hypothesis is confirmed by experiments with variable cake thicknesses. Thicker cakes tend to a more complete discharge. Variations in particle size also confirmed this observation. Against all expectations due to their higher adhesion, smaller particles were not found to lead to lower discharge rates, but only particles with a smaller specific area loading. Here the multi-variability of the regeneration process becomes clear.

Summarizing the experience gained from all experiments, it can be stated that the success of discharge is a question of momentum. A great momentum can be created by changing various variables. In the worst case, regeneration quality decreases during liquid discharge, gas discharge is only made possible in this way. In addition, in contrast to liquid discharge, a significant pressure influence can be detected.

CRedit authorship contribution statement

Patrick Morsch: Conceptualization, Methodology, Software, Formal analysis, Investigation, Validation, Resources, Writing - original draft, Project administration. **Pascal Ginisty:** Investigation, Writing - review & editing. **Harald Anlauf:** Supervision, Writing - review & editing, Funding acquisition. **Hermann Nirschl:** Supervision, Writing - review & editing, Funding acquisition.

Declaration of Competing Interest

The authors declare that they have no known competing financial interests or personal relationships that could have appeared to influence the work reported in this paper.

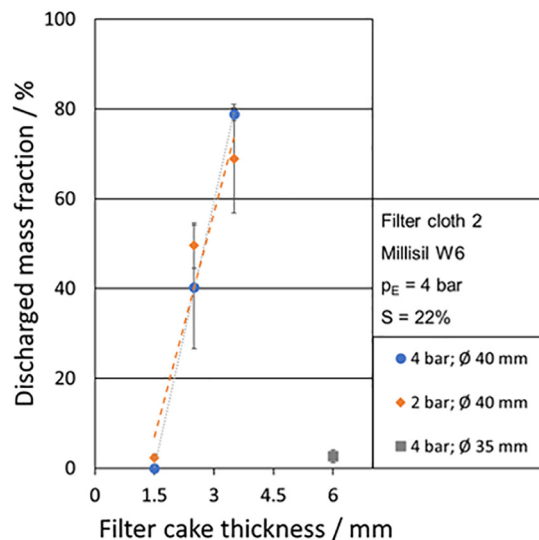


Fig. 9. Discharged mass fraction for the lab-scale candle filter as a function of the filter cake thickness H_{FC} for different diameters of the filter cloth 2 and backwashing pressure.

Table 1

Break-up stresses (Eq. (4)) and break-up energies (Eq. (5)) measured for filter cloth 1 and filter cloth 2.

Filter cloth number	Break-up stress [$\text{N}\cdot\text{m}^{-2}$]	Break-up energy [$\text{J}\cdot\text{m}^{-2}$]
1	323.33 ± 102.77	0.31 ± 0.11
2	408.47 ± 125.33	0.34 ± 0.07

Acknowledgement

The IGF Project 18591 N is supported via German Federation of Industrial Research Associations (AiF) within the programme for promoting the Industrial Collective Research (IGF) of the German Ministry of Economic Affairs and Energy (BMW), based on a resolution of the German Parliament. The authors would also like to thank the IFTS (Institut de la Filtration et des Techniques Séparatives) in France, especially Ms. Kristin Neubauer. We would also like to thank Mr. Sven Fietz for his support in writing the paper. Last, but not least, the authors thank all colleagues and students for the support of this paper.

References

- [1] S. Stahl, C. Leipert, H. Nirschl, *Sep. Purif. Technol.* 110 (2013).
- [2] C. Leipert, H. Nirschl, *F & S Int. Ed.* 11 (2012).
- [3] A. Dittler, M.V. Ferer, P. Mathur, P. Djuranovic, G. Kasper, D.H. Smith, *Powder Technol.* 124 (2002) 1–2.
- [4] A.J. Carleton, N.I. Heywood 20 (1983) 5.
- [5] H.R. Muller, R. Kern, W. Stahl, *Filtration & Sep.* 24(1) (1987).
- [6] K. Morris, R. Allen, R. Clift, *Filtration & Sep.* 24(1) (1987).
- [7] J.N. Israelachvili, *Intermolecular and surface forces*, Elsevier Acad. Press, Amsterdam, 2011 [eng].
- [8] A. Rushton, A.S. Ward, R.G. Holdich, *Solid-Liquid Filtration and Separation Technology*, Wiley-VCH, Hoboken, 2008 [eng].
- [9] J. Sievert, F. Löffler, *Chem. Eng. Process. Process Intensif.* 26 (1989) 2.
- [10] H.R. Müller, R. Kern, W. Stahl, *Filtr. Sep.* 24 (1987).
- [11] C. Weidemann, S. Vogt, H. Nirschl, *J. Food Eng.* 132 (2014).
- [12] K. Morris, R.W. Allen, R. Clift, *Filtr. Sep.* 24 (1987).
- [13] S. Illies, H. Anlauf, H. Nirschl, *Drying Technol.* 34 (2015) 8.
- [14] R.J. Wakeman, *Filtr. Sep.* 11 (1974).
- [15] J. Sievert, F. Löffler, *Filtr. Sep.* 24 (1987) 2.
- [16] S. Ripperger, *Filtrieren und Separieren* 22(2) (2008).
- [17] T. Weigert, S. Ripperger, *F & S Int. Ed.* 3 (2003).
- [18] T. Weigert, S. Ripperger, *F & S Int. Ed.* 2 (2002).
- [19] P. Morsch, P. Ginisty, H. Anlauf, H. Nirschl, *Chem. Eng. Sci.* (2019).

J. Attached publication [5]

Verification of the contribution from the co-authors

Title: In-situ cleaning process of chamber filter presses with sensor-controlled and demand-oriented automation

Journal: Separation and Purification Technology

Authors: P. Morsch, A. Arnold, H. Schulze, R. Werner, H. Anlauf, D. U. Geier, T. Becker, H. Nirschl

Position in the dissertation:

The content of this paper has been included in Chapter 4.7 and 5.1

Contribution of Patrick Morsch

Conceptualization, Methodology, Software, Formal analysis, Investigation, Validation, Resources, Writing - Original Draft, Project administration

Contribution of Adrian Arnold

Investigation, Writing - Review & Editing

Contribution of Henning Schulze

Investigation, Writing - Review & Editing

Contribution of Roman Werner

Investigation, Writing - Review & Editing

Contribution of Harald Anlauf

Supervision, Writing- Reviewing and Editing, Funding acquisition

Contribution of Dominik U. Geier

Supervision, Writing- Reviewing and Editing, Funding acquisition

Contribution of Thomas Becker

Supervision, Writing- Reviewing and Editing, Funding acquisition

Contribution of Hermann Nirschl

Supervision, Writing- Reviewing and Editing, Funding acquisition



In-situ cleaning process of chamber filter presses with sensor-controlled and demand-oriented automation

Patrick Morsch^{a,*}, Adrian Arnold^a, Henning Schulze^a, Roman Werner^b, Harald Anlauf^a, Dominik U. Geier^b, Thomas Becker^b, Hermann Nirschl^a

^a Karlsruhe Institute of Technology (KIT), Institute for Mechanical Process Engineering and Mechanics – Process Machines, Strasse am Forum 8, 76131 Karlsruhe, Germany

^b Technical University of Munich, TUM School of Life Sciences Weihenstephan, Institute of Brewing and Beverage Technology, BioPat and Digitalization, Weihenstephaner Steig 20, 85354 Freising, Germany

ARTICLE INFO

Keywords:

Filter cloth cleaning
Image analysis
Chamber filter
Automatic surface cleaning
Nozzle cleaning
Surface cleaning on demand

ABSTRACT

The content of this paper is the cleaning of filter surfaces from remaining filter cakes. Remaining dirt on filter surfaces is a widespread problem. To counteract this, increasingly automated cleaning systems are being integrated, which clean these surfaces with great cleaning effort. The reduction of the cleaning effort can be achieved by the combination of a camera with a surface contamination detection software. The advantages for the cleaning process are a more efficient cleaning, less produced wastewater and an effective documentation of the cleaning. The cleaning procedure is carried out using 3 steps: It starts with the recording of a picture. Then, an algorithm detects contamination, generates corresponding coordinates and a nozzle path. These coordinates are then approached by means of a xyz table and the contamination is cleaned by a jet stream. Different nozzles and cleaning parameters were tested and their influence on the cleaning effectiveness is discussed in the context of this study.

1. Introduction

The cleaning of plants for the chemical industry is essential to avoid cross-contamination, particularly in batch operation, and therefore safe production [1]. This is especially true for solid–liquid separation processes and for filtration [2]. These devices have special cleaning requirements due to the surfaces of filter cloths, which are difficult to clean [3]. The cleaning of filters is therefore often designed conservatively which is equivalent to excess cleaning. A demand-oriented cleaning method based on image evaluation offers a lot of potential for optimization in this area to reduce the necessary cleaning agent, document the cleaning result, and reduce the amount of wastewater produced. The latter point is particularly interesting considering the trend of rising wastewater costs in recent years.

Basis of this demand-oriented cleaning is the development of an optical residue detection coupled with an automated nozzle system with a pulsatory and/or continuously operated nozzle lance for chamber filters. The cleaning process is then carried out using the following points:

1. Detection of the contaminated areas.
2. Assignment of coordinates.
3. Approaching and cleaning of the defined coordinates.

The combination of these components enables demand-oriented cleaning and thus represents an efficient, optimized, and resource-saving cleaning method. A tissue-nozzle variation based on this cleaning procedure has already been carried out and shows the effectiveness of the process. The focus of this paper is on the presentation of the image evaluation and the automation, which is based on process parameters such as nozzle pressure, distance, type and contamination matrix [4].

Fig. 1 a shows an example of organic contamination on a filter fabric. Fig. 1 b shows the detection of the contaminated surfaces based on the image evaluation and Fig. 1 c the assignment with coordinates. The automated and demand-oriented cleaning is investigated in laboratory tests and relevant parameters are determined. Simultaneously, the algorithm for the documentation of the contamination is developed. The validation is carried out on a laboratory scaled chamber filter press using

* Corresponding author.

E-mail addresses: patrick.morsch@kit.edu (P. Morsch), roman.werner@tum.de (R. Werner).

URL: <http://www.mvm.kit.edu> (P. Morsch), <http://www.lbgt.wzw.tum.de> (R. Werner).

<https://doi.org/10.1016/j.seppur.2020.117793>

Received 9 December 2019; Received in revised form 8 July 2020; Accepted 21 September 2020

Available online 28 September 2020

1383-5866/© 2020 Elsevier B.V. All rights reserved.

a model contamination. The cleaning technology presented here can thus be transferred to other filter systems (backwashing filters, surface cleaning of containers, etc.), so that the research results can be used to increase purity in a wide range of applications, avoid contamination and increase product safety.

2. Method

The realization of this project is based on the coupling of mechanical cleaning components and the development of a residue detection system. The cleaning process can be traced using the flowchart shown in Fig. 2 and is divided into three groups, which are also listed in the Introduction chapter. After the image capturing (1) the dirt detection is done by means of prefabricated solution algorithms with subsequent determination of coordinates based on a defined origin (2). Based on this knowledge it is now possible to check whether the surface is clean or dirty. If no dirt is detected the cleaning procedure is completed immediately. Otherwise, the system checks whether the same procedure has already been performed several times using the same image section. In this case an irregularity (damage to the surface, etc.) must be assumed, which cannot be eliminated by a simple cleaning.

The automated detection of surface impurities starts by recording the surface of a laboratory scaled chamber filter with a camera (1. Image capturing). Within the scope of this project the image is captured using a camera unit with a resolution of 2 megapixels that is as low as possible (Microsoft LifeCam Studio from Microsoft Corporation). This measure is intended to ensure that the system can also be used effectively with less expensive structures. Points to be considered during image capturing are enough lighting so that the contrast between contamination and surface (filter fabric) can be seen and the camera must be protected against splashing water. As part of this project a housing was designed for the camera unit. After the step 1. Image capturing the step 2. Dirt analysis & output of coordinates is carried out with the calculation of coordinates of the dirty areas. The image analysis is carried out using the GRSR (Gradient-Reduction-Threshold-Reduction) evaluation algorithm. This dirt analysis works as follows:

The dynamic image evaluation by the GRSR method goes through several iteration steps for the elaboration of the contamination areas based on a reference image. These steps can be summarized using the following points:

- I. Clean reference fabric: transformation of the RGB image into HSV space and HS combination stored (HashSet)
- II. Iteration of the HashSet on contaminated tissue
- III. (Multiple) Reduction(-s) for image noise minimization
- IV. Threshold post-filtering
- V. (Multiple) Reduction(-s) for image noise minimization

First, it is necessary to have a clean tissue as a reference (Fig. 3 a). This image is transferred from the RGB image to the HSV color space and stored as the HS image. This reference image (HashSet) is reduced by the

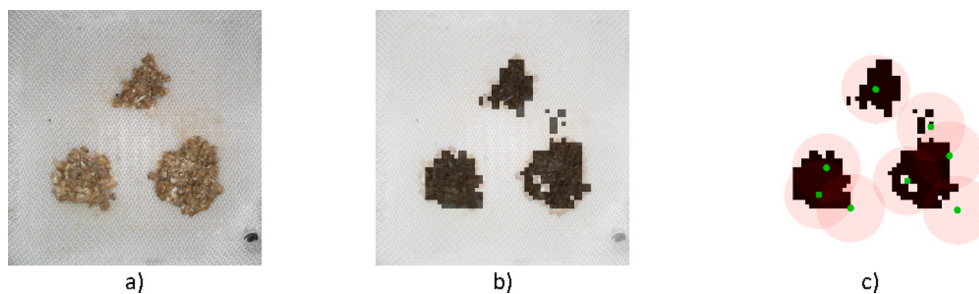


Fig. 1. Representation of an organic impurity matrix on a filter fabric (a), the detected contamination (black) over the impurity matrix (b), and the coordinates (green points) at a fixed nozzle diameter (red circles) for covering the surface (c). (For interpretation of the references to color in this figure legend, the reader is referred to the web version of this article.)

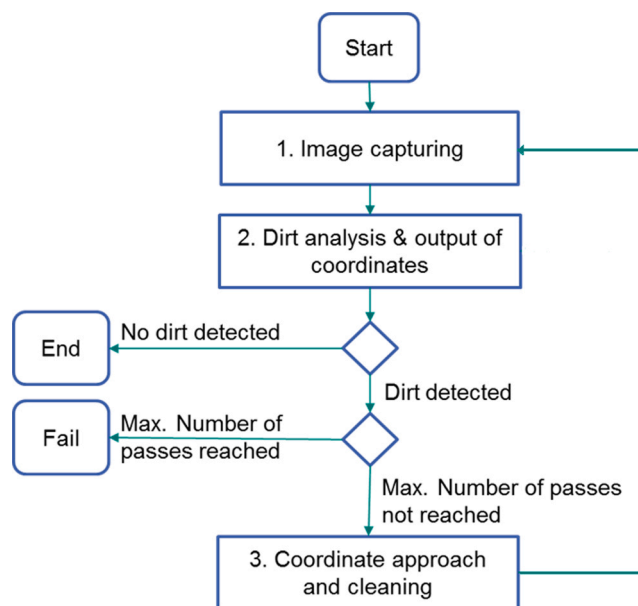


Fig. 2. Schematic representation of the flow chart for detection of impurities with subsequent cleaning.

light intensity V (Value) so that the reference image does not depend on the light intensities. Once the reference image is available it can be used to iterate over the dirty tissue (Fig. 3 b). Since a used tissue shows dirt everywhere relative to a clean tissue, it is characterized as “dirty” at many pixels (Fig. 3 c). For this reason, reduction steps are required to reveal the actual contamination (Fig. 3 d–f), as well as a threshold post-filter (Fig. 3 g) with subsequent reduction steps (Fig. 3 h). This sequence is carried out several times until the actual contamination is worked out (Fig. 3 h–j). For this reason, the procedure is also referred to as the GRSR procedure. Thus, the pollution can be worked out effectively depending on the iteration steps. In addition, the HashSet is dynamically adapted before the threshold-step by correcting it for the clean surface of the soiled tissue. Accordingly, the procedure should also effectively consider the ageing phenomenon of fabrics/surfaces. A further advantage is the robust behavior towards differences in illumination. However, they require an increased computing effort.

While the investigation, it turned out that the GRSR method was particularly suitable for the applied pollution and for the detection of dirt compared to the canny edge detection and histogram methods which were also tested. For this reason, the evaluation is based on this dirt detection algorithm.

After dirt detection the coordinates for coupling the software (1. Image evaluation and 2. Dirt analysis & output of coordinates) with the hardware (3. Coordinate approach and cleaning) are calculated. This is a part of step 2 and done if an effective radius of the cleaning nozzle has

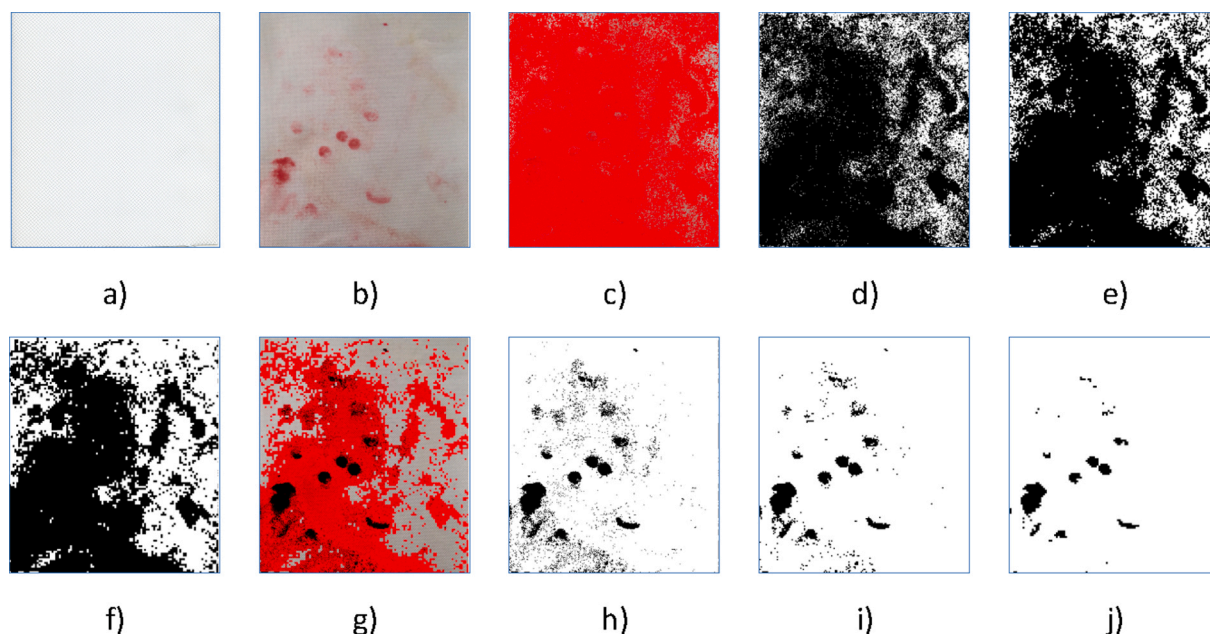


Fig. 3. Representation of dirt detection based on development using the GRSR method.

been specified by surface alignment of the cleaning surfaces with the dirt surface. For this purpose, enough effective circuits of the nozzle are placed over the dirt surfaces until they are completely covered. Subsequently, insignificant effective circles are removed, and the centers of the circles are the coordinates of the cleaning unit to be approached in relation to a previously defined origin. Fig. 4 a–d shows an example of the definition of coordinates based on pollution with the reduction of coordinating points by a fusion of two circles. Fig. 4 e shows the result with 34 coordinate points in comparison to the optimal solution Fig. 4 f with 29 coordinates.

After the coordinates have been defined the shortest path for the nozzle to the individual coordinate points must be clarified. This is illustrated in Fig. 5. After the contamination matrix (Fig. 5 a) has been converted into a binary image (Fig. 5 b - c) and the coordinates have been determined (Fig. 5 d) the calculation of the optimal path is based on a start value (Fig. 5 e, center). The *Traveling Salesman problem* [5] of determining the shortest path can only be solved numerically and thus allows the shortest cleaning path to be determined for the cleaning unit. The algorithm uses a monte carlo-based TSP-approximator with simulated annealing, which yields near optimal results for the shortest path.

Based on these steps and the coupling of image evaluation, determination of coordinates, sequence of start-up (software), and the cleaning unit hardware (consisting of nozzle and CNC control) the demand-oriented cleaning of surfaces can now take place. The

quantification is based on the decrease of the occupied surface over time and the necessary cleaning quantity. For this, the dirty pixels during and at the end of cleaning procedure A are related to the dirty pixels defined at the beginning of cleaning A_0 . This is called “Standardized degree of contamination” α_{Measured} and is calculated by the dirty pixels at time t during cleaning divided by the dirty pixels at the beginning of cleaning (See Eq. (1)). [4]

$$\alpha_{\text{Measured}} = A/A_0 \tag{1}$$

This value is between 1 and 0. In combination with the defined cleaning times, the necessary cleaning agent is measured and related to the filter area. This “Specific cleaning amount” can now be assigned to any “Standardized degree of contamination” α_{Measured} and allows a description of the decrease of contamination on the surface with the cleaning effort. On this basis different cleaning parameters and their effects can be compared and quantified [4].

3. Materials

In the following chapter, the test materials used are discussed in more detail. After some details on the fabric used, the contamination matrix, the sample application, and the various nozzles are illuminated.

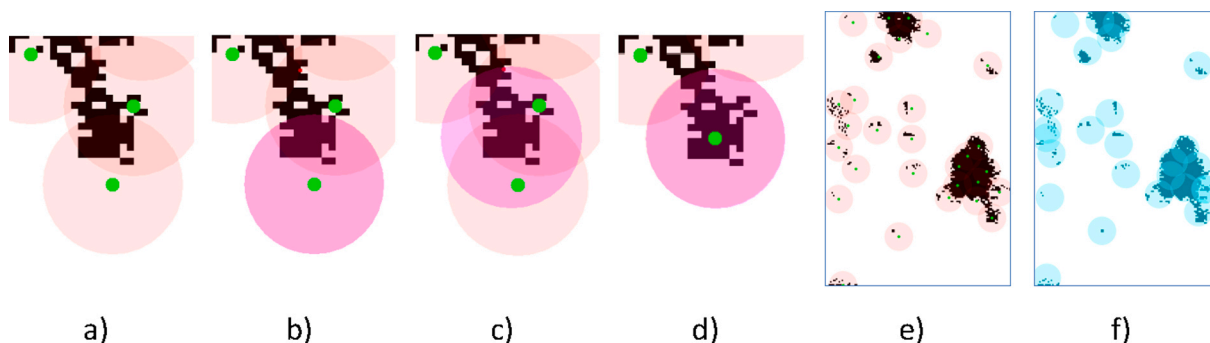


Fig. 4. Representation of the coordinate definition (a–b) with subsequent reduction step (c–d) and the results using a real pollution (e) (34 coordinate points) compared to the optimal result (f) (29 coordinate points).

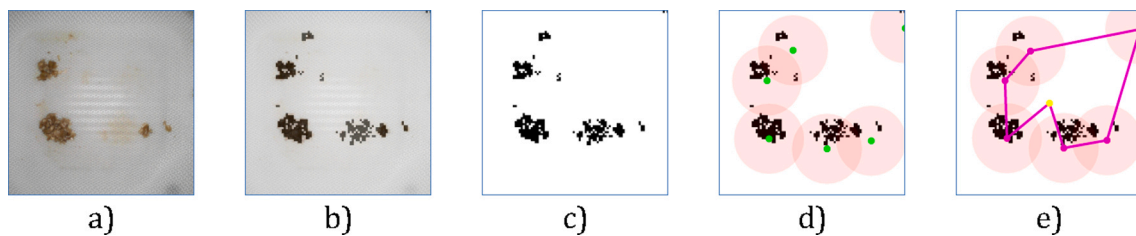


Fig. 5. Determination of the shortest path between the coordinate points (Traveling Salesman problem) based on a selected impurity.

3.1. Tissue

The evaluation of the nozzle selection was carried out on a multifilament fabric mounted on a laboratory scaled chamber filter [4]. Due to the loose fibrils and the rough structure of this multifilament fabric, it is expected that this fabric is difficult to clean compared to other multifilament fabrics. [6] This increased adhesion of dirt to the fabric and the resulting difficult cleaning situation are selection criteria for the polypropylene body fabric (Fig. 6). This is characterized according to DIN ISO 9354 with the abbreviation: 20–02 02–01–02 01–02 03. The first part 20 is the binding abbreviation and represents a twill fabric. 02–01–02 01 specifies the counted warp lifting and lowering. Lastly, 02 specifies the thread and 03 the offset. The binding cartridge resulting from this standard is also shown in Fig. 6, whereby the start for counting is also marked with a red dot in the laser microscope image. The different sizes of the warp and weft threads are striking: The weft threads with a measured diameter d_{weft} of 768 μm are considerably thinner than the warp threads with a d_{warp} of 1248 μm . With its properties, the fabric is specially optimized for filter presses and offers a high optical contrast with its white fibers. The large fabric thickness of 990 μm ensures high stability, but also a high basis weight of 505 g per square meter. Fig. 6 provides an overview of all fabric specifications and the binding cartridge:

Abbreviation according to DIN ISO 9354:	20-02 02-01-02 01 02 03
Weave type:	Twill
Material:	Polypropylen (PP)
$D_{\text{Bubble Point}}$:	7 μm
Air permeability at 20 mm water height:	40 $\text{l}\cdot\text{m}^{-2}\cdot\text{s}^{-1}$
Weight:	505 $\text{g}\cdot\text{m}^{-2}$
Thickness:	990 μm
S_q (DIN ISO 25178):	96 μm
d_{warp} :	1248 μm
d_{weft} :	768 μm

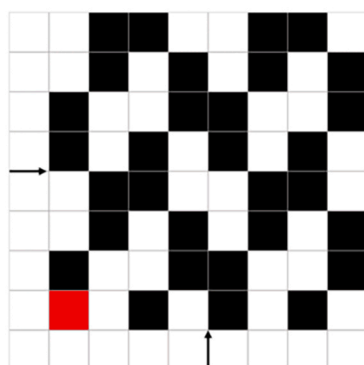
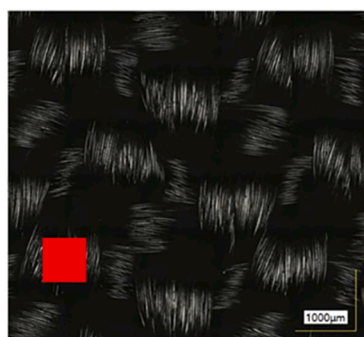


Fig. 6. Laser microscopy image, details and weave pattern of the used multifilament fabric.

3.2. Contamination matrix

In the experiments, the tissue described is contaminated with a contamination matrix of spent grains, a waste product of the beer industry [7] (Fig. 7). This is an insoluble residue of malt grain that remains in the mash and must be separated for further processing. For the first trials pure Pilsner malt was mashed with the particle size distribution shown in Fig. 7 a. The temperature control followed that of the congress mashing process (mashing at 45 °C, 1st rest 30 min at 45°, heating 25 min at 1 °C/min, 2nd rest 60 min at 70 °C) [7].

3.3. Nozzles

Three different nozzle types were tested in the first trials in order to achieve software optimizations and better degrees of cleaning. The same jet angle with flow rates as similar as possible was used to characterize the round and flat jet nozzles (see Table 1).

3.4. Sample application

To ensure that samples are applied as uniform as possible and have similarly high adhesive forces, we prepared all samples according to a fixed scheme:

- First, four heaps of the same weight were formed

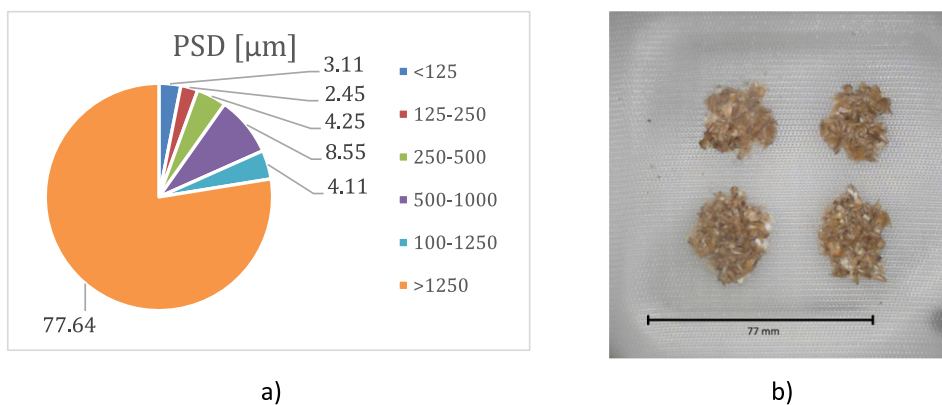


Fig. 7. Particle size distribution of the crushed malt sample (a) and the sample preparation on the tissue for one test run (b).

Table 1

Overview of tested nozzles. The nozzles were selected on the basis of similar flow rates with different flow profiles.

nozzle	nozzle type	volume flow [l·min ⁻¹ at 2 bar]	jet angle	jet shape (exemplary)
1	full cone nozzle	1.00	Round, 45° at 2 bar	
2				
3	full jet nozzle flat spray nozzle	1.00 1.25	Point shaped Flat, 45° at 2 bar	

- The samples were also moistened in a defined way, which further improved the adhesion between the sample and the filter cloth.
- The sample is then pressed on at a defined pressure of 185 Newtons per square centimeter.

The high pressure guarantees that the dirt adheres securely to the filter cloth. Depending on the expansion of the spent grains during pressing, the degree of contamination on the image evaluation surface of the filter cloth was between 7 and 12 percent. The contamination (see Fig. 7 b) could best be covered with circles with a diameter of 35 mm.

4. Results - Interpretation

To improve and characterize the new cleaning system a variation of different relevant parameters for the cleaning was performed. The following variations are investigated for their relevance and significance for cleaning in the system:

- Pressure variation
- Variation of the nozzle distance
- Variation of the nozzle type
- Influence of the contamination matrix

As expected, a higher pressure ensures better cleaning and a smaller distance between nozzle and filter cloth cleans more intensively and thoroughly. When varying the nozzle type it was necessary to find the best one for the XYZ table and when varying the contamination matrix to investigate a viscous contamination.

4.1. Pressure variation

A cleaning pressure of 5 bar served as reference pressure for further tests. This was well feasible at the experimental setup and showed a good cleaning effect in the first cleaning tests. At a reference distance of 35 mm to the filter fabric the full-cone nozzle cleaned with a fixed pulse duration of 250 ms. To achieve a better degree of cleaning and to accelerate the cleaning process the cleaning pressure was increased. The pressure was increased to 6.5 and 8 bar. Fig. 8 shows the influence of the increased pressure. The X-axis shows the consumption of cleaning agent normalized to the filter surface, while the vertical axis shows the contamination normalized to the initial value. The almost identical initial slope of the curves is conspicuous and indicates this as a nozzle characteristic. Only a cleaning pressure of 8 bar showed a slightly better cleaning result after the first cleaning. Between 5 and 6.5 bar no significant difference could be found in the result. In the further course of the cleaning a small pressure influence shows up in the examined pressure range. In general, the strong flattening of the curve after the first cleaning is also noticeable. This is due to the significantly lower residual contamination: To remove the remaining contamination increased solvent consumption is required. Therefore, cleaning is no longer as effective as at the beginning.

4.2. Variation of the nozzle distance

The next criterion considered was the influence of distance on detergent efficiency. The hypothesis is that with increasing distance the cleaning intensity and thus the effect of the nozzle, decreases. The full-cone nozzle was tested at a constant pressure of 5 bar at distances of 25,

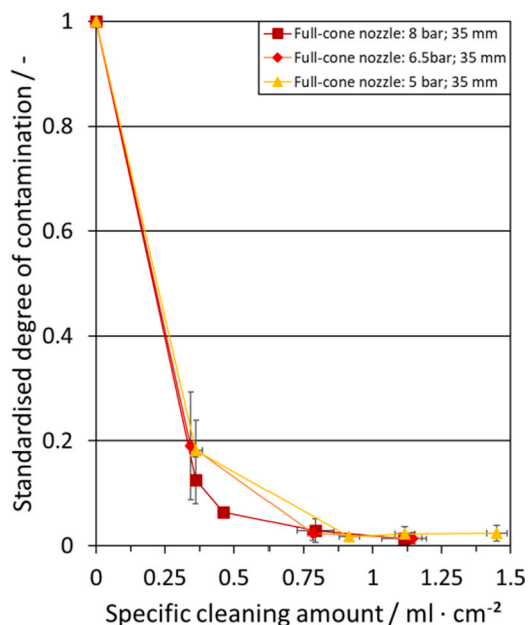
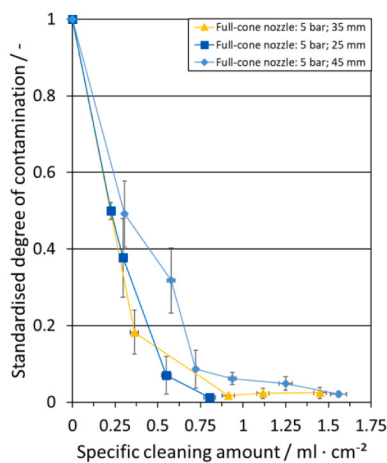


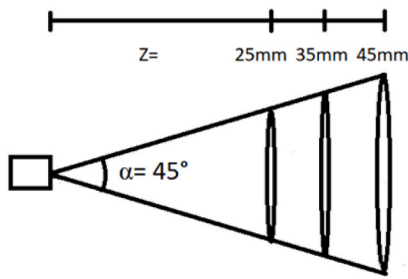
Fig. 8. Results of the pressure variation of the full-cone nozzle. The almost identical course shows only slightly improved cleaning results at a higher pressure of 8 bar.

35, and 45 mm from the filter cloth. A visualization of the resulting cleaning area and the results are shown in Fig. 9.

In Theory, a smaller distance improves the cleaning quality due to the resulting higher cleaning intensity since the performance of the nozzle remains largely the same and the power input takes place on a smaller area. This proved to be the case. However, the reduced distance of 25 mm required more cleaning points as the resulting cleaning radius was reduced. In some cases, the recognition software covered a contamination with several small circles. Therefore, the machine had to approach several times. This slightly increases the consumption of cleaning agent at the beginning and during the removal of the last residues of dirt. Nevertheless, this distance shows the best cleaning process and the smallest required cleaning volume until the end of a sequence. This is mainly due to the increased intensity. With a distance increase to 45 mm between nozzle and filter cloth the intensity decreased again. Compared to 35 mm and just at the beginning of the cleaning process it was not completely enough to remove the pressed-on particles from the



a)



Distance [mm]	25	35	45
Cleaning area [mm ²]	3239	4040	5680

b)

Fig. 9. Results and clarification of the distance variation (a) of the full-cone nozzle at 25–45 mm and their effect on the occupied area (b).

filter cloth.

This slow separation process is clearly visible in the curve in Fig. 9. Not only does cleaning require more cleaning agent at the beginning, but more cleaning agent had to be applied to remove any remaining residue. To achieve the best possible efficiency, the distance should be adapted to the diameter of the dirt. By determining the diameter, the coordinate generator could calculate an optimum distance to each contamination.

4.3. Variation of the nozzle type

In addition, various nozzles in the automated cleaning system were examined. Special attention was paid to the different power densities. A point jet, a flat jet, and a full cone nozzle were used. Fig. 10 shows the cleaning process of the three nozzles tested.

The nozzle with the highest power density, the full jet nozzle,

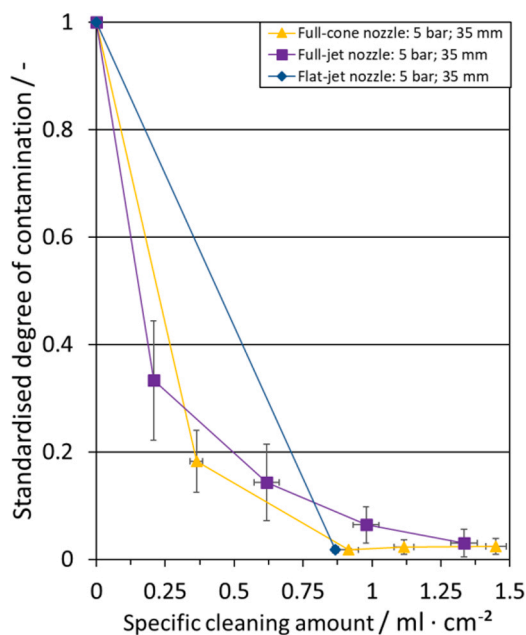


Fig. 10. Results of the nozzle variation: Full jet nozzle in purple, full cone nozzle in yellow and flat jet nozzle with only one cleaning point and the best cleaning shown in blue. (For interpretation of the references to color in this figure legend, the reader is referred to the web version of this article.)

showed the best cleaning agent efficiency at the beginning of the cleaning process. This is demonstrated from the largest gradient at the beginning of the cleaning curve. However, as the process progresses the cleaning efficiency decreases radially as the dirt spreads over the filter fabric. As soon as the initially local and compactly applied dirt has spread, the nozzle's small effective radius becomes apparent: a great deal of cleaning agent must be used to clean the entire filter cloth surface. In addition, the cleaning result is poorer, as only a spot-white cloth is cleaned even in deeper layers. Furthermore, this results in stronger discoloration due to residues in the fabric which can lead to detection problems.

In contrast to the full jet nozzle the full cone nozzle has the lowest power density of all tested nozzles. Cleaning with the full-cone nozzle showed good results but the distance between the nozzle and the filter cloth is particularly important for the cleaning effect. The selected reference distance of 35 mm did not prove to be the optimum in the distance investigations, but it showed advantages especially at the end of the cleaning process due to the large cleaning radius at low intensity (compared to the other nozzles).

The flat jet nozzle offers a high cleaning intensity with its linear cleaning profile. At the beginning of the experiments it was only usable with a continuous liquid flow. Because of and despite these limitations a very good degree of cleaning is achieved after a single cleaning run of the program. This leads to the conclusion that even better cleaning results are possible with a better implementation of the flat jet nozzle with an adapted coordinate generation on a square basis (instead of circles) and an additional pulsation [8].

The overall conclusion is that both the power density of a nozzle and the area cleaned by it are decisive for optimum cleaning agent efficiency. With its jet profile the flat jet nozzle showed the strengths of the two other nozzles tested during cleaning whilst moving operation: the intensity of the full jet nozzle and the surface cleaning of the full cone nozzle.

4.4. Influence of the contamination matrix

The last variation tested used counting contaminants and dried contaminants from the food industry. Pudding and spent grains dried overnight on the filter cloths were used for this purpose.

Contrary to expectations Fig. 11 shows that the viscous soiling (light green) did not show a worse cleaning process than the wet and dried draffs. The final degree of cleaning was even increased with a viscous contamination.

In contrast to the viscous sample it was much more difficult to remove the dried draffs (in dark green). Contrary to logical expectations the cleaning curve showed a maximum after the first cleaning process. However, this can be explained by the following factors: The dried, low-contrast draffs are detected more poorly in the beginning. Furthermore, the contamination swelled up during the first remoistening. This results in a higher percentage value for the original contamination during standardization. To avoid this factor, the curve in the corrected version was standardized to the highest detected degree of soiling and reflects the previously difficult to recognize situation well: The first cleaning of the filter cloth hardly cleaned any soiling, as this is only to be remoistened for removal. After remoistening the cleaning behavior is slightly worse.

5. Conclusion

During the investigation a systematic variation of factors, which are assumed to have an influence on the surface cleaning of filter cloths, was carried out. The following parameter variations were made for this purpose:

- Pressure
- Cleaning distance

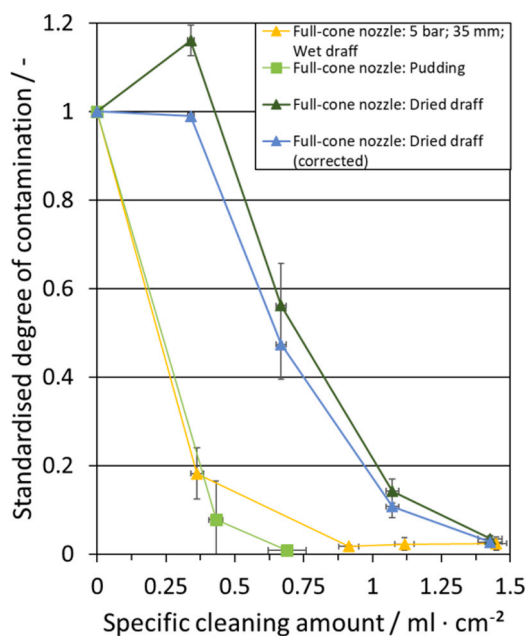


Fig. 11. Variation of contamination when using the full-cone nozzle at 35 mm distance, yellow: the comparison series (Wet draff), dark green: dried draff (as measured and in blue the corrected curve), light green: pudding. (For interpretation of the references to color in this figure legend, the reader is referred to the web version of this article.)

- Nozzle type
- Contamination

The low influence of the pressure on the surface cleanliness in the range of 5–8.5 bar is noticeable. Industrial cleaning systems operate at higher pressures thereby effective cleaning can also take place at pressures in this range. The variation of the cleaning intensity with the help of the nozzle types and the distance showed that these as well as the surface cleaned by the nozzle are relevant for an optimal utilization of the solvent. The low influence of the cleaning pressure in the tested area draws the conclusion that although a higher pressure is helpful. The selected distance between nozzle and filter cloth plays a significantly greater role in questions of cleaning efficiency. It was also found that in the case of local and compact soiling the cleaning distance in the coordinate generation should be adapted to the soiling diameter. This can be done by determining the diameter: In the image evaluation, the largest horizontal and vertical diameter is determined, then this value is set as the diameter of the cleaning circuit in round jet nozzles. The optimum distance can now be calculated with a given nozzle angle. A horizontal diameter analysis can also determine and optimize the cleaning distance for flat jet nozzles. With the nozzle variations the flat spray nozzle showed the most promising results even though it was not completely implemented at the time of the tests. In these experiments the generation of coordinates was still based on the circles of a full-cone nozzle. The solid jet nozzle showed advantages due to its intensity at the beginning of the cleaning process but led to poorer cleaning and efficiency results due to the punctual cleaning in the further course. The full-cone nozzle showed an overall good cleaning behavior. However, the choice of the optimum distance is an efficiency decision as this has a decisive influence on the cleaning intensity of the nozzle.

The variation of the soiling clearly showed that cleaning should be carried out promptly during operation as drying the soiling leads to a higher cleaning effort. This is also in the user's interest, as it saves both time and cleaning agent.

Compared to a reference cleaning, which is based on a conventional cleaning of the filter fabric, a significant saving of cleaning agents was achieved with all tests. The comparative cleaning was performed with a

continuous jet of the full-cone nozzle from left to right and required $\sim 2.25 \text{ ml/cm}^2$. The savings thus vary between 30 and 60 percent in relation to the cleaning agent used, which is standardized for the filter area.

6. Outlook

After elaboration of essential cleaning parameters within the surface cleaning various further developments of this system are conceivable. These can be divided into the following two groups:

- Further developments in process technology
- Anthropomatic developments

Further experiments with different nozzle parameters such as jet angles and pulsation times should be carried out for the further development of the process technology. Based on these results different fabrics [6] and nozzle combinations with additional pulsation [8] will be investigated for their cleaning effect. The aim is to find improved tissue, contamination-based detection parameters and, to expand the range of applications of the new system.

For the further antropomatic development, the software should implement a user interface within the framework of a GUI (graphical user interface) with further automation of the steps. Furthermore, the development of the coordinate generation system for flat jet nozzles and their resulting jet shape is conceivable. To achieve an even better efficiency, different approaches could be tested:

- Automatic distance determination: This determines the largest diameter of the contamination and generates the optimum distance for cleaning with the fixed spraying angle.
- Nozzle change following the example of the head change of a CNC milling machine: Depending on the existing cleaning situation, the nozzle can be changed, and strengths can be specifically played out.
- Intelligent pulse times and pulse number variation: Depending on the required cleaning quality and the existing cleaning situation the program can define pulse times, pause times, and repetitions.
- Movable nozzle head: Targeted cleaning using angles smaller than 90°

In summary, the new system can be retrofitted into existing semi-automated cleaning systems and requires only minimal additional costs and has a significant savings potential in cleaning agents. However, several improvements and tests on a laboratory and pilot scale still must be carried out before the system is ready for the market.

CRedit authorship contribution statement

Patrick Morsch: Conceptualization, Methodology, Software, Formal

analysis, Investigation, Validation, Resources, Writing - original draft, Project administration. **Adrian Arnold:** Investigation, Writing - review & editing. **Henning Schulze:** Software, Writing - review & editing. **Roman Werner:** Investigation, Writing - review & editing. **Harald Anlauf:** Supervision, Writing - review & editing, Funding acquisition. **Dominik U. Geier:** Supervision, Writing - review & editing, Funding acquisition. **Thomas Becker:** Supervision, Writing - review & editing, Funding acquisition. **Hermann Nirschl:** Supervision, Writing - review & editing, Funding acquisition.

Declaration of Competing Interest

The authors declare that they have no known competing financial interests or personal relationships that could have appeared to influence the work reported in this paper.

Acknowledgement

The IGF Project 19716 N of the IVLV e.V is supported via AiF within the programme for promoting the Industrial Collective Research (IGF) of the German Ministry of Economic Affairs and Energy (BMWi), based on a resolution of the German Parliament. The authors would also like to thank all colleagues and students for the support in writing this paper. Special thanks go to the students Thomas Kadow and Roman Lehmann for their support in this project.

References

- [1] World Health Organization, WHO Expert Committee on Specifications for Pharmaceutical Preparations. Forty-eighth Meeting Report. Geneva: World Health Organization (Technical Report Series), 2014. Online verfügbar unter <http://search.ebscohost.com/login.aspx?>
- [2] S. Ripperger, Reinigung, Desinfektion und Sterilisation von verfahrenstechnischen Anlagen: Die Reinigung verfahrenstechnischer Anlagen (Teil 1), in: *Filtern & Separieren*, Vol. 3, VDL-Verlag GmbH, Rödermark 2004, pp. 110–116.
- [3] S. Ripperger, Reinigung, Desinfektion und Sterilisation von verfahrenstechnischen Anlagen: Die Reinigung der Membrananlagen (Teil 2), in *Filtern & Separieren*, Vol. 4, 2004, pp. 162–166.
- [4] P. Morsch, J. Kühn, R. Werner, H. Anlauf, D.U. Geier, T. Becker, H. Nirschl, *Chem. Eng. Sci.* (2020).
- [5] V. Černý, Thermodynamical approach to the traveling salesman problem: an efficient simulation algorithm, *J. Optim. Theory Appl.* 45 (1) (1985) 41–51, <https://doi.org/10.1007/BF00940812>.
- [6] C. Weidemann, S. Stahl, H. Nirschl, Development of a qualitative test method for the cleanability of polymer woven filter media, *Food Bioprod. Process.* 91 (2013) 515–524.
- [7] Jacob Fritz (Hg.) MEBAK brautechnische Analysenmethoden - Rohstoffe. Rohfrucht, Gerste, Malz, Hopfen und Hopfenprodukte: Methodensammlung der Mittteleuropäischen Brautechnischen Analysenkommission. Mittteleuropäische Brautechnische Analysenkommission. Freising-Weihenstephan: Selbstverlag der MEBAK, 2016.
- [8] C. Weidemann, S. Vogt, H. Nirschl, Cleaning of filter media by pulsed flow – Establishment of dimensionless operation numbers describing the cleaning result, *J. Food Eng.* 132 (2014) 29–38.

K. Attached publication [6]

Verification of the contribution from the co-authors

Title: Influence of the filter cloth and nozzles type on the in-situ cleaning procedure of filter presses

Journal: Chemical Engineering Science

Authors: P. Morsch, J. Kühn, R. Werner, H. Anlauf, D. U. Geier, T. Becker, H. Nirschl

Position in the dissertation:

The content of this paper has been included in Chapter 4.7 and 5.1

Contribution of Patrick Morsch

Conceptual design and construction of the test setup, as well as planning of the test procedure, choosing the test material and, Execution of regeneration tests and data evaluation, Summary of the data and evaluation of the results, Writing the paper and performing the source research

Contribution of Jérôme Kühn

Execution of regeneration tests and data evaluation, Support by collecting the data, Support by writing the paper

Contribution of Roman Werner

In framework of a cooperation, the concept of a lab-scaled and pilot-scaled test setup was designed collaboratively, Support of the work by references in literature, test setup, test procedure. Proofreading of the paper (technical).

Contribution of Harald Anlauf

Support of the work by references in literature, test setup, test procedure. Proofreading of the paper (technical).

Contribution of Dominik U. Geier

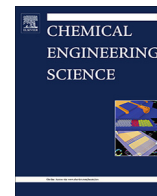
Support of the work by references in literature, test setup, test procedure. Proofreading of the paper (technical).

Contribution of Thomas Becker

Support of the work by references in literature, test setup, test procedure. Proofreading of the paper (technical).

Contribution of Hermann Nirschl

Support of the work by references in literature, test setup, test procedure. Proofreading of the paper (technical).



Influence of the filter cloth and nozzles type on the in-situ cleaning procedure of filter presses



Patrick Morsch^{a,*}, Jérôme Kühn^a, Roman Werner^{b,*}, Harald Anlauf^a, Dominik U. Geier^b, Thomas Becker^b, Hermann Nirschl^a

^a Karlsruhe Institute of Technology (KIT), Institute for Mechanical Process Engineering and Mechanics (MVM), Process Machines, Strasse am Forum 8, 76131 Karlsruhe, Germany

^b Technical University of Munich, TUM School of Life Sciences Weihenstephan, Institute of Brewing and Beverage Technology, BioPat and Digitalization, Weihenstephaner Steig 20, 85354 Freising, Germany

HIGHLIGHTS

- The surface contamination is lower with smaller meshes within the same weave type.
- Calendering of the fabric surface does not lead to less surface contamination.
- Multifilament fabrics have the lowest surface contamination with the smallest amount of cleaning agent.
- Mathematical description of the cleaning process by a regressive model possible.
- Full jet nozzle to be preferred for surface cleaning.
- Optimization of the dirt detection by variation with colour filters and light sources possible.

GRAPHICAL ABSTRACT

Exemplary representation of the contaminated surface and the resulting binary image with coordinate generation based on the effective radius of the cleaning nozzle and the shortest way of cleaning procedure (left to right).



ARTICLE INFO

Article history:

Received 10 March 2020
 Received in revised form 4 June 2020
 Accepted 7 June 2020
 Available online 11 June 2020

© 2020 Elsevier Ltd. All rights reserved.

1. Introduction

In particle technology, separation by means of filters is a widespread application and is closely linked to the weaving industry. The filter cloths produced there are used for the separation of particle-loaded streams in the apparatuses. The chamber filter/filter press, which is particularly suitable for separating the finest

particles due to the high possible filtration pressures, is particularly widespread. Independent of the separation during the filtration phase, the interaction of particles and filter cloth requires regular regeneration of the cloth. For this purpose, the process engineering offers various cleaning possibilities, as acid/alkaline cleaning, backwashing and more.

For effective cleaning, a precise definition of the contamination on the cloth is required. A distinction must be made between the contamination in the cloth (intra weave contamination) and remaining filter cake fragments on the cloth surface (surface contamination). In the case of intra weave contamination, the pores are clogged by bleeding and clogging (Purchas and Sutherland, 2002), which can be removed by various cleaning steps (Leipert

* Corresponding authors.

E-mail addresses: patrick.morsch@kit.edu (P. Morsch), roman.werner@tum.de (R. Werner).

URLs: <http://www.mvm.kit.edu> (J. Kühn), <http://www.mvm.kit.edu> (H. Anlauf), <http://www.lbgt.wzw.tum.de> (D.U. Geier), <http://www.lbgt.wzw.tum.de> (T. Becker), <http://www.mvm.kit.edu> (H. Nirschl).

Nomenclature

Symbol	Description [Unit]	Symbol	Description [Unit]
A	Covered area at time $t > t_0$ [-]	$\alpha_{\text{Approximated}}$	Approximated degree of contamination [-]
A_0	Covered area at time t_0 [-]	α_{Measured}	Standardised degree of contamination [-]
F^+ ; F^-	False-positive (+) and false-negative (-) errors [-]	β	Final contamination degree [-]
S_{F^+} ; S_{F^-}	Standard deviation of F^+ and F^- [-]	γ	(Cleaning) Kinetic [$\text{cm}^2 \cdot \text{ml}^{-1}$]
w_+ ; w_-	Weighting factor for standard deviation of F^+ and F^- [-]	ε	Specific cleaning amount [$\text{ml} \cdot \text{cm}^{-2}$]
x_{F^+}	Weighting factor. $x_{F^+} + (1 - x_{F^+}) = 1$ [-]		

and Nirschl, 2012; Stahl et al., 2013; Weidemann et al., 2014; Weidemann et al., 2013). The remaining particles in the meshes lead to an increase in the initial resistance of the filter cloth and thus to a reduced hydraulic performance (Purchas and Sutherland, 2002).

However, the decisive pressure loss is caused by the filter cake that has built up and thus the filter cake fragments on the cloth surface. This increases with decreasing particle size of the particle collective to be filtered. For this reason, especially the cake on the cloth surface must be removed with regard to the hydraulic system. The current state of the art is that these remaining surface coatings are removed by a manpower using a water jet in a lavish and cost-intensive process. There is no documentation of the cleaning result, which is usually associated with an excessive use of cleaning agents.

The industry has already taken up this grievance and offers cleaning systems that replace human labour by using automated nozzle lances on a sled. The resulting detergent use is still not demand-oriented, but the human component is replaced by a reproducible cleaning procedure. This cleaning concept can then be coupled with various measuring techniques for dirt detection. (Decker, 2019)

The cleaning of filter cloths by demand-controlled nozzle cleaning is an issue that has been insufficiently dealt with in the past for application using filter cloths. One finds demand-based cleaning in the food sector, plant components, production technology and other industrial sectors. Cleaning after filtration is mainly a topic from the food industry for membrane applications in beer filtration and the cleaning of apparatus parts from the dairy industry (Gibson et al., 1999; Goode et al., 2013). Especially in the dairy industry, hygienic cleaning is an important topic for saving cleaning agents because of the constant price pressure in this industry

sector. The cleaning process investigated in this context describes above all the reduction of fouling effects to avoid cross-contamination with perishable substances. The focus of the research is on smooth surfaces such as container tanks. (Gibson et al., 1999; Goode et al., 2013; Shi et al., 2014; D'Souza and Mawson, 2005; Kazemimoghadam and Mohammadi, 2007)

(Filter) cloth as a source of contamination has only moved into the focus of research in the food sector (large bakeries) in recent years (Moeller and Nirschl, 2017). Based on this, a more in-depth investigation was carried out with a focus on the ageing phenomenon of cloths and the resulting change in roughness and the consequences for the adhesion forces, also for the bakery industry (Moeller et al., 2018). The transfer of these experiences resulted in the development of a concept for the cleaning of the filter cloth according to the needs with targeted cleaning (Moeller and Nirschl, 2018).

Within the scope of this project, the implementation is carried out using a direct, imaging measurement system in reference to (Moeller and Nirschl, 2018). Based on this trend of automated cleaning, this paper deals with the effective removal of these surface contaminants by demand-oriented, automated cleaning. The basis for this is an image evaluation, coupled with a cleaning system (nozzle). Both in combination detect dirt and clean it from the surface of the filter cloth. The content of this investigation is the influence of the choice of cloth and nozzle on the cleaning result. Since filter cloths can be characterized as particularly difficult to clean due to their structure (periodic sequence of high roughness elevations [thread wrap] on a small cloth section), the cleaning system presented here, and the results of the nozzle selection can also be transferred to other cleaning systems (container cleaning, etc.) and contribute to increasing process and product safety.

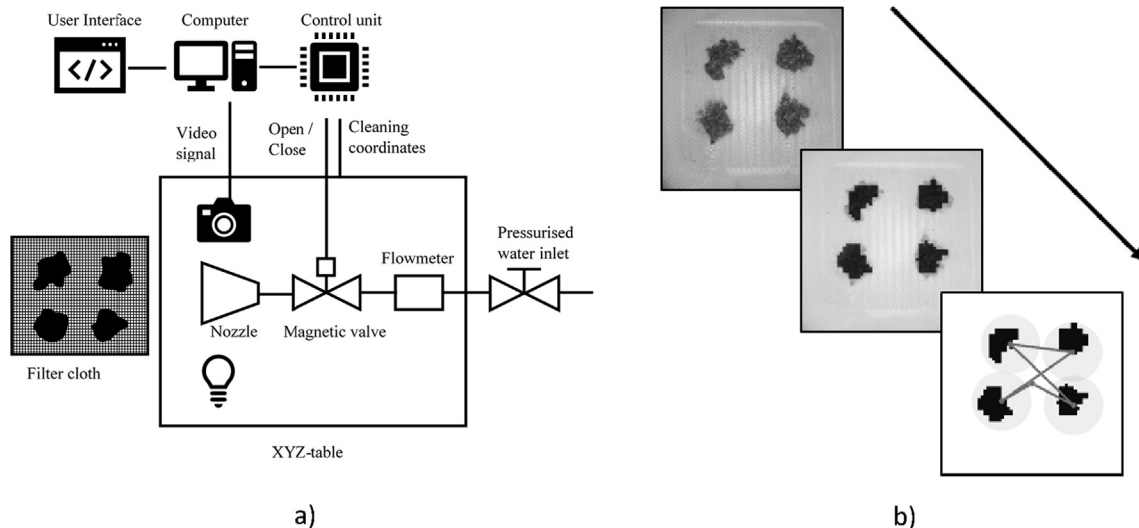


Fig. 1. Schematic representation of the test setup (a) and exemplary representation of the image evaluation of a test run (b).

2. Method

The basis of the demand-oriented, automated cleaning is an optical dirt detection system, which is coupled with a nozzle system. For this unit a dirt detection system was developed, which enables the connection of both components. The cleaning step takes place on a laboratory chamber filter with a filter plate dimension of 109 cm² surface. The contaminated area covers about 15% of the surface. This is a practical value after the cake is discharged. If the contaminated surface area is larger, the selection of the filter cloth should be reconsidered. The cleaning can then be reduced to three essential steps:

- Detection of the contaminated areas. [image analysis]
- Assignment of coordinates. [image processing]
- Approaching and cleaning of the defined coordinates. [cleaning]

In Fig. 1 a) the structure of the system is shown schematically. The detection of the contaminated areas is carried out by connecting a standard camera with an image analysis system. In order to ensure that the image analysis used has general validity, a low-cost camera with the trade name Microsoft LifeCam Studio from Microsoft Corporation with a resolution of 1080p (HD 1920 × 1080 pixels) was used. The image analysis is a self-developed product based on OpenSource software. Basis of the used procedure is a gradient-reduction-saturation-reduction procedure (GRSR) for the evaluation of the contaminated areas based on a clean cloth as reference image. Based on this image, a gradient between clean and unclean pixels is defined, the resulting image is reduced (smoothing image noise), pre-filtered with a threshold and reduced again. This procedure takes place in several passes (up to 3 times). The definition of the clean pixel is dynamically adjusted according to the iteration steps. This allows an effective detection of contaminated areas.

These unclean areas are then assigned coordinates, which are then approached by a CNC-controller and cleaned with a nozzle cleaning system. The steps of the image evaluation are shown in Fig. 1 b) as an example. The captured image (top left) is binarized (center) and then provided with coordinate points corresponding to the radius of action of the nozzle and the shortest path of the sequence is calculated with the starting point in the centre (bottom right). A cleaning impulse with a duration of 250 ms is used for cleaning when approaching the contaminated areas. This means that a jet of water will act on the contaminated area for this duration. This procedure continues until the cloth has been completely cleaned or until 10 cleaning passes have taken place. Here it is assumed that after 10 measurements a clean surface should be achieved for economical operation.

The combination of these components enables demand-oriented cleaning and thus represents an efficient, optimized and resource-saving cleaning method. The focus of this work is on the cleanability of different filter cloths with variable nozzle types. This is done by comparing the decrease of the filter surfaces covered with filter cake with the required cleaning agent input for different filter cloth and nozzle combinations. Therefore, a parameter has been defined to describe this (see Eq. (1)). The standardised degree of contamination α_{Measured} (Eq. (1)), which describes the decrease in the area occupied by filter cake $A(t > t_0)$, relative to the area originally occupied by the filter cake $A_0(t = t_0)$, during cleaning (with reference to (Stahl et al., 2007)). This value is determined directly from the evaluation of the surface cleaning (measured value). The standardised degree of contamination α_{Measured} therefore assumes values of 1 at the time before cleaning and then tends towards 0 for perfect cleaning. The values ≥ 0 for the final

contamination state can then be used between the cloths and nozzle types to describe the cleanability of the cloths regarding a stationary contamination state.

$$\alpha_{\text{Measured}} = A/A_0 \quad (1)$$

The description of the measured course of the decrease in the standardised degree of contamination α_{Measured} was carried out by approximating this curve using the mathematical model shown in Eq. (2). For this purpose, the course $\alpha_{\text{Approximated}}$ is described using a regressive model with the quantities final contamination degree β and the (cleaning) kinetic γ . The approximated curve depends on the specific cleaning amount ε and allows the comparison based on a pair of values. A high kinetic value goes hand in hand with a good, equivalent to a fast, decrease of the occupied area over the necessary specific cleaning quantity. In addition, the value final contamination degree describes the surface pollution after 10 cleaning steps and should be interpreted as remaining contamination on the filter cloth. Based on these values the comparison between the cloths and the different nozzles is possible.

$$\alpha_{\text{Approximated}} = (1 - \beta) \cdot \text{Exp}(-\gamma \cdot \varepsilon) + \beta \quad (2)$$

In addition to the parameter variation of cloth and nozzle type to create a model for the description of the cleaning process, the image evaluation is also optimized. For this purpose, the dirt detection is supplemented by the use of colour filters and changes in the light source and their influence on the dirt detection is evaluated.

The present parameters for image evaluation, which are used to evaluate white filter cloths, lead to increased false results when used a coloured filter cloth. This means that dirty areas are not recognized (false-negative result) or clean areas are recognized as dirty (false-positive result). The parameters must therefore be adjusted to achieve better contamination detection. This can increase the efficiency of automated cleaning, as false-positive findings lead to an increase in the amount of cleaning agent required, as clean areas are then also approached. On the other hand, false-negative findings lead to insufficient cleaning of the filter cloth, as contamination remains undetected. The parameter that influences the error detection in the image evaluation is the threshold value. This describes the maximum difference between the image pixel and the reference value, so that the image pixel is still considered clean. Thus, a reduction of this threshold value leads to a decrease in the number of false-negative errors. In the opposite direction, however, the false-positive findings can accumulate. Colour filters are used in front of the camera as a further adjustment option. These shift the colour spectrum and thus affect image recognition. By varying different colour filters and the threshold value, an optimum for image recognition can be determined. For this purpose, cleaning tests are carried out in which the state of contamination is documented with the different colour filters in front of the camera lens. Thus, the same contamination conditions can be evaluated with the different colour filters. This is then done automatically, whereby each image also undergoes a threshold value variation. This means that each contamination state is analysed with the different filters as well as with the threshold values. The filters used are listed and characterized in Table 1 with their RGB values. To determine the RGB values, the colour filters were photographed in a strongly lighted room and the histogram of the RGB values of the photograph was determined. Table 1 lists the mean value and the standard deviation of the respective R, G and B-values.

By using colour filters and adjusting the image analysis, a wide range of adjustment possibilities is created from which the optimal recognition parameters are extracted. For this purpose, the evaluated recognitions must be evaluated according to their accuracy. Therefore, a score σ is defined (Eq. (3)), which gives a weighted

Table 1
Overview of the colour filters used for image acquisition.

No.	Colour Filter Description	RGB-values (colour intensity 0–255)		
		R	G	B
–	<Filter cloth No. 10> No Filter	232 ± 6	179 ± 10	9 ± 31
1	Red	82 ± 4	0 ± 0	0 ± 0
2	Grey	32 ± 2	25 ± 2	17 ± 2
3	Yellow	231 ± 2	154 ± 3	0 ± 0
4	Orange	214 ± 3	76 ± 4	0 ± 0
5	Brown	34 ± 2	14 ± 3	0 ± 1
6	Blue	0 ± 1	2 ± 2	61 ± 2

representation of the false-positive and false-negative errors and their fluctuations between the tests.

$$\sigma = (F^+ + w_+ \cdot s_{F^+}) \cdot x_{F^+} + (F^- + w_- \cdot s_{F^-}) \cdot (1 - x_{F^+}) \quad (3)$$

This score must be minimized, analogous to an objective functional, for optimal dirt detection. F^+ is the mean value of false-positive errors over the tests. F^- is the mean value of the false-negative errors. x_{F^+} is a weighting factor that weights the false-positive and false-negative errors against each other. Standard deviation s_{F^+} and s_{F^-} are the standard deviations of the errors for F^+ and F^- . The Factors w_+ and w_- weights these deviations and their importance. In this way, less reproducible results could be considered. In this evaluation, $x_{F^+} = x_{F^-} = w_+ = w_- = 0.5$, so that both errors and their deviation are equally reflected in the score σ . From the determined score for each threshold value and colour filter, the optimum threshold values for each colour filter can be determined directly, to compare them with each other.

3. Materials

The chapter Materials includes the presentation of the filter cloths used with their specific properties. The selection is based on the mesh sizes specified by the manufacturer and the differentiation into the mesh types Plain, Twill und Satin. In the following subchapter the cloth selection is defined. In addition to the variation of the cloths, there was also a variation of different nozzles for selected filter cloths. With regard to the nozzles, attention was focused on the common cleaning jets flat jet, full cone nozzle and spot jet. The nozzles are described in subchapter 3.2. The chapter Material concludes with a short description of the contamination matrix used.

3.1. Filter cloths

With reference to (Purchas and Sutherland, 2002), cloths can be divided into major groups according to the fibres used (single fibre or multiple fibres (fibrils)):

- Monofilament Cloth
- Multifilament Cloth

In addition to these two groups, there are also blended cloths where one yarn direction (warp/weft) is multifilament and the other monofilament. To illustrate these groups of cloths, a selection of monofilament cloths and multifilament cloths is therefore made, which are summarized in Table 2.

The first cloths, which are grouped together as Group 1, comprise twill weaves, according to manufacturer information, with different mesh sizes but the same material. This makes it possible to investigate an influence of the mesh size in the range of 215 μm to 20 μm . The surface roughness is also reduced with decreasing

mesh size. Tests of the filter cloth according to DIN ISO 9354 have shown that the cloths are not only twill weaves but also a satin cloth. In addition, weave type is similar for the 215 and 120 μm mesh, but different from the 43 and 20 μm mesh. The reason for this is that as the mesh size decreases, the weave must be adjusted so that the desired mesh size can be achieved at all.

As the values for mesh size and roughness in group 1 show a similar tendency, the correlation mesh size and roughness can only be investigated with the help of another cloth group. For this step the investigation has been extended to polyamide-based cloths (group 2). These are, according to the manufacturer's specifications, specially calendered cloths with mesh sizes of 66 and 38 μm and another normally calendered cloth with 80 μm . These three cloths have similar roughnesses between 49 and 66 μm . The determination of the weave according to DIN ISO 9354 has also shown here that there are two twill weaves (80 and 66 μm), as well as a satin cloth (38 μm), with partly elaborate weave patterns (66 μm cloth).

In addition to the monofilament cloths in groups 1 and 2, a further investigation was carried out using multifilament cloths with 7 and 33 μm , as well as a mixed cloth of mono- and multifilament fibres (35 μm), which should demonstrate the cleanability of this type of cloth in direct comparison to monofilament cloths. The comparison should therefore be made with the mixed cloth of 35 μm . Due to the weave, multifilament cloths have a significantly smaller mesh width if this is based on a bubble-point test. However, the cloths examined are directly intended for use in filter presses and are therefore included in this investigation. The background to this is also that the surface roughness is in a similar range to that of the monofilament cloths from Group 1 examined. Previous studies are based on the multifilament cloth (No. 8) and are now extended in this paper. Another special feature of cloth No. 2 and No. 11 is that they are made of yellow (11) and black (2) dyed cloth fibres, while all other cloths are made of white fibres. Here an adjustment of the image evaluation is necessary, which will be shown exemplarily in the course of the investigation.

3.2. Nozzles

Three different nozzle types were tested in the first trials in order to achieve software optimizations and better degrees of cleaning. The same jet angle with flow rates as similar as possible was used to characterize the round and flat jet nozzles (see Table 3).

3.3. Contamination matrix and sample application

Within the scope of this study, the cleaning result is evaluated by means of a contamination matrix from mash, the crushed and processed malt sample from the beer filtration. This mash produced according to the so-called congress mash process, has a very

Table 2
Summary of the examined cloths for the demand-oriented and automated nozzle cleaning.

No.	Group/ Weave type / mesh size in μm / material		Weave according to DIN ISO 9354		Weight per unit area	Surface roughness (ISO 25178)	Thread thickness warp/ weft	Cloth thickness (ISO 5084)	Image (The scale equals to 1000 μm)	
										$\text{g}\cdot\text{dm}^{-2}$
1	1	Twill Mono	215*	PP	20-02 02-01-01	2.5	215	363/507	480	
2		Twill	164*	PP	20-02 02-01-01	3.3	104	319/472	560	
3		Twill	120*	PP	20-02 02-01-01	2.7	99	404/594	480	
4		Satin	43*	PP	30-08 02-02-04	3.65	81	195/216	540	
5		Twill	20*	PP	20-04 02-02-02	3.65	28	208/213	500	
6	2	Twill	80*	PA 6.6.	20-03 01 02 02-02- 02	3.6	66	214/271	520	
7		Twill	66*	PA 6.6.	20 21-03 01 02 02 02 02 01 03-02 02-04 04 **	3.6	49	197/164	520	
8		Satin	38*	PA 6.6.	30-08 02-02-04	4	52	184/187	470	
9	3	Twill Multi	7	PP	20-02 02-01-02 01 02 03	5.05	96	1248/768	990	
10		Plain	33	PP	10-01 01-01-00	3.3	75	916/911	780	
11		Satin Mono/ Multi	35*	PP	30-04 01-01-02	3.1	47	208/1080	500	

* Manufacturer information.

** In the style of DIN ISO 9354.

Table 3
Summary of the three nozzle types.

No.	Nozzle type	Spray angle °	Flow rate l·min ⁻¹
1	Flat jet nozzle	45	1.0 at 5 bar
2	Full cone nozzle	45	1.0 at 2 bar
3	Point jet nozzle	–	0.63 at 2 bar

broad particle size distribution and can therefore be characterised as difficult to clean and makes contamination reproducible (Jacob, 2016). The proportions of the different particle sizes based on the total mass between <1250 μm and >125 μm is shown in Fig. 2 a).

For a reproducible behaviour of the filter cake during cleaning, it is applied to the filter surface with a defined pressure. For this purpose, four samples are measured, moistened and applied to the filter cloth at defined points. Re-moistening is necessary because saturation has a decisive influence on the adhesive forces acting. The samples are then pressed onto the cloth at 185 $\text{N}\cdot\text{cm}^{-2}$. The pressure guarantees that the particle system penetrates the surface structure of the cloth and thus adheres to it. The applied spent grains on the filter surface are shown in Fig. 2 b).

4. Results and discussion

For a more detailed description of cloth selection and nozzle type on the cleaning behaviour, the cloths and nozzles described in the chapter Material are now examined in the automated cleaning system on a laboratory scale. The results should facilitate the selection of suitable cloths and nozzles. For this reason, in addition to the course of the coated surface via the necessary specific cleaning agent expenditure, the cleaning behaviour will be compared across materials with a kinetic value for cleaning and the possible final contamination after the cleaning procedure.

4.1. Variation of the filter cloth

The variation of the filter cloths is carried out with the cloths summarized in Table 2. The cleaning of the cloths number 2 and 11 is to be adjusted in the image evaluation due to the dyeing of warp and weft threads. This problem is considered separately due to its practical relevance. The working hypothesis is based on experience and assumptions from previous investigations in the field of regeneration and cleanability (Morsch et al., 2020a, 2020b; Ripperger, 2004). These hypotheses can be formulated as follows:

- Hypothesis 1: Rougher filter cloths can be regenerated less sufficient. The roughness may depend on the mesh size (Group 1). For this reason, lower cleaning efficiency can be expected with increasing mesh size.
- Hypothesis 2: Multifilament cloths are harder to clean than monofilament cloths because of the warp and weft threads consisting of many fibrils.
- Hypothesis 3: Treatment of the cloth (calendering etc.) has an immediate and positive effect on cleanability, as the roughness of the filter cloth decreases.

In addition to the hypotheses, an optimization of the image evaluation for colored filter cloths (No. 2 and 11) and a mathematical description of the cleaning process by means of a model are carried out. This is described in the sections Optimization of the image evaluation and Cleaning kinetics.

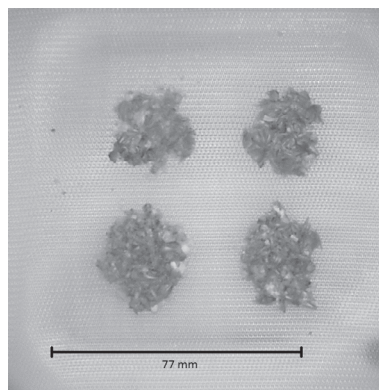
4.1.1. Hypothesis 1: Influence of mesh size

To describe the cleanability, the filter cloths are plotted over the standardised degree of contamination and the specific quantity of cleaning agent used to achieve this surface cleanliness (see Fig. 3).

By definition, all cleaning starts at a normalized value of one. 215 μm cloth No.1 (monofilament cloth with the twill weave) can be reduced to 0.35 with a detergent application of 1.5 $\text{ml}\cdot\text{cm}^{-2}$. The curve then flattens out and after 10 cleaning steps a final contamination level of ~ 0.15 at 4.25 $\text{ml}\cdot\text{cm}^{-2}$ is achieved. A better cleaning within group 1 filter cloth is achieved with cloth No.3, with a mesh size of 120 μm (monofilament, twill). Here, a surface cleanliness of ~ 0.2 can be achieved at 1.5 $\text{ml}\cdot\text{cm}^{-2}$ and after 10 cleanings the surface cleanliness is 0.1 at a cleaning agent consumption of 4 $\text{ml}\cdot\text{cm}^{-2}$. Here, an improvement in cleanability within the same cloth group with decreasing mesh size and roughness can be observed. This trend can also be observed with cloth No.4 and No.5. These cloths are to be classified within the same group, even if the weave shows clear differences. Cloth No.4 has a surface cleanliness of 0.15 at a detergent consumption of 1.5 $\text{ml}\cdot\text{cm}^{-2}$ and decreases to 0.1 after 10 cleanings. Here, a significant decrease in the removal rate is observed, since for a further reduction of 0.05 in surface coverage, the cleaning effort is almost tripled. For cloth No.5 the surface cleanliness is 0.05 at 1.5 $\text{ml}\cdot\text{cm}^{-2}$ and decreases insignificantly with further cleaning steps. The hypothesis 1 can therefore be confirmed using filter cloth of group 1. However, this is different when filter cloth of group 2 is included. In this case, the 80 μm cloth No.6 has a better cleanability, with regard to removal and final contamination, compared to the cloth No.7 with 66 μm mesh size. While filter cloth No.6 shows a similar

Mesh size μm	Percentage %
< 125	3.11
125 – 250	2.45
250 – 500	4.25
500 – 1000	8.44
1000 – 1250	4.11
> 1250	77.64

a)



b)

Fig. 2. Particle size distribution of the mash (a) and the sample preparation on the filter cloth (b).

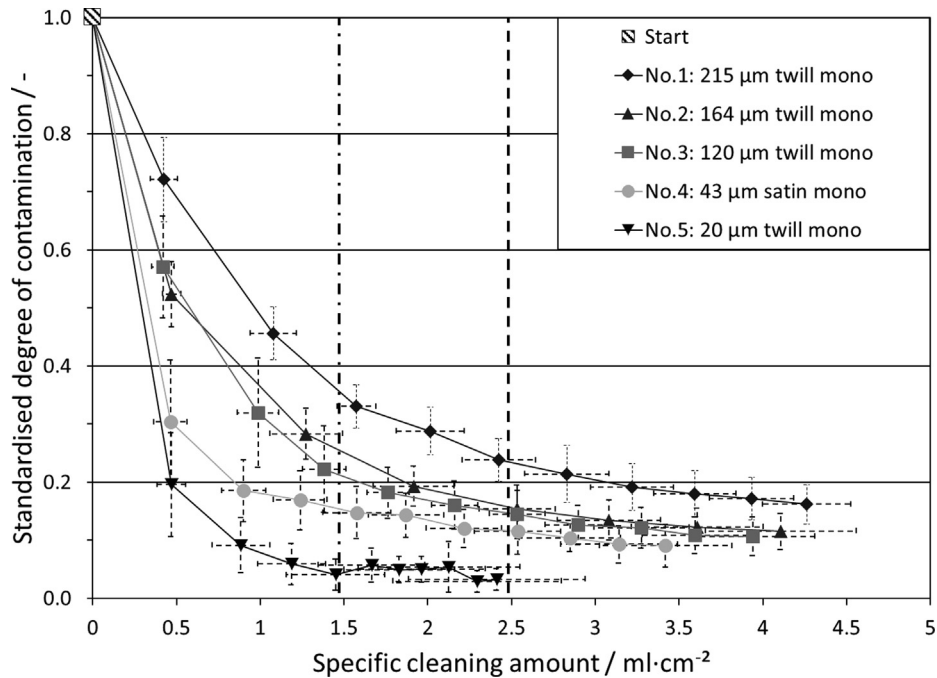


Fig. 3. Results of the filter cloth variation for filter cloths No. 1 to 5 (Group 1). The full cone nozzle (Nozzle No.2) was used for the measurements.

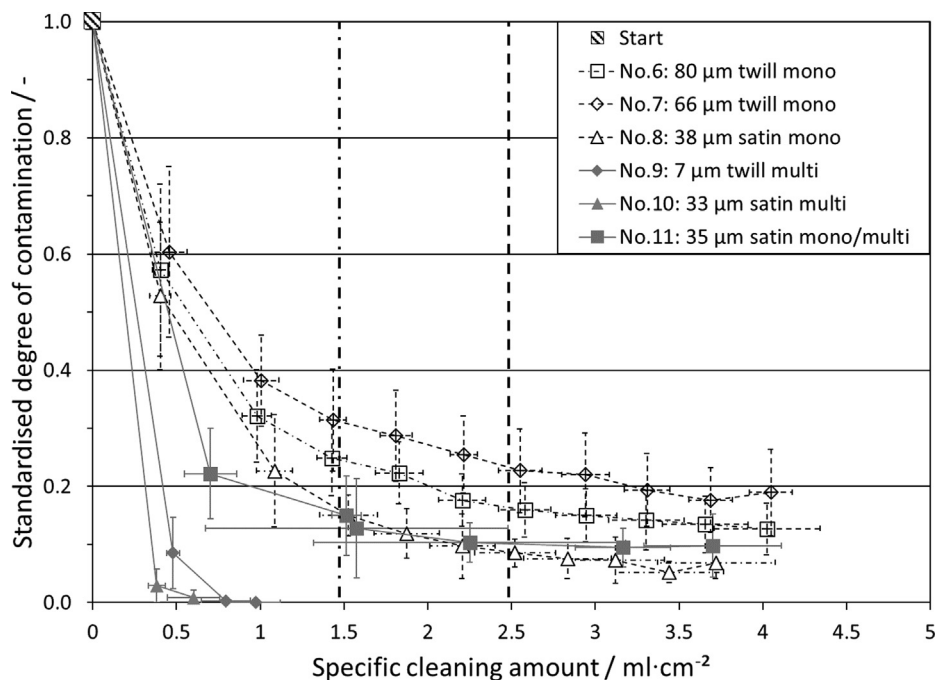


Fig. 4. Results of the filter cloth variation for filter cloths No. 6 to 11 (Group 2 and Group 3). The full cone nozzle (Nozzle No.2) was used for the measurements.

reduction as No.3, despite higher final contamination, No.7 can be compared to No.1. Mesh size of No.8 is similar to No.4 but has a better final contamination level of ~ 0.075 .

In case of cloth group 2, no tendency between roughness and mesh size can be detected (Fig. 4). The reason for this may be the clearer difference in weave within group 2 compared to group 1. The cloths also differ in the type of after-treatment (calendering). This leads to the conclusion that hypothesis 1 can be correct within a cloth group, but that the weave has too big influence on mesh size and roughness. A general tendency is therefore difficult to

establish and laboratory tests on cleanability are still required, especially for special weaves such as those in cloth group 2.

4.1.2. Hypothesis 2: Multifilament cloths are more difficult to clean

Based on cloth No. 9 till 11 (See Fig. 4), multifilament cloths are also included in this investigation. While cloth No. 9 has a mesh size of 7 μm , cloth No. 10 and 11 are coarser at 33 μm and 35 μm . Nevertheless, hypothesis 1 cannot be confirmed for this group of cloths either, because the 33 μm cloth has a slightly better cleanability. Regarding hypothesis 2, it can also be said that the

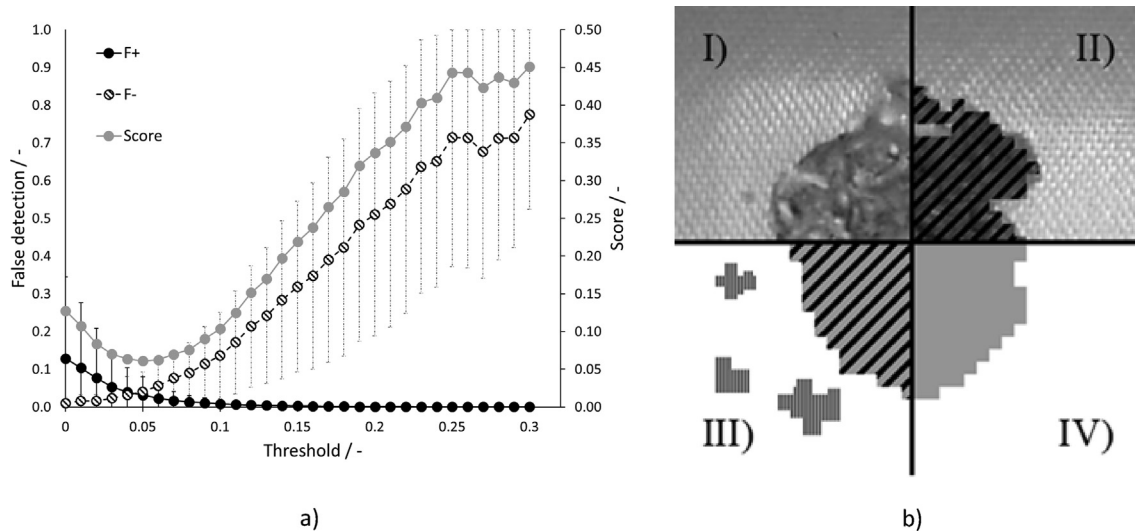


Fig. 5. a) Error detection divided into false-positive (black), false-negative (hatched) and score (grey) plotted over the threshold value exemplary for the tests with the standard reference image without yellow filter for $n = 13$ tests. b) Contaminated area (I) with ideal cover (diagonally hatched in II and III), as well as false-positive findings (vertical lines in III) and false-negative findings (IV).

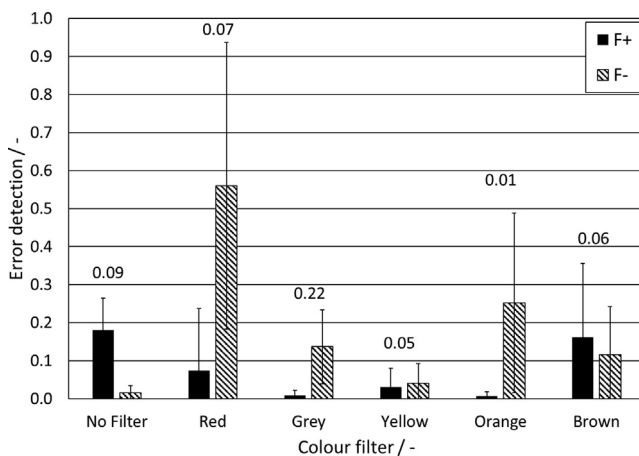


Fig. 6. Display of different colour filters for the image evaluation of filter cloth No. 11.

multifilament cloths are much easier to clean, with regard to surface cleanliness. Intra-filament cloth impurities are not considered here. It can be expected that the final contamination degree will tend to be stable with further cleaning of the surface. This value can be 0, for filter cloth that can be completely freed from contamination (No. 9 and 10). As expected, however, this value will be > 0 , because impurities penetrate into the meshes of the cloths, which were not cleaned by convective cleaning jets on the surface but by convective cleaning through the mesh and/or diffusive displacement. That the cleaning process is not completed becomes clear with cloth No. 1–8 by means of the standard deviation in the lower limit value. This is always > 0 and is therefore to be interpreted as an actual fluctuation of the contamination and not as a measurement error.

The results correspond to the backwashing filtration and confirms that multifilament cloths are not adhesion dominated. The adhesion between the cloth and the particle system must be low, as interpreted from the fast surface cleanability. Hypothesis 2, which relates to surface cleanability, can therefore not be confirmed. Multifilament cloths can be cleaned very well from filter

cake residue on the surface. In the following, we will discuss the difficulty of evaluating cloth No. 11 and make suggestions for improved image evaluation of such cloths. Afterwards the cloths are classified according to the kinetic term.

4.1.3. Optimization of the image evaluation

The evaluation of the images based on Eq. (3) and the different colour filter and light source in Table 1 and starts with a manual marking of all contaminations. These serve as a reference so that the evaluations can then be automatically compared with the actual contamination. In the process, it is checked whether a pixel of the computer recognition matches the manual one. If this is not the case, it is checked whether the result is false-negative or false-positive. The total number of false errors is systematically output in a file at the end. For each threshold value, each false-positive and false-negative value is output for each experiment. From this, the score defined above can be calculated. The required values are defined by determining the mean value of the false results and the standard deviation of these over the different experiments. By including the deviation in the score, stable values for the evaluation should be found. This means that these values should be able to cope with any distribution of the contamination matrix in experiments and should give good detection results.

For clarification, the course of error detection is shown schematically in Fig. 5 a) + b). In the ideal case, the contaminated area (I) is completely detected (II). However, due to the image evaluation there is no sharp boundary between dirty areas and clean areas. This leads to an increase of the dirty areas as a result of the image evaluation. Even areas that are already clean can be detected as dirty (F^+) and lead to a cleaning of these areas. This increases the amount of cleaning agent used but does not lead to a reduction in the cleaning result (III). On the other hand, there is the F^- finding, i.e. a non-detection of the soiled areas (IV). This is directly associated with a reduction of the cleaning result and should therefore be avoided.

With a balanced weighting of both errors, i.e. with an $x_{F^+} = 0.5$ and w_+ and $w_- = 0.5$, the lowest score at threshold = 0.09 for no colour filter is obtained. Here, the false-positive result is at $18\% \pm 8.5\%$ and the false-negative result at $1.6\% \pm 1.9\%$.

The score can now be used to determine the best threshold settings for each colour filter. The error detections at these settings

are then compared with each other. Figure 6 shows the lowest scores of the different colour filters. Above the errors is the corresponding threshold-value. It can be clearly seen that only the yellow and grey colour filters have an advantage compared to the tests without colour filters. Thus, the false-positive error can be reduced to $0.9\% \pm 1.3\%$ for grey, whereas the false-negative error increases to $13.7\% \pm 9.8\%$. For the yellow colour filter, the false-positive result is at $4.1\% \pm 4.9\%$ and the false-negative result is at $4.1\% \pm 5.2\%$. Thus, the yellow colour filter has the lowest score of all tested variations with a threshold-value of 0.05. Referring to Table 1, the yellow colour filter with an RGB-value of 230.9, 153.5 and 0 is very close to that of Filter Cloth No.11 with 232.2, 178.5 and 8.7. It seems that a similar RGB-value of the colour filter to the cloth filter leads to a better dirt detection or at least favours it. This is disproved by the grey colour filter, which has the second-best dirt detection, instead of the orange colour filter. Here, further tests are required with filter cloths that are difficult to evaluate. Finally, a similar colour value between the colour filter and the filter cloth provides the best image recognition in this investigation.

The success of the colour filters depends mainly on how far the colour spectrum of the reflections is shifted. The reflections are decisive for the high false-positive results of the yellow filter cloth, as they have similar hue and saturation values as the contaminations. Due to the yellow and grey colour filter, the H and S values of the reflections are like those of the filter cloth and are then no longer detected incorrectly.

The same procedure does not lead to a successful determination of a detection optimum for black filter cloth No. 2. The colour filters do in part lead to better recognition, but with still very large fluctuations and errors. Therefore, the use of a colour filter is not sufficient in this case. In order to achieve sufficient dirt detection

despite this, a further approach was taken with the black cloth. Instead of the normal lighting with an LED ring, a UV lamp is now used as the illuminant. This is to avoid the reflections on the cloth, which are the cause of the fault detection, and thus enable the dirt to be detected. It should be noted, that in the case of the black cloth the reflections lead to false-negative errors, instead of false-positive errors as with the yellow cloth. This is the case because on the reference image the reflections have H and S values like the contaminations later on the images to be evaluated.

The procedure with the UV illumination is the same as for the colour filters. A sample is always prepared, and an image of the contamination status is created once under normal lighting conditions, i.e. with LED light and ambient lighting, and once with UV lighting. The tests are then evaluated with a threshold variation. The result is that the UV light can be used to determine the contamination with high accuracy and low susceptibility to errors. The optimal threshold value in this case is 0. It should also be noted that the images are taken with the UV light without any further illumination source in order to avoid reflections on the cloth.

4.1.4. Hypothesis 3: Calendering of the cloths leads to better cleanliness

By adjusting the image evaluation for cloth No. 2 and cloth No. 11, it is now also possible to compare them with the other filter cloths. For this purpose, the course of the normalized contamination of Fig. 3 and Fig. 4 at $1.5 \text{ ml}\cdot\text{cm}^{-2}$ and $2.5 \text{ ml}\cdot\text{cm}^{-2}$ for filter cloths 1–7, as well as No. 11 is shown in Fig. 7. The representation is not chronological as a result of the following interpretation. As already noted in Fig. 3, the normalized degree of contamination of cloth No. 1 to No. 5 is steadily decreasing. The cloths of group

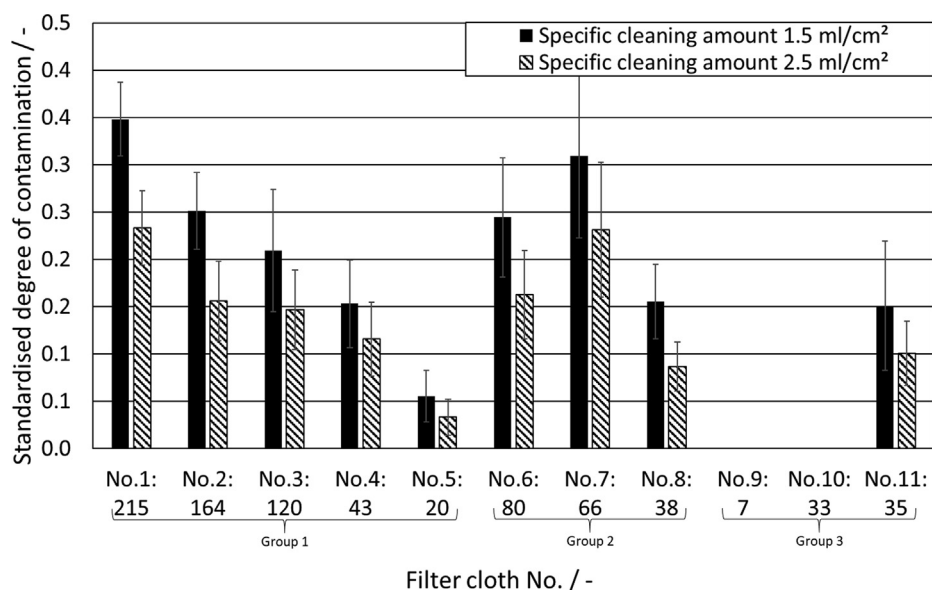


Fig. 7. Results of the filter cloth variation for $1.5 \text{ ml}\cdot\text{cm}^{-2}$ and $2.5 \text{ ml}\cdot\text{cm}^{-2}$ from Fig. 3 and Fig. 4.

Table 4

Summary of kinetics and final contamination level for filter cloth variation.

	Filter cloth No. Group 1			Filter cloth No. Group 2			Filter cloth No. Group 3				
	1	2	3	4	5	6	7	8	9	10	11
Kinetic / $\text{cm}^2 \text{ ml}^{-1}$	0.95	1.44	1.51	3.17	3.85	1.56	1.38	1.66	5.25	9.79	2.85
Final contamination level / -	0.15	0.12	0.12	0.12	0.05	0.14	0.20	0.07	0.00	0.01	0.11

1 thus become cleaner with decreasing mesh size and roughness for the same specific amount of detergent. Cloth No. 2, which can now be tested, also follows the trend. The cleaning process is better than the coarser cloth No. 1, but worse than the finer mesh cloth No. 3. In the case of Group 2 cloths, this tendency is only visible between the two specially calendered cloths (No. 7 and No. 8). Cloth No. 6 of cloth group 2 has a lower surface coverage than cloth No. 7. No tendency can be seen here. Hypothesis 3, which refers to the intensity of the after-treatment, can therefore not be confirmed. The specially calendered cloths No. 7 and No. 8 have no better cleanability than the cloths of group 1 with the same or similar mesh size.

An interesting finding can be seen when comparing cloth No. 4, No. 8 and No. 11. All cloths have a similar mesh size (35–43 μm) but the roughness of No. 8 and No. 11 differs from No. 4. When comparing the weave, it is noticeable that the weaves are similar, even though they differ in threading and therefore in the number of loops. In total, however, all three shows similar behaviour with regard to final contamination and the specific amount of cleaning agent required. From the comparison of the cloths it becomes clear that the weave and the resulting mesh size is a better indication for similar cleaning behaviour across cloths instead of roughness values. Furthermore, blended cloth No. 11, consisting of monofilament and multifilament, tends to behave more like a monofilament than a multifilament.

4.1.5. Cleaning kinetics

For further quantification of the discharge, an evaluation of the discharge kinetics is now carried out by defining a kinetic value

dependent on the filter cloth-nozzle-combination, in the unit $\text{cm}^2 \cdot \text{ml}^{-1}$, the final degree of contamination and a Cleaning quality to increase the coefficient of determination of the fit. The kinetics is to be understood as a decrease of the contaminated area per volume cleaning agent and it is important to note that for large values a rapid decrease can be expected. The final contamination degree is the remaining particles on the surface and inside the filter cloth meshes, after 10 cleaning steps. And the cleaning quality describes the overall reduction of surface contamination. The sum of final contamination degree and cleaning quality is ~ 1 . The values for filter cloths 1–11 are summarized in Table 4.

As already shown in Figs. 3 and 4, for filter cloths 1–5 the kinetic increases as a result of the faster decrease, while the final contamination level decreases. It starts with filter cloth No.1 and $0.95 \text{ cm}^2 \cdot \text{ml}^{-1}$ and rises until $3.85 \text{ cm}^2 \cdot \text{ml}^{-1}$ for No.5. A final surface contamination < 0.1 can only be reached with filter cloth No.5. Here, a direct dependence between kinetics and final contamination can be observed. If the surface contamination decreases faster, the filter cloth can also be cleaned more cleanly.

For group 2, no such tendency can be seen, but filter cloth No. 8 shows a low level of final contamination despite moderate kinetics. Comparing filter cloth No. 4, 8 and 11, the kinetic value for No. 3 and No. 11 is similar (3.17 and $2.85 \text{ cm}^2 \cdot \text{ml}^{-1}$), while this value differs for filter cloth No. 8 ($1.66 \text{ cm}^2 \cdot \text{ml}^{-1}$). Nevertheless, the final surface cleanliness after $n = 10$ cleaning steps is similar in the range of 0.1. The cloth No. 8 shows a smaller Final contamination degree (0.07) although it has a smaller cleaning kinetic. Here, too, the multivariability of regeneration becomes clear.

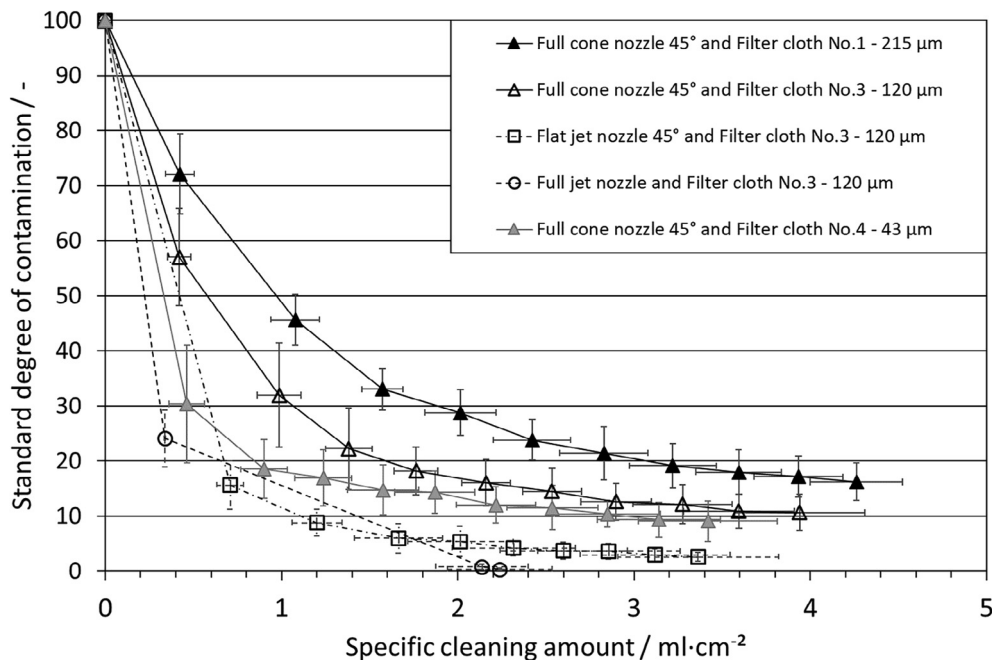


Fig. 8. Variation of nozzle types for cloths No.1, 3, 4 at a nozzle pressure of 5 bar and a nozzle distance to the surface of 35 mm.

Table 5

Summary of kinetics and final contamination level for nozzle variation.

No.	Nozzle type	Filter cloth				Final contamination level / -		
		No.1	No.3	No.4	No.1	No.3	No.4	
		Kinetic / $\text{cm}^2 \cdot \text{ml}^{-1}$						
1	Flat jet nozzle	1.86	2.86	4.83	0.06	0.04	0.02	
2	Full cone nozzle	0.94	1.46	3.30	0.15	0.12	0.13	
3	Full jet nozzle	3.10	4.25	7.98	0.01	0.01	0.01	

In the case of multifilament filter cloths, the highest kinetic values of 5.2 for No. 9 and 9.8 for No. 10 are found. In summary, it can be said that for cloths with kinetics ≥ 3.8 a good cleaning process can be determined with the present combination of cloth and nozzle.

4.2. Variation of the nozzle type

Analogous to the variation of the meshes with the full-cone nozzle, a variation of the nozzle type (flat-jet nozzle, full-cone nozzle and full jet nozzle) is now carried out with the filter meshes No. 1, 3, 4. The course is shown exemplarily in the standardised contamination - specific cleaning quantity graph and again discussed using the kinetic value from equation (3). Fig. 8 shows the curve for the 120 μm mesh No. 3 for the variable nozzle types and the full cone nozzle with variable mesh type (No. 1, 3, 4). However, the transferability of the image evaluation between the nozzle types is not directly possible. The reason for this is the generation of coordinates for approaching the soiled areas. This coordinate generation is based on the geometrically existing effective area of the nozzle as a function of the jet angle and the distance. In the case of the full cone nozzle, this is based on an effective cleaning area at a distance of 30–35 mm. For the full jet nozzle this effective radius is reduced to 10 mm. This does not include statements about the intensity of the cleaning jet on the cleaned surface. The coordination generation of the flat jet nozzle is based on an elongated geometry to cover the contamination.

If the nozzle type is varied, the full cone nozzle has a much worse cleaning performance compared to the flat jet nozzle. The best way to clean here is to use the full jet nozzle. As a summary, it can be said that the tendency could be observed for all 3 cloths within group 1. The full cone nozzle cleans worst, whereas flat jet and full jet give better results. Spot blasting always cleans the surface to the lowest degree of final contamination.

Analogous to the filter cloths, this behaviour can also be characterized by kinetic and final contamination state. This is summarized in Table 5. For flat jet nozzle, the kinetics for the 215 μm No. 1 increase from 1.86 $\text{cm}^2 \cdot \text{ml}^{-1}$, over 2.86 $\text{cm}^2 \cdot \text{ml}^{-1}$ for the 120 μm No. 3 to 4.83 $\text{cm}^2 \cdot \text{ml}^{-1}$ for No. 4 with 43 μm . A good final contamination level of < 0.1 can be achieved for all 3 cloths. In the case of the full cone nozzle, the behaviour is as described in the subchapter 4.1 Variation of the filter cloth and high final contamination degree of up to 0.151 remain even after 10 cleaning steps. The full jet nozzle in turn has kinetics of > 3 for cloth No. 1 (3.10 $\text{cm}^2 \cdot \text{ml}^{-1}$), No. 3 (4.25 $\text{cm}^2 \cdot \text{ml}^{-1}$) and No. 4 (7.98 $\text{cm}^2 \cdot \text{ml}^{-1}$). Analogous to the variation of the filter cloths, very small final impurities towards 0 can also be observed here with the high kinetics. In summary, it can be said that there is a large nozzle influence. The full jet nozzle has proven to be a good cleaning nozzle for targeted cleaning. This is due to the high intensity of the cleaning. With the variation of the nozzles it becomes clear that already a kinetic value > 3 leads to good cleaning results of the surface. Thus, it is possible to achieve fast and good surface cleanliness by choosing the appropriate nozzle, although the cloth has rather poor cleaning properties (No.1) compared to for example multifilament cloth.

5. Conclusion

In the course of the investigation a systematic variation of factors, which are assumed to have an influence on the surface cleaning of filter cloths, was carried out. The parameters filter cloth type and nozzle type were varied for this purpose.

Within a cloth group of calendared cloths in the range of 20–215 μm a dependence of the mesh size and the surface roughness on the cleaning behaviour could be observed. This behaviour could

only be confirmed to a certain extent for other cloth groups. It is important in this comparison that the weave and after-treatment (calendering) are similar within the cloth group. A generally valid correlation between the cleaning process and mesh width/roughness is therefore not possible. Multifilament cloths have proven to be extremely suitable for surface cleaning. The assumption that the fibrils make dropping difficult has not been confirmed. Effects on contamination within the filter are not the subject of this study. The cleaning results of the surface can now easily be transferred to the absolute cleaning of a X m^2 filter surface. For this purpose, the area-specific application by the standard degree of contamination is simply to be equated with the actual occupied filter area of the filter to be cleaned. This step enables the estimation of the specific cleaning quantity to determine the necessary cleaning application.

Positive effects of calendaring on the cleanability of the cloths could not be determined. The cloths with a stronger calendaring process showed worse cleaning behaviour with smaller and equal mesh sizes than normal calendared cloths.

Furthermore, it could be shown that simple changes in the image acquisition in difficult cases of contamination detection can significantly increase this. For example, colour filters or UV illumination can be used if the required dirt detection fails, due to too low contrast or in the case of error detection due to reflections. By means of small test series an optimum for dirt detection can be found.

In the case of the nozzle variation, the behaviour of group 1 filter cloths could be confirmed. Furthermore, it was shown that, when cleaning is required, the spot jet nozzle is preferable to the flat jet nozzle and full cone nozzle.

The kinetic value in combination with the degree of final contamination has proved to be a good way of quantifying the cloth-nozzle combination by means of two variables. For kinetics > 3 good cleanliness and final contamination levels can be achieved.

Declaration of Competing Interest

The authors declare that they have no known competing financial interests or personal relationships that could have appeared to influence the work reported in this paper.

Acknowledgment

The IGF Project 19716N of the IVLV e.V is supported via AiF within the programme for promoting the Industrial Collective Research (IGF) of the German Ministry of Economic Affairs and Energy (BMWi), based on a resolution of the German Parliament. The authors would also like to thank all colleagues and students for the support in writing this paper. Special thanks go to the students Adrian Arnold and David Dumancic for their support in this project through their skills in computer science.

References

- A. Decker, FILTECH 2019 – Proceedings (FILTECH, Meerbusch, 2019, L14).
- D'Souza, N.M., Mawson, A.J., 2005. Crit. Rev. Food Sci. Nutr. 45, 2.
- Gibson, H., Taylor, J.H., Hall, K.E., Holah, J.T., 1999. J. Appl. Microbiol. 87, 1.
- Goode, K.R., Asteriadou, K., Robbins, P.T., Fryer, P.J., 2013. Compr. Rev. Food Sci. Food Saf. 12, 2.
- Jacob, Fritz (Hg.) (2016): MEBAK brautechnische Analysenmethoden - Rohstoffe. Rohfrucht, Gerste, Malz, Hopfen und Hopfenprodukte : Methodensammlung der Mitteleuropäischen Brautechnischen Analysenkommission. Mitteleuropäische Brautechnische Analysenkommission. Freising-Weihenstephan: Selbstverlag der MEBAK.
- Kazemimoghadam, M., Mohammadi, T., 2007. Desalination 204, 1–3.
- Leipert, C., Nirschl, H., 2012. F & S International Edition 12, 13–18.
- Moeller, R.-S., Nirschl, H., 2017. J. Food Eng. 194, 99–108.
- Moeller, R.-S., Nirschl, H., 2018. Sep. Purif. Technol. 207, 336–343.
- Moeller, R.-S., Duchardt, A., Nirschl, H., 2018. J. Food Eng. 214, 218–225.
- Morsch, P., Ginisty, P., Anlauf, H., Nirschl, H., 2020. Chem. Eng. Sci. 213 (23). <https://doi.org/10.1016/j.ces.2019.115372>.

- Morsch, P., Ginisty, P., Anlauf, H., Nirschl, H., 2020a. *Sep. Purif. Technol.* 249. <https://doi.org/10.1016/j.seppur.2020.117073>.
- Purchas, D.B., Sutherland, K., 2002. *Handbook of filter media*. Elsevier Advanced Technology, Oxford.
- Ripperger, S., 2004. *Filtrieren Separieren* 4, 162–166.
- Shi, X., Tal, G., Hankins, N.P., Gitis, V., 2014. *J. Water Process Eng.* 1.
- Stahl, S., Siggelkow, S., Nirschl, H., 2007. *Engineering Life Science* 7, 136–142.
- Stahl, S., Leipert, C., Nirschl, H., 2013. *Sep. Purif. Technol.* 110, 196–201.
- Weidemann, C., Stahl, S., Nirschl, H., 2013. *Food Bioprod. Process.* 91, 515–524.
- Weidemann, C., Vogt, S., Nirschl, H., 2014. *J. Food Eng.* 132, 29–38.

L. Extended investigation of [4]

Filter Cloth for Backwashing Treatment into Gas-Phase after Liquid Filtration

Introduction

The separation of a solid-liquid mixture is one of the basic tasks of mechanical process engineering. A frequently used process is the cake-forming filtration. This is used, for example, in the pharmaceutical, chemical and food industries as well as in wastewater treatment. The separation of a suspension is realized by the liquid phase flowing orthogonally through a porous filter medium due to a driving pressure difference, while the dispersed solids are retained on the surface of the medium. The separated particles form a continuously growing filter cake on the filter surface, the so-called filter cake.

The formation of the continuously growing filter cake leads to a steady increase in the flow resistance. In cake-forming filtration under constant pressure, this is reflected in a regressive decrease of the filtrate flow over time. It is therefore necessary to regularly remove the deposited particles from the filter. A frequently used method for cleaning the filter medium is backwashing. In this case, a fluid flows through the filter medium against the direction of filtration, forcing the previously filtered debris to be discharged. This process can take place in both liquid and gaseous phase. While the detachment of the filter cake during gas discharge is characterized by an impulse, the discharge in liquid phase takes place by the flow and detachment of the filter cake in the same way. [1,2,4]

While the theory of cake filtration has been comprehensively analyzed and documented, filter backwashing is an insufficiently investigated application. Knowledge of the theoretical principles of backwashing and the resulting correct choice of cleaning parameters are decisive for the economic operation of a filter system. Particularly in view of the large number of filter fabrics used, it is not known which fabrics are particularly suitable for backwashing in gas and/or liquid phase.

While backwashing filtration with discharge in the liquid phase and the choice of mesh for this purpose is already the subject of investigations [1,2], backwashing filtration in the gas phase still needs to be extended by a further mesh variation [4]. For this reason, filter fabrics (type of fabric, mesh size, etc.) are used for cake filtration in liquid and regeneration in gas phase. The aim is to provide manufacturers and users of backwashing filter a tool for fabric selection.

Theory

Due to the permanent deposition of particles on and in the filter medium, cake filtration becomes increasingly impractical and uneconomical over time. After a certain time, the operating limit of the filtration is reached. This is clearly shown by the reduction of the filtrate

flow or by reaching the maximum allowable/possible pressure difference. After a certain filtration time, the filter medium must therefore be replaced or cleaned of the deposited particles.

In cake filtration, the main cleaning task is to remove the filter cake that has formed. In addition to techniques for nozzle-supported cleaning of filter fabrics, there is also the possibility of cake discharge by backwashing [6]. A fluid flows through the filter against the filtration direction and the cake is thrown off. A prerequisite for the detachment of the filter cake is, that the forces due to the backwashing exceed the adhesive forces between filter cake and filter cloth [100,129,130,160].

The process of backwashing can be divided by the environment of discharge (discharge in gas or liquid phase) and the type of discharge [101].

In the gas phase, the discharge takes place mainly by means of a pulse and is known as "patchy cleaning" if the filter cake is completely detached from the gas filtration [101]. However, small fragments can also come loose and lead to partial regeneration. Here a rest of the Filter cake remains on the surface, which leads to a decrease of the filtration performance in the following filtration cycle. The "patchy cleaning" from the gas discharge is known as a complete discharge in the liquid discharge and produces the best cake release. In addition to complete detachment, the liquid discharge process also includes incomplete, good and bad, and resuspended discharge. This depends mainly on the particle collective and the cake thickness. With very thin cakes, resuspension of the cake takes place and after backwashing, considerable particle residues are still present on the fabric. Here there is no cake throwing in the actual sense, but a cleaning of the meshes according to the model [172,173].

The reason for an incomplete discharge at low cake heights is that the backwash not only overcomes the adhesion between cake and fabric but also the cohesion within the filter cake. The former is necessary for cake discharge. However, overcoming the cohesion leads to the destruction of the cake structure, resulting in individual fragments. With thicker filter cakes there is a higher cohesion, which favors complete separation. Furthermore, these considerations lead to the conclusion that the backwash pressure must exceed a minimum value to overcome the adhesive forces between filter and cake, but must not exceed a maximum value, otherwise the cake will break. [100,129,130,160]

The focus of this work is the gas phase discharge with different tissue types. The tissues are characterized according to their properties and compared with the regenerability by cake release. For this reason, the work is based on [4] and extends it by the aspect of tissue selection. By means of this investigation it is now possible to assess the backwashing properties of

different types of fabric and to take measures for the use on backwash filters in favor of a good regenerability.

Method

The test is carried out according to the schematic diagram (I to III.b) shown in Figure 12 for discharging in gaseous environments (II and III) . Each test series starts with the introduction of the suspension into the process chamber and filtration to a defined filter cake thickness.

After successful filtration (I), the suspension is led out of the process chamber and the filter cake is dried with compressed air (II.b). After reaching a defined saturation, a pressure pulse follows from the inside of the candle filter (III.b). This accelerates the tissue and the cake, while the former stops and thus detaches the cake from the tissue. The detached cake falls onto a collecting grid, which allows easy removal of the dropped cake. In addition, the remaining cake can be mechanically removed from the fabric and removed. This allows a percentage of mass discharged to be defined as a function of the process parameters for quantification. The underlying equations for calculating the saturation and the discarded mass fraction are summarized in Eq. 21 and Eq. 22. For this purpose, the discarded wet cake mass is $m_{\text{removed, wet}}$ dried at 100 °C ($m_{\text{removed, dry}}$). With the density ρ_{Liquid} , the volume of the filter cake $V_{\text{Filter cake}}$ and its porosity $\epsilon_{\text{Filter cake}}$ the saturation can be determined. The same procedure applies to the proportion of cake fragments thrown off. For this purpose, the mass thrown off is m_{removed} in relation to the total mass of the filter cake, consisting of mass thrown off and remaining cake mass on the filter candle m_{remain} (see Eq. 22). The procedure has proven its worth and follows the implementation according to. [4]

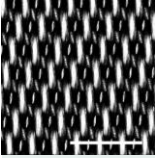
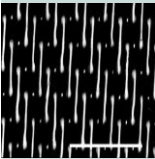
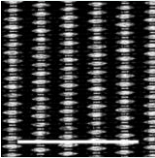
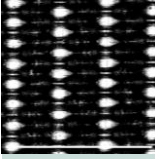
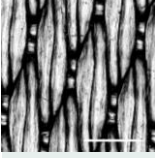
Material

The investigation is based on 5 filter fabrics of different weave (plain, twill, satin) and mesh size ($\leq 20 \mu\text{m}$), summarized in Table 7. These fabrics are characterized regarding their weave (DIN ISO 9354), filter mean resistance (VDI 2762-2), basis weight, surface roughness (ISO 25178), thread thickness, fabric thickness (ISO 5084) and modulus of elasticity in force-elongation measurements based on.

According to this, backwash tests are carried out as shown in Figure 12 with the orthorhombic particle system "Millisil W6" presented in [4], with a specific cake resistance of $5.7 \cdot 10^{13} \text{ m}^{-2}$ at a particle diameter $x_{50.3}$ of $36 \mu\text{m}$ ($x_{10.3} = 3.4 \mu\text{m}$ and $x_{90.3} = 114.5 \mu\text{m}$).

The fabrics are mounted on a laboratory candle filter with a diameter of 30 mm and a filter length of 110 mm and filter cakes of various cake thicknesses are filtered and discharged. In the following chapter, the mass percentage dropped is summarized in XY graphs and the discharge quality is discussed.

Table 7: Tissues used for the test series and selected characterization parameters.

Fabric type / mesh size in μm / material		Weave according to DIN ISO 9354	Filter cloth resistance according to VDI 2762-2 $\text{m}^{-1} *$	Weight per unit area g/dm^2	Surface roughness (ISO 25178) μm	Thread thickness warp/ weft μm	Fabric thickness (ISO 5084) μm	Young's modulus warp/weft (stretching area) N/mm^2	Image (The scale equals to 1 mm)	
Monofile/Monofile Filter Cloth										
Twill	14	PP	20-02 01-01-02	$1.52 \cdot 10^{10} \pm 1.40 \cdot 10^9$	1.25	40	168 / 161	200	457.08 (0% $\leq\epsilon_D<0.15\%$) / 88.39 (0% $\leq\epsilon_D<0.33\%$)	
	20	PET	20-03 01-01-03	$1.56 \cdot 10^{10} \pm 3.33 \cdot 10^9$	2	30	128 / 160	260	130.07 (0% $\leq\epsilon_D<0.35\%$) / 105.9 (0% $\leq\epsilon_D<0.33\%$)	
Plain	12	PET	10-01 01-01-00	$2.03 \cdot 10^{10} \pm 1.89 \cdot 10^9$	0.5	9	100 / 45	80	225.98 (0% $\leq\epsilon_D<0.50\%$) / 236.63 (0% $\leq\epsilon_D<0.39\%$)	
	14	PA6.6		$9.41 \cdot 10^9 \pm 1.37 \cdot 10^9$	1	86	100 / 75	160	196.69 (0% $\leq\epsilon_D<0.17\%$) / 77.3 (0% $\leq\epsilon_D<0.35\%$)	
Satin	18	PP	30-04 02-02-04	$5.07 \cdot 10^{10} \pm 1.26 \cdot 10^{10}$	4.25	7	227 / 443	714	306.36 (0% $\leq\epsilon_D<0.36\%$) / 142.57 (0% $\leq\epsilon_D<0.77\%$)	

*: Based on mean filter cloth resistance measured with Particle system P1, P2 and P3 (see table 4)

Interpretation

Within the framework of the investigation, the variation is carried out, following [4], on the basis of 4 parameter variations:

- I. Backwashing pressure
- II. Filter cake thickness
- III. Filter cloth diameter
- IV. Filter cloth type

This variation is intended to clarify the sensitivity of the discharge quality of different fabrics regarding the backwash pressure (I) and the filter cake thickness (II). In addition, it is necessary to find out which type of fabric requires a stronger relative movement of the fabric by changing the fabric diameter (III) for a good throw-off. For this purpose, the tissue type (IV) should be used for classification. All parameter variations are introduced with the help of a hypothesis, which must be proved.

I. Backwashing pressure: an increase in this variable increases the stress on the filter cake and can according to [100] improve the discharge and this can be expected.

The subject of this variation is to determine the influence of the backwash pressure on the cake mass thrown off at a constant cake height of 1.5 mm. The tests are carried out on the tissues from Table 1 with a tissue diameter of 40 mm on the 30 mm filter candle (5 mm possible movement of the filter fabric). The backwash pressure varies between 1 and 4 bar. The discharge curves of the used meshes are shown in Figure 21.

The 12 μm plain weave, measured according to [4], clearly shows the most favorable discharge behavior. Already at a backwashing pressure of 1.25 bar more than half of the filter cake is discharged. A linear approximation, with a coefficient of determination of 0.98, describes the course and thus indicates a discharge of 21.6 % per bar backwash pressure. A complete discharge of approx. 99 % can thus be achieved by backwashing at 3.25 bar. In addition to other favorable properties, this fabric also has a particularly low weight per unit area.

The 14 μm plain weave also shows a progressive course of the discharged cake fragments. The linear approach achieves a similar gradient of 22 % per bar backwashing pressure. However, here only about half of the 12 μm plain weave is discharged at one bar backwash pressure. With a backwashing pressure of 2 bar, a throw-off of 31 % is achieved and rises to 80 % with 4 bar. Despite the similar rising behavior, the 12 μm plain weave is preferred for backwashing a 1.5 mm thick cake in gas phase due to the more efficient discharge at low backwash pressures. The plain weave with 12 μm mesh width is only half as thick as the 14 μm weave and, due to its only half the weight per unit area and thus lower inertia, discharges significantly better when the backwash pressure is varied. The very smooth surface of the 12 μm mesh also favors the discharge at even low pressures.

The 14 μm twill fabric behaves exceptionally well in backwash pressure variation tests due to its peak at 2 bar. This behavior was not expected, so the test series was repeated. This behavior was also measured during renewed measurements. Since this behavior is contrary to the expected observations, an approximately constant behavior can be assumed. This means that an

increase of the release force via the backwashing pressure has no significant influence on the release behavior. At $1.25 \text{ g}\cdot\text{dm}^{-2}$, the basis weight of this fabric is more than twice as high as that of the $12 \mu\text{m}$ fabric and thus has a rather inert behavior. Furthermore, the very high modulus of elasticity means that the speed of the fabric's own movement is not sufficiently accelerated by the high stiffness.

Even the $18 \mu\text{m}$ satin fabric does not show any expected increase in the discharge masses due to the increase in backwash pressure. With a fabric thickness of $714 \mu\text{m}$, this is a particularly thick fabric with a very high basis weight of $4.25 \text{ g}\cdot\text{dm}^{-2}$ and is therefore difficult to regenerate. The air passage of only $30 \text{ l}\cdot\text{m}^{-2}\cdot\text{s}^{-1}$ also contributes to the poor cleaning of the fabric, as a low air passage is equivalent to a low porosity.

After this measuring point at 4 bar, only very small parts of the $20 \mu\text{m}$ fabric can be removed. Due to the limitation of the backwash pressure no further pressure increase took place. Again, the fabric is difficult to accelerate due to its thickness of $260 \mu\text{m}$ and a relatively high basis weight of $2 \text{ g}\cdot\text{dm}^{-2}$, so that the backwashing pressure has no influence on the removal behavior. In general, the investigations of the hypothesis that a higher backwash pressure leads to a higher acceleration of the fabric and thus to more discharge can only be partially confirmed.

The influence of the backwash pressure is particularly evident for fabrics with low basis weight and low modulus of elasticity. Furthermore, the fabric thickness is also an influencing factor.

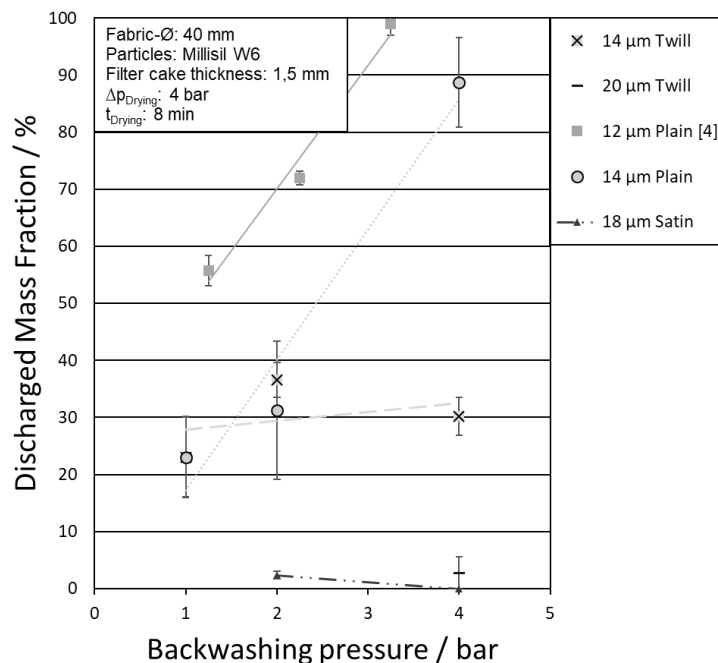


Figure 21: Variation of the backwashing pressure for a cake height of 1.5 mm and 40 mm fabric diameter for backwashing filtration in gas phase.

II. Filter cake thickness: in case of filter presses, heavier filter cakes can be discharged more easily [6]. This behavior can also be expected for candle filters, because the force of inertia increases with the filter cake thickness.

In this chapter the influence of the cake height on the mass discharged in case of gas discharge is determined. For this purpose, the 40 mm diameter fabric used is stretched over the 30 mm diameter candle. After the filtration follows the backwashing with 2 bar backwashing pressure. The variation of the cake height is from 0.5 mm to 4.5 mm and is shown in Figure 22.

The 12 μm plain weave provides the best discharge behavior. At a cake thickness of 1.5 mm and 2 bar backwash pressure, almost 70 % of the filter cake is discharged. In the case of the 14 μm mesh weave, no discharge is observed at a cake height of 0.5 mm. At 1.5 mm, the drop increases to 31 % until the complete drop is reached at a cake height of 2.5 mm. An approximately linear observation of this mesh, with a coefficient of determination of $R^2=0.96$, yields about 48 % per millimeter of cake height starting at 0.5 mm. The comparison with the 14 μm twill fabric with the same mesh size and similar fabric thickness shows that the masses dropped are similar at 0.5 mm and 1.5 mm. From a cake thickness of 2.5 mm the difference is clearly visible. For the twill fabric, a drop of approx. 92 % only occurs at a cake height of 3.5 mm. A complete discharge can only be achieved at 4 mm. This process can be described as linear with 30 % of the mass thrown off per millimeter of cake height. In a comparison of the two 14 μm mesh fabrics, the plain weave is more easily regenerated than the twill weave and is therefore to be preferred for backwashing filtration regarding the thrown-off mass with gas discharge. The long-term behavior will not be investigated in this paper. Compared to the stiffer twill weave, the 14 μm plain weave has twice as much surface roughness (ISO 25178) and a much lower air resistance (14 μm plain weave: $300 \text{ l}\cdot\text{m}^{-2}\cdot\text{s}^{-1}$; 14 μm twill: $100 \text{ l}\cdot\text{m}^{-2}\cdot\text{s}^{-1}$). From this it can be concluded that the stiffness of the fabric has a greater influence on the drop than the surface roughness. Therefore, the fabric with a low modulus of elasticity and higher surface roughness has the better discharge behavior. The basis weight of $1 \text{ g}\cdot\text{dm}^{-2}$ of the plain weave is also lighter than that of the twill weave and is therefore less inert and can therefore be accelerated more easily. Furthermore, as expected, the fabric with higher porosity shows better backwashing behavior.

Particularly noticeable is the almost identical discharge pattern of the 14 μm twill fabric and the 12 μm plain weave with a fabric diameter of 35 mm. A comparison of these two fabrics in terms of fabric properties shows that, in addition to the difference in material and weave, the remaining factors also differ greatly. Here it can be seen that the 12 μm plain weave has much

finer threads than the 14 μm twill weave. Furthermore, the 12 μm fabric has a significantly lower surface roughness and a modulus of elasticity that is only half as high. The basis weight of the 14 μm fabric is also 2.5 times greater than that of the 12 μm fabric. However, the air permeability of the fabrics is similar (12 μm fabric: $84 \text{ l}\cdot\text{m}^{-2}\cdot\text{s}^{-1}$). In addition, the 12 μm fabric with a diameter of 35 mm requires only half as much acceleration distance as the 14 μm fabric with a diameter of 40 mm. In general, the higher strength of these two tissues compared to the 14 μm twill tissue can be observed here. So, the decisive factor for good discharge behavior is low stiffness.

The 20 μm twill weave and the 18 μm satin weave are clearly different from the 12 and 14 μm weave. The first discharges of these fabrics of less than 10 % only occur at a cake height of 1.5 mm and thus differ significantly. Here the 20 μm mesh still has an advantage over the 18 μm mesh. The observation of the confidence intervals at 2.5 and 3.5 mm cake height shows the difference in position of the measuring points, but due to the scattering of the error of the measuring points a similar discharge behavior can be assumed. By interpolation, the complete discharge of the 18 μm diameter satin fabric is achieved at about 4.25 mm and 4.75 mm for the 20 μm twill fabric. About the fabric properties, the 20 μm twill fabric has comparatively more favorable properties for the discharge behavior than the 18 μm satin fabric ($30 \text{ l}\cdot\text{m}^{-2}\cdot\text{s}^{-1}$), especially regarding fabric thickness, surface roughness and air resistance ($185 \text{ l}\cdot\text{m}^{-2}\cdot\text{s}^{-1}$). Regarding the mass discharge, the impression can be gained that the rougher 18 μm fabric has a relatively better discharge behavior. This contrasts with the significantly smaller roughness compared to the 20 μm fabric and is therefore difficult to interpret. The problem of the 18 μm fabric is the significantly increased residual load

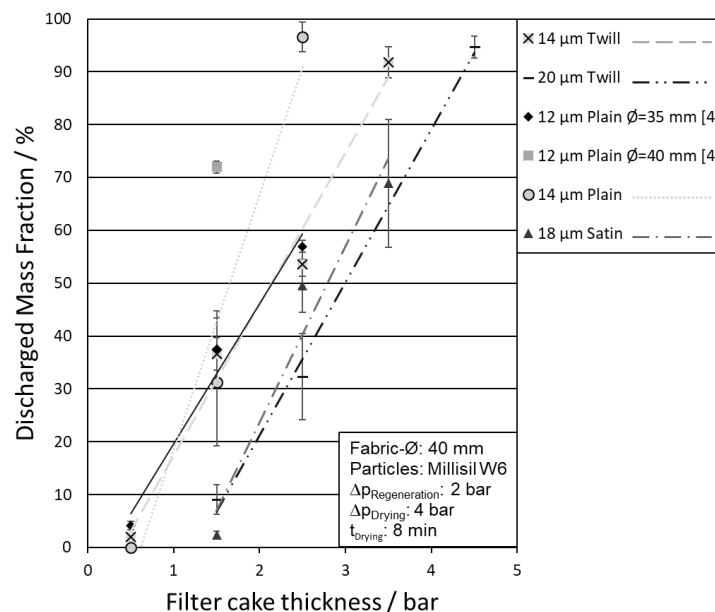


Figure 22: Variation of the cake height at a backwashing pressure of 2 bar for backwashing filtration in gas phase.

III. Filter cloth diameter and IV. Filter cloth type: An increase in the filter cloth diameter relative to the filter element (e.g. candle filter) increases the acceleration distance and the detachment force [197].

This section deals with the investigation of the influence of the fabric diameter, with constant candle diameter, on the regeneration of the filter fabric. For this purpose, the 14 µm twill fabric and the 18 µm satin fabric with diameters of 35 and 40 mm are examined at a constant pressure of 2 bar and a constant cake height of 1.5 mm. For comparison, the data according to [4] of the 12 µm plain weave are discussed. The drying time here is always 480 seconds at a drying pressure of 4 bar. For each measuring point five tests with the same basic conditions are carried out.

For a 35 mm diameter fabric, the average acceleration path of the fabric is 2.5 mm in each direction of the cross section without considering the inherent elongation. For 40 mm, a maximum acceleration path of 5 mm shall be achieved. From the discharge in gas phase after previous gas filtration, the equation Eq. 26 is known for the calculation of the maximum speed, depending on pressure increase, acceleration path and specific weight per unit area [197].

$$v_{\max} = (9 \cdot s^2 \cdot 0.5 \cdot W^{-1})^{1/3} \cdot (d(\Delta p)/dt)^{1/3} \quad \text{Eq. 26}$$

The free path length s of the fabric is the maximum acceleration path of the fabric and filter cake and W is the basis weight. The gas impulse with the set backwash pressure initiates the natural movement of the fabric. The weight per unit area W in Eq. 26 also influences the speed of the fabric. Here, a small basis weight favors a greater maximum speed and thus also regeneration.

The discharge on characteristics of the 12 µm plain weave according to [4] shows a strong dependence on the diameter. The measuring points shown for the discharged mass of the 40 mm diameter fabric are in all cases approx. twice as large as the discharge mass of a fabric with a 5 mm smaller diameter. The equation according to [198,199] for the maximum speed describes that with a larger distance, i.e. larger diameter, a higher speed and thus a better throw-off can be achieved ($v_{\max} \sim s^{2/3}$). Furthermore, a small weight per unit area has an effect in favor of good release ($v_{\max} \sim W^{-1/3}$). It is particularly noticeable here that the 35 mm fabric can be discharged with 3.25 bar, even with a 40 mm fabric with only 1.25 bar backwash pressure. This makes the influence of the fabric diameter clear. The observation of the 12 µm plain weave with diameters of 35 and 40 mm confirms the results to be expected from Eq. 3.

The 18 µm mesh with diameters of 35 and 40 mm at constant backwashing pressure and cake height variation are content of [4]. With increasing cake thickness, the inertia of the filter cake

increases. It is therefore true that cakes of higher thickness can be thrown off better than thin cakes up to a discharge of 70 % for 2 and 4 bar backwashing pressure. Due to the greater distance, the maximum speed of the 40 mm fabric is also greater here due to the gas impulse than with 35 mm diameter. For the same fabric with a diameter of 35 mm a worse discharge behavior is to be expected. After an evaluation of the cake heights, no discharge can be determined even with a cake of 6 mm thickness, thus confirming the expectation. This can be explained by the influencing, very high weight per unit area of $4.25 \text{ g}\cdot\text{dm}^2$, which inhibits the movement of the fabric.

The $14 \mu\text{m}$ twill fabric is observed both at constant cake height and at constant backwashing pressure. The courses of the cake discharge at a constant cake height of 1.5 mm behave similarly. As already mentioned, the high point at 2 bar was initially classified as a measurement error. However, this error can be reproduced by repeating the series of measurements. With reference to Eq. 3, however, this is not to be expected. For this reason, a linear dependence is assumed in the examined pressure range of the $14 \mu\text{m}$ fabric. The linear approximations are shown in Figure 23 a) and are very similar. In general, the $14 \mu\text{m}$ fabric is difficult to clean under these conditions, regardless of the fabric diameter.

The cake height variation of the $14 \mu\text{m}$ mesh is shown in Figure 23 b) for the mesh diameters 35 and 40 mm. Even with the variation of the mesh diameter, this mesh does not behave as expected. In linear approximation, the straight line of the 35 mm diameter is steeper than the tissue of larger diameter, so that the tissue of smaller diameter is preferred for regeneration. This contradicts the hypothesis that tissue with a larger acceleration path can be regenerated more efficiently. First impulse in the interpretation of these measured values suggests a systematic error. These may be, for example, incorrect fixation or poorer drying. Since a systematic error could also be excluded, this behavior must be attributed to the diameter. One possible explanation for this would be that the difference in diameter does not change the specific weight, but the absolute weight of the 40 mm fabric is greater than that of the 35 mm fabric and thus influences the discharge behavior. Due to the greater mass, the fabric behaves more inertly.

All in all, it can be said that the stable $14 \mu\text{m}$ twill fabric and the $18 \mu\text{m}$ satin fabric has a significantly poorer cleanability than the $12 \mu\text{m}$ plain fabric made of [4]. If the choice of fabric is nevertheless made for such a stable/rigid fabric, for example because of the filtration performance, the regeneration parameters must be determined empirically.

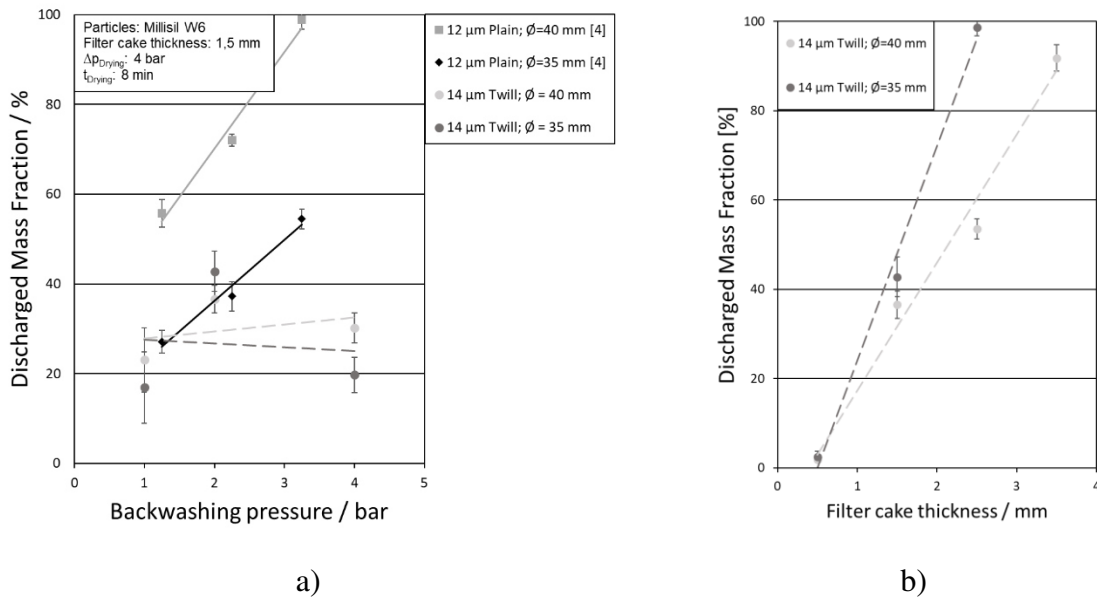


Figure 23: Influence of the fabric diameter on the cake discharge for different backwashing pressure at 1.5 mm filter cake thicknesses (a) and for different filter cake height at 2 bar backwashing pressure (b) for the 14 μm twill weave.

Conclusion

About the backwashing behavior of the fabric, the fabric properties have a decisive influence on the regenerability. Here, small elastic moduli and basis weights are particularly advantageous for the self-movement of the fabric, as shown on the 14 μm plain weave in comparison to the 14 μm twill weave. However, the surface roughness isn't decisive for the separation of the filter cake from the filter medium, as the comparison of 12 μm plain weave with 18 μm satin weave shows. A larger diameter fabric achieves higher speeds in a dry environment than a smaller diameter fabric. The comparison of the 12 μm plain weave makes it clear that with a diameter of 40 mm a considerably lower backwash pressure is required for a throw-off of over 50 % than with a diameter of 35 mm on the 30 mm lab candle filter. So that a fabric with a larger diameter is preferable.

The influence of the mesh sizes can be seen by examining the mesh by varying the cake height at constant backwashing pressure. According to [160], fabrics with a larger mesh size throw off more efficiently than finer fabrics due to weaker adhesion forces. However, in this work a better throw-off was achieved with smaller mesh sizes than with larger ones. The 12 μm fabric has the most efficient discharge behavior compared to the other fabrics. The twill weave with 14 μm mesh width is almost identical to the 12 μm plain weave with a diameter of 35 mm. With the 14 μm plain weave, these three fabrics achieve a drop of between 30 and 40 % at a cake height of only 1.5 mm. The fabrics with mesh sizes of 18 and 20 μm, on the other hand, only achieve a comparable drop with a cake height of 2.5 mm.

The influence of a variation of the backwashing pressure can only be seen with the two plain weaves with 12 and 14 μm . On the other hand, the discharge of the twill fabric and the satin fabric cannot be increased by increasing the backwashing pressure. Therefore, about the variation of the backwashing pressure, a plain fabric is recommended. The 12 μm plain weave behaves more favorably than the 14 μm one, with unfavorable discharge behavior, especially for fabrics of high stability (high modulus of elasticity and basis weight).

The 12 μm plain weave is distinguished by the results of this work as the fabric with the best cleaning behavior. With its particularly smooth surface and a low weight per unit area for gas phase discharge, it has excellent properties. Long-term tests on this fabric are not part of this study, but due to its low stability and thickness, this fabric may not be suitable for long-term use.

The 14 μm plain weave also shows a favorable discharge behavior, especially for large cake heights. For backwashing at high pressures, the mesh with 12 μm diameter is preferable.

The low influence of the backwashing pressure on the 14 μm twill weave allows a waste of approx. 30 % already at 1 bar backwashing pressure. Fabrics with high tensile strength are not suitable for backwashing with low pressure and small cake thickness, as they are difficult to accelerate. These achieve better discharge results in liquid phase (see [1]).

To make general statements about the influence of the mesh on the backwashing filtration with regeneration in gas phase, further experiments with larger meshes/ more pores per filter are and particle systems as well as with different candle geometries are necessary. Special focus should be placed on fabrics with a gradation of strength with respect to the young's moduli and similar roughness to further investigate this influence. Similarly, fabrics of different roughness and similar young's moduli are to be considered. Special attention should be paid to satin fabrics to ensure that these fabrics, such as the 18 μm weave used here, are indeed not suitable for backwashing in gas phase. As already mentioned in this chapter, the best backwashing properties are found in the 12 μm plain weave, which has breaking strengths due to its filigree structure. Long-term tests are of interest here, which, especially in the case of mineral sharp-edged products, consider the properties of the fabric regarding service life and regenerability at wear and tear.

Symbols

Symbol	Description	Unit
$\Delta p_{\text{Regeneration}}$	Backwashing pressure	bar
Δp_{Drying}	Dehumidification pressure	bar
H_{FC}	Filter cake thickness	m
m_{remain}	Mass fraction remaining on filter surface	g
$m_{\text{remain, dry}}$	Mass fraction remaining on filter surface after drying	g
$m_{\text{remain, wet}}$	Mass fraction remaining on filter surface with liquid	g
m_{removed}	Discharged mass fraction	g
$m_{\text{removed, dry}}$	Discharged mass fraction after drying	g
$m_{\text{removed, wet}}$	Discharged mass fraction with liquid	g
S	Saturation	-
s	Acceleration distance s	m
S_{∞}	Limit saturation	-
t	time	s
t_{Drying}	Dehumidification time	s
v_{max}	Maximum velocity of the filter cloth	$\text{m} \cdot \text{s}^{-1}$
W	Surface weight	$\text{kg} \cdot \text{m}^{-2}$
$X_{i, 3}$	Descriptive Mass/volume-related modal value of particle distribution ($i = 10, 50, 90 \%$)	μm
ρ_{Liquid}	Density of the liquid phase	$\text{kg} \cdot \text{m}^{-3}$

References

- [1] Morsch P, Ginisty P, Anlauf H, Nirschl H. Factors influencing backwashing operation in the liquid phase after cake filtration. *Chemical Engineering Science* 2020;213:115372.
- [2] Morsch P, Anlauf H, Nirschl H. The influence of filter cloth on cake discharge performances during backwashing into liquid phase. *Separation and Purification Technology* 2021;254:117549.
- [3] Morsch P, Bauer M, Kessler C, Anlauf H, Nirschl H. Description of the filter cloth deformation during backwashing filtration. *Separation and Purification Technology* 2020;253:117504.
- [4] Morsch P, Ginisty P, Anlauf H, Nirschl H. Influence of regeneration variables during backwashing treatment into gas-phase after liquid filtration. *Separation and Purification Technology* 2020;249:117073.
- [5] Morsch P, Arnold A, Schulze H, Werner R, Anlauf H, Geier DU et al. In-situ cleaning process of chamber filter presses with sensor-controlled and demand-oriented automation. *Separation and Purification Technology* 2021;256:117793.
- [6] Morsch P, Kühn J, Werner R, Anlauf H, Geier DU, Becker T et al. Influence of the filter cloth and nozzles type on the in-situ cleaning procedure of filter presses. *Chemical Engineering Science* 2020:115889.
- [7] Anlauf H. Fest/Flüssig-Trennung. *Chemie Ingenieur Technik* 2018;90(12):1929–38.
- [8] Anlauf H. Evolution in der Trenntechnik - technische Entwicklung durch Mutation und Selektion. *Filtrieren und Separieren* 2012, 2012:150–7.
- [9] Anlauf H. Fest/Flüssig-Trenntechnik in Karlsruhe. *Filtrieren und Separieren* 1998, 1998:207–13.
- [10] Anlauf H, Romani X. Superposed Filtration Mechanism during Clarification of Very Low Concentrated Suspension with a Paperstack Candle Filter. *Chemical Engineering Technology* 2010, 2010:1–8.
- [11] Luckert K (ed.). *Handbuch der mechanischen Fest-Flüssig-Trennung*. Essen: Vulkan-Verl; 2004.
- [12] Anlauf H. Mechanische Fest/Flüssig-Trennung im Wandel der Zeit. *Chemie Ingenieur Technik* 2003;75(10):1460–3.
- [13] Henry Darcy. *Les fontaines publiques de la ville de Dijon*. Paris: Dalmont; 1856.
- [14] Fourier JBJ. *The analytical theory of heat*. [Charleston, SC]: [BiblioLife]; 2009.
- [15] Fick A. Ueber Diffusion. *Ann. Phys. Chem.* 1855;170(1):59–86.

- [16] Brown GO. The History of the Darcy-Weisbach Equation for Pipe Flow Resistance. In: Rogers JR, Fredrich AJ, editors. Environmental and Water Resources History. Reston, VA: American Society of Civil Engineers; 10172002, p. 34–43.
- [17] Poiseuille JLM. Recherches experimentales sur le mouvement des liquides dans les tubes de tres petits diametres;; II. Influence de la longueur sur la quantité de liquide qui traverse les tubes de très petits diamètres. III: Influence du diamètre sur la quantité qui traverse les tubes de très petits diamètres. C. R. Acad. Sci. 1840;11:1041–8.
- [18] Poiseuille JLM. Recherches experimentales sur le mouvement des liquides dans les tubes de tres petits diametres;; I. Influence de la pression sur la quantité de liquide qui traverse les tubes de très petits diamètres. C. R. Acad. Sci. 1840;11:961–7.
- [19] Poiseuille JLM. Recherches experimentales sur le mouvement des liquides dans les tubes de tres petits diametres;; IV. Influence de la temperature sur la quantité de liquide qui traverse les tubes de très petits diamètres. C. R. Acad. Sci. 1841;12:112–5.
- [20] Hagen GHL. Über die Bewegung des Wassers in engen cylindrischen Röhren. 46 1839:423–42.
- [21] Suter SP, Skalak R. The History of Poiseuille's Law. Annu. Rev. Fluid Mech. 1993;25(1):1–20.
- [22] Bohl W. Technische Strömungslehre: Stoffeigenschaften von Flüssigkeiten und Gasen, Hydrostatik, Aerostatik, inkompressible Strömungen, kompressible Strömungen, Strömungsmesstechnik. 12th ed. Würzburg: Vogel; 2002.
- [23] Brieghel-Miller A. Die Entwicklung und der jetzige Stand der Theorie der Filtration von Suspensionen. Kolloid-Zeitschrift 1940;92(3):285–99.
- [24] Bück A, Wirth K-E. Druckverlust in durchströmten Schüttungen. In: Jousten K, editor. Handbuch Vakuumtechnik. Wiesbaden: Springer Fachmedien Wiesbaden; 2017, p. 1–6.
- [25] Gupte AR. Experimentelle Untersuchung der Einflüsse von Porosität und Korngrößenverteilung im Widerstandsgesetz der Porenströmung. Dissertation. Karlsruhe; 1970.
- [26] Inayat A, Schwerdtfeger J, Freund H, Körner C, Singer RF, Schwieger W. Periodic open-cell foams: Pressure drop measurements and modeling of an ideal tetrakaidecahedra packing. Chemical Engineering Science 2011;66(12):2758–63.
- [27] Carman PC. Fluid flow through granular beds. Trans. Inst. Chem. Eng. 1937;15:150-166.
- [28] Kozeny J. Über kapillare leitung der wasser in boden. Royal Academy of Science 1927;Proc. Class I(136):271–306.

- [29] Forchheimer P. Wasserbewegung durch boden. Z. Ver. Deutsch, Ing. 1901;45:1782–8.
- [30] LIAKOPOULOS AC. DARCY'S COEFFICIENT OF PERMEABILITY AS SYMMETRIC TENSOR OF SECOND RANK. International Association of Scientific Hydrology. Bulletin 1965;10(3):41–8.
- [31] Ergun S. Fluid flow through packed columns. 48 1952:89–94.
- [32] Tien C, Ramarao BV. Can filter cake porosity be estimated based on the Kozeny–Carman equation? Powder Technology 2013;237:233–40.
- [33] Anlauf H, Romani X. Klärung sehr gering konzentrierter Suspensionen mit expandierbaren Papier-Spaltfilterkerzen. Filtrieren und Separieren:110–6.
- [34] Hermia J. Etude analytique des lois de filtration a pression constante. Rev Univ Mines 2:45–51. Rev Univ Mines 1966;2(45–51).
- [35] Hermia J. Constant pressure blocking filtration laws: application to power-law non-Newtonian fluids. Trans. Inst. Chem. Eng. 1982;60(3):183–7.
- [36] Shirato M, ARAGAKI T, IRITANI E. Blocking filtration laws for filtration of power-law non-newtonian fluids. J. Chem. Eng. Japan / JCEJ 1979;12(2):162–4.
- [37] P. H. Hermans, H. L. Bredée. Zur Kenntnis der Filtrationsgesetze. Recueil des Travaux Chimiques des Pays-Bas 1935;54(9):680–700.
- [38] Purchas DB, Sutherland K. Handbook of filter media. 2nd ed. Oxford: Elsevier Advanced Technology; 2002.
- [39] Ripperger S, Fernández Puga J, Tichy J. Einfluss des Filtermittelwiderstandes und der Strömungswiderstände im Filtratablauf bei kontinuierlich betriebenen Filtern mit hohem Feststoffdurchsatz. Filtrieren und Separieren 2005(19 Nr. 2):58–62.
- [40] Tichy JW. Zum Einfluss des Filtermittels und der auftretenden Interferenzen zwischen Filterkuchen und Filtermittel bei der Kuchenfiltration. Zugl.: Kaiserlautern, Techn. Univ., Diss., 2007. Düsseldorf: VDI-Verl; 2007.
- [41] Rushton A. Effect of filter cloth structure on flow resistance, bleeding, blinding and plant performance. THE CHEMICAL ENGINEER;1970:88–92.
- [42] Hatschek E. The mechanism of filtration. J. Chem. Technol. Biotechnol. 1908;27(11):538–44.
- [43] Chase GG, Arconti J, Kanel J. The Effect of Filter Cakes on Filter Medium Resistance. Separation Science and Technology 1994;29(16):2179–96.
- [44] Keller Y. Ueber den Einfluss der Filtertuch-Unterlage auf den Filtrationsverlauf; 1962.
- [45] Petersen L, Ripperger S. Einfluss der Geometrie des Filtratablaufs auf die Kinetik der Kuchenfiltration. Filtrieren und Separieren 2012;26(5):322–5.

- [46] Bächle V, Morsch P, Fränkle B, Gleiß M, Nirschl H. Interaction of Particles and Filter Fabric in Ultrafine Filtration. *Eng* 2021;2(2):126–40.
- [47] Purchas DB. *Solid-Liquid Separation Technology: Chapter 3*. Croydon: Uplands Press; 1981.
- [48] Heertjes PM, Zuideveld PL. Clarification of liquids using filter aids Part I. Mechanisms of filtration. *Powder Technology* 1978;19(1):17–30.
- [49] Heertjes PM, Zuideveld PL. Clarification of liquids using filter aids Part II. Depth filtration. *Powder Technology* 1978;19(1):31–43.
- [50] Heertjes PM, Zuideveld PL. Clarification of liquids using filter aids Part III. Cake Resistance in surface filtration. *Powder Technology* 1978;19(1):45–64.
- [51] Petersen L. *Untersuchung der Tiefenfiltration wässriger Suspensionen mit Vliesen*. Kaiserslautern: Technische Universität Kaiserslautern; 2016.
- [52] Schollmeier S. *Beladungskinetik von Faserfiltern - Beladungskinetik einzelner Filterfasern*: Karlsruhe; 2008.
- [53] Damm A. *Experimentelle Untersuchungen zur Kuchenfiltration in tuchbespannten Kerzenfiltern, insbesondere zur Aufklärung des Sedimentationseinflusses*. Diplomarbeit. Cologne; 1995.
- [54] Ives KJ. *Scientific basis of filtration: Capture mechanisms in filtration*: Springer Netherlands; 1975.
- [55] Kolb HE, Schmitt R, Dittler A, Kasper G. On the accuracy of capillary flow porometry for fibrous filter media. *Separation and Purification Technology* 2018;199:198–205.
- [56] Gupta K, Jen A. Characterization of pore structure of filter media. *Fluid - Particle Separation Journal* 2002;14(3):227–41.
- [57] S.Ripperger CS. *Die Barrierewirkung von Geweben: Teil 1: Textiltechnische Charakterisierung und Barrieremechanismen*. *Filtrieren und Separieren* 2005, 2005:110–7.
- [58] S. Ripperger. *Die Barrierewirkung von Geweben: Teil 2: Experimentelle methoden zur Bestimmung von Gewebeeigenschaften*. *Filtrieren und Separieren* 2005, 2005:166–73.
- [59] Rideal G. Filter calibration: high precision method. *Filtration & Separation* 2001;38(2):26–8.
- [60] Anlauf H. Bestimmung der größten Pore in Filtermedien unterschiedlicher Struktur durch Messung des kapillaren Eintrittsdrucks. *Chemie Ingenieur Technik* 1996;68(11):1476–9.

- [61] Schubert H. Kapillarität in porösen Feststoffsystemen. Berlin, Heidelberg usw.: Springer; 1982.
- [62] S. Ripperger. Die Barrierewirkung von Geweben: Teil 3: Auswahl von Geweben zur Kuchenfiltration. *Filtrieren und Separieren* 2005, 2005:284–9.
- [63] S. Ripperger. Die Barrierewirkung von Geweben: Teil 6: Einfluss des Filtermittels auf die Kuchenfiltration. *Filtrieren und Separieren* 2008, 2008:6–9.
- [64] S. Ripperger, M. Stompor, P. Fiala. Experimentelle Methoden zur Charakterisierung der Barrierewirkung von Gewebe gegenüber Flüssigkeiten und Partikeln. *Filtrieren und Separieren* 2002, 2002:130–7.
- [65] Esser U, Peuker U. Filtrationsexperiment und Simulation, wie gut stimmen Ergebnisse überein? Merseburg; 2018.
- [66] Hund D, Schmidt K, Ripperger S. Numerische Berechnung der Strömung und Partikelabscheidung in Filtrationsgeweben. *Filtrieren und Separieren* 2014;28(4):221–5.
- [67] Ripperger S, Schmidt K. Entwicklung von Geweben als Filtermedien unter Berücksichtigung der numerischen Strömungssimulation. *Filtrieren und Separieren* 2015;29(6):378–81.
- [68] Hund D, Schmidt K, Ripperger S, Antonyuk S. Direct numerical simulation of cake formation during filtration with woven fabrics. *Chemical Engineering Research and Design* 2018;139:26–33.
- [69] Schnitzer C, Ripperger S. Die Barrierewirkung von Geweben: Teil 5: Modellierung der Durchströmung von Multifilamentgeweben mit Methoden der numerischen Strömungssimulation. *Filtrieren und Separieren* 2007;21(6):336–8.
- [70] Schnitzer C, Ripperger S. Barrierewirkung von Geweben: Teil 4: Modellierung der Durchströmung von Multifilamentgeweben. *Filtrieren und Separieren* 2007;21(4):226–31.
- [71] VDI-Guideline. Mechanical solid-liquid separation by cake filtration - Determination of filter cake resistance: 2762-2; 2010.
- [72] Straumann R. Einfluß der Sedimentation auf die Filtration. *Chemie Ingenieur Technik* 1963;35(10):715–20.
- [73] Bothe C, Esser U, Fechtel T. Experimentelle und theoretische Untersuchungen zur Filtration mit überlagerter Sedimentation in Drucknutschen. *Chemie Ingenieur Technik* 1997;69(7):903–12.
- [74] Bockstal F, Fouarge L, Hermia J, Rahier G. Constant Pressure Cake Filtration with Simultaneous Sedimentation. *Filtration & Separation* 1985;22(4):255–7.

- [75] Chellappah K, Tarleton ES, Wakeman RJ. Filtration and sedimentation behaviour of fibre/particle binary suspensions. *Filtration* 2009(9 (4)):286–94.
- [76] Wiedemann T. Das Schrumpfs- und Reißungsverhalten von Filterkuchen. Zugl.: Karlsruhe, Univ., Diss., 1996. Düsseldorf: VDI-Verl; 1996.
- [77] Erk A. Rheologische Eigenschaften feindisperser Suspensionen während ihrer Fest-Flüssig-Trennung in Filtern und Zentrifugen. Zugl.: Karlsruhe, Univ., Diss., 2006. Aachen; 2006.
- [78] Chellappah K, Tarleton ES, Wakeman RJ. The Porosity, Permeability and Restructuring of Heterogeneous Filter Cakes. *Chem. Eng. Technol.* 2010;33(8):1283–9.
- [79] Chellappah K, Tarleton ES, Wakeman RJ. Aggregation effects in the cake filtration of interacting binary mixtures. *Chemical Engineering Science* 2010;65(24):6407–14.
- [80] Wakeman R. The influence of particle properties on filtration. *Separation and Purification Technology* 2007;58(2):234–41.
- [81] Johnson KL, Kendall K, Roberts AD. Surface energy and the contact of elastic solids. *Proc. R. Soc. Lond. A* 1971;324(1558):301–13.
- [82] Derjaguin BV, Muller VM, Toporov YP. Effect of contact deformations on the adhesion of particles. *Journal of Colloid and Interface Science* 1975;53(2):314–26.
- [83] Chen Y, Best A, Butt H-J, Boehler R, Haschke T, Wiechert W. Pressure distribution in a mechanical microcontact. *Appl. Phys. Lett.* 2006;88(23):234101.
- [84] Huber MT. Zur Theorie der Berührung fester elastischer Körper. *Ann. Phys. Chem.* 1904;319(6):153–63.
- [85] Cornehl B. Bruch von Proteinkristallen im mechanischen Trennprozess: Karlsruhe; 2014.
- [86] Tiller FM, Kwon JH. Role of porosity in filtration: XIII. Behavior of highly compactible cakes. *AIChE J.* 1998;44(10):2159–67.
- [87] Alles CM. Prozeßstrategien für die Filtration mit kompressiblen Kuchen. Karlsruhe, Univ., Diss., 2000.
- [88] Bender W, Redeker D. Fortschritte bei der mechanischen Flüssigkeitsabtrennung durch Filtration. *Chemie Ingenieur Technik* 1981;53(4):227–36.
- [89] Rushton A, Ward AS, Holdich RG. *Solid-Liquid Filtration and Separation Technology*. Hoboken: Wiley-VCH; 2008.
- [90] Wirth K-E. Die Grundlagen der pneumatischen Förderung. *Chemie Ingenieur Technik* 1983;55(2):110–22.

- [91] Werther J. Mathematische Modellierung von Wirbelschichten. *Chemie Ingenieur Technik* 1984;56(3):187–96.
- [92] Illies S. Darstellungen zur Entfeuchtung von zu Rissbildung neigenden Filterkuchen. Dissertation. Karlsruhe; 2017.
- [93] Ripperger S. Reinigen, Desinfizieren und Sterilisieren von verfahrenstechnischen Anlagen; Teil 1: Die Reinigung verfahrenstechnischer Anlagen. *Filtrieren und Separieren* 2004;18(3):110–6.
- [94] Ripperger S. Reinigen, Desinfizieren und Sterilisieren von verfahrenstechnischen Anlagen; Teil 2: Die Reinigung von Membrananlagen. *Filtrieren und Separieren* 2004;18(4):162–6.
- [95] Ripperger S. Reinigen, Desinfizieren und Sterilisieren von verfahrenstechnischen Anlagen; Teil 3: Die Desinfektion und Sterilisation verfahrenstechnischer Anlagen. *Filtrieren und Separieren* 2004;18(5):218–22.
- [96] Ripperger S. Reinigen, Desinfizieren und Sterilisieren von verfahrenstechnischen Anlagen; Teil 4: Hygienic Design. *Filtrieren und Separieren*. *Filtrieren und Separieren* 2004;18(6):272–6.
- [97] Werner RA, Geier DU, Becker T. The Challenge of Cleaning Woven Filter Cloth in the Beverage Industry—Wash Jets as an Appropriate Solution. *Food Eng Rev* 2020;12(4):520–45.
- [98] Gibson H, Taylor JH, Hall KE, Holah JT. Effectiveness of cleaning techniques used in the food industry in terms of the removal of bacterial biofilms. *Journal of Applied Microbiology* 1999;87(1):41–8.
- [99] D'Souza NM, Mawson AJ. Membrane cleaning in the dairy industry: a review. *Critical reviews in food science and nutrition* 2005;45(2):125–34.
- [100] Morris K, Allen RWK, Clift R. Adhesion of Cakes to Filter Media. *Filtration & Separation* 1987, 1987:41–5.
- [101] Dittler A, Ferer MV, Mathur P, Djuranovic P, Kasper G, Smith DH. Patchy cleaning of rigid gas filters—transient regeneration phenomena comparison of modelling to experiment. *Powder Technology* 2002;124(1-2):55–66.
- [102] Ferer M, Smith DH. A simple model of the adhesive failure of a layer: Cohesive effects. *Journal of Applied Physics* 1997;81(4):1737–44.
- [103] Zsifkovits HE, Altendorfer-Kaiser S (eds.). *Logistische Modellierung: 2. Wissenschaftlicher Industrielogistik-Dialog in Leoben (Wild)*. 1st ed. Mering: Rainer Hampp Verlag; 2014.

- [104] CORN M. The adhesion of solid particles to solid surfaces. I. A review. *Journal of the Air Pollution Control Association* 1961;11:523–8.
- [105] Rumpf H. Grundlagen und Methoden des Granulierens. *Chemie Ingenieur Technik* 1958;30(3):144–58.
- [106] Schubert H. Grundlagen des Agglomerierens. *Chemie Ingenieur Technik* 1979;51(4):266–77.
- [107] Ripperger S, Hartmüller J. Die Haftung von Partikeln an Bauteiloberflächen: Teil 1: Theoretische Abschätzung von Haftkräften aufgrund der van der Waals-Kraft. *Filtrieren und Separieren* 2014, 2014:212–6.
- [108] Ripperger S, Hartmüller J. Die Haftung von Partikeln an Bauteiloberflächen: Teil 2: Theoretische Abschätzung von Haftkräften aufgrund von Flüssigkeitsbrücken. *Filtrieren und Separieren* 2014, 2014:274–7.
- [109] Ripperger S, Hartmüller J. Die Haftung von Partikeln an Bauteiloberflächen: Teil 3: Methoden zur experimentellen Bestimmung von Haftkräften. *Filtrieren und Separieren* 2014, 2014:350–4.
- [110] Schönfeld F. Kapillarfluss-Porometer. *CITplus* 2019;22(10):31–2.
- [111] Schubert H. Kapillardruck und Zugfestigkeit von feuchten Haufwerken aus körnigen Stoffen. *Chemie Ingenieur Technik* 1973;45(6):396–401.
- [112] Redeker D, Steiner K-H, Esser U. Das mechanische Entfeuchten von Filterkuchen. *Chemie Ingenieur Technik (CIT)* 1983;55(11):829–39.
- [113] Anlauf H. Untersättigung und/oder Konsolidierung - Grenzen der mechanischen Entfeuchtung von Filterkuchen. *Chemie Ingenieur Technik* 2014;86(1-2):149–60.
- [114] Ozcan O, Ruhland M, Stahl W. The effect of pressure, particle size and particle shape on the shear strength of very fine mineral filter cakes. *International Journal of Mineral Processing* 2000;59(2):185–93.
- [115] Wiedemann T, Stahl W. Schrumpfs- und Reißungsverhalten feinkörniger Filterkuchen bei der Gasdifferenzdruckentfeuchtung. *Chemie Ingenieur Technik* 1995;67(11):1486–9.
- [116] Hamaker HC. The London—van der Waals attraction between spherical particles. *Physica* 1937;4(10):1058–72.
- [117] London F. The general theory of molecular forces. *Trans. Faraday Soc.* 1937;33:8b.
- [118] Derjaguin B. Untersuchungen über die Reibung und Adhäsion, IV. *Kolloid-Zeitschrift* 1934;69(2):155–64.

- [119] Lehmann MJ, Schmidt E. Numerische Berechnung von Van-der-Waals-Haftkräften zwischen beliebig strukturierten Partikeln. *Chemie Ingenieur Technik* 1998;70(10):1318–21.
- [120] Bobe U. Die Reinigbarkeit technischer Oberflächen im immmergierten System. Doctor thesis. München; 2008.
- [121] Lee S-w, Sigmund WM. AFM study of repulsive van der Waals forces between Teflon AF™ thin film and silica or alumina. *Colloids and Surfaces A: Physicochemical and Engineering Aspects* 2002;204(1-3):43–50.
- [122] Israelachvili JN. Intermolecular and surface forces. 3rd ed. Amsterdam: Elsevier Acad. Press; 2011.
- [123] Lagaly G, Schulz O, Zimehl R. Dispersionen und Emulsionen. Heidelberg: Steinkopff; 1997.
- [124] Laitinen O, Bauer K, Niinimäki J, Peuker UA. Validity of the Rumpf and the Rabinovich adhesion force models for alumina substrates with nanoscale roughness. *Powder Technology* 2013;246:545–52.
- [125] Götzinger M, Peukert W. Dispersive forces of particle–surface interactions: Direct AFM measurements and modelling. *Powder Technology* 2003;130(1-3):102–9.
- [126] Götzinger M, & Peukert W. Haftkraftverteilungen von rauen Haftsyste-men am Beispiel Kugel–Platte. *Chemie Ingenieur Technik* 2003;75(12):1848-1852.
- [127] Rabinovich, Adler, Ata, Singh, Moudgil. Adhesion between Nanoscale Rough Surfaces. *Journal of Colloid and Interface Science* 2000;232(1):10–6.
- [128] Weigert T. Haftung von Filterkuchen bei der Fest/Flüssig-Filtration. Zugl.: Dresden, Techn. Univ., Diss., 2000. Düsseldorf: VDI-Verl; 2001.
- [129] Weigert T, Ripperger S. Filter Cake Adhesion on Textile Filter Media. Part 2: Physical Description and Modeling. *F & S International Edition* 2003(3):12–9.
- [130] Weigert T, Ripperger S. Filter Cake Adhesion on Textile Filter Media. Part 1: Experimental Tests and their Evaluation. *F & S International Edition* 2002(2):32–8.
- [131] Schulze D. Pulver und Schüttgüter: Fliesseigenschaften und Handhabung. 1st ed. Berlin: Springer; 2007.
- [132] Schmelzle S. Numerische Untersuchungen zum Segregationsverhalten von trockenen und feuchten Schüttgütern im diskontinuierlichen Mischprozess: Karlsruhe; 2019.
- [133] Dueck J, Djatschenko E, Neesse T. Computersimulation von Filterkuchenstrukturen. *Chemie Ingenieur Technik* 2007;79(11):1913–9.

- [134] Menesklou P, Nirschl H, Gleiss M. Dewatering of finely dispersed calcium carbonate-water slurries in decanter centrifuges: About modelling of a dynamic simulation tool. *Separation and Purification Technology* 2020;251:117287.
- [135] Hammerich S, Stickland AD, Radel B, Gleiss M, Nirschl H. Modified shear cell for characterization of the rheological behavior of particulate networks under compression. *Particuology* 2020;51:1–9.
- [136] Mittal KL. *Surface Contamination: Genesis, Detection, and Control*. Boston, MA: Springer US; 1979.
- [137] Wildbrett G. *Reinigung und Desinfektion in der Lebensmittelindustrie*. 2nd ed. Hamburg: Behr; 2006.
- [138] Reiff F, Wissemeier H, Camphausen H, Ruf F. *Reinigungs- und Desinfektionsmittel im Lebensmittelbetrieb.: Handbuch der Lebensmittelchemie*. 9th ed; 1970.
- [139] Reuter H. Reinigen und Desinfizieren im Molkereibetrieb. *Stand des Wissens und der Technik. Chemie Ingenieur Technik* 1983;55(4):293–301.
- [140] Bénézech T. *A method for the assessment of in-place cleanability of food processing equipment*. 3rd ed. Chipping Campden: Published for EHEDG by CCFRA Technology; 2004.
- [141] Bénézech T. *A method for the assessment of in-line steam sterilisability of food processing equipment*. 2nd ed. Chipping Campden: Published for EHEDG by CCFRA Technology; 2004.
- [142] Bénézech T. *A method for the assessment of bacteria tightness of food processing equipment*. 2nd ed. Chipping Campden: Published for EHEDG by CCFRA Technology; 2004.
- [143] Rust U. Der Sinner'sche Kreis: Basis einer erfolgreichen Reinigung und Desinfektion. *Getränkeindustrie* 2004;11:98–104.
- [144] Müller-Steinhagen H. *Handbook [of] heat exchanger fouling: Mitigation and cleaning technologies = Wärmetauscher-Fouling Verminderung und Reinigungssysteme / editor: H. Müller-Steinhagen*. Essen: Publico Publications; Rugby Institution of Chemical Engineers; 2000.
- [145] Diery W. Entwicklungsstand der Rektifikationsböden. *Chemie Ingenieur Technik* 1975;47(23):964–70.
- [146] Moeller R-S. *Haftkräfte, Alterung und Überwachung funktionaler Oberflächen – Gärtücher im Gebrauch*: Karlsruhe; 2018.

- [147] Weidemann C. Reinigungsfähigkeit von Filtermedien mithilfe kontinuierlicher und pulsierender Strömung. Zugl.: Karlsruhe, KIT, Diss., 2014. Karlsruhe, Hannover: KIT Scientific Publ; Technische Informationsbibliothek u. Universitätsbibliothek; 2015.
- [148] Oliveira R. Understanding adhesion: A means for preventing fouling. *Experimental Thermal and Fluid Science* 1997;14(4):316–22.
- [149] Förster M, Augustin W, Bohnet M. Influence of the adhesion force crystal/heat exchanger surface on fouling mitigation. *Chemical Engineering and Processing: Process Intensification* 1999;38(4-6):449–61.
- [150] A.J. Charleton, N.I. Heywood. Can you Handle Sticky Cakes? *Filtration & Separation* 1983, 1983:357–60.
- [151] Goode KR, Asteriadiou K, Robbins PT, Fryer PJ. Fouling and Cleaning Studies in the Food and Beverage Industry Classified by Cleaning Type. *Comprehensive Reviews in Food Science and Food Safety* 2013;12(2):121–43.
- [152] Chmielewski RAN, Frank JF. Biofilm Formation and Control in Food Processing Facilities. *Comp Rev Food Sci Food Safety* 2003;2(1):22–32.
- [153] Srey S, Jahid IK, Ha S-D. Biofilm formation in food industries: A food safety concern. *Food Control* 2013;31(2):572–85.
- [154] Dunsmore DG, Twomey A, Whittlestone WG, Morgan HW. Design and Performance of Systems for Cleaning Product-Contact Surfaces of Food Equipment: A Review. *Journal of food protection* 1981;44(3):220–40.
- [155] Boulané-Petermann L. Processes of bioadhesion on stainless steel surfaces and cleanability: A review with special reference to the food industry. *Biofouling* 1996;10(4):275–300.
- [156] Stahl S, Siggelkow S, Nirschl H. A Microbiological Test Method to Determine the Cleanability of Filter Media in Solid-Liquid-Separation Applications. *Eng. Life Sci.* 2007;7(2):136–42.
- [157] Fränkle B, Morsch P, Nirschl H. Regeneration assessments of filter fabrics of filter presses in the mining sector. *Minerals Engineering* 2021;168:106922.
- [158] Leipert C, Nirschl H. Investigations of the cleanability of polymer filter media. *F & S International Edition* 2012(11):13–8.
- [159] Weigert T, Ripperger S. Filterkuchenhaftung an textilen Filtermedien: Teil 1: Experimentelle Untersuchungen und ihre Auswertung. *Filtrieren und Separieren* 2001(15):221–8.

- [160] Muller HR, Kern R, Stahl W. Adhesive Forces between Filter Cloth and Cake. *Filtration & Separation* 1987, 1987:27–32.
- [161] Ken-Ichiro Kurita. Device for releasing filter cake in filter press(US3669273A); 1970.
- [162] Franco Grigoletti. Unloading device for filter press(EP0554515A1); 11.08.93.
- [163] Fritz Trummel. Method and apparatus for dislodging a cake of a chamber filter press(US5449468A).
- [164] Richard Van Egdome. Filter press with a cake throw-off device(DE10061918B4); 2000.
- [165] Viktor Germanovic Ponomarenko, Valeri Fjodorovic Pavlenko, Viktor Anatolevic Cernikov, Oleksandr F Edorovc Picachci, Oleksandr Viktorovic Stankun, Viktor Michailovic Gutorov. Filter press for the filtration of suspensions(DE19546701A1).
- [166] Joel D. De Haan, Daniel De Haan, Gregory De Haan, David J. Spyker, David P. McLeod, Wesley G. Koops, Leonid B. Gelfand. Air-assist discharge of filter press cake(US5567327A).
- [167] Kunihiko Tsuchida KO. APPARATUS FOR REGENERATING FILTER CLOTHES OF FILTER PRESS(US5846415A).
- [168] 金望松. Automatic mud scraping and filter cloth cleaning device of full automatic filter press(CN2675222Y).
- [169] Baochang LIU QZ. Scraper device for discharging filter cake on filter plate of pressure filter(US8945382B2).
- [170] Wolfgang Hess, Manfred Scherer, Johann Feller, Bruno Hegnauer. Apparatus for removing a filter cake base layer(DE4330594C1).
- [171] Poul Bach, Henning Birger Moeller, Nicolai Pipper. Process for cleaning a filter unit and a filter unit for filtering gas(DK1027131T3).
- [172] Weidemann C, Vogt S, Nirschl H. Cleaning of filter media by pulsed flow – Establishment of dimensionless operation numbers describing the cleaning result. *Journal of Food Engineering* 2014;132:29–38.
- [173] Stahl S, Leipert C, Nirschl H. The cleanability of particle loaded woven filter media in solid–liquid separation. *Separation and Purification Technology* 2013;110:196–201.
- [174] Stahl S. Zum Reinigungsverhalten von Filtergeweben auf diskontinuierlichen Filterzentrifugen. @Karlsruhe, Karlsruher Inst. für Technologie, Diss., 2013.
- [175] Anlauf H. Standardfiltertests zur Bestimmung des Kuchen- und Filtermediumwiderstandes bei der Feststoffabtrennung aus Suspensionen. *Chemie Ingenieur Technik* 1994;66(8):1069–71.

- [176] Yim S-S, Kim J-H. An experimental and theoretical study on the initial period of cake filtration. *Korean J. Chem. Eng.* 2000;17(4):393–400.
- [177] Anlauf H. Filtermedien zur Kuchenfiltration – Schnittstelle zwischen Suspension und Apparat. *Chemie Ingenieur Technik* 2007;79(11):1821–31.
- [178] Riemenschneider H. Entfeuchten durch Pressen. Doctor thesis. Stuttgart; 1983.
- [179] Nicolaou I. Fortschritte in Theorie und Praxis der Filterkuchenbildung und -entfeuchtung durch Gasdruckdifferenz. Zugl.: Karlsruhe, Univ., Habil.-Schr., 1996. Düsseldorf: VDI-Verl; 1999.
- [180] Anlauf H. WET CAKE FILTRATION: Fundamentals, equipment, strategies. [Place of publication not identified]: WILEY VCH; 2020.
- [181] Smith J, Sheridan C, van Dyk L, Naik S, Plint N, Turrer HDG. Optimal ceramic filtration operating conditions for an iron-ore concentrate. *Minerals Engineering* 2018;115:1–3.
- [182] Thor W, Loncin M. Reinigen, Desinfizieren und Nachspülen in der Lebensmittel-Industrie. *Chemie Ingenieur Technik* 1978;50(3):188–93.
- [183] S. Ripperger. Optimierung von Rückspülfiltern für Flüssigkeiten. *Filtrieren und Separieren* 2008, 2008:68–72.
- [184] Bargel H-J, Schulze G (eds.). *Werkstoffkunde*. 12th ed. Berlin, Germany: Springer Vieweg; 2018.
- [185] Heymann J, Bottcher P. Textile Filtermedien-Beschaffenheit und Eigenschaften. *Filtrieren und Separieren* 1997;11(2):43.
- [186] Müller H. Method of cleaning filter elements(US4443346A); 1981.
- [187] Wegner A. Filter candle for a filter and method for operating a filter(WO2001056680A1); 2001.
- [188] Haldipur GB, Dilmore WJ. Filtering Apparatus(US5143530A); 1990.
- [189] Meier H-P. Spiral Multiple-Tube Filter(US6041944A).
- [190] Hong Xiang G. The modern large scale XMZ 1050/2000 m² automatic filter press for dewatering fine materials. Karlsruhe (Germany); 1991.
- [191] Wu S, Cai R, Zhang L. Research progress on the cleaning and regeneration of PM2.5 filter media. *Particuology* 2021.
- [192] Siebert F. Untersuchungen zum Foulingverhalten keramischer Hohlfasermembranen; 2017.
- [193] Schuhmann S. Schnelle MRI zur Charakterisierung von Filtrationsprozessen: Karlsruhe; 2020.

- [194] Nasr W, Nasr K. Laser Induced Shockwave Surface Cleaning(US 2011/0083696A1); 2010.
- [195] Sobieski W, Trykozko A. Darcy's and Forchheimer's laws in practice. Part 1. The experiment. Technical Sciences 2014;17(4):321 to 335.
- [196] Sobieski W, Trykozko A. Darcy's and Forchheimer's laws in practice. Part 2. The numerical model. Technical Sciences 2014;17(4):337 to 350.
- [197] Sievert J. Physikalische Vorgänge bei der Regenerierung des Filtermediums in Schlauchfiltern mit Druckstossabreinigung. Zugl.: Karlsruhe, Univ., Diss., 1987. Düsseldorf: VDI-Verl; 1988.
- [198] Sievert J, Löffler F. Cleaning mechanisms in pulse-jet fabric filters. Filtration & Separation 1987(24 (2)):110–3.
- [199] Sievert J, Löffler F. Fabric cleaning in pulse-jet filters. Chemical Engineering and Processing: Process Intensification 1989;26(2):179–83.

Publications

1. P. Morsch, P. Ginisty, H. Anlauf, H. Nirschl
Factors influencing backwashing operation in the liquid phase after cake filtration
Chemical Engineering Science **213** (2020)
DOI: 10.1016/j.ces.2019.115372
2. P. Morsch, H. Anlauf, H. Nirschl
The influence of filter cloth on cake discharge performances during backwashing into liquid phase
Separation and Purification Technology **254** (2021)
DOI: 10.1016/j.seppur.2020.117549
3. P. Morsch, M. Bauer, C. Kessler, H. Anlauf, and H. Nirschl
Description of the filter cloth deformation during backwashing filtration
Separation and Purification Technology **253** (2020)
DOI: 10.1016/j.seppur.2020.117504
4. P. Morsch, P. Ginisty, H. Anlauf, and H. Nirschl
Influence of regeneration variables during backwashing treatment into gas-phase after liquid filtration
Separation and Purification Technology **249** (2020)
DOI: 10.1016/j.seppur.2020.117073
5. P. Morsch, A. Arnold, H. Schulze, R. Werner, H. Anlauf, D. U. Geier, T. Becker, and H. Nirschl
In-situ cleaning process of chamber filter presses with sensor-controlled and demand-oriented automation
Separation and Purification Technology **256** (2021)
DOI: 10.1016/j.seppur.2020.117793
6. P. Morsch, J. Kühn, R. Werner, H. Anlauf, D. U. Geier, T. Becker, and H. Nirschl
Influence of the filter cloth and nozzles type on the in-situ cleaning procedure of filter presses
Chemical Engineering Science **226** (2020)
DOI: 10.1016/j.ces.2020.115889

7. B. Fränkle, P. Morsch, and H. Nirschl
Regeneration assessments of filter fabrics of filter presses in the mining sector
Minerals Engineering **168** (2021)
DOI: doi.org/10.1016/j.mineng.2021.106922
8. V. Bächle, P. Morsch, B. Fränkle, M. Gleiß, and H. Nirschl
Interaction of Particles and Filter Fabric in Ultrafine Filtration
MDPI Eng **2** (2021)
DOI: doi.org/10.3390/eng2020009
9. V. Bächle, P. Morsch, M. Gleiß, and H. Nirschl
Influence of the Precoat Layer on the Filtration Properties and Regeneration Quality of
Backwashing Filters
MDPI Eng **2** (2021)
DOI: doi.org/10.3390/eng2020012

Posters and presentations

14	04/2021	AFS FiltCon 2021, AMERICAN FILTRATION AND SEPERATIONS SOCIETY (AFS) , Virtual Conference. Presentation: "In-situ cleaning process of chamber filter presses with sensor-controlled and demand-oriented automation"
13	10/2019	FILTECH 2019, THE FILTRATION EVENT , Cologne. <ul style="list-style-type: none"> • Presentation: "Influencing parameters to improve the regeneration efficiency of backwashing filters" • Presentation: "In-situ cleaning process of chamber filter presses with sensor-controlled and demand-oriented automation" • Presentation (Co-Author): "Investigation about cohesion and adhesion in backwashing filtration based on penetrometry and tension tests"
12	04/2019	PARTEC 2019, INTERNATIONAL CONGRESS ON PARTICLE TECHNOLOGY , Nürnberg. Poster: "Influence of backwashing pressure and filter cake thickness during backwash regeneration into liquid phase"
11	04/2019	AFS 2019, AMERICAN FILTRATION AND SEPERATIONS SOCIETY (AFS) – Spring Conference , Cypress Hill, New Jersey (USA). <ul style="list-style-type: none"> • Presentation: "Influencing parameters to improve the regeneration efficiency of backwashing filters" • Presentation: "Influence of filter cloth, backwashing pressure and filter cake thickness during backwash treatment into gas phase"
10	03/2019	ProcessNet 2019, JAHRESTREFFEN DER PROCESSNET FACHGRUPPEN MECHANISCHE FLÜSSIGKEITSABTRENNUNG , Bamberg. <ul style="list-style-type: none"> • Presentation: "Einfluss der Gewebewahl auf die Regeneration von Rückspülfiltern in flüssiger und gasförmiger Umgebung" • Poster: "Beschreibung der Gewebedehnung während der Rückspülfiltration" • Poster: "Einflussgrößen beim Kuchenabwurf in gasförmige Umgebung nach vorheriger Flüssigfiltration"
9	02/2019	52. Technologisches Seminar 2019, LEHRSTUHL FÜR BRAU- UND GETRÄNKETECHNOLOGIE WEIHENSTEPHAN , Freising. Presentation: "Bedarfsorientierte Reinigung von Membranfilterpressen durch Bildanalyse"
8	10/2018	FPS 2018, EUROPEAN CONFERENCE ON FLUID-PARTICLE SEPARATION , Lyon (Frankreich). <ul style="list-style-type: none"> • Presentation: "Influence of backwashing pressure and filter cake thickness during backwash regeneration into liquid phase" • Presentation (Co-Author): "Influence of cake formation and discharge on the filter media cleanability"
7	04/2018	8th WCPT 2018, 8TH WORLD CONGRESS ON PARTICLE TECHNOLOGY , Orlando, Florida (USA). Presentation: "Influence of filter cake thickness during backwash regeneration"
6	03/2018	FILTECH 2018, THE FILTRATION EVENT , Köln. Presentation: "Influence of filter cake thickness during backwash regeneration"
5	02/2018	ProcessNet 2018, JAHRESTREFFEN DER PROCESSNET FACHGRUPPEN MECHANISCHE FLÜSSIGKEITSABTRENNUNG , Merseburg. Presentation: "Einfluss der Filterkuchendicke bei der Regeneration von Rückspülfiltern"
4	11/2017	4th HSN-Symposium, 4. FACHSYMPOSIUM DES VEREINS HYBRIDSENORNET E.V. , Karlsruhe). Poster: "Bildanalytische Schmutzerkennung auf Filtertüchern"
3	10/2017	10th WCCE 2017, 10TH WORLD CONGRESS OF CHEMICAL ENGINEERING 2017 , Barcelona. Presentation: "Removal of fine-grained and thin filter cakes by a countercurrent backwash treatment"
2	03/2017	ProcessNet 2017, JAHRESTREFFEN DER PROCESSNET FACHGRUPPEN MECHANISCHE FLÜSSIGKEITSABTRENNUNG , Cologne. Presentation: "Ablösung feinstkörniger dünner Partikelschichten von Filtermedien durch Rückspülung"
1	10/2016	FILTECH 2016, THE FILTRATION EVENT , Cologne. Presentation: "Removal of fine-grained and thin filter cakes by a countercurrent backwash treatment" - LECTURE AWARD